VOT 74507

ZEOLITE BASED CATALYSTS FOR FINE CHEMICALS

(MANGKIN MIKROLIANG BERASASKAN ZEOLIT UNTUK BAHAN KIMIA KHUSUS)

ZAINAB BINTI RAMLI

JABATAN KIMIA
FAKULTI SAINS
UNIVERSITI TEKNOLOGI MALAYSIA

2007

ACKNOWLEDGEMENTS

Alhamdulillah, All Praises to Allah, The supreme Lord of the universe who has granted me everything and makes it possible for me to finish this project (Project No.: 09-02-06-0057 SR0005/09-03**)** with success. Peace and blessing to Rasulullah S.A.W., all the prophets and families, his close friend and all muslim.

I would like to express my gratitude to Ministry of Science Technology and Innovation, MOSTI, Malaysia, for financial support under IRPA Grant Vot 74507. My appreciation also goes to Research Management Centre, UTM for the effective management of the project, and also to the Ibnu Sina Institute for Fundamental Science for support of instruments for the solid state characterizations.

Thank to all the main research team in this project, Prof. Dr. Halimaton Hamdan, Assoc. Prof. Dr. Salasiah Endud, Assoc Prof. Dr. Farediah Ahmad and Dr. Hadi Nur for the contribution of idea for the successful of this project. To those post graduates, final year project students and research assistants, thank you for the hard work, dedication and patience. Without your contribution the success of this project could not be realized. Thanks also to other project teams in the Research Programme "Development of Zeolites and its Derivatives as Catalysts in the Production of Fine Chemicals" for the cooperation, idea and sharing instruments.

Last but not least, thank to all the laboratory assistants of Department of Chemistry and Physic, Faculty of Science, and technicians from Material Laboratory, Mechanical Faculty UTM for the operation of the instruments for characterization and to the individuals who have directly on indirectly contributed in this project.

ASSOC. PROF. DR. ZAINAB RAMLI
Research Leader

ABSTRACT

Several new zeolite-based catalysts have been developed for chemical processes namely the Friedel Crafts acylation and alkylation, and consecutive oxidative acidic reactions of olefin to diol in which the products from theses reactions are valuable chemicals and intermediates in the pharmaceutical and polymer industries. Most of these zeolite based catalysts have been successfully prepared by using rice husk ash as silica source. Ferrierite (Fer), zeolite Beta with different Si/Al ratios and zeolitic mesoporous ITQ-6, have been obtained in pure form in a shorter crystallization time whereas titanium silicalite (TS-1) and zeolite X were also obtained by using commercial silica and natural zeolite respectively. The synthesized zeolites catalysts are modified in order to suit the named processes. For Friedel Crafts reaction, alkylation of resorcinol and acylation of anisole were carried out. Zeolite Beta in modified form: hydrogen-Beta(H-Beta), niobium-Beta(Nb-Beta), gallium-Beta(Ga-Beta) and ITQ-6 and Nb-ITQ-6 were tested their reactivity in alkylation of resorcinol with *tert*-butyl alkylation agent to obtain antioxidants 4-*tert*-butyl resorcinol and 4,6-*di*-*tert*-butyl resorcinol as main products. Nb-Beta was found to be the most active catalyst for the reaction with more than 90% conversion and nearly 100% selectivity for the 4,6-*di*-*tert*-butyl resorcinol while Ga-Beta gave nearly 100% selectivity for 4-*tert*-butyl resorcinol. The strength of antioxidant property of the reaction products is 4X higher than the resorcinol. The reactivity of the catalysts for the reaction depends mostly on the strength of Brönsted acidity together with high zeolite crystallinity rather than the mesoporous property of the catalysts. For the acylation of anisole with propionic anhydride catalysed by H-Fer with Si/Al ratio ~6, gave the highest conversion (60%) and 80% selectivity for *p*-methoxypropiophenone in which slightly lower activity as compared to H-Beta (~ 80% conversion) due to the smaller pore size of H-Fer. In another reaction process, a consecutive oxidative acidic reaction of olefin to diol, bifunctional oxidative acidic TS-1 zeolite catalysts have been developed and was tested on the consecutive transformation of 1-octene to 1,2-octanediol via 1,2-epoxyoctane formation as model reaction. The bifunctional catalysts were prepared by incorporating acidic metal oxides/sulphates on oxidative TS-1: tungsten oxides (WO_3/TS-1), niobium oxide (Nb/TS-1), sulfated zirconia (SZ/TS-1) and sulfated acid (SO_4^{2-}/TS-1) in such a way the location of oxidative sites are inside the pore while the acidic sites located on the external surface of the catalyst. Brönsted acid sites were found in all prepared catalyst except in SO_4^{2-}/TS-1. All catalysts showed significant increased in the rate of formation of 1,2-epoxyoctane compared to TS-1 alone. Brönsted acid sites from acidic oxides/sulphates was responsible for the formation of 1,2-octanediol, with Nb/TS-1 catalyst gave the highest yield of diol. The higher activity of bifunctional catalysts was due to the location of acidic sites in the immediate vicinity of the oxidative sites which enable the epoxidation product to undergo rapid hydrolysis at acid sites.

ABSTRAK

Beberapa jenis mangkin baru berasaskan zeolit telah dihasilkan untuk tindak balas pengasilan dan pengalkilan Friedel-Crafts serta tindak balas berturutan pengoksidaan berasid olefin kepada diol yang mana hasil daripada tindak balas ini sangat berguna dan merupakan bahan perantaraan dalam industri farmaseutikal dan industri polimer. Kebanyakan mangkin berasaskan zeolit ini berjaya disintesis dengan menggunakan abu sekam padi sebagai sumber silika. Ferrierit (Fer), zeolit Beta dengan nisbah Si/Al yang berbeza dan zeolit mesoliang ITQ-6 tulen telah diperoleh dengan masa penghabluran yang pendek, manakala titanium silikalit (TS-1) dan zeolite-X masing-masing diperoleh dengan menggunakan silika dan zeolit asli. Mangkin zeolit yang telah disintesis kemudiaannya, diubahsuai untuk disesuaikan dengan proses-proses tersebut. Pengalkilan resorsinol dan pengasilan anisol telah dijalankan untuk tindak balas Friedel-Crafts. Kereaktifan zeolit Beta terubahsuai: hidrogen-Beta(H-Beta), niobium-Beta(Nb-Beta), gallium-Beta(Ga-Beta) dan ITQ-6 serta Nb-ITQ-6 telah diuji dalam tindak balas pengalkilan resorsinol dengan agen pengalkilan *tert*-butil untuk menghasilkan antioksida 4-*tert*-butil resorsinol dan 4,6-*di*-*tert*-butil resorsinol sebagai hasil utama. Mangkin Nb-Beta didapati paling reaktif untuk tindak balas tersebut dengan lebih daripada 90% pertukaran dan hampir 100% pemilihan untuk 4,6-*di*-*tert*-butilresorsinol manakala Ga-Beta memberikan hampir 100% pemilihan 4-*tert*-butilresorsinol. Kekuatan antioksidan bagi hasil tindak balas adalah 4X lebih tinggi daripada resorsinol. Kereaktifan mangkin untuk tindak balas tersebut lebih bergantung kepada kekuatan tapak asid Brönsted dan tahap kehabluran zeolit yang tinggi berbanding sifat mesoliang mangkin tersebut. Untuk pengasilan anisol dengan propionik anhidrida yang dimangkinkan oleh H-Fer dengan nisbah Si/Al ~6, memberikan peratus pertukaran yang tinggi (60%) dan 80% pemilihan untuk *p*-metoksipropiofenon yang mempunyai keasidan yang agak rendah berbanding H-Beta (~ 80% pertukaran) yang bergantung kepada saiz liang H-FER yang lebih kecil. Di dalam tindak balas yang lain, tindak balas berasid secara berturutan pengoksidaan olefin kepada diol, mangkin zeolit dwifungsi pengoksidaan berasid TS-1 telah dihasilkan dan diuji pada pembentukan pertukaran berturut 1-oktena kepada 1,2-octenadiol melalui 1,2-epoksioktana sebagai tindak balas contoh. Mangkin dwifungsi dihasilkan dengan menyelitkan logam oksida/sulfat berasid ke dalam oksida TS-1: tungsten oxida (WO_3/TS-1), niobium oksida (Nb/TS-1), zirconia sulfat (SZ/TS-1) dan sulfat (SO_4^{2-}/TS-1) supaya kedudukan tapak pengoksidaan terletak didalam liang manakala tapak asid berada pada permukaan luar mangkin. Tapak asid Brönsted didapati pada semua mangkin yang disintesis kecuali pada SO_4^{2-}/TS-1. Semua mangkin menunjukkan peningkatan yang positif pada kadar pembentukan 1,2-epoksioktana dibandingkan dengan TS-1 sahaja. Tapak asid Brönsted daripada oksida/sulfat berasid berperanan dalam pembentukan 1,2-oktanadiol, dengan mangkin Nb/TS-1 memberikan hasil diol yang paling tinggi. Kereaktifan mangkin bergantung kepada kedudukan tapak asid yang bersebelahan dengan tapak pengoksidaan, yang membolehkan hasil pengepoksidaan melalui proses hidrolisis yang pantas pada tapak asid.

Research Team

ASSOC. PROF. DR.. ZAINAB RAMLI (**Leader**)
ASSOC. PROF. DR. SALASIAH ENDUD (**Researcher**)
PROF. DR. HALIMATON HAMDAN (**Researcher**)
ASSOC. PROF. DR. FAREDIAH AHMAD (**Researcher**)
DR. HADI NUR (**Additional Researcher**)
DIDIK PRASETYOKO (**Ph.D student**)
HASLIZA BAHRUJI (**M.Sc. Student**)
MARZITA ABD. MAZAK (**M.Sc. Student**)
WONG KAH MAN (**M.Sc. student**)
AIMAN NAJATI AKMAR RAHMAN (**M.Sc. Student**)
NOOR AISHIKIN MOHD. YUSOFF (**M.Sc. Student**)
Hasidah Mohamad Arsat (**Research Assistant**)
Sheela Chandren (**Research Assistant**)
Che Rozid Bin Mamat (**RA-student working scheme**)
Mohd Fauzan Isa (**RA-student working scheme**)
Chong Kwok Fen (**RA-student working scheme**)
Emmi Shahida Marzuki (**RA-student working scheme**)
Rozaina Binti Saleh (**RA-student working scheme**)
Wong Ka Lun (**RA-student working scheme**)

e-mail: zainab@kimia.fs.utm.my
Tel no. : 07-5534491

Vot: 74507

TABLE OF CONTENTS

CHAPTER 1

INTRODUCTION

INTRODUCTION

1.1 Zeolite based catalysts for fine chemicals

Friedel Craft acylation and alkylation of aromatic materials is one of the important reactions in the production of fine chemicals for pharmaceutical and perfumery industries. Commercial antioxidant such as butyl hydroxy toluene, BHT and butyl hydroxy anisole, BHA (Koorneev et. al. *US Patent*, 1990) for example are the product of Friedel Crafts reactions which make use of homogeneous catalysis system namely mineral acids as catalyst (Cardillo et. al. *Tetrahedron Left.* 1972, **10**, 945). However, due to the economic associated in the separation process and the stringent environmental concern on the disposal of spent acidic catalyst makes the system environmentally unfavorable.

Research on the used of solid catalysts such as zeolite and clay as catalyst or as support for metal oxides are becoming popular in many organic reactions to produce fine chemicals. Friedel Crafts acylation and alkylation (Freese et. al *Catalysis Today*, (1999) **49**, 237), and metathesis (Hamdan *et. al*. *Stud. Sur Sci. Catal.* (1997) **105,** (57) etc. of organic materials have been carried out by using various zeolite-based catalysts with good yield and selectivity. Friedel Crafts reaction is catalysed by Bronsted and Lewis acids. Since modified H-zeolite is a solid acid catalyst (Ramli et. al Malay. *J. Anal. Sci*. (2001) **(2)**, it has great potential to substitute minerals acid in many Friedel Crafts reactions. Friedel Crafts reactions using solid catalysts (Narayanan *et a*l. *Applied catalysis A*, 2001, 273) such as zeolites are in the rise due their capability in catalyzing as solid acid in the reactions with good conversion and selectivity. Acylation of anisole over H-zeolite beta synthesized from rice husk ash (Ramli. Z. et. al., *Buletin Kimia*, 2000, 32) produce ~ 80% conversion and 70% selectivity for the main product. The structure and pore size of the zeolites catalyst seems to determine the acidity, reactivity and

selectivity of the catalysts towards the chosen reaction. The activity of catalyst for such reactions can be increased by modification on the zeolite frame work to optimize the acid properties of the catalyst.

In this project zeolites with different structures, pore sizes and acidities project zeolite were utilized in order to study the actual parameter governing the reactivity of zeolite-based catalyst in the Friedel Crafts reaction. Zeolites such as Ferrierite (medium pore: ϕ ~ 5Å), Beta (large pore.ϕ ~ 7Å) and ITQ-6 (mesopore .ϕ ~ 40Å) will be used based on the difference in pore size system that might affect the product output from the Friedel Crafts reaction. The reactivity of the prepared zeolites based catalysts was tested in the alkylation of resorcinol as model reaction (Eq. 1.1) as the chemical products from the reaction have antioxidant properties supposed to be higher strength than commercial BHA and BHT and .

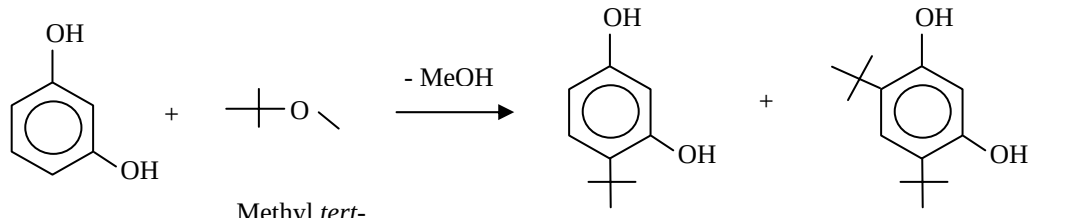

……(eq. 1.1)

One of the crucial points for the development of catalysts is to design the active sites for catalytic processes. The efficiency of a catalytic process in general greatly depends on the performance of the catalyst, rendering the development of efficient catalytic materials one of the foremost challenges in catalysis research. In many of catalytic processes a stream of reactant is passed over tiny particles (atomic or cluster) of active sites on an oxide support surface. One of the challenges is to design highly-functionalized catalysts by a combination of oxidative and acidic active sites for consecutive oxidation and acid catalytic reactions. Therefore the project was also

extended to the used of zeolites based catalyst for other process for producing fine chemicals. In this study the properties of zeolites was tailored in such a way that it acts as bifunctional oxidative acidic catalysts capable of catalyzing direct transformation of alkene to diol. As shown in Figure 1.1 for the bifunctional oxidative acidic catalyst, as a model reaction, Ti site acts as oxidative site for oxidation of 1-octene to 1,2-epoxyoctane (as intermediate) and niobic acid acts as acidic site for transformation of 1,2-epoxyoctane to 1,2-octanediol

Several bifunctional oxidative and acid catalysts have been prepared by incorporation of trivalent metal ions (Al^{3+}, B^{3+}, Fe^{3+}, Ga^{3+}) and titanium ion (Ti^{4+}) together in the framework of silica based molecular-sieves (Trong On *et al*., 2003; van

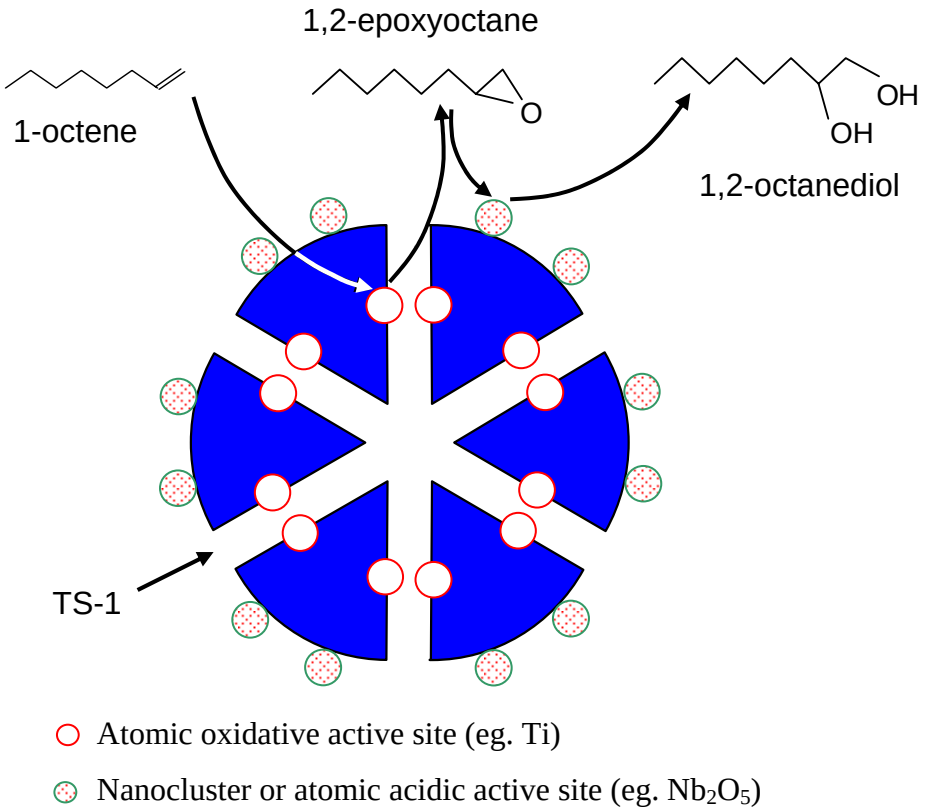

Figure 1.1: Oxidative and acidic catalyst for consecutive oxidation and acid catalytic reactions.

der Wall *al.*, 1998; Krijnen *et al.*, 1999). The catalysts being active both in the oxidation reactions due to the presence of tetrahedral Ti^{4+} and in acid catalyzed reactions as the substitution of the trivalent cations in the framework of silica generates acid sites. In a previous study, some research groups (van der Wall *et al.*, 1998; Davies *et al.*, 2001; Sashidaran *et al.*, 2002) have demonstrated that Ti-Al-beta and Ti-beta zeolites can lead to acid-catalyzed consecutive reaction. The catalysts were active in epoxidation of alcohol or bulky alkenes and selective in diol formation. These products are useful intermediates in the production of pharmaceutical, pesticide, fragrance and other fine chemicals.

1.2 Objectives of the projects

Original objectives of the project as proposed were (i) –(iv). However the objectives of the projects were extended to the tailoring of the actives sites zeolites for bifunctional oxidative acidic catalysts for production of other fine chemicals (objectives v -)

i) to prepare the microporous zeolite-based catalyst of different zeolites types from silica rice husk ash
ii) to modify the as prepared microporous zeolite catalyst for Friedel Crafts acylation and other organic reactions
iii) to compare the reactivity of various microporous zeolite based catalysts for Friedel Crafts acylation and alkylation
iv) to determine the most active catalyst for Friedel Crafts acylation.

Extended objectives

v) to prepare oxidative titanium silicalite (TS-1)
vi) to incorporate the acidic metal oxides into TS-1 for the preparation of bifunctional oxidative acidic catalysts
vii) To test the prepared catalysts for the one pot reaction of alkene to diol via alkene oxide.

1.3 Scope of the project

The project was started by preparing zeolites with different types zeolites and pore sizes and Si/Al ratios using most of the time the rice husk ash as silica source. Zeolites that have been chosen were zeolite Beta and zeolite X & Y (large pore), ferrierite and prefer, and titanium silicalite (TS-1) instead of ZSM-5 (medium pore zeolite), and mesoporous ITQ-6.

For the Friedel Craft alkylation and acylation which proceed in the presence Bronsted and Lewis acid, the prepared zeolites were modified into (i) the H-form, (ii) by introducing metals oxides, and also (iii) by changing the Si/Al ratios of the zeolite framework, in order to create the acidity at different strength. Metal oxides that have been chosen were niobium oxide (Nb_2O_5. xH_2O) and gallium oxide (GaOx) because of their properties as Bronsted acid and Lewis acid respectively. The incorporation of metal oxides were carried by impregnation method while zeolite at different Si/Al ratios were obtained by direct synthesis using different silica/alumina ratios of the initial gel composition. The prepared catalysts were tested their reactivity in the (i) Friedel Crafts alkylation of resorcinol with *tert*-butyl alkyl agents namely *tert*-butanol and methyl *tert*-butyl ether (MTBE) and (ii) Friedel Craft acylation of anisole with propionic and acetic anhydrides as acyl agents.

In the preparation of bifunctional oxidative acidic zeolite based catalyst, titanium silicalite (TS-1) which already contains oxidative sites, were incorporated by wet incipient or impregnated method with selected metal oxides/sulphates. The metal oxides/sulphates that have been chosen were known to have Bronsted acid properties were tungsten oxides (WO_3), niobium oxide and niobic acid Nb_2O_5. xH_2O, sulfated zirconia (SZ) and titanium oxides (TiO_2) and sulfated ions (SO_4^{2-}) from sulfuric acid. The prepared catalyst were tested their reactivity in the one pot transformation of olefin to diol with the transformation of 1-octene to 1,2-octanediol as model reaction. The reactivity was monitored on the rate of reaction.

All prepared catalysts were characterized by XRD and FTIR for the crystal phase identification, Field Emission SEM for crystal morphology, and Diffuse Reflectance UV-Vis for identification of coordinated structure. Acidity studies were done by pyridine adsorption monitored by FTIR, and temperature desorption of NH_3. The catalytic testing

was done in batch reactor equipped with condenser. The liquid samples from the reaction were separated and identified by GC-FID and some components were identified using GC-MSD. For antioxidant properties, the product from Friedel Crafts reaction were characterized by ESR using 1,1-diphenyl-2 picryl-hydrazyl (DPPH) as antioxidant scavenger.

1.4 Organization of the reports

Most of the outcomes of this research are documented in the form of journal publications and theses. The following chapters described about the outcome results in the form of compilation of all publications and theses of based on the subjects: CHAPTER II: Friedel Crafts alkylation/acylation catalysed by zeolite based catalyst, CHAPTER III: Bifunctional catalysts and CHAPTER IV: Zeolites as basic catalysts.

References:

Cardillo, B., Merlini, L. and Servi, S. (1972). Alkylation of resorcinols with monoterpenoid allylic alcohols in aqueous acid: synthesis of new cannabinoid derivatives. *Tetrahedron Lett.* 13: 945-948.

Davies, L. J., McMorn, P., Bethell, D., Page, P. C. B., King, F., Hancock, F. E. and Hutchings, G. J. (2001). Oxidation of crotyl alcohol using Ti-β and Ti-MCM-41 catalysts. *J. Mol. Catal. A: Chemical* 165: 243–247.

Krijnen, S., Sánchez, P., Jakobs, B. T. F. and van Hooff, J. H. C. A. (1999). controlled post-synthesis route to well-defined and active titanium Beta epoxidation catalysts. *Microporous and Mesoporous Mater.* 31: 163-173

Liu, Jue-Chen, Wang, Jonas C.T,: Mohammaed Yusuf, (1995). Ketocanazole shampoo containing butylated hydroxyl anisole. US Patent 5,456,851.

Narayanan, S., and Murthy, K.V.V.S.B.S.R., (2000). Montmorillonite as a versatile solid acid catalyst for *tert*.-butylation of resorcinol. *Appl. Catal. A:General* 213: 273–278

Sasidharan, M., Wu, P. and Tatsumi, T. (2002). Direct Formation of Pinacols from Olefins over Various Titano–Silicates, *J. Catal.* 209: 260-265.

Trong On, D., Nguyen, S. V., Hulea, V., Dumitriu, E. and Kaliaguine, S. (2003) Mono- and bifunctional MFI, BEA and MCM-41 titanium-molecular sieves. Part 1. Synthesis and characterization. *Microporous and Mesoporous Mater.* 57: 169–180.

U. Freese, F. Heinrich and F. Roessner (1999) Acylation of aromatic compounds on H-Beta zeolites. *Catal. Today*. 49: 237-244.

Waal, J. C., Kooyman, P. J., Jansen, J. C. and van Bekkum, H. (1998). Synthesis and characterization of aluminum-free zeolite titanium beta using di(cyclohexylmethyl) dimethylammonium as a new and selective template. *Microporous and Mesoporous Mater.* 25(1-3): 43-57

CHAPTER 2

SYNTHESIS OF ZEOLITES FROM RICE HUSH ASH

(Compilation of Paper Publications, Seminars & Conferences and Abstract of Theses)

SYNTHESIS OF SELECTED ZEOLITES FROM RICE RUSK ASH: SCANNING ELECTRON MICROGRAPHS OF ZEOLITES CRYSTALS

Introduction:

In Malaysia, the local annual production of rice leaves behind about 2.4 million tones of husk as waste product (Kim *et al.*, 2000). Rice husk, a major agricultural waste, is a fibrous material with high silica content, cellulose and lignin (James and Rao., 1986). Silica ash which is transformed from the husk by complete burning constitutes 15-20% of the total weight of the husk. Rice husk ash contains 90-99% SiO_2 and 20% of the white ash residue left after the combustion causes air and water pollution (Pariente *et al*., 1987). Because of its nonbiodegradable property, the presence of the silica ash causes a number of problems to the environment. In order to solve these problems, useful applications of the waste product are desirable.

Silica from rice husk finds it uses as a constituent of low cost cements and as a source for metallurgical as well as semiconductor-grade silicon. Silica is one of the basic raw materials in the glass and ceramic industries. Here, rice husk can be employed with advantage. As the ash is obtained as a fine powder, it does not require further grinding. Also the firing temperature is expected to be lower than normal because of the reactive nature of silica in ash. Silica in rice husk has also been employed for preparing silicon carbide whiskers at temperature lower than normal (James and Rao., 1986).

The large amount silica freely obtained from this source provides an abundant and cheap alternative of silica for many industrial uses, including the synthesis of zeolites (Kapur *et al*., 1998). The reactivity of the silica depends on the method of preparation and extraction from the rice husk. Controlled burning at 800ºC for 10 hours produces rice husk ash in amorphous form, whereas silica crystal from rice husk ash with tridymite and cristobalite structures are formed in uncontrolled burning at higher temperatures (> 800ºC) (Chen and Yeoh., 1992). The chemical compositions of rice husk ash are listed in Table 2.1.

Table 2 .1: The composition of compounds in rice husk ash (Chen and Yeoh, 1992)

Compound	SiO_2	Al_2O_3	Fe_2O_3	CaO	MgO	Na_2O	K_2O	LOI	Total
Percentage, wt%	95.12	0.19	0.07	0.32	0.51	0.01	1.64	2.14	100.0

LOI = Loss on ignition

Synthesis of a few types of zeolites from rice husk ash has been reported (Chen and Yeoh., 1992; Listiorini *et al.*, 1996). Zeolite Beta also has been synthesized successfully using crystalline silica from rice husk ash containing cristobalite and tridymite which is obtained directly from uncontrolled burning (Didik, 2001). Therefore, the transformation of crystalline silica from rice husk ash to zeolite is possible when amorphous silica is normally been used in the zeolite synthesis. Amorphous silica obtained by combustion under controlled temperature contains only $Si(OSi)_4$ tetrahedral units and has proved to be the most reactive silica source in the synthesis of zeolite as compared to silica prepared by either chemical extraction or uncontrolled burning of rice husk. The presence of crystalline cristobalite and tridymite phases and SiOH group render the silica less active. The properties of silica obtained from rice husk ash are strongly influenced by the temperature of formation and the duration of heating (Hamdan *et al*., 2000).

In this project besides the mentioned zeolites produced from rice husk ash in the previous project, the search for synthesizing other type of zeolites using rice husk ash as silica source was continued. Selected zeolite with different pore sizes type and should be suitable for as catalysts for Friedel Crafts alkylation and acylation were chosen: zeolite Beta (large pore), Ferrierite (medium pore), zeolite P (small pore) and zeolitic mesoporous ITQ-6(mesoporous), while for the consecutive oxidative acidic reaction of alkene to oxidative titanium silicalite TS-1 was chosen. This article summarizes the zeolites obtained from this projects which were characterized by SEM methods only. Results from other characterizations methods were described in detailed in the theses.

Experimental

All methods for producing zeolites in this project are described in details in the Ph.D and M.Sc theses carried out by research students in this project. In general all zeolites synthesis involves hydrothermal synthesis at selected temperature and at atmospheric pressure.

Method of synthesis of zeolite Beta with different Si/Al ratios of the framework are described in the thesis of Wong Kah Man (M. Sc. Thesis, 2005) and Marzita Abd Mazak (M.Sc Thesis, 2006). The methods for synthesizing gallosilicate zeolite Beta was performed by Aiman Najati (M.Sc. Thesis 2007). The medium pore ferrierite with composition optimization was described in detailed in Hasliza Bahruji (M.Sc. Thesis 2005) while the method for transforming zeolitic microporous FREFER to mesoporous ITQ-6 was undertaken by Nor Aishikin Mohd Yusoff (M.Sc Thesis, in press).Didik Prasetyoko (Ph.D. Thesis 2006) has reported the method of synthesizing titanium silicalite TS-1 at different Ti/Al ratios.

Results

This project has proved the reactivity of rice husk ash (RHA) as silica source for producing many kinds of zeolites. Almost all kind of zeolites have successfully formed when using RHA as silica source. In this project zeolite P (small pore) Zeolite Ferrierite (FER), precursor of ferrierite (PREFER) (medium pore zeolite), zeolite Beta and zeolite X has have been synthesized in pure and highly crystalline form. The evidence of the formation of those zeolites was described in detailed in their respective theses by XRD and IR methods.

Zeolite P was obtained from oxides composition 6.0-6.2 Na_2O: Al_2O_3: $8SiO_2$: 112 H_2O within 1 day at 100 ^oC . . The morphologies of zeolite P at different magnification are presented in Figure 1 showing rose-like crystals. For a small pore zeolite P can be formed in 1 days time at 100^oC using 6.0-6.2 Na_2O : Al_2O_3 : 8 SiO_2 : 112 H_2O gel composition. For half day crystallization time at the same temperature and composition produced zeolite X or Y instead, indicating that zeolite X and Y are metastable zeolites which will transform to other phases.

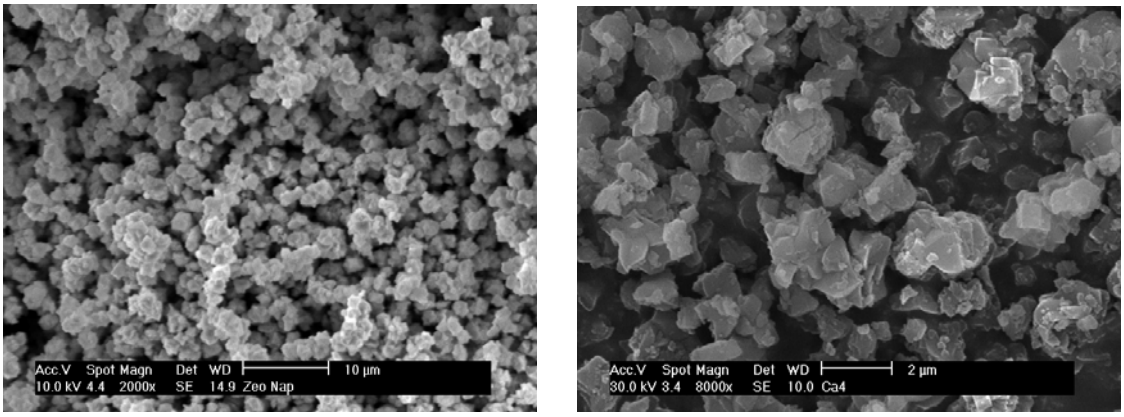

(a) (b)

Figure 1: SEM of zeolite P (a) 2000x (b) 8000x magnification

Pure ferrierite zeolite FER phase was obtained from gel compositions in the range of 1.31 – 1.5 Na_2O : Al_2O_3 : 10 – 30 SiO_2 : 4.0 – 10.0 Pyrrolidine : 410 H_2O with narrow range of SiO_2/Al_2O_3 ratios from 10 to 30. The stable FER was obtain in 4 days crystallization time at 200^oC, shorter than when using commercial silica source like fume silica, which usually take 8-12 days. SEM for the formation of ferrierite at different crystallization period are shown in Figure 2.

Figure 3 shows SEM of some morphologies of Al- zeolite Beta and galosilicate zeolite Beta with granule-like morphologies with various sizes. Pure zeolite Beta phase is obtained from the oxide gel ratios of 1.9-8 Na_2O: Al_2O_3: 27-90 SiO_2: 5-20 TEA_2O:

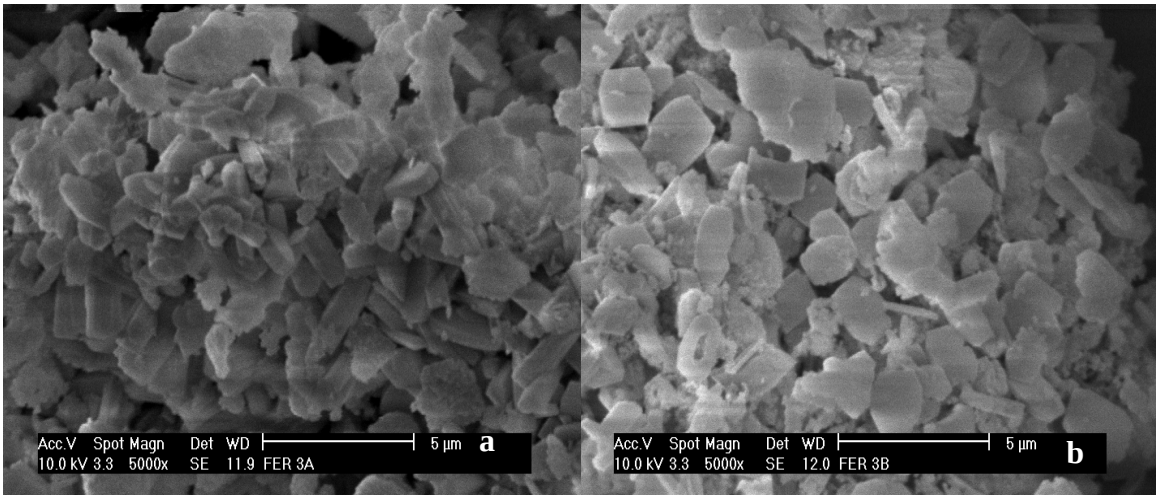

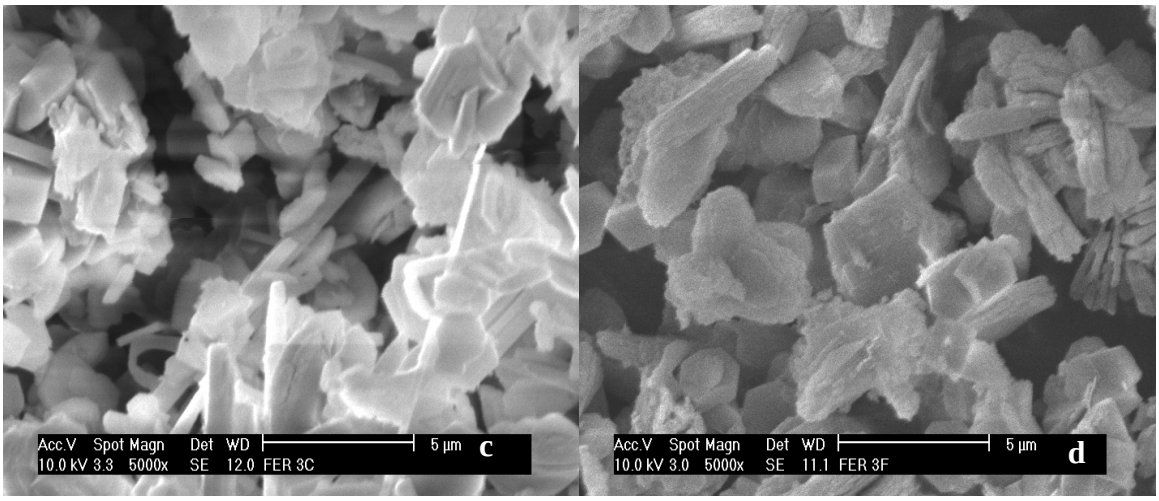

Figure 2: Scanning electron micrograph for ferrierite at different crystallization period (a) 1 day (b) 5days (c) 9 days (d) 12 days

240-800 H_2O at 150^oC for 7 days crystallization. Silicieous zeolite Beta (aluminium free) failed to obtain due to the presence of aluminium containment which facilitates the formation of Al-Beta. However gallosilicate zeolite Beta (aluminium free zeolite Beta containing gallium in the framework) has been successfully synthesized from hydrothermal synthesis at 135^oC with molar oxide composition of 6.0 Na_2O : 67 SiO_2 : Ga_2O_3 : 13.3 TEA_2O : 1000 H_2O. Another successful formation of zeolite PREFER was obtained from gel composition in the range of 10-60 SiO_2 : 0.5-1Al_2O_3 : 7.5-15NH_4F : 2.5-5HF : 10 (4-amino-2,2,6,6- tetramethylpiperidinr) : 50-100H_2O at 175^oC for 5 days crystallization time.

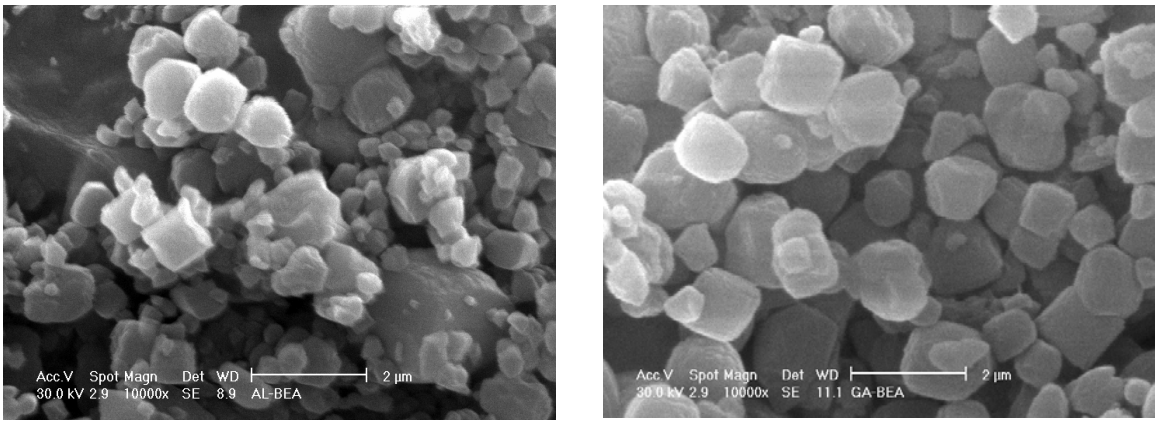

(a) (b)

Figure 3 : SEM of (a) Al-zeolite Beta (b) Gallosilicate zeolite Beta

Another successfull attemp in producing zeolitic mesoporous zeolite PREFER and ITQ-6 amphasized the reactivity of rice RHA as silica source. In all cases the RHA must be in amorphous form. Figure 4 shows some of morphologies of the precursor of ferrierite, PREFER with flake-like crystal and its mesoporous zeolitic ITQ-6 obtained from rice husk ash. The morphology of ITQ-6 clearly shows the distroyed crystal of the precursor PREFER as the result of delamination treatment on the PREFER precursor which involved swelling with organic template, followed by sonication and calcination to eliminate the organic template. XRD of ITQ-6 shows the amorphous material as evidence from the SEM picture shown Figure 5. However the microporous PREFER has transform to the mesoporous material of ITQ-6 (

.

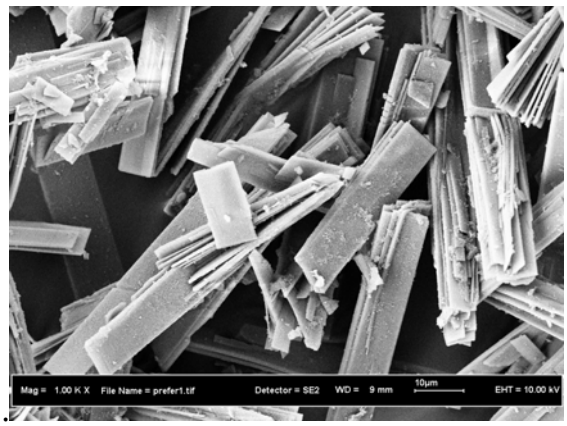

(a) 1000x magnification

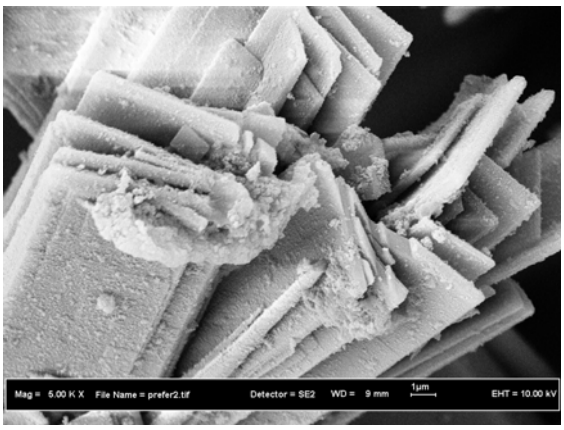

(b) 5000x magnification

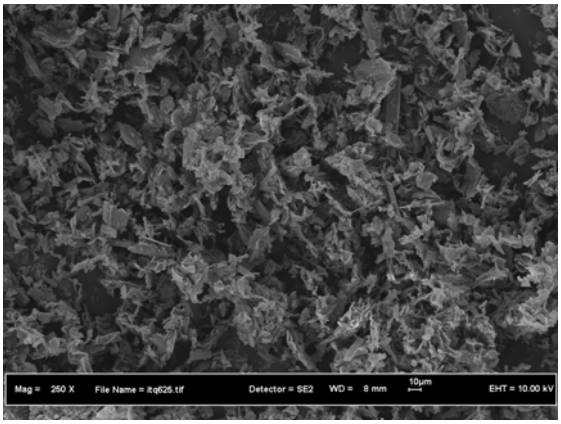

(c) 250 x magnification

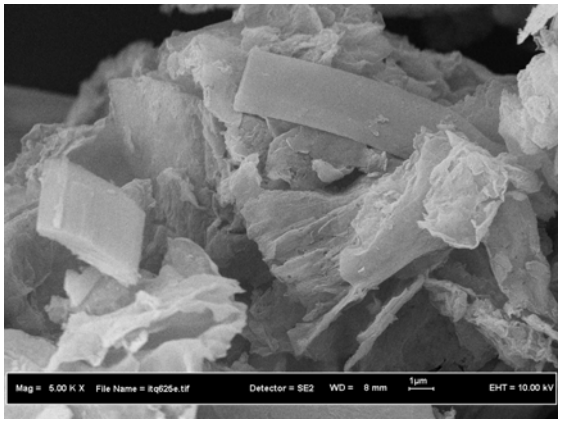

(d) 5000x magnification

Figure 4: FESEM of PREFER (a) and (b) and ITQ-6 (c) & (d)

The morphology of samples titanium silicalite TS-1 at different content of Ti were presented in Figure 5 showing hexagonal crystals. The crystallinity of samples TS-1 is slightly increased as titanium content increased from 1% to 3%. Meanwhile, crystallinity of sample TS-1 (4%) decreased markedly compared to that of samples TS-1 (1-3%). This result suggests that at the titanium loading higher than 3%, the titanium species in the gel may retard the growth of TS-1 crystals. It is known that for samples TS-1, the titanium species are located in the framework structure of silicalite, therefore, no TiO_2 can be observed by XRD technique. However, the structure of titanium in the molecular structure cannot be confirmed by XRD technique, but by UV-Vis DR

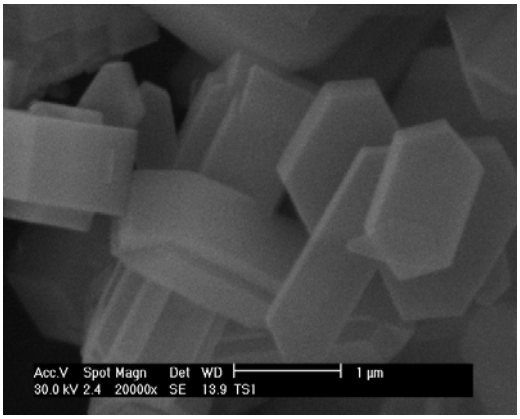

(a) 1%wt Ti- 20,000x magnification

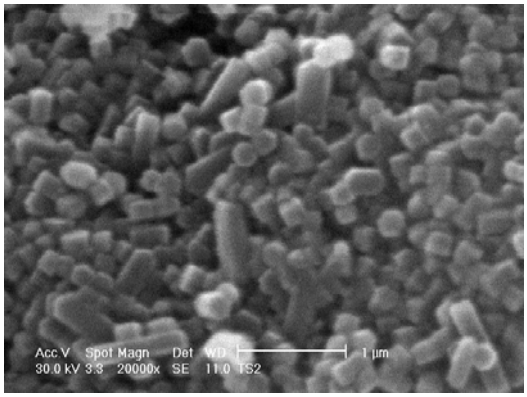

(b) 2%wt Ti - 10,000 x magnification

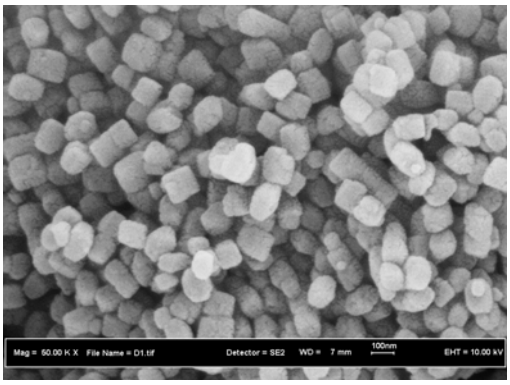

(c) 3 wt% Ti- 10,000x magnification

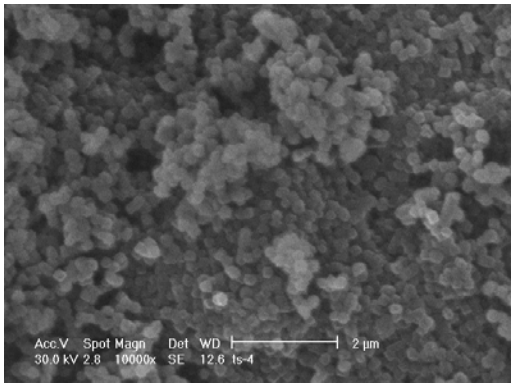

(d) 4 wt% Ti - 10,000x magnification

Figure 5 : FESEM of TS-1 at different wt% Ti : (a) 1 wt% Ti (b) 2 wt% Ti (c) 3 wt% Ti (d) 4 wt% Ti

technique, which is also reported in Didik Prasetyoko (Ph.D. Thesis, 2006). Well form TS-1 hexagonal crystal was obtained in the micro size range from the gel containing only 1 %wt. Ti. With the increased of Ti content in the gel, the size of TS-1 cystals reduces to near nano range (~100-200 nm) with not so well form of crystals as can be seen from the SEM pictures in Figure 5.

References:

Aiman Najati Akmar binti Rahman (2007) Gallium Modified Zeolite Beta for Friedel Crafts Alkylation of Resorcinol. M.Sc Thesis , UTM

Chen, S. S., and Yeoh, A. K. (1992). Development of zeolite NaY from Rice Husk Ash. *Journal of Industrial Technology*. 2. SIRIM, Malaysia

Didik, P. (2001). *Pengoptimuman sintesis zeolite beta daripada abu sekam padi:pencirian dan tindakbalas pemangkinan Friedel-Crafts.* UTM. Tesis MSc

Didik Prasetyoko (2006) Bifunctional oxidative and Acidic Titanium Silicalite (TS-1) Catalysts for One Pot Synthesis of 1,2-octenediol from 1-octene. Ph. D Tesis, UTM

Hasliza binti Bahruji (2005) Synthesis of zeolite Ferrierite from Rice Husk Ash, Characterization and Activity Towards Friedel Crafts Acylation of Anisole with propyl anhydride M.Sc Thesis, UTM

James, J.and Rao, M. S.(1986) Characterization of Silica in Rice Husk Ash. *American Ceramic Society Bulletin*.65: 1177-1180.

Listiorini, E., Ramli, Z., and Hamdan, H.(1996) "Optimization and Reactivity study of Silica in The synthesis of zeolites from Rice Husk Ash." *J. Teknologi*.25: 27-35.

Marzita Abd. Mazak (2006) "Modified Zeolite Beta as Catalysts in Friedel Crafts alkylation of Resorcino*l*. M.Sc Tesis, UTM

Pariente, J. P., Martens, J. A. and Jacobs, P. A. (1987). Crystallization and Mechanism of Zeolite Beta from TEA_2O, Na_2O and K_2O Containing Silicates Gels. *App. Cat. A.* 31: 35 – 64.

Wong Kah Man (2004) Acid-base Properties of Modified Zeolite Beta: Modification, Characterization and Catalytic Testing. M.Sc Thesis, UTM

Proceeding of Annual Fundamental Science Seminar 2003, pg 147-152

EFFECT OF MOLAR OXIDES COMPOSITION IN THE SYNTHESIS OF FERRIERITE FROM RICE HUSK ASH

Zainab Ramli[a], Halimaton Hamdan[a], Bogdan Sulikowsk[b]i, Hasliza Bahruji[a]

[a]Institute Ibnu Sina, Universiti Teknologi Malaysia
81310 Skudai, Johor
[b]Polish Academy of Sciences, Krakow Institute of Catalysis and Surface Chemistry,
Ul. Niezapominajek 8, PL30-639 Krakow, Poland
Tel: +(607) 5534491
Email: myhas-075@hotmail.com

ABSTRACT

Ferrierite, a rare and siliceous zeolite has great potential as heterogeneous catalyst and catalyst support. In this *study, ferrierite type zeolite has been synthesized for the first time using rice husk ash as silica source. The crystallization process of ferrierite was carried out hydrothermally in the presence of organic template pyrrolidine, py. The effect of reaction parameters including the variation of* SiO_2 / Al_2O_3 *and Py /* Al_2O_3 *molar ratios in the starting reaction mixtures were studied in order to determine the optimum conditions for the formation of ferrierite. Solid products obtained from the synthesis were characterized by XRD, FTIR and SEM. Characterization result showed that ferrierite can be formed from the initial reaction mixture in the range of 1.31 – 1.5* Na_2O *: 1* Al_2O_3 *: 12 – 30* SiO_2 *: 6.67 – 10.0 Py : 410* H_2O*. The decrease in the pyrrolidine concentration resulted in the formation of analcime phase.*

1. INTRODUCTION

Ferrierite is a siliceous zeolite and widely employed as catalyst in skeletal isomerization of *n*-butene and for reduction of nitrous oxide gaseous. It was first discovered by W. F. Ferrier. Ferrierite is a medium pore zeolite with pore sizes between 4.5 Å to 6.5 Å. Ferrierite formed in two types, monoclinic and orthorhombic. The ferrierite framework contains two systems of mutually perpendicular one-dimensional channel of 10- and 8-membered rings. The main channel is parallel to the orthorhombic c-axis of the crystal and is outlined by the elliptical 10-membered of the rings (sized 4.3 Å x 5.5 Å in diameter). The side channels are formed by 8-membered of the rings (3.4 Å x 4.8 Å in diameter), which parallel to the b-axis of the crystal [1].

Since the discovery of the ferrierite and its potential in many applications particularly in the nitrous oxide gaseous reduction, a lot of research have been carried out to improve the synthetic method and the quality of the product as well as to reduce the cost of producing ferrierite. Ferrierite can only be found in three places, at the Kamploops Lake, Canada; Gotaloves, Yugoslavia; and Chernichino, Bulgaria. Because the difficulty in finding ferrierite in other places, scientific research on finding an alternatives way to obtain ferrierite has become important. Synthetic ferrierite was first obtained by hydrothermal high-pressure crystallization (up to 165 bar at 350^{o}C and 120 bar at 325^{o}C) by Kibby et al.[1]**.** Silicon and organic template are the important components in the synthesis of ferrierite because both reactants will influence in the development of ferrierite structure. In synthesizing ferrierite, normally pyrrolidine, piperidine or ethylenediamine was used as organic template and crystallization temperature was set around 150^{o}C to 200^{o}C. The template is used as structure directing agent as well as charge balancing cation.

Commercial ferrierite was produced by using commercial silica sources in the form of gel, sol and amorphous fumed silica. However, highly silica content of waste materials such as rice husk ash and fly ash are potential silica sources for zeolite synthesis. In this study, rice husk ash was used as a source of silica which is never been done before. Previous studies have shown that the utilization of rice husk ash has successfully produced zeolite A, Y, ZSM-5, mordenite and Beta. The successful of rice husk ash in preparing ferrierite will give an alternative in producing a low cost ferrierite.

2. EXPERIMENTAL

The following reagents were used for the ferrierite synthesis: NaOH (Merck), sodium aluminate (Chem-Tech), pyrrodiline (Merck), piperidine (Merck), glycerol (Merck) ethylenediamine (Merck) and distilled water. Rice husk ash obtained from BERNAS Rice Mill, Kuala Selangor, Selangor initially contains 90% of SiO_2 as silica source. Other constituent in the rice husk ash are MgO, Na_2O, K_2O, CuO, Al_2O_3 and Fe_2O_3. Synthesis of ferrierite was carried out in a variety of mole oxides ratios with different type of template as shown in Table 1. In a typical zeolite synthesis, the ash was added to an aqueous NaOH solution with stirring. The template was then added and following with the solution of sodium aluminate solution. The oxides mixture obtained by mixing of ash, sodium hydroxide solution, template, sodium aluminate solution and distilled water, was stirred at room temperature for 6 hours and then sealed in a stainless steel autoclave. The conversion to ferrierite was carried out at 200^{o}C for 7 days. The solid phase was filtered, thoroughly washed with distilled water and dried overnight at 100^{o}C. The dried powder was calcined at 550^{o}C for at least 6 hours to remove the organic template. The synthesis product was characterized using XRD, FTIR and SEM to confirm the formation of ferrierite. To optimize the formation of ferrierite from rice husk ash, ferrierite was performed by hydrothermal crystallization of a mixture of molar composition 1.31 Na_2O : 1 Al_2O_3 : 20 SiO_2 : 6.67 Py : 410 H_2O, (py is pyrrolidine). The synthesis procedure was repeated by changing the SiO_2, Na_2O and pyrrolidine content in the range of 1.31 – 5.00 Na_2O : 1 Al_2O_3 : 12.00-50.00 SiO_2 : 2 .00 – 10.00 Py : 410 H_2O.

3. RESULTS AND DISCUSSION.

Figure 1 shows the X-ray diffraction pattern of the products synthesized in the presence of three different types of organic templates. The X-ray diffraction pattern in Figure 1 reveals that only sample Fer-3-Py using pyrrolidine as template show similar XRD pattern when compared to the XRD pattern of ferrierite from previous research [2] which indicates that ferrierite has been successfully formed. Other samples that using glycerol, ethylenediamine and piperidine as template, they was failed to formed ferrierite. However, ferrierite was able to form from those templates, when using commercial fumed silica as silica sources [3], [4], [5]. It shows that the phase purity of crystalline products prepared using rice husk ash as silica sources is most likely dependent on the type of template used. The formation of ZSM-5 in sample Fer-2, when ethylenediamine was used as template is expected since all organic template used in this study can serve as structure directing agents for ZSM-5 formation. Jongkind *et al*. [6] and Yang *et al*.[4] found that ZSM-5 can be formed using ethylenediamine, piperidine and pyrrolidine as template.

Each zeolite species has a typical infrared pattern for structural vibration which consist of four main peaks; the asymmetric and symmetric peaks of TO_4 (T = Al, Si) at 1250 – 1000 cm^{-1} and 750 – 650 cm^{-1} respectively and T–O bending at 500 – 400 cm^{-1}. The IR spectra of the samples are shown in Figure 2. All bands that correspond to the IR spectra of ferrierite are present in the IR spectra of sample Fer-3. it is further confirmed that Fer-3-Py was successfully synthesis from rice husk ash. Table 1 lists the initial reaction mixture of the ferrierite synthesized from rice husk ash using varieties of templates and the phase product from each molar oxides ratio. Figure 3 shows a scanning electron micrograph of ferrierite which it shows the star-shaped particles of ferrierite.

Table 1: The initial mole oxides ratio for each sample

Sample	Template	Product	Mole Oxide Ratio	SiO_2/Al_2O_3
Fer-1-Gly	Glycerol	MOR	11.97 Na_2O : 1 Al_2O_3 : 9.85 SiO_2 : 198.8 Gly : 158.15H_2O,	9.85
Fer-2-En	Ethylenediamine	ZSM-5	1.85 Na_2O : 1 Al_2O_3 : 51 SiO_2 : 19.7 En : 592 H_2O,	51
Fer-3-Py	Pyrrolidine	FER	1.51 Na_2O : 1 Al_2O_3 : 30 SiO_2 : 10 Py : 370 H_2O,	30
Fer-4-Py	Pyrrolidine	FER	1.31 Na_2O : 1 Al_2O_3 : 20 SiO_2 : 6.67 Py : 410 H_2O,	20
Fer-7-Pn	Piperidine	Analcime	6.78 Na_2O : 1 Al_2O_3 : 22.7 SiO_2 : 8.99 Pn : 368 H_2O,	22.7

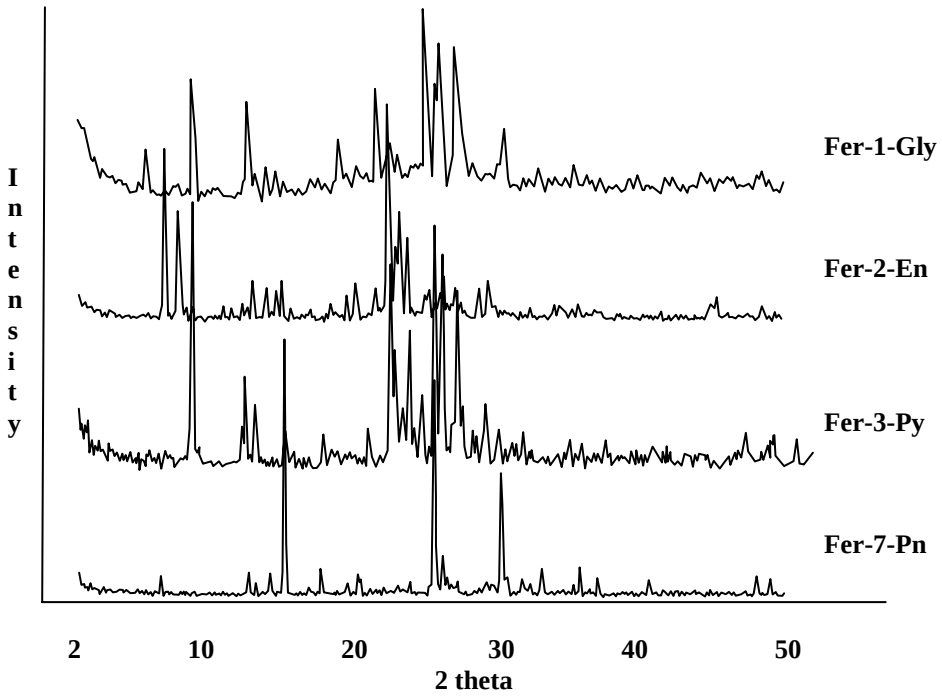

Fig. 1 X-Ray Diffractogram for sample Fer-1-Gly, Fer-2-En, Fer-3-Py, Fer-7-Pn and Fer-8-PnGly.

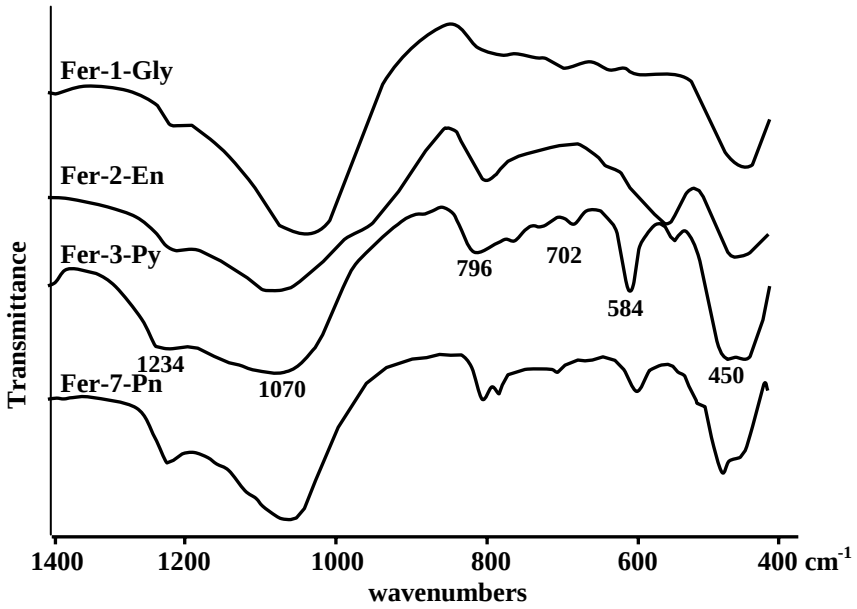

Fig. 2 FTIR spectra for sample Fer-1-Gly, Fer-2-En, Fer-3-Py, Fer-7-Pn and Fer-8-PnGly

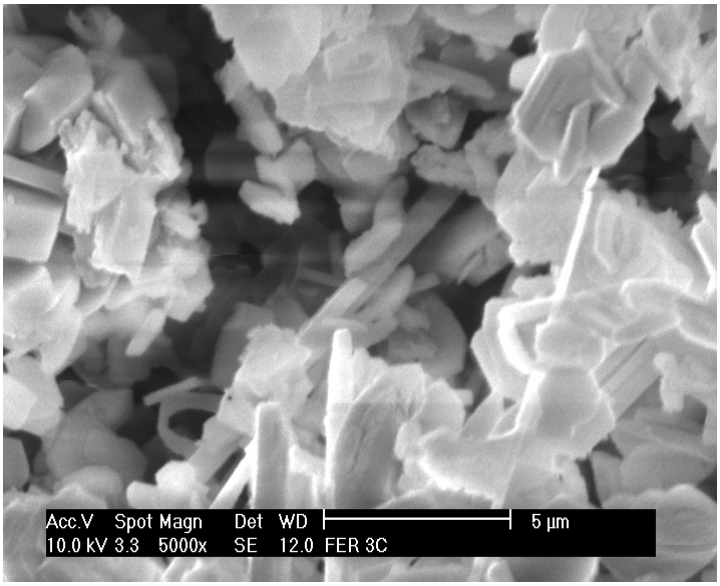

Fig 3: Scanning Electron Micrograph for ferrierite

3.1 Effects of SiO_2 / Al_2O_3 and Py / Al_2O_3 molar ratios on the synthesis of ferrierite

In order to test whether ferrierite can be prepared with a reduced amount of organic template pyrrolidine when rice husk ash was used as silica source, we have attempted ferrierite synthesis using 1.31 Na_2O : 1 Al_2O_3 : 12 SiO_2 : X Py : 410 H_2O mole oxides which X were varied from 10 to 3. The X-ray diffraction patterns given in Figure 5 reveal that ferrierite with a high crystallinity can be prepared, even though the Py / Al_2O_3 ratio of the reaction mixture is reduced from 10 to 4. When the Py / Al_2O_3 ratio of the reaction mixture is lower than 4, there is no phase of ferrierite was formed. From XRD pattern for sample with Py / Al_2O_3 is 3 in Figure 5 shows that quartz rather that ferrierite is the main phase when the amount of pyrrolidine was reduced to 3.

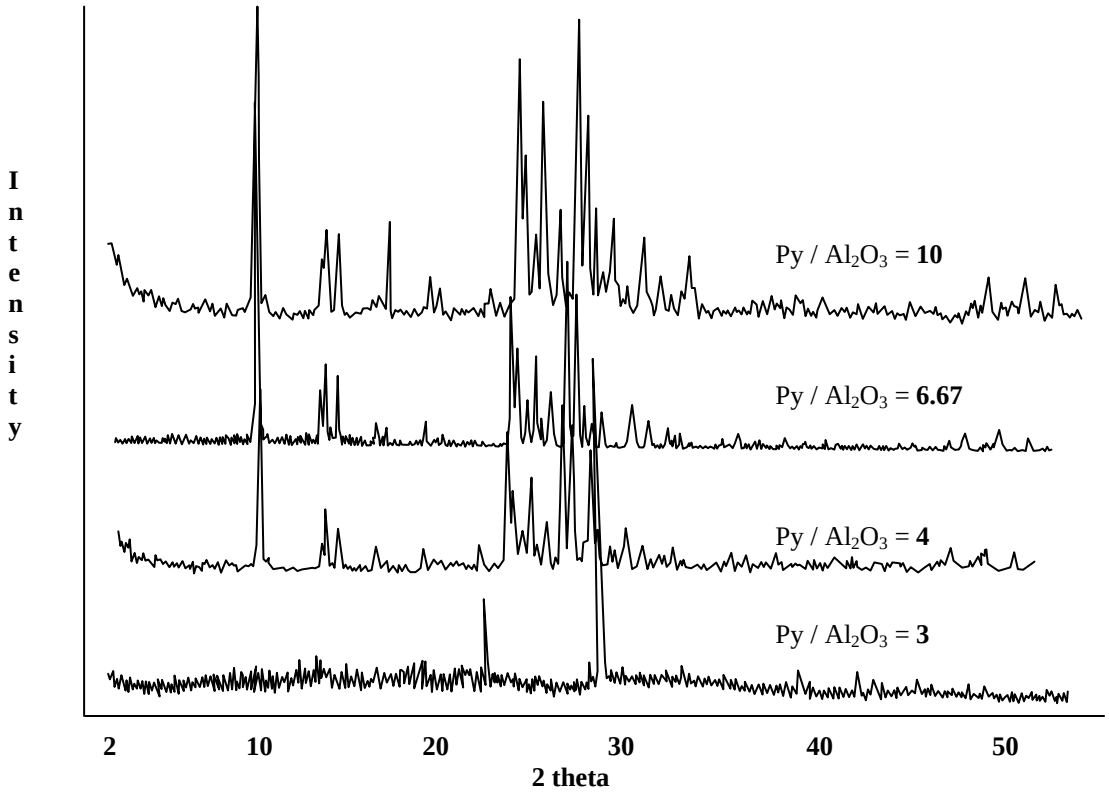

Fig. 4: XRD pattern of ferrierite synthesis with different concentrations of pyrrolidine.

Table 2: Variation of SiO_2 / Al_2O_3 ratios in the synthesis of ferrierite

Sample	Mole Oxide ratio	SiO_2 / Al_2O_3 ratio	Product
Si-12	1.31 Na_2O : 1 Al_2O_3 : 12 SiO_2 : 6.67 Py : 410 H_2O,	12	FER
Si-20	1.31 Na_2O : 1 Al_2O_3 : 20 SiO_2 : 6.67 Py : 410 H_2O,	20	FER
Si-30-P-10	1.51 Na_2O : 1 Al_2O_3 : 30SiO_2 : 10 Py : 410 H_2O,	30	FER
Si-30	1.31 Na_2O : 1 Al_2O_3 :30 SiO_2 : 6.67 Py : 410 H_2O,	30	amorphous
Si-40-P-10	1.51 Na_2O : 1 Al_2O_3 : 40 SiO_2 : 10 Py : 410 H_2O,	40	analcime
Si-40	1.31 Na_2O : 1 Al_2O_3 : 40 SiO_2 : 6.67 Py : 410 H_2O,	40	amorphous
Si-50	1.31 Na_2O : 1 Al_2O_3 : 50 SiO_2 : 6.67 Py : 410 H_2O,	50	amorphous
Si-30-P-3-N-5	5 Na_2O : 1 Al_2O_3 : 30 SiO_2 : 3 Py : 410 H_2O,	30	quartz

Table 2 summarizes the results obtained from ferrierite synthesis performed using the rice husk ash as silica source. It is found that the SiO_2 / Al_2O_3 ratio range leading to the successful ferrierite formation is very narrow. A highly crystalline ferrierite can be obtained only from the reaction mixture with SiO_2 / Al_2O_3 ratio is 10 to 30. However, ferrierite with SiO_2 / Al_2O_3 30 can only be obtained when the pyrrolidine as structure directing content was increased to 10 as shown in sample Si-30-P-10. For sample Si-40-P-10, when the SiO_2 / Al_2O_3 ratio is increased to 40 with the amount of pyrrolidine is 10, the formation of analcime was occur, while no crystalline material was formed from the synthesis mixtures with SiO_2 / Al_2O_3 ratios more than 30 and the Py / Al_2O_3 ratio is 6.67.

From Figure 6, it can be seen that the mole percent of SiO_2 should vary from 60% to 70% and that for pyrrolidine from 30% to 40% and for Na_2O is around 5%. When the silica to alumina ratio increase, the alkalinity of solution will reduce and it will affect the formation of ferrierite [7]. The alkalinity or crystallization time need to increase in order to transform all silica to the product [8].

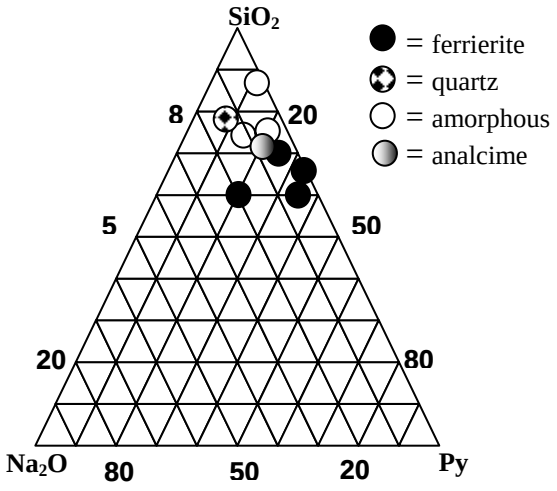

Fig 6: Phase diagram showing the reaction mixture composition for ferrierite formation after 12 days at 200°C

4. CONCLUSION

The overall results of this study reveal that ferrierite can be successfully synthesized from rice husk ash when the reaction mixtures have the gel compositions 1.31 – 1.5 Na_2O : 1 Al_2O_3 : 12 – 30 SiO_2 : 4.0 – 10.0 Py : 410 H_2O. The crystallization rate is strongly dependent on the crystallization temperature which it reached the optimized value within 3 days. In this study, pyrolidine is suitable to be used as template within the molar oxides ranges when rice husk ash is the source of silica.

REFERENCES

1. C. L. Kibby, A. J. Perrotta and F. E. Massoth, *J. Catal.*, 14 (1974), 45
2. K. A. Ranjit, A. N. Kotasthane, B. Roa, S.M Abijit and B. D. Kulkarni., *J. Colloid and Interface Science.* 263 (2000), 47
3. H. Robson (ed), "Verified Synthesis of Zeolitic Materials", Elsevier, 2001
4. Y. Sanyuang, A. G. Vlessidis, and N. P. Exmiridis, *Microporous Materials*, 9, (1997), 273
5. J. K. Tae, S. A. Wha, B. H. Suk, *Microporous Materials*, 7, (1996), 35
6. H. Jongkind, K. P. Datema, S. Nabuurs, A. Sieve and W. H. J. Stork *Microporous Materials*, 10, (1996), 149-161
7. R. F. Neils and V. C. R Lovat, *Zeolites*, 15, (1995), 444
8. J. M. Francisco, C. M. Lopez, M. A. Centeno, and C. Urbina, *Micoporous and Mesoporous Materials*, 26, (1999), 133

Paper presented at Malaysian Science and Technology Congress 2005, 18-20, 2005

SYNTHESIS AND CHARACTERIZATION OF [Ga]-BETA ZEOLITES FROM FIBROUS AGRICULTURAL PRODUCT

Aiman Najati Akmar Rahman, Zainab Ramli* and Farediah Ahmad
Department of Chemistry, Faculty of Sciences, University Technology of Malaysia, 81310 UTM Skudai, Johore Bahru, Johore
Telephone no : +07-5534491; Fax no : +607-5566162; e- mail : aiem82@yahoo.co.uk, zainab@kimia.fs.utm.my

ABSTRACT

Rice husk is a fibrous abundant waste of agricultural production obtained from rice milling. It was usually disposed off by combustion. The ash left is known to contain more than 90 % of silica with remaining metal oxides and carbonaceous materials. The large amount of silica freely obtained from this source provides abundant and cheap alternative silica for many industrial uses such as fertilizer, additive for cement and concrete fabrication and also in zeolite synthesis. Rice husk ash (RHA) has proven to be active in the synthesis of several types of zeolites. In this study, amorphous silica of RHA and commercial silica (fume silica and colloidal silica) were used in the synthesis of gallium containing zeolite beta ([Ga]-Beta). Incorporation of gallium into zeolite beta was done via hydrothermal synthesis. Molar oxide composition of gel ratio consisting of SiO_2; Ga_2O_3 ; $(TEA)_2O$; H_2O and Na_2O was used in the synthesis. The synthesized samples were characterized using X-Ray Diffraction (XRD) and Fourier Transformation Infrared (FTIR) spectroscopy to determine the structure and crystallinity of samples. XRD result shows that RHA is the preferred silica source as the synthesized of solid samples formed pure zeolite beta with the highest crystallinity as compared to other silica source used in this study. Characterization of [Ga]-Beta using FTIR shows identical spectra of zeolite beta with shifting of double ring peaks and T-O asymmetric vibration towards lower frequencies compared to aluminium zeolite beta ([Al]-Beta). Hydroxyl study of [Ga]-Beta shows shifting of the band assigned to bridging hydroxyl of Si-(OH)-Ga group towards higher frequencies as compared to [Al]-Beta, indicating gallium had been successfully incorporated into the framework. Scanning Electron Micrograph (SEM) images of samples show that the morphology of [Ga]-Beta from RHA are cubic crystal of various sizes in the range of 0.5μm to 2.0 μm.

Keywords : zeolite beta, gallium zeolite beta, rice husk ash, isomorphous substitution, gallosilicate

INTRODUCTION

Zeolite can be synthesized using various type of silica source such as tetramethylorthosilicate (TMOS), tetraethylorthosilicate (TEOS), water glass, colloidal silica and fumed silica. Previous researches had shown that rice husk ash (RHA) had also been found active in the synthesis of several types of zeolites, such as zeolite beta[1], zeolite Y[2] , zeolite A, ZSM-5, zeolite L and mordenite[3] .

Gallium doped zeolites were found active in the transformation of light alkanes into aromatics, dehydrogenation or oxidative dehydrogenation of alkanes and also in the benzoylation of aromatics. Incorporation of gallium into zeolite is believed to alter the chemical nature and acidity of zeolite. The highly dispersed gallium in the pores of zeolites was assumed to play the key role in both reaction activity and selectivity[4,5]. The catalytic properties were mainly originated from the acidic properties which created when the protons or metal ions are incorporated in the framework of zeolite. Techniques such as hydrothermal synthesis, impregnation, ion exchange and mechanical mixing have usually been applied to introduce

gallium into zeolites. Gallium may be deposited in the form of clusters or cluster oxides in the porous network or on the external surface of the crystalline zeolites depending on the synthesis condition. Isomorphous substitution and replacement of exchangeable cations are important ways to modify zeolite properties in order to obtain specific characteristics for practical applications and have received great attention in the field of zeolite science.

This paper reports the introduction of gallium into zeolite by direct synthesis. In this work RHA was chosen as the silica source as it has been proven that RHA is an active source of silica for synthesis of zeolites. Zeolite beta, being the large pore class zeolites provide better catalytic activity in the synthesis of large organic molecules.

EXPERIMENTAL

Amorphous rice husk ash (RHA) with 0.5 % carbon content obtained from control burning in fluidized bed reactor, fume silica Cab-O Sil 5 (97 %, Fluka Chimika), colloidal silica LUDOX (40 % in water) were used as raw material for the silica source to synthesize zeolite beta. Other chemicals involved in the synthesis are tetraethylammonium hydroxide (40 % TEAOH solution % w/w, Fluka Chimika), sodium aluminate (54 % Al_2O_3; 41 % Na_2O % w/w, Riedel de Haan), gallium nitrate (99.9 %, Aldrich), sodium hydroxide (99 %, MERCK), ammonium nitrate (99 %, MERCK) and deionized water.

Synthesis of gallosilicate zeolite beta was carried out using method described by Chao[6] et al. with gel of molar oxide composition of 6.0 Na_2O : 67 SiO_2 : 1 Ga_2O_3 : 13.3 TEA_2O : 1000 H_2O. Synthesis of aluminosilicate zeolite beta was carried out using method described by Didik[1] with gel of molar oxide composition of 4.0 Na_2O : 45 SiO_2 : 1 Al_2O_3 : 10 TEA_2O : 480 H_2O. Syntheses of samples were done under static condition at 135 ^oC for 14 days and 150 ^oC for gallosilicate and aluminosilicate samples respectively. The filtered solid was dried at 100 ^oC. **TABLE 1** lists the samples synthesized in this work.

SiO_2 sources	Al_2O_3/Ga_2O_3 sources	Notation
Rice husk ash	$Ga(NO_3)_3$	[Ga]-Beta-RHA
Fume silica	$Ga(NO_3)_3$	[Ga]-Beta-FS
Colloidal silica	$Ga(NO_3)_3$	[Ga]-Beta-CS
Rice husk ash	$NaAl_2O_3$	[Al]-Beta-RHA

TABLE 1 : Sources and Notation of Synthesized Zeolite Samples

Samples were characterized by powder x-ray diffraction (XRD) using a Bruker Advance D8 diffractometer with the CuKα (λ=1.5405 Å) radiation at 40 kV and 40 mA. The pattern was scanned in the 2θ ranges of 5^o to 45^o at a step 0.05^o and step time 1s. The hydroxyl group and T-O (T = Si, Al and Ga) vibration of samples were collected using Perkin Elmer Spectrum One Fourier Transformation Infrared (FTIR) Spectrometer, with a spectral resolution of 4 cm^{-1}, scan 10s at room temperature. KBr technique was applied for scanning of T-O vibration of samples. For the study of the hydroxyl group, wafer of hydrogen form samples (H-Beta), of 10–12 mg was locked in a cell equipped with CaF_2 windows, and evacuated at 400 ^oC under vacuum for 5 hours. The morphology and particle sizes of samples were determined using Scanning Electron Microscope (SEM). Samples were spread on stubs and coated with gold. Scanning of samples were done using SEM model Philip XL40 under vacuum with pressure of 5 barr.

RESULT AND DISCUSSION

The XRD patterns of all samples synthesized in this work is shown in **FIGURE 1.** The XRD shows the XRD pattern of prepared gallosilicate zeolite using different silica source. XRD diffractogram of zeolite beta shows 2θ peaks at 7.7^{o}, 16.5 ^{o}, 21.4 ^{o}, 22.4 ^{o}, 25.2 ^{o}, 26.8 ^{o}, 29.5 ^{o} and 43.5 ^{o} (± 0.1^{o}) for all solid samples. Based on the diffraction pattern, crystal having zeolite beta pure phase were identified for the [Ga]-Beta-CS and [Ga]-Beta-RHA samples of gallosilicate. Pattern also shows that the structure of zeolite beta is still preserved with the incorporation of gallium into the framework. However, the diffraction pattern of [Ga]-Beta-FS is slightly different from others. The obtained solid samples seemed to contain not only zeolite beta, but with impurities of other phases. **TABLE 2** shows that gallosilicate beta synthesized from RHA as silica source gives the highest crystallinity among the gallosilicate samples as compared to other silica sources.

FIGURE 2 shows the IR spectrum of T-O vibration of solid samples. IR spectra of the samples show pattern similar for zeolite beta. Vibration of solid samples were found for T-O asymmetry stretching (1219 cm^{-1}, 1063 cm^{-1}), T-O symmetry stretching (782 cm^{-1}), double ring vibration (567 cm^{-1}, 508 cm^{-1}) and T-O bending (463 cm^{-1}, 426 cm^{-1}). But for one noted that the peak assign to double ring shifted towards lower frequencies for gallosilicate samples. This double ring peak, which had usually been found at 520 cm^{-1} for aluminosilicate beta, shifted to 508 cm^{-1} for gallosilicate beta. The Ga-O (1.83 Å) bond is longer than Al-O (1.75 Å) bond and Si-O (1.62 Å) bond, the shifting suggest that the ability of framework to change its fine structure (bond angles and distances) by rotation, tilting or inversion of the tetrahedra which form the double ring in order to relax the strain created by the substitution of atom[7]. For [Ga]-Beta-CS and [Ga]-Beta-FS samples, a shoulder peak at 960 cm^{-1} assign to Si-O of silanol stretching vibration was found. This peak which is usually found in high silica zeolites such as Si-MCM41, silicalite and calcined zeolites suggest that only small amount of gallium had been incorporated into the framework which left defects sites of silanol nest. This band is missing in [Ga]-Beta-RHA samples suggest that more gallium has been incorporated into the framework as compared to other gallosilicate samples. We also found that the frequency for T-O asymmetric stretching vibration shifted to lower frequencies by introduction of gallium atoms into the framework for all samples as compared to the aluminosilicate sample. This indicates that incorporation of gallium atom occurs during the synthesis and the contribution of gallium atoms is greater than that from the incorporation of aluminium atoms. The shift towards lower wavenumber caused by incorporation of gallium atoms is due to the substitution of weaker Ga-O bond for Si-O bond and weightier gallium atom for silicon atom[8].

The hydroxyl, υ(OH) region of the IR spectrum of H-[Al]-Beta-RHA contain bands at 3734 cm^{-1} and 3610 cm^{-1} (**FIGURE 3**). The former has been assigned to terminal silanol while the latter is attributed to acidic bridging OH. As seen in spectrum, the frequencies of the second band for H-[Ga]-Beta-RHA is shifted to higher frequencies of 3616 cm^{-1}. The shifting of this peak indicates the successful incorporation of gallium into the framework of zeolite beta. The fact that this band is at higher frequency than 3610 cm^{-1} of H-[Al]-Beta-RHA suggest that the OH group in Si-(OH)-Ga is more covalent than [Al] isomorph and hence that this site is less acidic[9]. This finding had also been reported by Chao[6] et al,Oumi[10] et al and Ocelli[11] et al.

The SEM micrograph of [Ga]-Beta-RHA sample is shown in **FIGURE 4**. The images confirm the crystallinity of [Ga]-Beta-RHA sample. Images show that the morphology of [Ga]-Beta from amorphous RHA are cubic crystal of various sizes in the range of 0.5 μm to 2.0 μm.

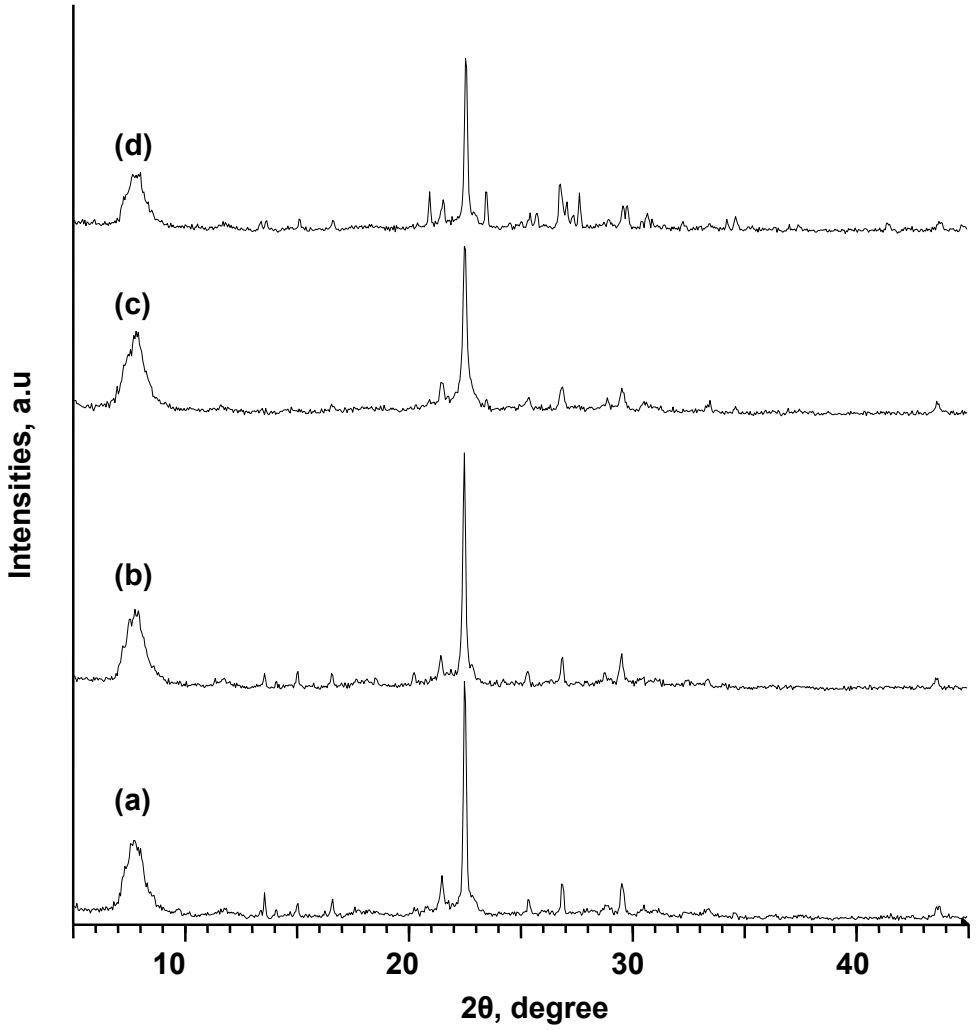

FIGURE 1 : XRD Diffractogram of Synthesized Solid Samples (a) [Al]-Beta-RHA, (b) [Ga]-Beta-RHA, (c) [Ga]-Beta-CS and (d) [Ga]-Beta-FS

Samples	Count per second, Cps	Crystallinity , %*
[Al]-Beta-RHA	1052	100.0
[Ga]-Beta-RHA	1050	99.8
[Ga]-Beta-CS	751	71.4
[Ga]-Beta-FS	772	73.4

* based on d_{302} peak of [Al]-Beta-RHA

TABLE 2 : Crystallinity of Synthesized Samples

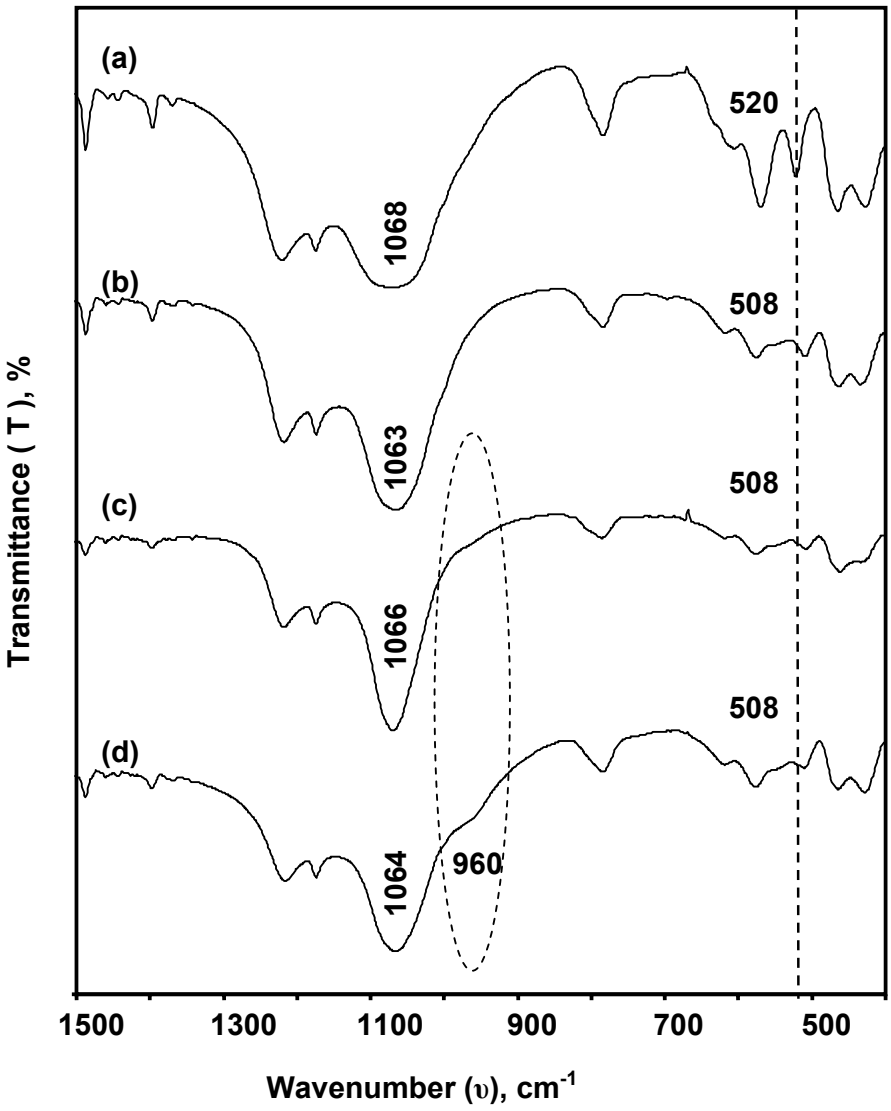

FIGURE 2 : IR Spectra of Solid Samples in the Region of T-O Vibration for (a) [Al]-Beta-RHA, (b) [Ga]-Beta-RHA, (c) [Ga]-Beta-CS and (d) [Ga]- Beta-FS

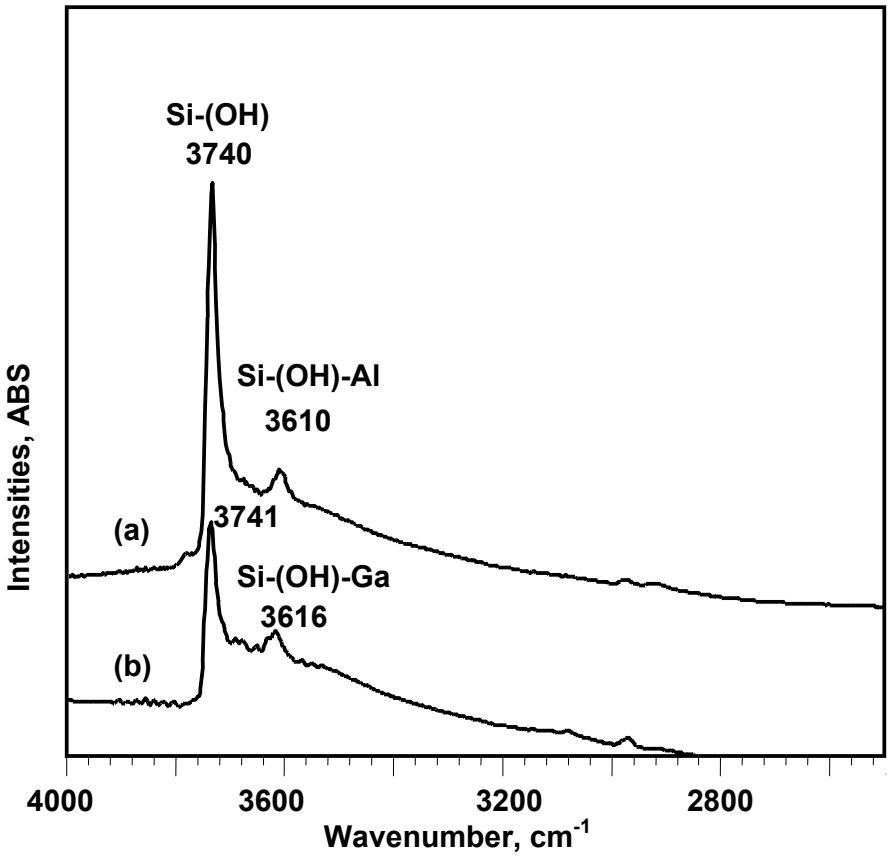

FIGURE 3 : IR Spectra of Hydroxyl Region of (a) [Al]-Beta-RHA and (b) [Ga]-Beta RHA

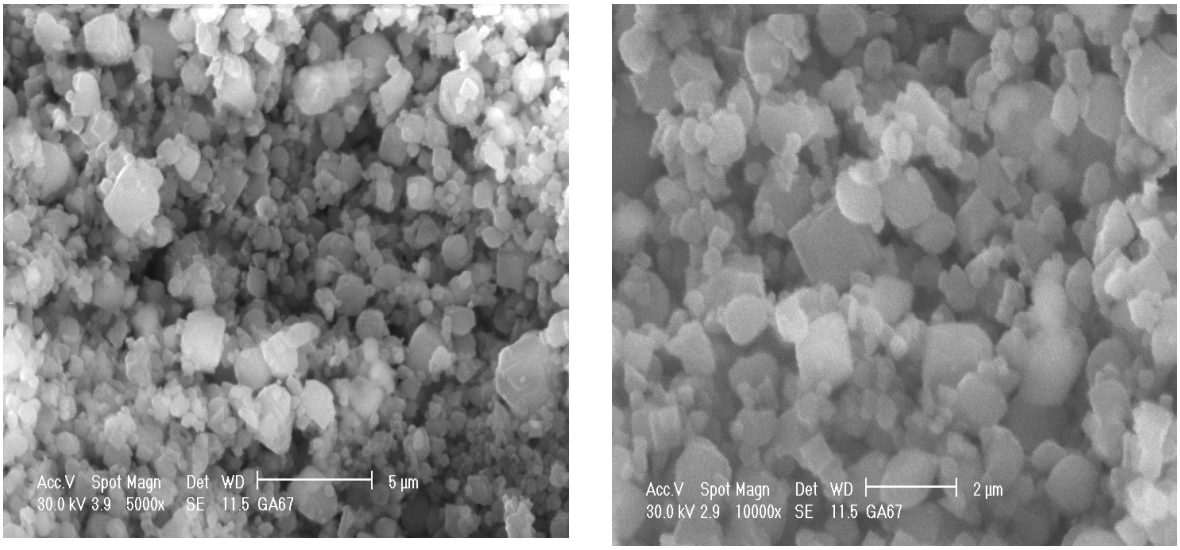

FIGURE 4 : SEM Images of [Ga]-Beta-RHA

CONCLUSIONS

Gallosilicate zeolite beta had been synthesized using different silica sources of amorphous RHA and commercial silica. The gallosilicate synthesized from RHA gives pure crystal having zeolite beta phases with highest crystallinity compared to others. IR spectra in the framework vibration and hydroxyl regions indicate gallium atoms had successfully been incorporated in the tetrahedral of zeolite framework during the synthesis. SEM images of [Ga]-Beta-RHA shows that the morphology of synthesized sample is cubic crystal of different sizes.

ACKNOWLEDGEMENT

1. Department of Chemistry, Faculty of Sciences, University Technology of Malaysia
2. Ibnu Sina Institute for Fundamental Science Studies, University Technology of Malaysia
3. IRPA : PROJECT NO : 09-02-06-0057 SR0005/09-03

REFERENCE

1. Didik Prasetyoko (2001). "Pengoptimuman Sintesis Zeolit Beta daripada Silika Sekam Padi : Pencirian dan Tindak balas Pemangkinan Friedel-Crafts". MSc Thesis. Universiti Teknologi Malaysia.

2. Hamdan, H., Muhid, M.N.M, Endud, S., Listiorini, E. and Ramli, Z. (1997). "^{29}Si MAS NMR, XRD and FESEM Studies of Rice Husk Silica for the Synthesis of Zeolites." *Journal of Non-Crystalline Solids*. **211**. 126-131.

3. Zainab Ramli. (1995). "Rhenium Impregnated Zeolites: Synthesis, Characterization and Modification as Catalysts in the Metathesis of Alkenes." Phd Thesis . UTM

4. Wei, A. C., Liu, P.H., Chao, K.J., Yang, E. and Cheng, H. (2001). "X-ray Absorption Measurement and Density Functional Theory Analysis of Gallium in Gallium-Containing Beta Zeolites." Microporous and mesoporous Materials. 47. 147-156

5. Choudhary, V.R., Jana, S.K., Patil, N.S. and Bhargava, S.K. (2003). "Friedel-Crafts Type Benzylation and Benzoylation of Aromatic Compounds over Hβ Zeolite Modified by Oxides or Chlorides of Gallium and Indium". *Microporous and Mesoporous Materials*. **57**. 21-35.

6. Chao, K.J., Sheu, S.P., Lin, L., Genet, M.J. and Feng, M.H. (1997). "Characterization of Incorporated Gallium in Beta Zeolite." *Zeolites*. **18**. 18-24.

7. Fricke, R., Kosslick, H., Lischke, G., and Richter, M. (2000). "Incorporation of Gallium into Zeolites: Syntheses, Properties and Catalytic Application." *Chem. Rev*. **100**. 2303-2405

8. Yang, C., Xu, Q. and Hu, C. (2000). "Boronation and Galliation of Zeolites β in an Alkaline Medium." *Materials Chemistry and Physics*. **63**. 55-66.

9. Chu, C. T-W. and Chang, C.D. (1985). "Isomorphous Substitution in Zeolite Frameworks. 1. Acidity of Surface Hydrohyls in [Fe]-, [Ga]-, and [Al]-ZSM-5." *J. Phys. Chem*. **89**. 1569-1571

10. Oumi, Y., Jintsugawa, I., Kikuchi, S., Nawata, S., Fukushima, T., Teranishi, T. and Sano, T. (2003). *Microporous and Mesoporous Materials*. **66**. 109-116

11. Ocelli, M.L., Eckert, H., Wolker, A., Auroux, A. (1999). "Crystalline galliosilicate Molecular Sieves with the Beta Structure." *Microporous and Mesoporous Materials*. **30**. 219-232.

CHAPTER 2

SYNTHESIS OF ZEOLITES FROM RICE HUSH ASH

(Compilation of Paper Publications, Seminars & Conferences and Abstract of Theses)

SYNTHESIS OF SELECTED ZEOLITES FROM RICE RUSK ASH: SCANNING ELECTRON MICROGRAPHS OF ZEOLITES CRYSTALS

Introduction:

In Malaysia, the local annual production of rice leaves behind about 2.4 million tones of husk as waste product (Kim *et al.*, 2000). Rice husk, a major agricultural waste, is a fibrous material with high silica content, cellulose and lignin (James and Rao., 1986). Silica ash which is transformed from the husk by complete burning constitutes 15-20% of the total weight of the husk. Rice husk ash contains 90-99% SiO_2 and 20% of the white ash residue left after the combustion causes air and water pollution (Pariente *et al*., 1987). Because of its nonbiodegradable property, the presence of the silica ash causes a number of problems to the environment. In order to solve these problems, useful applications of the waste product are desirable.

Silica from rice husk finds it uses as a constituent of low cost cements and as a source for metallurgical as well as semiconductor-grade silicon. Silica is one of the basic raw materials in the glass and ceramic industries. Here, rice husk can be employed with advantage. As the ash is obtained as a fine powder, it does not require further grinding. Also the firing temperature is expected to be lower than normal because of the reactive nature of silica in ash. Silica in rice husk has also been employed for preparing silicon carbide whiskers at temperature lower than normal (James and Rao., 1986).

The large amount silica freely obtained from this source provides an abundant and cheap alternative of silica for many industrial uses, including the synthesis of zeolites (Kapur *et al*., 1998). The reactivity of the silica depends on the method of preparation and extraction from the rice husk. Controlled burning at 800ºC for 10 hours produces rice husk ash in amorphous form, whereas silica crystal from rice husk ash with tridymite and cristobalite structures are formed in uncontrolled burning at higher temperatures (> 800ºC) (Chen and Yeoh., 1992). The chemical compositions of rice husk ash are listed in Table 2.1.

Table 2 .1: The composition of compounds in rice husk ash (Chen and Yeoh, 1992)

Compound	SiO_2	Al_2O_3	Fe_2O_3	CaO	MgO	Na_2O	K_2O	LOI	Total
Percentage, wt%	95.12	0.19	0.07	0.32	0.51	0.01	1.64	2.14	100.0

LOI = Loss on ignition

Synthesis of a few types of zeolites from rice husk ash has been reported (Chen and Yeoh., 1992; Listiorini *et al.*, 1996). Zeolite Beta also has been synthesized successfully using crystalline silica from rice husk ash containing cristobalite and tridymite which is obtained directly from uncontrolled burning (Didik, 2001). Therefore, the transformation of crystalline silica from rice husk ash to zeolite is possible when amorphous silica is normally been used in the zeolite synthesis. Amorphous silica obtained by combustion under controlled temperature contains only $Si(OSi)_4$ tetrahedral units and has proved to be the most reactive silica source in the synthesis of zeolite as compared to silica prepared by either chemical extraction or uncontrolled burning of rice husk. The presence of crystalline cristobalite and tridymite phases and SiOH group render the silica less active. The properties of silica obtained from rice husk ash are strongly influenced by the temperature of formation and the duration of heating (Hamdan *et al*., 2000).

In this project besides the mentioned zeolites produced from rice husk ash in the previous project, the search for synthesizing other type of zeolites using rice husk ash as silica source was continued. Selected zeolite with different pore sizes type and should be suitable for as catalysts for Friedel Crafts alkylation and acylation were chosen: zeolite Beta (large pore), Ferrierite (medium pore), zeolite P (small pore) and zeolitic mesoporous ITQ-6(mesoporous), while for the consecutive oxidative acidic reaction of alkene to oxidative titanium silicalite TS-1 was chosen. This article summarizes the zeolites obtained from this projects which were characterized by SEM methods only. Results from other characterizations methods were described in detailed in the theses.

Experimental

All methods for producing zeolites in this project are described in details in the Ph.D and M.Sc theses carried out by research students in this project. In general all zeolites synthesis involves hydrothermal synthesis at selected temperature and at atmospheric pressure.

Method of synthesis of zeolite Beta with different Si/Al ratios of the framework are described in the thesis of Wong Kah Man (M. Sc. Thesis, 2005) and Marzita Abd Mazak (M.Sc Thesis, 2006). The methods for synthesizing gallosilicate zeolite Beta was performed by Aiman Najati (M.Sc. Thesis 2007). The medium pore ferrierite with composition optimization was described in detailed in Hasliza Bahruji (M.Sc. Thesis 2005) while the method for transforming zeolitic microporous FREFER to mesoporous ITQ-6 was undertaken by Nor Aishikin Mohd Yusoff (M.Sc Thesis, in press).Didik Prasetyoko (Ph.D. Thesis 2006) has reported the method of synthesizing titanium silicalite TS-1 at different Ti/Al ratios.

Results

This project has proved the reactivity of rice husk ash (RHA) as silica source for producing many kinds of zeolites. Almost all kind of zeolites have successfully formed when using RHA as silica source. In this project zeolite P (small pore) Zeolite Ferrierite (FER), precursor of ferrierite (PREFER) (medium pore zeolite), zeolite Beta and zeolite X has have been synthesized in pure and highly crystalline form. The evidence of the formation of those zeolites was described in detailed in their respective theses by XRD and IR methods.

Zeolite P was obtained from oxides composition 6.0-6.2 Na_2O: Al_2O_3: $8SiO_2$: 112 H_2O within 1 day at 100 ^oC . . The morphologies of zeolite P at different magnification are presented in Figure 1 showing rose-like crystals. For a small pore zeolite P can be formed in 1 days time at 100^oC using 6.0-6.2 Na_2O : Al_2O_3 : 8 SiO_2 : 112 H_2O gel composition. For half day crystallization time at the same temperature and composition produced zeolite X or Y instead, indicating that zeolite X and Y are metastable zeolites which will transform to other phases.

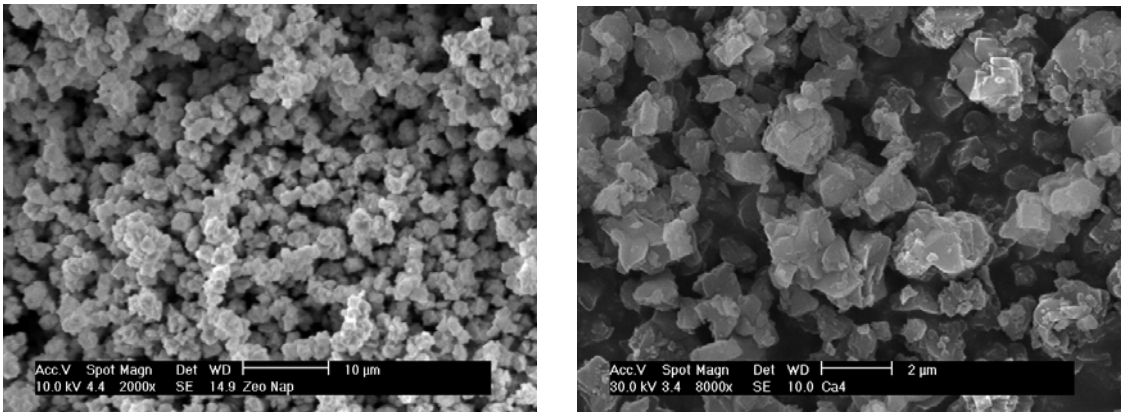

(a) (b)

Figure 1: SEM of zeolite P (a) 2000x (b) 8000x magnification

Pure ferrierite zeolite FER phase was obtained from gel compositions in the range of 1.31 – 1.5 Na_2O : Al_2O_3 : 10 – 30 SiO_2 : 4.0 – 10.0 Pyrrolidine : 410 H_2O with narrow range of SiO_2/Al_2O_3 ratios from 10 to 30. The stable FER was obtain in 4 days crystallization time at 200^oC, shorter than when using commercial silica source like fume silica, which usually take 8-12 days. SEM for the formation of ferrierite at different crystallization period are shown in Figure 2.

Figure 3 shows SEM of some morphologies of Al- zeolite Beta and galosilicate zeolite Beta with granule-like morphologies with various sizes. Pure zeolite Beta phase is obtained from the oxide gel ratios of 1.9-8 Na_2O: Al_2O_3: 27-90 SiO_2: 5-20 TEA_2O:

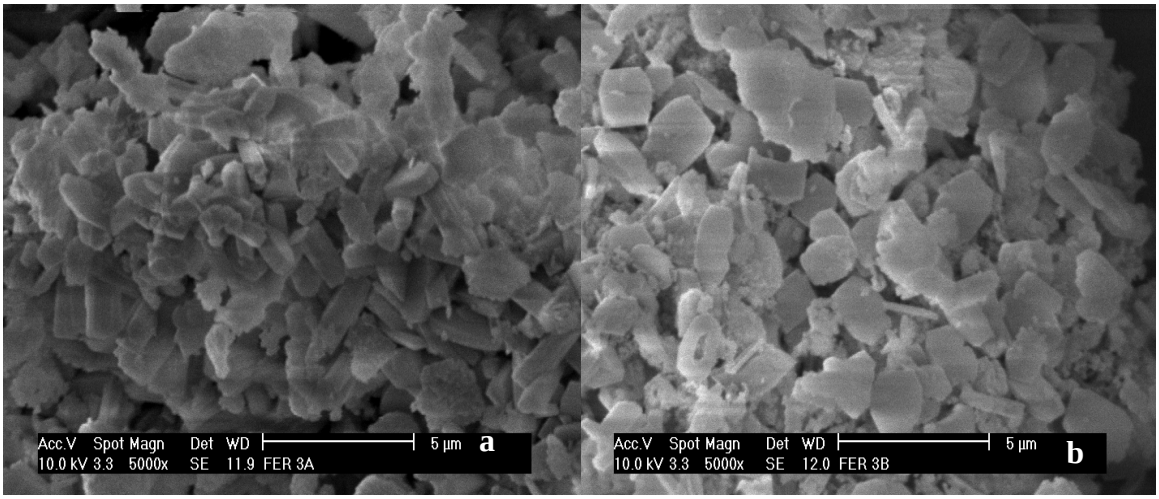

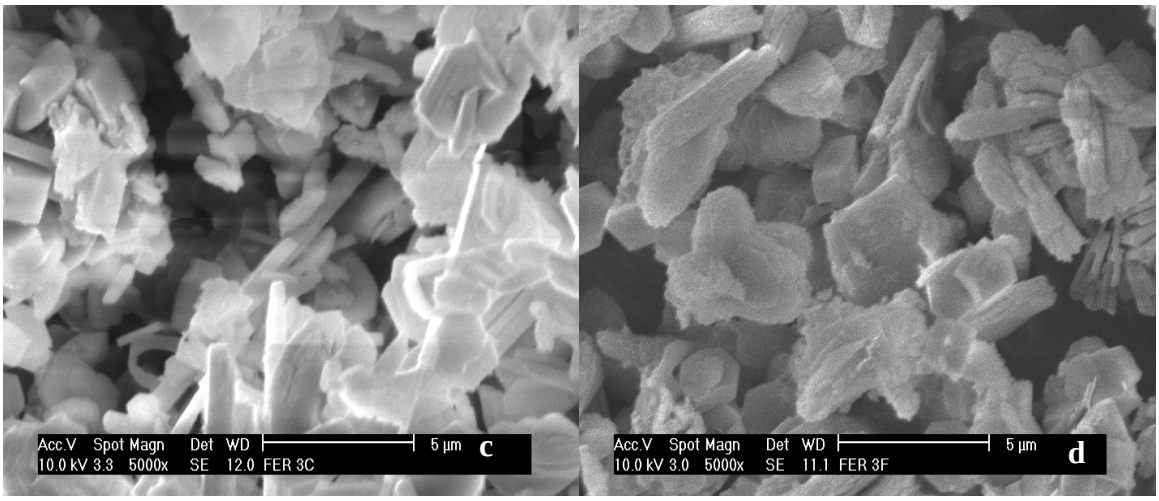

Figure 2: Scanning electron micrograph for ferrierite at different crystallization period (a) 1 day (b) 5days (c) 9 days (d) 12 days

240-800 H_2O at 150^oC for 7 days crystallization. Silicieous zeolite Beta (aluminium free) failed to obtain due to the presence of aluminium containment which facilitates the formation of Al-Beta. However gallosilicate zeolite Beta (aluminium free zeolite Beta containing gallium in the framework) has been successfully synthesized from hydrothermal synthesis at 135^oC with molar oxide composition of 6.0 Na_2O : 67 SiO_2 : Ga_2O_3 : 13.3 TEA_2O : 1000 H_2O. Another successful formation of zeolite PREFER was obtained from gel composition in the range of 10-60 SiO_2 : 0.5-1Al_2O_3 : 7.5-15NH_4F : 2.5-5HF : 10 (4-amino-2,2,6,6- tetramethylpiperidinr) : 50-100H_2O at 175^oC for 5 days crystallization time.

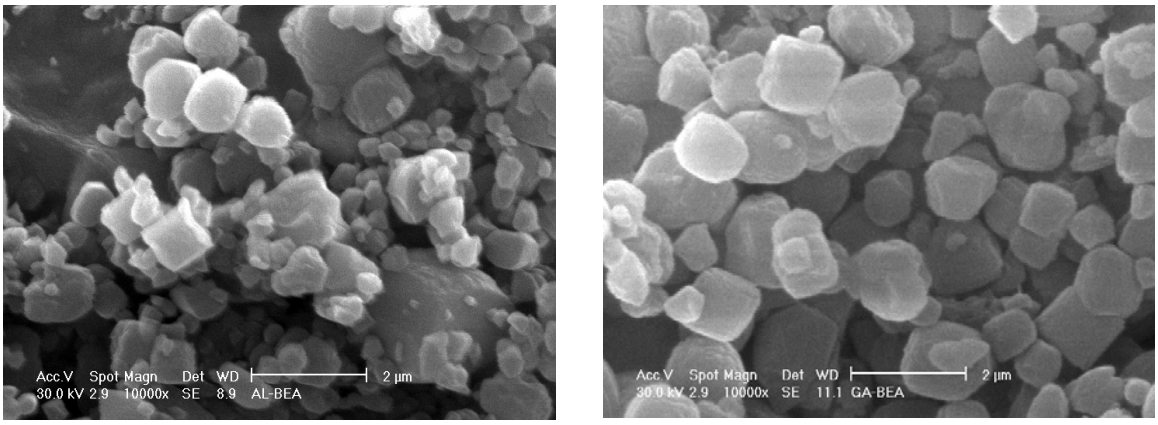

(a) (b)

Figure 3 : SEM of (a) Al-zeolite Beta (b) Gallosilicate zeolite Beta

Another successfull attemp in producing zeolitic mesoporous zeolite PREFER and ITQ-6 amphasized the reactivity of rice RHA as silica source. In all cases the RHA must be in amorphous form. Figure 4 shows some of morphologies of the precursor of ferrierite, PREFER with flake-like crystal and its mesoporous zeolitic ITQ-6 obtained from rice husk ash. The morphology of ITQ-6 clearly shows the distroyed crystal of the precursor PREFER as the result of delamination treatment on the PREFER precursor which involved swelling with organic template, followed by sonication and calcination to eliminate the organic template. XRD of ITQ-6 shows the amorphous material as evidence from the SEM picture shown Figure 5. However the microporous PREFER has transform to the mesoporous material of ITQ-6 (

.

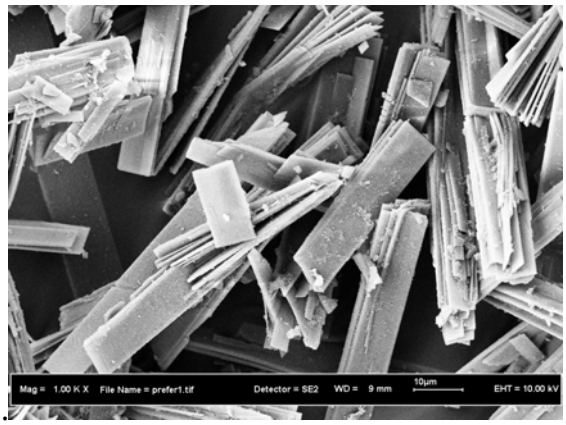

(a) 1000x magnification

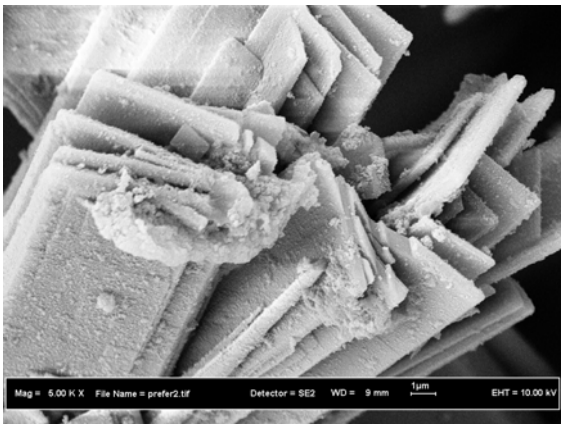

(b) 5000x magnification

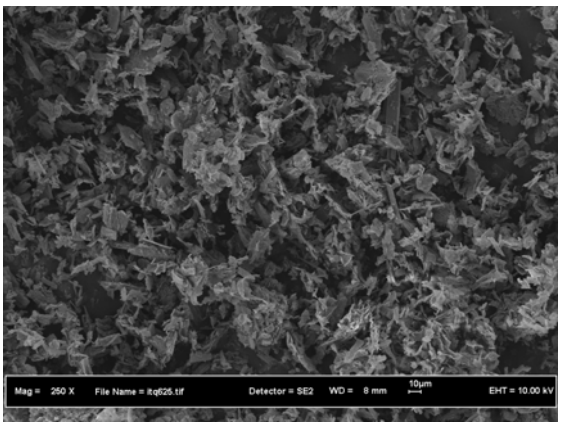

(c) 250 x magnification

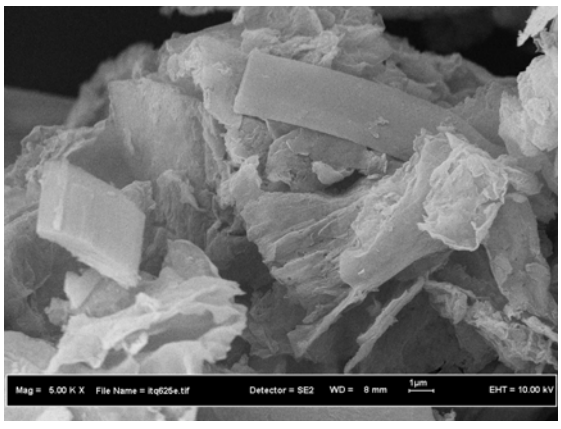

(d) 5000x magnification

Figure 4: FESEM of PREFER (a) and (b) and ITQ-6 (c) & (d)

The morphology of samples titanium silicalite TS-1 at different content of Ti were presented in Figure 5 showing hexagonal crystals. The crystallinity of samples TS-1 is slightly increased as titanium content increased from 1% to 3%. Meanwhile, crystallinity of sample TS-1 (4%) decreased markedly compared to that of samples TS-1 (1-3%). This result suggests that at the titanium loading higher than 3%, the titanium species in the gel may retard the growth of TS-1 crystals. It is known that for samples TS-1, the titanium species are located in the framework structure of silicalite, therefore, no TiO_2 can be observed by XRD technique. However, the structure of titanium in the molecular structure cannot be confirmed by XRD technique, but by UV-Vis DR

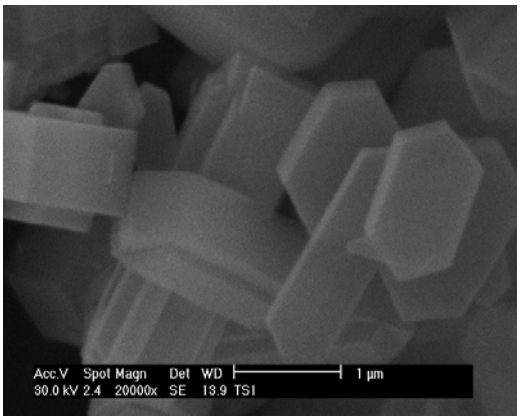

(a) 1%wt Ti- 20,000x magnification

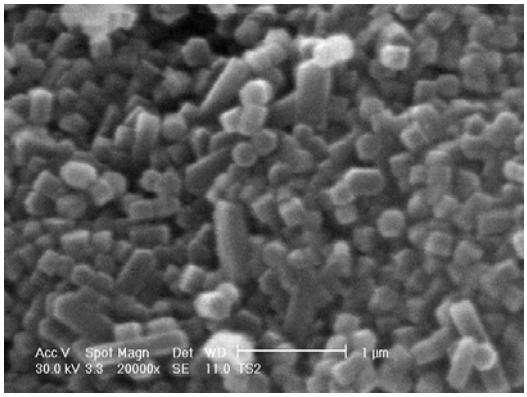

(b) 2%wt Ti - 10,000 x magnification

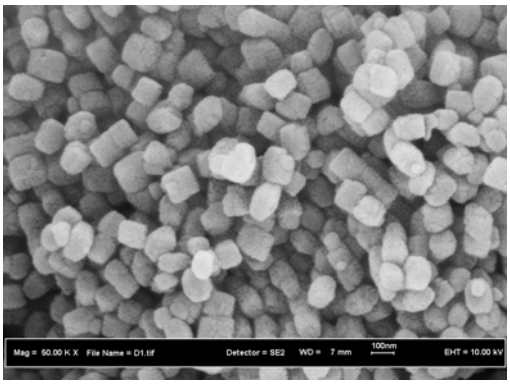

(c) 3 wt% Ti- 10,000x magnification

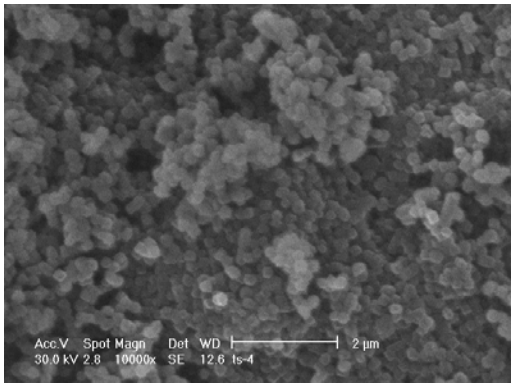

(d) 4 wt% Ti - 10,000x magnification

Figure 5 : FESEM of TS-1 at different wt% Ti : (a) 1 wt% Ti (b) 2 wt% Ti (c) 3 wt% Ti (d) 4 wt% Ti

technique, which is also reported in Didik Prasetyoko (Ph.D. Thesis, 2006). Well form TS-1 hexagonal crystal was obtained in the micro size range from the gel containing only 1 %wt. Ti. With the increased of Ti content in the gel, the size of TS-1 cystals reduces to near nano range (~100-200 nm) with not so well form of crystals as can be seen from the SEM pictures in Figure 5.

References:

Aiman Najati Akmar binti Rahman (2007) Gallium Modified Zeolite Beta for Friedel Crafts Alkylation of Resorcinol. M.Sc Thesis , UTM

Chen, S. S., and Yeoh, A. K. (1992). Development of zeolite NaY from Rice Husk Ash. *Journal of Industrial Technology*. 2. SIRIM, Malaysia

Didik, P. (2001). *Pengoptimuman sintesis zeolite beta daripada abu sekam padi:pencirian dan tindakbalas pemangkinan Friedel-Crafts.* UTM. Tesis MSc

Didik Prasetyoko (2006) Bifunctional oxidative and Acidic Titanium Silicalite (TS-1) Catalysts for One Pot Synthesis of 1,2-octenediol from 1-octene. Ph. D Tesis, UTM

Hasliza binti Bahruji (2005) Synthesis of zeolite Ferrierite from Rice Husk Ash, Characterization and Activity Towards Friedel Crafts Acylation of Anisole with propyl anhydride M.Sc Thesis, UTM

James, J.and Rao, M. S.(1986) Characterization of Silica in Rice Husk Ash. *American Ceramic Society Bulletin*.65: 1177-1180.

Listiorini, E., Ramli, Z., and Hamdan, H.(1996) "Optimization and Reactivity study of Silica in The synthesis of zeolites from Rice Husk Ash." *J. Teknologi*.25: 27-35.

Marzita Abd. Mazak (2006) "Modified Zeolite Beta as Catalysts in Friedel Crafts alkylation of Resorcino*l*. M.Sc Tesis, UTM

Pariente, J. P., Martens, J. A. and Jacobs, P. A. (1987). Crystallization and Mechanism of Zeolite Beta from TEA_2O, Na_2O and K_2O Containing Silicates Gels. *App. Cat. A.* 31: 35 – 64.

Wong Kah Man (2004) Acid-base Properties of Modified Zeolite Beta: Modification, Characterization and Catalytic Testing. M.Sc Thesis, UTM

Available online at www.sciencedirect.com
ScienceDirect
Waste Management 26 (2006) 1173–1179
wasteWmanagement
www.elsevier.com/locate/wasman

Conversion of rice husk ash to zeolite beta

Didik Prasetyoko [a], Zainab Ramli [a,*], Salasiah Endud [a], Halimaton Hamdan [a], Bogdan Sulikowski [b]

[a] Department of Chemistry, Faculty of Science, Universiti Teknologi Malaysia, 81310 Johor, Malaysia
[b] Institute of Catalysis and Surface Chemistry, Polish Academy of Sciences, Niezapominajek 8, 30-239 Cracow, Poland

Accepted 15 September 2005
Available online 7 November 2005

Abstract

White rice husk ash (RHA), an agriculture waste containing crystalline tridymite and α-cristobalite, was used as a silica source for zeolite Beta synthesis. The crystallization of zeolite Beta from RHA at 150 °C in the presence of tetraethylammonium hydroxide was monitored by XRD, FTIR and ^{29}Si MAS NMR techniques. It was found that zeolite Beta started to form after 12 h and the complete crystallization of zeolite Beta phase was achieved after 2 d. XRD, ^{29}Si MAS NMR and solid yield studies indicate that the transformation mechanism of silica present in RHA to zeolite Beta involves dissolution of the ash, formation of an amorphous aluminosilicate after 6 h of crystallization, followed by dissolution in the mother liquor and final transformation to pure zeolite Beta crystals.

1. Introduction

Zeolites are hydrated crystalline aluminosilicates with open three-dimensional framework structures, made up of SiO_4 and AlO_4 tetrahedral linked by sharing their oxygen atom to form regular intracrystalline cavities and channels of atomic dimensions. Zeolites are conventionally prepared by the hydrothermal method of the gel containing silica, alumina, cation, template and water. Different types of silica are known to produce different types of zeolites from the same gel mixture (Barrer, 1982). Most of the silica sources used in the synthesis of zeolite are commercially available in the form of a solution, a gel, a fumed solid, a colloid, and an organic derivative such as tetraethylorthosilicate.

It is well known that many plants have an ability to accumulate silicon compounds. One example comprises a perennial plant horsetail (*Equisetum arvense*), used previously as a grinding and a polishing agent; another is rice (*Oryza sativa*), one of the major cultivated plants in the world. World production in 2002 was 576 million t; production in Malaysia was 2.1 million t. During production of rice, huge amounts of rice husk are left as waste product. Husk is usually disposed of by combustion, thus giving rice husk ash (RHA). This by-product is produced in many places world-wide and constitutes an environmental problem due to air and water pollution. On the other side, chemical analysis shows that a white variety of RHA can contain up to 90–99% silica. It is, therefore, not unusual that this cheap source of silica may be of interest for numerous industrial uses, including the large-scale synthesis of zeolites. Preliminary efforts were made in the synthesis of zeolites using this source. Thus, Bajpai et al. (1981) obtained mordenite and Wang et al. (1998) obtained ZSM-48 type zeolite using RHA as a silica source, and we have succeeded in bench-scale experiments aimed at crystallization of zeolite Y (Ramli et al., 1996), X and ZSM-5 (Ramli, 1995; Ramli and Bahruji, 2003). In our previous work amorphous silica extracted from crystalline RHA was used as a starting material. In this paper, our objective was focused on preparation of the wide-pore zeolite Beta, a potentially interesting aluminosilicate for many catalytic applications.

Zeolite Beta was explored as a powerful catalyst in petrochemical applications and fine chemical synthesis,

* Corresponding author. Tel.: +607 5534491; fax: +607 5566162.
E-mail address: zainab@kimia.fs.utm.my (Z. Ramli).

0956-053X/$ - see front matter © 2005 Elsevier Ltd. All rights reserved.
doi:10.1016/j.wasman.2005.09.009

including epoxidation (Wall et al., 1998), transalkylation (Lee et al., 1998), isomerization (Jansen et al., 1997) and acylation (Freese et al., 1999). It is a large pore zeolite with the formula $Na_n\{Al_nSi_{64-n}O_{128}\}$, $n < 7$ (Meier et al., 1996). The Si/Al ratio may vary, starting from 8, going through more siliceous (dealuminated) forms and ending with an aluminium-free homologue.

Zeolite Beta has a very complex structure composed of the intergrowth of the two distinct structures, termed as polymorphs A and B. The polymorphs are closely related structures and contain 12-membered oxygen rings, with channel intersections of the straight channels {1 0 0} (7.6×6.4 Å) and sinusoidal channels {0 0 1} (5.5×5.5 Å), respectively. The intergrown hybrid of the polymorphs does not significantly affect the pores in those two dimensions (Higgins et al., 1988). Because of its structure and high silica content, zeolite Beta exhibits high acid strength, high thermal stability and is stable upon acid treatment. In a recent study by Freese et al. (1999), zeolite Beta was found to be the most active catalyst for acylation of aromatic compounds, in comparison with the performance of zeolite Y and ZSM-5. Jacob et al. (1999) explored zeolite Beta as a heterogeneous Lewis acid. It was shown to be the most efficient and selective catalyst for benzoylation of *o*-xylene with benzoyl chloride (in comparison with ZSM-5, Beta, H-mordenite, and Na–Y type zeolites).

Generally zeolite Beta were prepared by the hydrothermal method (Barrer, 1982), the dry gel method and steam-assisted crystallization methods (Matsukata et al., 2002). In the synthesis of zeolite Beta, the main reagents are a silica source and organic templates. In the original synthesis of zeolite Beta patented by Wadlinger et al. (1967), tetraethylammonium hydroxide was used both as a templating and a structure-directing agent. Several commercially available silica sources, such as aqueous silica sol (Cannan and Hinchey, 1992), a colloidal silica (Rubin, 1992) and tetraethyl-orthosilicate (Eapen et al., 1994) have been widely used in the synthesis of zeolite Beta. Zeolite Beta with high silica content was synthesized from precipitated silica (Saxton and Zajacek, 1996). Inoue and Hiroshi (1995) prepared zeolite Beta by reacting a granular amorphous aluminosilicate, prepared by continuously reacting an aqueous solution of an alkali metal silicate and an aqueous solution containing aluminium. An amorphous silica aerogel has also been used in the synthesis of zeolite Beta with low template content (Maria et al., 1997). Other organic templating agents, such as dibenzyl-1,4-diazabicyclo(2,2,2) octane chloride dibenzyl-dimethylammonium ion (Calvert et al., 1987), 4,4′-trimethylenebis(*N*-benzyl-piperidine) (Lohse et al., 1996), TEA halide-diethanolamine (Saxton and Zajacek, 1996), TEAOH–TEA halide–triethanol–amine, TEABr–NH_4OH and TEAOH–TEABr chelates (Chang et al., 1987) were explored for the synthesis of zeolite Beta. A detailed study of the synthesis of zeolite Beta using silica gel as a low cost silica source has been published (Ramanath and Kumar, 1990).

The objective of this paper is to explore the synthesis of zeolite Beta using white rice husk ash as the silica source. We also document how a crystalline form of silica, present in the RHA, is transformed into zeolite Beta.

2. Experimental

White RHA obtained from a rice field in northern Malaysia contained 94 wt% SiO_2, 0.19 wt% Al_2O_3, 0.32 wt% CaO, and 1.64 wt% K_2O. Other materials used were tetraethylammonium hydroxide (40% TEAOH solution in water, supplied by Fluka Chimika), sodium aluminate (54 wt% Al_2O_3: 41 wt% Na_2O, technical grade), sodium hydroxide (Merck) and distilled water. A commercial silica source, i.e., Ludox (30 wt% SiO_2 in water), was used as comparison in the synthesis of zeolite Beta.

The reaction mixture was prepared at room temperature with the appropriate amounts of reagents needed to obtain a total weight of 50 g as follows. A 11.1 g portion of RHA was added to the solution of 0.36 g NaOH in 9 g of water in a Teflon beaker to give mixture A. Sodium aluminate (1.21 g) was dissolved in the TEAOH solution (23.71 g), which was previously diluted with a small amount of water (4.60 g), to yield solution B. Solution B was added slowly to mixture A with vigorous stirring and homogenized for at least 2 h. The chemical composition of the initial gel was 1.96 Na_2O:27 SiO_2:Al_2O_3:5 TEA_2O:240 H_2O. The gel obtained was transferred to a stainless steel autoclave and heated at 150 °C under autogeneous pressure for 6 d. After hydrothermal crystallization, a solid was separated from the mother liquor by filtering and was washed with distilled water until neutral. Finally, the solid was dried at 110 °C overnight.

In order to study the transformation of RHA to zeolite Beta, the hydrothermal crystallization was carried out using the gel as above at various periods of time (0.25–12 d). After filtration, washing and drying, the solids were calcined at 550 °C for 16 h. The temperature of calcination was increased gradually at 5 °C/min until the final temperature was reached. The resultant solid was cooled to the ambient temperature and weighed.

All of the products were characterized by powder X-ray diffraction (XRD) for the crystallinity and purity of the solid materials, using a Siemens 5000 diffractometer with the Cu Kα radiation as the diffracted monochromatic beam. The pattern was acquired in the 2θ 5–45° range. The intensity of the peak at 22.5° was taken as a measure of the solid crystallinity. Infrared spectra of the samples in the transmission mode were collected on a Shimadzu 8000 FTIR (spectral resolution of 2 cm^{-1}, 15 scans) at 20 °C using a standard KBr method. The spectra were recorded in the zeolite framework vibration region (1300–400 cm^{-1}). The ^{29}Si MAS NMR spectra were recorded on a Varian Unity INOVA 400 MHz spectrometer, at a spinning rate of 5.5 kHz, a pulse length of 3.0 μs and a recycle delay of 12 s. The ^{29}Si chemical shifts were reported relative to external TMS. The estimated values of the

chemical shift corresponding to different environments of the SiO_4 unit were obtained by Gaussian signal deconvolution. The signals were used for calculation of the Si/Al ratios in the framework of samples, using the known formula (Engelhardt and Michel, 1987).

3. Results and discussion

3.1. Powder X-ray diffraction

Fig. 1 illustrates the XRD patterns of the RHA and solid products obtained at various crystallization times. As seen, the parent material RHA is crystalline and consists of α-cristobalite and tridymite (Fig. 1(a)). We have found that the crystalline phase of the RHA was transformed to the pure zeolite Beta phase after 2 d of hydrothermal synthesis. The sample recovered after 6 h showed the XRD pattern (Fig. 1(b)) with the main characteristic signals at 21.8°, 31.4°, 36.1°; and 20.6°, 23.3°, 27.5°, 28.1°, 30.2°, 36.1°, which were assigned to α-cristobalite and tridymite, respectively. These are typical of the two main phases found previously in the RHA (Ramli et al., 1996) and confirmed further in experiments now. The two phases were transformed into zeolite Beta phase after 6 h of crystallization. Such an evolution is marked, upon close inspection of XRD spectra, by disappearance of tridymite, followed by disappearance of α-cristobalite after 24 h.

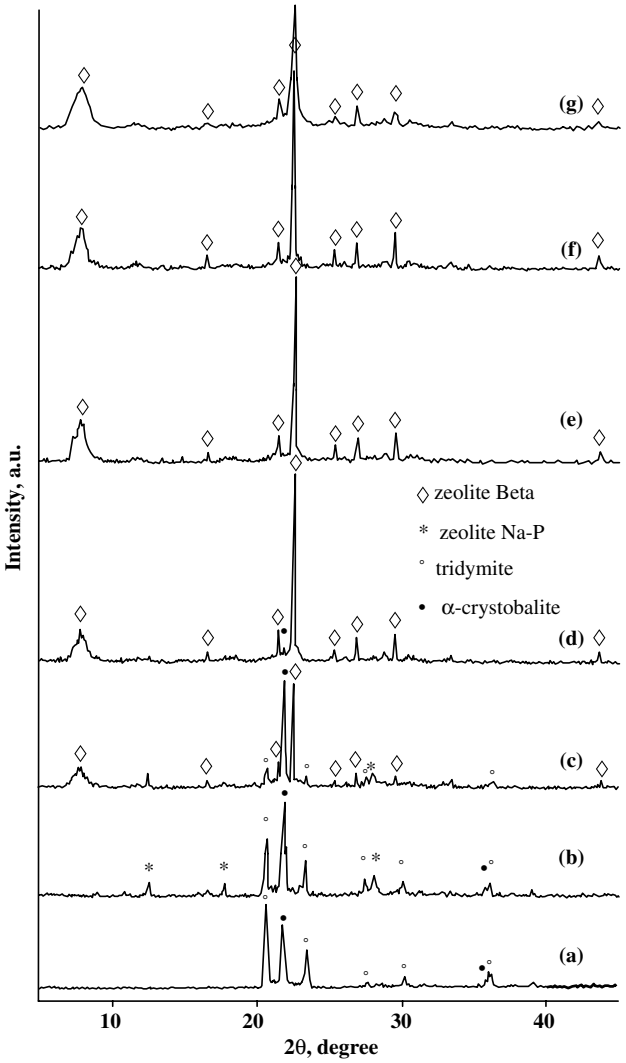

Fig. 1. XRD patterns of the rice husk ash (RHA) (a), solid products obtained after (b) 6 h (c) 12 h (d) 24 h (e) 48 h and (f) 96 h of crystallization time, and (g) BEA from colloidal silica.

Additional peaks with low intensity at 12.48° and 17.79° were also discerned in the sample after 6 h. The two signals, which became significant after 1 d of crystallization, were assigned as a trace of Na–P type zeolite. However, this zeolitic phase disappeared completely after 2 d of crystallization. The formation of zeolite Beta was detected as low intensity signals at 7.8°, 22.5° and 43.2° present already in the sample after 12 h of crystallization. Apart from zeolite Beta, α-cristobalite, tridymite and zeolite Na–P are clearly seen in this sample (Fig. 1(c)). As the time of crystallization was increased, the intensities of the diffraction peaks associated with the zeolite Beta also increased, thus indicating a progress in crystallization. The evolution of crystalline phase of zeolite Beta reached its maximum after 2 d of crystallization, when no further increase of the peak intensity at $2\theta = 22.5°$ was observed. In addition, the XRD patterns of zeolite Beta from rice husk ash (BEA-RHA) and colloidal silica (BEA-CS) are similar, characteristic of the BEA structure (Wadlinger et al., 1967; Perez-Pariente et al., 1987).

3.2. Solid yield at different crystallization times

The solids were recovered at different crystallization times, dried and calcined at 550 °C for 16 h before the XRD spectra were acquired. Fig. 2 shows the relationship

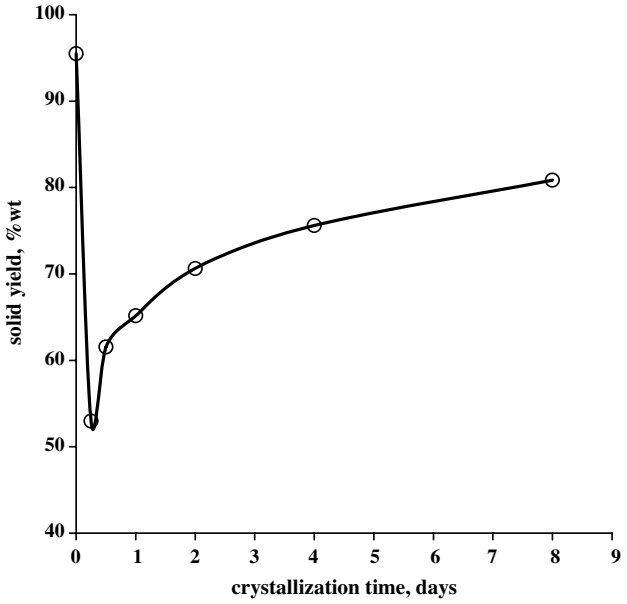

Fig. 2. Solid yield (wt%) as a function of crystallization time.

between the solid yield (wt%) and crystallization time of the initial mixture containing RHA. The graph shows that the amount of solids in the reaction mixture drops significantly from about 95 wt% at the beginning of the experiment to reach minimum at 53% after 6 h, followed by a continuous increase up to 80% after 8 d. It is seen that the increase is insignificant after 2 d of crystallization, and changes from 70% to 80% within the next 6 d of crystallization.

The graph can be rationalized in terms of the dissolution of the parent solid, which is predominantly RHA. Before the initial mixture is heated, only about 5 wt% of the solid phase is dissolved. This is due to the presence of the crystalline α-cristobalite and tridymite in the RHA, both forms of silica known to be very difficult to dissolve (Iler, 1979). However, as the temperature is increased to 150 °C, the two phases present originally in RHA start to dissolve and after the first 6 h about half of the RHA is dissolved. At the same time, traces of Na–P type zeolite are formed in the solid phase, as evidenced in the XRD spectrum (Fig. 1(b)). Upon prolonging the crystallization time, this zeolitic phase disappears completely. The formation of minor amounts of zeolite Na–P affects the solid weight increase to a minor extent. As the amount of the solid product starts to increase by about 10% after 12 h, this weight gain is attributed predominantly to the formation of the zeolite Beta (cf. XRD). It is also clear that the rate of growth of zeolite Beta is higher than the rate of dissolution of the starting material. Formation of pure zeolite Beta is observed with prolonged crystallization time.

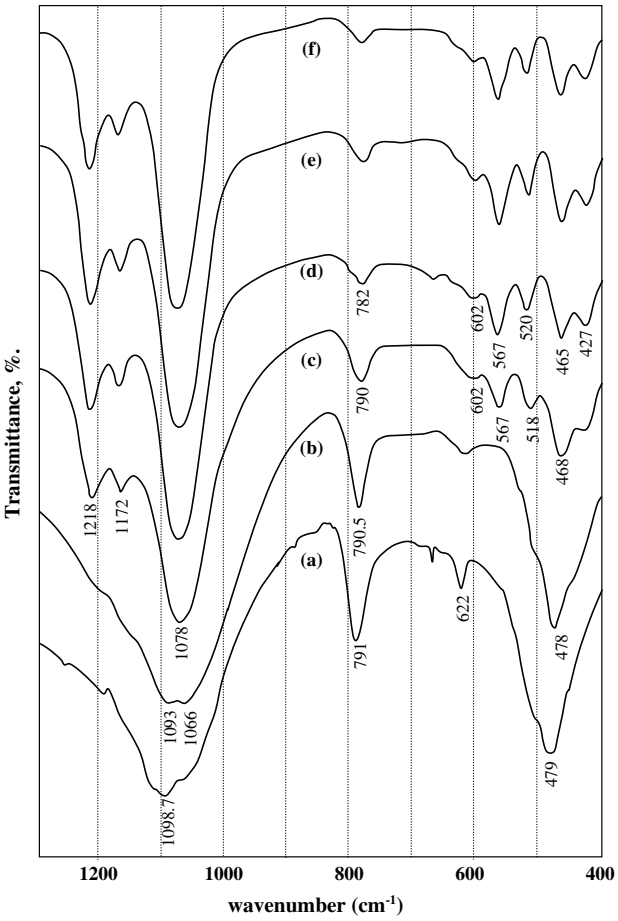

Fig. 3. FTIR spectra of the rice husk ash (RHA) and solid products recovered during the synthesis of zeolite Beta at various crystallization times: (a) RHA; (b) 6 h; (c) 12 h; (d) 24 h; (e) 48 h; (f) 96 h.

3.3. Infrared spectroscopy

The progress in the transformation of RHA to zeolite Beta and evolution of its crystallinity with time of crystallization can be conveniently monitored by infrared spectroscopy. The spectra were taken in the lattice vibration region of zeolite, i.e., 400–1300 cm^{-1}, as shown in Fig. 3. In Fig. 3(a) the infrared spectrum of RHA is visualized. Three main signals are seen, a strong broad band at 1099 cm^{-1} accompanied with a hump at 1066 cm^{-1}, a sharp medium band at 791 cm^{-1} and a strong band at 479 cm^{-1}. The strongest vibration in the 950–1250 cm^{-1} region was commonly observed in (alumino)silicates and silica polymorphs due to ← OT → ← O stretching modes, where T = Si, Al (Flanigen et al., 1971). The signal at 1099 cm^{-1} is therefore assigned to the asymmetric stretching vibrations of tetrahedra SiO_4, while a band at 791 cm^{-1} is due to symmetric stretching vibrations of the same units. The third signal at 479 cm^{-1} is assigned to the Si–O bending mode. Additionally, one can discern a very weak band at 622 cm^{-1}, which is characteristic of the crystalline cristobalite. No significant changes in the spectrum are noticed after 6 h of crystallization, and all main features already observed in the starting mixture are seen. However, the onset of the zeolitic phase formation can be clearly discerned as a set of small signals, which are developed further upon increasing the crystallization time. Also, the broad band at 1099 cm^{-1} becomes more pronounced and splits into two signals with the maxima at 1093 and 1066 cm^{-1}. All of the stretching modes are sensitive to zeolite framework Si/Al composition and generally shift to a lower frequency with increasing aluminium content, due to the longer Al–O bond, 1.75 Å, as compared to the Si–O bond, 1.61 Å (Sulikowski, 1996). Therefore, lowering the vibration frequency from 1099 to 1093 cm^{-1} indicates incorporation of tetrahedral aluminium in the framework of zeolite Beta. As an average shift is 25.3 cm^{-1} per 0.1 Al (Flanigen et al., 1971), the shift of 22 cm^{-1} corresponds here to 0.087 Al, or to the Si/Al ≈ 10 ratio in the zeolite framework. The estimation of Si/Al ratio by this method may, however, bear an error, as there was a significant scatter of data in the original relationship.

After 12 h of crystallization, several new bands appear in the spectrum (Fig. 3(c)). These bands can be rationalized as being typical of the zeolite phase. In general, the zeolite vibrations can be divided into two families, structure sensitive and structure insensitive. Structure sensitive bands change with topology and building units of the zeolite framework and occur in four regions of the spectrum, 300–420, 500–600, 750–820 cm^{-1} and as a shoulder at

1050–1150 cm^{-1} (Flanigen et al., 1971). Thus, a medium intensity vibration at 1217 cm^{-1} is assigned to the asymmetric stretching mode of the external TO_4 linkages, a sharp band at 568 cm^{-1} is assigned to the double ring vibration, and sharp bands at 466 and 426 cm^{-1} are assigned to the bending T–O mode. The appearance of double ring vibration indicates that the framework of zeolite Beta begins to form, as the secondary building unit of this aluminosilicate consists of double 6-membered rings. Another indication that crystallization is in progress and aluminium is being incorporated into tetrahedral zeolite sites can be evidenced by observing the shift of asymmetric stretching vibration of TO_4units from 1099 to 1078 cm^{-1} (vide supra) and also from 791 to 782 cm^{-1}. Finally, a small sharp band at 1171 cm^{-1} is assigned to the tetrahedral stretching vibrations of the organic template; this band seen in the as-prepared samples disappears completely after template removal by calcination.

As the time of crystallization is increased, the corresponding spectra (Fig. 3(d)–(f)) reveal no significant changes, but the enhancement of vibrations. For those samples, the asymmetric stretching signals of TO_4 at 1218 and 1078 cm^{-1} become sharper. The characteristic vibrations of zeolite Beta at 1219, 1172, 566, 519, 464, and 427 cm^{-1} also developed into the sharper signals, thus indicating an increase in crystallinity. Finally, vibration at 478 cm^{-1} assigned to the pore opening (Eapen et al., 1994) shifts gradually to 464 cm^{-1} with crystallization time, thus being in good agreement with observations made above and XRD studies.

FTIR can be also conveniently used for monitoring crystallinity of zeolite Beta during the hydrothermal synthesis, as reported earlier by Perez-Pariente et al. (1987) and Ramanath and Kumar (1990). The intensity changes of the characteristic signals corresponding to the double rings vibration at 566 and 520 cm^{-1} were used to study the progress in crystallization (Perez-Pariente et al., 1987; Ramanath and Kumar, 1990). In our work, the band at 466 cm^{-1} is selected as a reference band, because its intensity remains essentially constant with the time of crystallization. Fig. 4 shows relative crystallinity of samples expressed by the intensity ratio of the 566 and 520 cm^{-1} signals to the 466 cm^{-1}, respectively. As seen, both curves depict a very similar trend and therefore both can be effectively used for monitoring the hydrothermal process. A very fast increase in crystallinity is observed within 24 h, followed by minor changes with time. After 48 h both traces level up and then remain constant. The results are in good agreement with the XRD-based findings.

3.4. Solid state ^{29}Si MAS NMR

The ^{29}Si MAS NMR spectra in Fig. 5 depict evolution of short-range silicon environments with the time of crystallization. The spectrum in Fig. 5(a) shows the characteristic ^{29}Si MAS NMR pattern of RHA, with only one intense signal located at −113.3 ppm. The signal is assigned

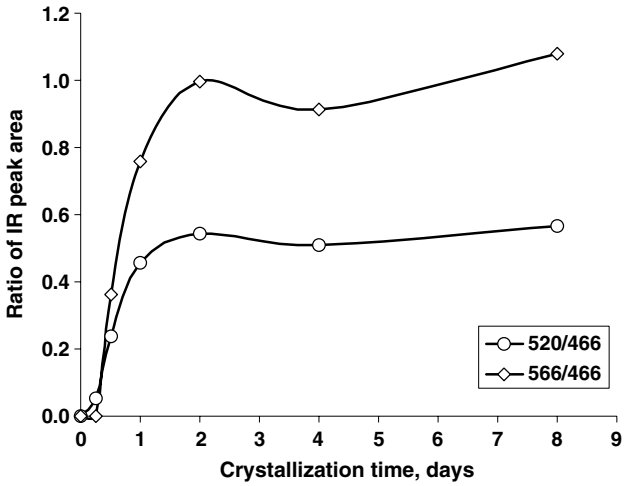

Fig. 4. Relative crystallinity of the zeolite Beta based on the intensity ratio of the infrared bands at 520/466 and 566/466 cm^{-1}.

to SiO_4 unit surrounded by four tetrahedral SiO_4 in its first coordination sphere, (Q^4)–Si(4Si,0Al), due to the presence of α-cristobalite and tridymite. The spectrum is, however, not resolved into a (physical) mixture of the two forms of silica. In particular, the fine structure of tridymite with the chemical shifts ranging from −109.3 to −114.0 ppm (Smith and Blackwell, 1983) is not seen in the spectrum of RHA.

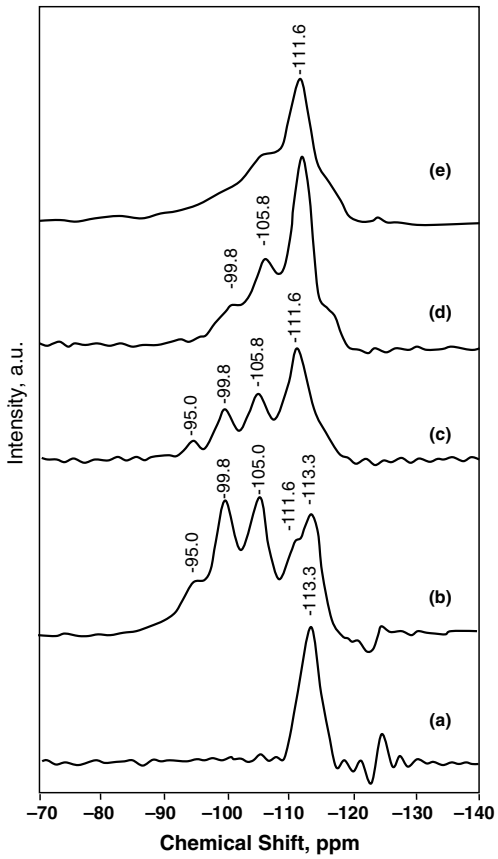

Fig. 5. ^{29}Si MAS NMR spectra of the RHA and solid materials obtained at various crystallization times: (a) RHA; (b) 6 h; (c) 12 h; (d) 24 h; (e) 96 h.

Monitoring of the solid during the hydrothermal synthesis demonstrates clearly how the silicon signal of the RHA in the parent sample transforms into several non-equivalent tetrahedral SiO_4 in zeolite Beta. The sample after 6 h of crystallization (Fig. 5(b)) reveals three signals and two shoulders centered at −113.3, −105.0, −99.8, and −111.6, −95.0 ppm, respectively. The signals at −111.6 and −113.3 ppm are still in the range of the siliceous region (Q^4) between −110 and −116 ppm, which can be attributed to Si(4Si,0Al) groupings located at different crystallographic sites (Stelzer et al., 1998). The appearance of a signal at −111.6 ppm indicates the formation of different Q^4 environments, which in this case are attributed to the Si(4Si,0Al) sites of aluminosilicates formed in the solid phase. The signals at −105.0, −99.8, and −95.0 ppm can be attributed as Q^4 type for Si(3Si,1Al) sites, as Q^3 type for Si(3Si,1OH) sites containing silanol groups, and as Q^4 type for Si(2Si,2Al) sites, respectively. Similar features of the zeolite Beta spectra were reported previously (Camblor and Valencia, 1998). As the crystallization time increases, the intensities of the signals associated with Si(4Si,0Al), Si(3Si,1Al), the silanol site Si(3Si,1OH) and the Si(2Si,2Al) at −113.3, −105.8, −99.8 and −95.0 ppm all decrease, as depicted in the spectrum of the sample after 12 h of crystallization (Fig. 5(c)). However, the signal associated with Si(4Si,0Al) at −111.6 ppm increases in intensity, suggesting that the framework is becoming more siliceous. Furthermore, successive decrease in the intensities of the low field signals occur concurrently with the increase in intensities of the signals at the higher field with the increasing time of crystallization, until a strong peak emerges at −111.6 ppm accompanied by a shoulder at −105.8 ppm for the sample obtained after 4 d of crystallization (Fig. 5(e)). At this stage, all of the Q^4 type signals associated with the tetrahedral environment of silicon Si(4Si,0Al) in the parent sample at −113.3 ppm are hardly discerned, indicating therefore that most of the RHA has been transformed into zeolite Beta. These results are complementary to and support earlier findings based on the XRD patterns analysis, according to which the formation of zeolite Beta from RHA was completed after 2 d of crystallization.

Gaussian deconvolution of the ^{29}Si MAS NMR traces yields the intensity of each signal. Taking this into account, the Si/Al framework ratio of the solid products was calculated using a known formula (Engelhardt and Michel, 1987). Table 1 lists deconvoluted values corresponding to the signals of different chemical environments for each solid product together with their Si/Al ratios. We note that the Si/Al ratio changes significantly from 6.8 after 6 h to 13.6 after 4 d of synthesis time. It is, therefore, clear that the initial aluminosilicate is aluminium-rich. Evidently, aluminium is released from the tetrahedral sites of the aluminosilicate during the course of the synthesis, thus forming a much more siliceous solid phase of zeolite Beta.

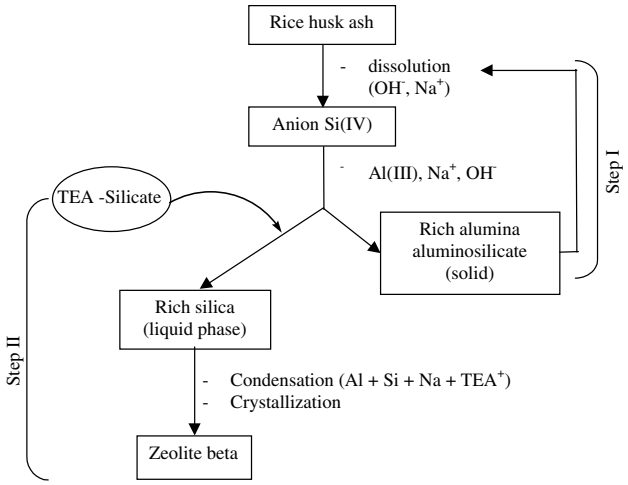

Fig. 6. A suggested mechanism of the transformation of RHA into Beta (BEA) type zeolite.

3.5. Transformation mechanism of silica of RHA into zeolite Beta

Taking into account the XRD, FTIR and NMR results, it is obvious that the transformation of silica present in RHA to zeolite Beta proceeds via the formation of aluminosilicate species and, to a minor extent, also via traces of the metastable zeolite Na–P (Fig. 6). At the initial stage of crystallization, the mechanism involves dissolution of crystalline silica of RHA in the NaOH base to yield silicate ions. This is demonstrated by the presence of silanols in the ^{29}Si NMR spectra and also by a drastic drop in the weight of solid products, recovered after 6 h of crystallization. At the same time, amorphous aluminosilicate species are being formed, with local silicon environments corresponding to the Si(3Si,1Al), Si(2Si,2Al) and Si(4Si,0Al) groupings. Some of them can be attributed to the framework of low silica zeolite P. From the solid yield of the sample after 6 h of crystallization, showing that half of the starting material was dissolved, it is evident that the

Table 1
Chemical shifts and signal intensity from Gaussian deconvolution of the ^{29}Si MAS NMR spectra

Crystallization time (h)	Chemical shift (ppm) and relative intensities (in parentheses)					Si/Al
	Q^4 (2Si, 2Al)	Q^3 (3Si,1OH)	Q^4 (3Si,1Al)	Q^4 (4Si,0Al)$_I$	Q^4 (4Si,0Al)$_{II}$	
Parent RHA	–	–	–	–	−113.3 (1.00)	–
6	−95.0 (0.09)	−99.8 (0.31)	−105.0 (0.29)	−111.6 (0.10)	−113.3 (0.21)	6.8
12	−95.0 (0.05)	−99.8 (0.19)	−105.8 (0.36)	−111.6 (0.37)	−113.3 (0.03)	7.4
24	–	−99.8 (0.11)	−105.8 (0.30)	−111.6 (0.57)	−113.3 (0.02)	12.0
96	–	−99.8 (0.09)	−105.8 (0.26)	−111.6 (0.60)	−113.3 (0.04)	13.6

aqueous phase is rich in Na^+, OH^-, TEA^+ and silicates ions. In the presence of those ions, the dissolution of aluminosilicate species into aluminate and silicate species takes place, thus forming the TEA–silicates species (Perez-Pariente et al., 1987). These species, in the presence of Na^+ ions, form the silica-rich zeolite Beta nuclei, as was inferred from NMR and IR studies. Since the yield of the solid products remains constant once zeolite Beta has been formed, it is clear that the rate of the formation of zeolite Beta framework is higher than the rate of silica dissolution. The study also shows the role of TEA as a structure-directing agent for the formation of zeolite Beta. The organic template (TEA) is involved in the zeolite formation at the latter synthesis stage, i.e., after formation of aluminosilicate species. Finally, our work shows that without the template, the synthesis would be stopped at the formation of zeolite P.

4. Conclusion

Zeolite Beta has been synthesized by a direct hydrothermal route, using crystalline silica of rice husk ash (RHA) as a silica source and tetraethylammonium hydroxide as the structure-directing agent. We have demonstrated, therefore, that the natural source of silica consisting of the two crystalline polymorphs of silica (α-cristobalite and tridymite), can be used conveniently for hydrothermal zeolite synthesis. In particular, we have shown that highly crystalline zeolite Beta can be obtained from the RHA silica source. Rice husk ash was completely transformed to pure zeolite Beta phase after just 2 d of hydrothermal synthesis at 150 °C. The transformation of RHA involves dissolution of the silica in the highly basic reaction mixture, followed by the formation of an aluminosilicate, crystallization of the metastable zeolite Na–P and finally the pure zeolite Beta phase.

Acknowledgements

The authors thank Universiti Teknologi Malaysia and The Ministry of Science and Environment Malaysia for financial support, under IRPA Grant Vot 72117.

References

Bajpai, P.K., Rao, M.S., Gokhale, K.V.G.K., 1981. Synthesis of mordenite type zeolite using silica from rice husk ash. Ind. End. Chem. Prod. Res. Dev. 20, 721–726.

Barrer, R.M., 1982. Hydrothermal Chemistry of Zeolites. Academic Press, New York, USA.

Calvert, R.B., Chang, C.D., Rubin, M.K., Valyocsik, E.W., 1987. Process for the preparation of zeolite Beta using dibenzyldimethylammonium ions and the product produced. US Patent 4642226.

Camblor, M.A., Valencia, S., 1998. Characterization of nanocrystalline zeolite beta. Micropor. Mesopor. Mat. 25, 25–74.

Cannan, T.R., Hinchey, R.J., 1992. Synthesis of zeolite beta. US Patent 5139759.

Chang, C.D., Rubin, M.K., Valyocsik, E.W., 1987. Process for the preparation of zeolite Beta using dibenzyldimethylammonium ions and the product produced. US Patent 4642226.

Eapen, M.J., Reddy, K.S.N., Shiralkar, V.P., 1994. Hydrothermal crystallization of zeolite beta using tetraethylammonium bromide. Zeolites 14, 295–302.

Engelhardt, G., Michel, D., 1987. High-Resolution Solid-State NMR of Silicates and Zeolites. Wiley, Chichester, UK.

Flanigen, E.M., Khatami, H., Szymanski, H.A., 1971. Adv. Chem. Series 101, 201–228.

Freese, U., Heinrich, F., Roessner, F., 1999. Acylation of aromatic compounds on H-beta zeolites. Catal. Today 49, 237–244.

Higgins, J.B., LaPierre, R.B., Schlenker, J.L., Rohrman, A.C., Wood, J.D., Kerr, G.T., Rohrbaugh, W.J., 1988. The framework topology of zeolite beta. Zeolites 8, 446–452.

Iler, R.K., 1979. The Chemistry of Silica: Solubility, Polymerization, Colloid, and Surface Properties, and Biochemistry. Wiley, New York.

Inoue, T., Hiroshi, W., 1995. Method of producing zeolite beta. US Patent 5427765.

Jacob, B., Sugunan, S., Singh, A.P., 1999. Selective benzoylation of *O*-xylene to 3,4-dimethylbenzophenone using various zeolite catalyst. J. Mol. Catal. A Chem. 139, 43–53.

Jansen, J.C., Creighton, E.J., Njo, S.L., Koningsveid, H., van Bekkum, H., 1997. On the remarkable behaviour of zeolite beta in acid catalysis. Catal. Today 38, 205–212.

Lee, Y.K., Park, S.H., Rhee, H.K., 1998. Transalkylation of toluene and 1,2,4-trimethylbenzene over large pore zeolites. Catal. Today 44, 223–233.

Lohse, U., Altrichter, B., Denath, R., Fricke, R., Jancke, K., Parlitz, B., Schrier, E., 1996. Synthesis of zeolites beta. Part 1. Using TEAOH/Br with addition of chelates as templating agents. J. Chem. Soc., Faraday Trans. 92, 159–165.

Maria, W., Carvalho, N.C., Cardosa, D., 1997. In: Chon, H., Ihm, S.K., Uh, Y.S. (Eds.), Progress in Zeolite and Microporous Materials. 105, 349–356.

Matsukata, M., Osaki, T., Ogura, M., Kikuchi, E., 2002. Crystallization behavior of zeolite beta during steam-assisted crystallization of dry gel. Micropor. Mesopor. Mat. 56, 1–10.

Meier, W.M., Olson, D.H., Baerlocher, Ch., 1996. Atlas of Zeolite Structure Types, fourth ed. International Zeolite Association, Netherlands.

Perez-Pariente, J., Martens, J.A., Jacobs, P.A., 1987. Crystallization mechanism of zeolite beta from TEA_2O, Na_2O, and K_2O containing silicate gels. Appl. Catal. 31, 35–64.

Ramanath, N.B., Kumar, R., 1990. Synthesis of zeolite beta using silica gel as a source of SiO_2. J. Chem. Biotechnol. 48, 453–466.

Ramli, Z., 1995. Rhenium-impregnated zeolites: synthesis, characterization and modification as catalysts in the metathesis of alkenes. Ph.D. thesis, UTM, Malaysia.

Ramli, Z., Listiorini, E., Hamdan, H., 1996. Optimization and reactivity study of silica in the synthesis of zeolites from rice husk. J. Teknologi UTM 25, 27–35.

Ramli, Z., Bahruji, H., 2003. Synthesis of ZSM-5 type zeolite using crystalline silica of rice husk ash. Malaysian J. Chem. 5, 48–55.

Rubin, M.K., 1992. Synthesis of zeolite Beta. US Patent 5164170.

Saxton, R.J., Zajacek, J.G., 1996. Method of making essentially silicic zeolite beta. US Patent 5554356.

Smith, J.V., Blackwell, C.S., 1983. Nuclear magnetic resonance of silica polymorphs. Nature 303, 223–225.

Stelzer, J., Paulus, M., Hunger, M., Weitkamp, J., 1998. Hydrophobic properties of all-silica zeolite beta. Micropor. Mesopor. Mat. 22, 1–8.

Sulikowski, B., 1996. Isomorphous replacement in the zeolitic frameworks: recent advances and implications. Heterogen. Chem. Rev. 3, 203–268.

Wadlinger, R.L., Kerr, G.T., Rosinski, E.J., 1967. Synthesis zeolite beta. US Patent 3308069.

Wall, J.C., Rigutto, M.S., van Bekkum, H., 1998. Zeolite titanium beta as a selective catalyst in the epoxidation of bulky alkenes. Appl. Catal. A Gen. 167, 331–342.

Wang, H.P., Lin, K.S., Huan, Y.J., Li, M.C., Tsaur, L.K., 1998. Synthesis of zeolite ZSM-48 from rice husk ash. J. Hazard. Mater. 58, 147–152.

Malaysian Journal of Chemistry, 2003, Vol **5**, *No. 1, 48-55*

SYNTHESIS OF ZSM-5-TYPE ZEOLITE USING CRYSTALLINE SILICA OF RICE HUSK ASH.

Zainab Ramli and Hasliza Bahruji

Department of Chemistry,
Faculty of Science,
Universiti Teknologi Malaysia,
81310 UTM Skudai, Johor, Malaysia

Abstract*: White rice husk ash obtained from uncontrolled burning of rice husk contain >90 % silica in the crystalline form. In this study the ash was used as a silica source in the preparation of ZSM-5, a highly siliceous zeolite used as a catalyst in the petrochemical industries and in organic synthesis. The synthesis of ZSM-5 was carried out at different initial molar composition of the oxides in order to determine the range of SiO_2 : Al_2O_3 ratio that can form pure ZSM-5. The initial molar oxides ratios in the range of 5.4 – 10.0 Na_2O : 24.0 – 100.0 SiO_2 : 1.0 – 2.9 Al_2O_3 : 1800 – 3600 H_2O : 3 - 6 TPA, were used and hydrothermally treated at 150 ^oC for 7 days at static condition. The resulting solid products were characterized by XRD and FTIR. Results showed that pure ZSM-5 was successfully formed from all initial oxides ratios without the formation of other zeolite phases. Rice husk ash in samples with initial silica to alumina ratio ≤ 30 has been successfully transformed to ZSM-5 phase. On the other hand products obtained from initial silica to alumina ratios > 30, showed the presence of unreacted rice husk ash. The initial gel composition with low TPABr and without alumina respectively produced small quantities of ZSM-5.*

Abstrak*: Abu sekam padi putih yang didapatkan daripada pembakaran sekam padi tidak terkawal mengandungi >90 % silika berhablur. Dalam kajian ini abu ini digunakan sebagai punca silika dalam sintesis ZSM-5, suatu zeolit bersilika tinggi yang digunakan sebagai mangkin dalam industri petrokimia dan dalam sintesis organik. Sintesis ZSM-5 dilakukan pada komposisi molar oksida awal yang berbeza-beza untuk mendapatkan julat nisbah silika kepada alumina yang boleh membentuk ZSM-5 tulen. Julat nisbah molar oksida awal 5.4 – 10.0 Na_2O : 24.0 – 100.0 SiO_2 : 1.0 – 2.9 Al_2O_3 : 1800 – 3600 H_2O : 3 - 6 TPA digunakan dalam sintesis yang dilakukan secara hidroterma pada suhu 150 ^oC selama 7 hari tanpa pengacauan. Hasil pepejal dicirikan oleh kaedah XRD dan FTIR. Keputusan menunjukkan ZSM-5 berjaya dibentuk daripada semua nisbah komposisi oksida yang digunakan tanpa pembentukan fasa zeolit lain. Sampel daripada nisbah silika kepada alumina awal ≤ 30 berjaya menukarkan semua abu kepada fasa ZSM-5. Sebaliknya hasil daripada nisbah silika kepada alumina awal > 30 masih mengandungi silika abu sekam padi yang tidak bertindak balas. Hanya sedikit ZSM-5 terbentuk daripada komposisi yang mengandungi kurang TPABr dan komposisi tanpa aluminium.*

Keyword: zeolite ZSM-5, rice husk ash, silica to alumina ratio.

Introduction

Zeolite ZSM-5 (Mobil Synthetic Zeolite-5) is a highly siliceous zeolite, widely employed as a catalyst in organic synthesis, petroleum refining and petrochemical industries. It was first developed in 1972 by Argauer and Landolt [1,2]. ZSM-5 is categorised as a medium pore class zeolite, having channels system with pore sizes between 4.5 Å to 6.5 Å, formed by two types of 10-membered oxygen rings. The first type is a straight and elliptical channel, with a free cross-section of 5.5 x 5.1 Å. The second type, perpendicular to the first channel is a sinusoidal channel with a cross-section of 5.6 x 5.4 Å [3]. Its catalytic properties are due to its acidity while the unique pore systems gives the catalyst its shape selective character [4].

Since the discovery of the highly siliceous zeolite ZSM-5 and its potential in many applications, a lot of research have been carried out to improve the synthetic methods and the quality of the product as well as to reduce the cost of production of zeolite ZSM-5 [5]. ZSM-5 crystallizes normally at temperature higher than 100 ^{o}C in the presence of organic base template particularly tetrapropylammonium cations [6]. The organic template functioned as a structure directing agent as well as a charge balancing cation. However, ZSM-5 has also been reported to form in the absence of the template [7,8]. Wha Jung Kim *et al*. [9] reported the possibility of synthesizing the ZSM-5 at atmospheric pressure and temperature as low as 100 ^{o}C. Recently, Coker *et al*. [10] succeeded in synthesising ZSM-5 in a low gravity environment.

Commercial ZSM-5 is produced from commercial silica sources in the form of gel, sol and amorphous fumed silica. However, waste materials with high silica content such as rice husk ash (RHA) and fly ash are potential silica sources for zeolite synthesis.

Previous studies [11-15] have shown that the utilization of RHA has successfully produced zeolites A, Y, ZSM-5, mordenite, and zeolite beta. In all cases, the silica of the rice husk ash was in amorphous form obtained either by extraction of the silica from the crystalline RHA or by controlled burning of the rice husk.

Rice husk, one of the major agricultural waste, is a fibrous material containing more than 90% SiO_2. The ash obtained from complete uncontrolled burning of rice husk usually consists of crystalline silica in a mixture of tridymite and crystoballite and occasionally quartz phase if the burning is prolonged [13]. Silica in this form is not active and is usually not suitable for zeolite synthesis. However in this study, attempt was made to use ash from the uncontrolled burning of the rice husk without further treatment in the synthesis of zeolite ZSM-5. Previous studies have shown that it was possible to use crystalline ash to produce pure zeolite beta [16]. Similarly, this study aims at finding the correct combination of the initial molar oxides ratios in the synthesis of pure ZSM-5.

Experimental

ZSM-5 was crystallized in the mixed oxides form of Na_2O: Al_2O_3: SiO_2: H_2O: tetrapropylammonium oxide (TPA_2O). Crystalline rice husk ash (RHA) obtained from BERNAS Rice Mill, Kuala Selangor, Selangor, containing 90.43% w/w SiO_2 was used as the silica source. Other constituents in the RHA in percentage of weight are Al_2O_3 (0.02%), K_2O (3.72%), Na_2O (0.04%), CaO (0.43%), MgO (0.16%), Fe_2O_3 (0.09%) and LOI (5.11%), which are considered as impurities. The synthesis of ZSM-5 was carried out at different initial molar composition of the oxides as tabulated in Table 1. In a typical zeolite synthesis the ash (2.78 g) was added to an aqueous tetrapropylammonium bromide (TPABr) (2.33 g) solution with stirring. An aqueous solution of sodium

aluminate; prepared separately by mixing calculated proportion of sodium aluminate (0.25 g) and sodium hydroxide (0.62 g) was slowly added to the alkaline silica mixture, followed by vigorous stirring to ensure a homogeneous solution. The resulting gel has a molar composition of $6Na_2O$: Al_2O_3 : $30SiO_2$: $1800H_2O$: 6TPABr. Crystallization of ZSM-5 was carried out by placing the gel in a stainless steel autoclave and heated in air oven at 150 ^oC for seven days. At the end of the period, the autoclave was quenched with water to room temperature to stop the crystallization. The product was removed, filtered and washed with distilled water before drying at 100 ^oC overnight. The dried powder was calcined at 550 ^oC for at least five hours to remove the organic template. The procedure was repeated by changing the oxides composition in the range of 5.4 – $10.0Na_2O$: 24.0 – $100.0SiO_2$: 1.0 – $2.9Al_2O_3$: 1800 – $3600H_2O$: 3 - 6TPABr. The product was characterized by XRD and FTIR to confirm the formation of ZSM-5.

Table 1: Initial molar composition of oxides in the reaction mixture.

Sample	Na_2O	SiO_2	Al_2O_3	H_2O	TPABr
S-1	6	30	1	1800	6
S-2	6	28	1	1800	6
S-3	6.45	30.24	1.89	1800	6
S-4	5.46	25	1	1800	6
S-5	10.02	24.07	2.94	1800	6
S-6	6	50	1	3600	6
S-7	6	70	1	3600	6
S-8	6	100	1	3600	6
S-9	6	30	0	1800	6
S-10	6	30	1	1800	5
S-11	6	30	1	1800	3

Results and Discussion

Crystalline silica from rice husk ash was used as the silica source in the synthesis of ZSM-5 and its XRD diffractogram is shown in Figure 1. Structural characterization of the rice husk ash by XRD shows that the ash consists mainly of silica in the form of crystobalite and tridymite phases. The presence of crystobalite is indicated by diffraction peaks at 2θ 21.7^{o} and 36.0^{o}, while the presence of tridymite is typically shown at 2θ 20.5^{o} and 29.0^{o}. The formation of ZSM-5 phase was confirmed by comparing the diffractograms of all the as-synthesized samples to the diffractogram of the reference ZSM-5 [17]. The as-synthesized S-1 sample gave similar diffraction pattern to that of the reference sample ZSM-5. This indicates that the as-synthesized S-1 sample has a ZSM-5 like structure. The successful transformation of all the RHA to pure zeolite ZSM-5 suggests that the impurities in RHA did not affect the formation of the aluminosilicate framework of zeolite ZSM-5.

1. Effect of the SiO_2 Content

X-ray Diffraction Pattern

A fine white fine solid obtained from the synthesis after calcination at 550^{o}C was characterized using X-ray diffraction technique. Figure 2 represents the XRD patterns of the as-synthesized samples S-1 to S-11 from the different oxides composition. All the diffractograms showed similar XRD patterns as compared to that of the reference ZSM-5, indicating that ZSM-5 like zeolite was formed from all the different reaction mixtures.

However, some samples do indicate the presence of unreacted RHA. The absence of other zeolite phases suggests that all the initial oxides ratios in this study facilitated in the

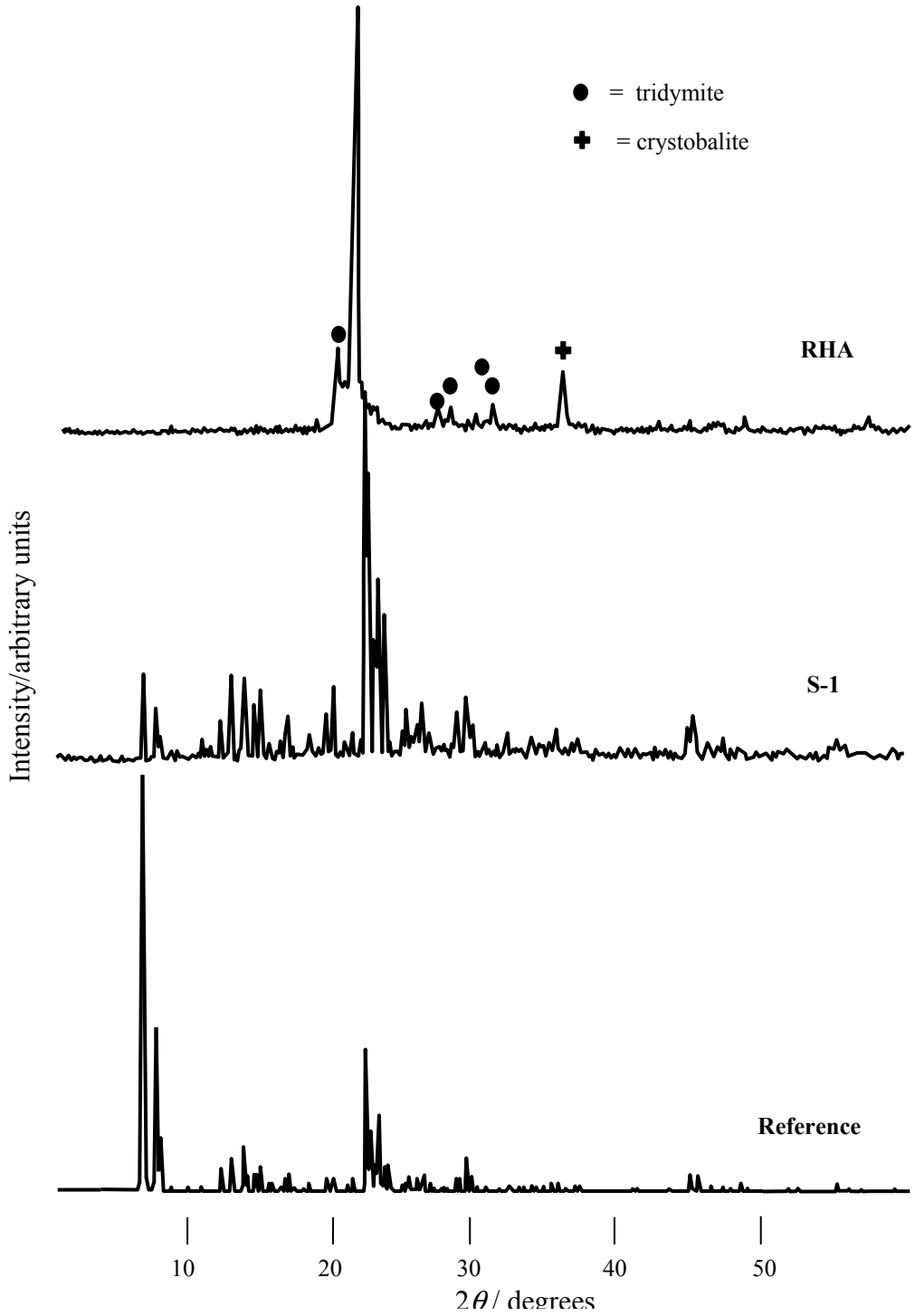

Figure 1: XRD diffractograms of rice husk ash (RHA), sample S-1 and reference ZSM-5

formation of ZSM-5 crystals in the presence of template TPA cation which acted as a structure directing agent. The presence of ZSM-5 phase is indicated by the existence of all peaks corresponding to ZSM-5 phase with the three intense peaks at 2θ 23.14°, 23.33° and 23.69°. The splitting of these peaks is clearly observed indicating that the ZSM-5 is in a monoclinic phase. Detailed results of the phase formation of the as-synthesized products are summarized in Table 2.

It is observed that the initial reaction mixtures with SiO_2 / Al_2O_3 ratio of 30 or less (samples S-1 to S-5) produced pure and highly crystalline ZSM-5 phases. The diffractograms showed high intensity of the diffraction peaks for these samples. However, when the initial SiO_2 / Al_2O_3 ratios were increased to more than 30, as in samples S-6, S-7 and S-8, an additional peak appeared at 2θ 22.07° corresponding to the

Table 2**:** Results from each synthesized zeolite ZSM-5 from rice husk ash (RHA).

Sample	SiO_2/Al_2O_3	% Crystallinity of ZSM-5	Phase crystallinity
S-1	30	100.0	**ZSM-5**
S-2	28	95.7	**ZSM-5**
S-3	16	91.4	**ZSM-5**
S-4	25	93.5	**ZSM-5**
S-5	8	92.2	**ZSM-5**
S-6	50	72.3	**ZSM-5** (major), RHA
S-7	70	72.2	**ZSM-5**, RHA
S-8	100	27.1	**ZSM-5**, RHA major)
S-9*	30	14.3	**ZSM-5**, RHA(major)
S-10**	30	32.9	**ZSM-5**, RHA(major)
S-11***	30	29.4	**ZSM-5**, RHA(major)

* Free alumina system
** 5 TPABr
*** 3 TPABr

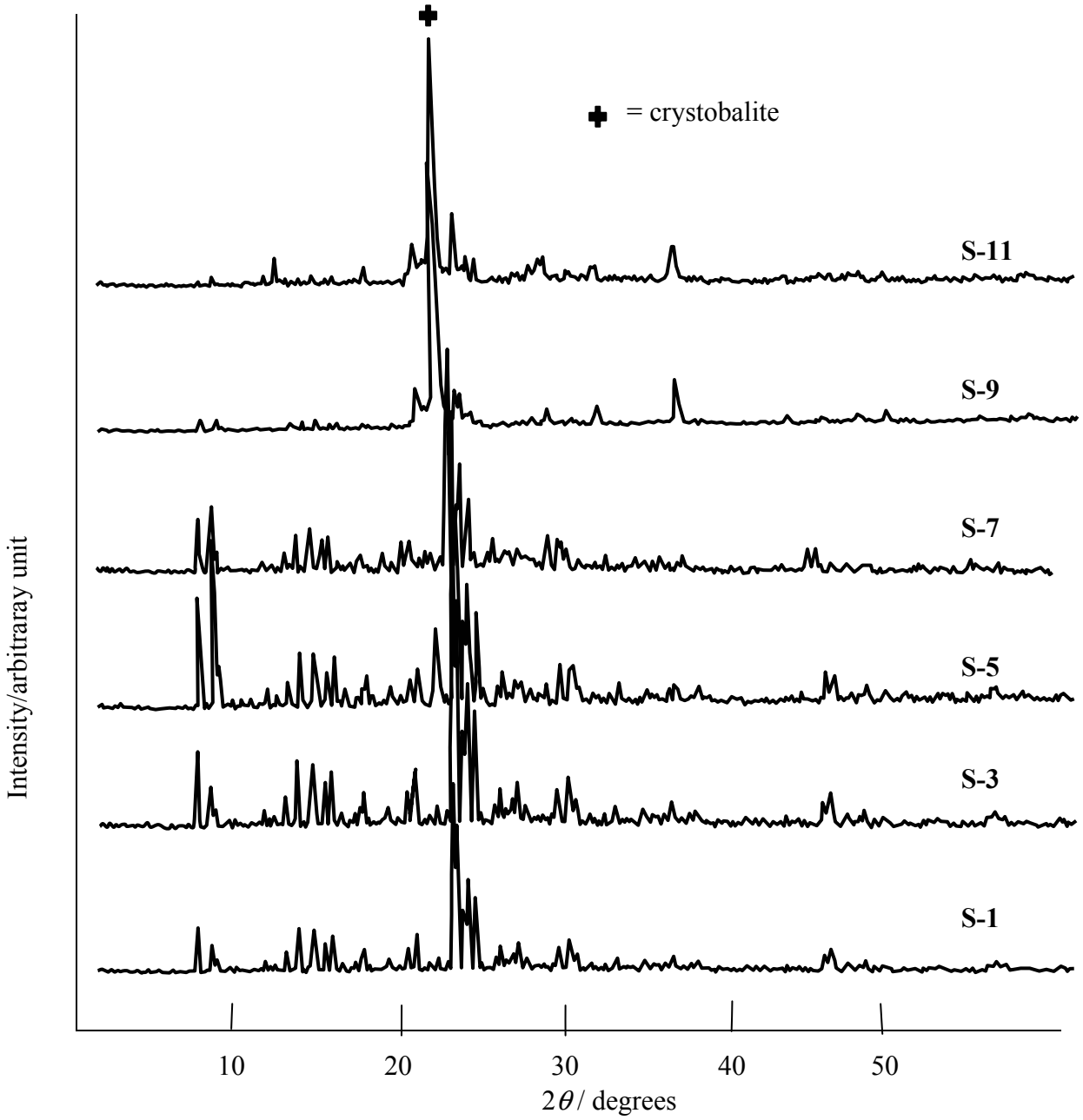

Figure 2: XRD diffractograms of samples S-1, S-3, S-5, S-7, S-9 and S-11

crystobalite of the RHA. The intensity of the peaks increased with the increase of silica in the initial reaction mixtures. These results indicated that crystalline silica of the type crystobalite still remain, suggesting the difficulty of crystobalite to dissolve in the reaction mixture and to be transformed to ZSM-5 crystal phase. Table 2 shows the percentage of crystallinity of ZSM-5 for each sample relative to sample S-1 i.e. the most intense peaks of ZSM-5 like sample produced from this synthesis.

Fourier Transform Infrared (FTIR).

Each zeolite species has a typical infrared structural vibration pattern consisting of four main peaks; the asymmetric and symmetric stretching of TO_4 (T= Al, Si) at 1250 – 1000 cm^{-1} and 750 – 650 respectively, T-O bending at 500 – 400 cm^{-1} and the double ring vibration at 550 cm^{-1} [18]. The IR spectra of the samples are shown in Figure 3. Most of the bands corresponding to the IR spectra of zeolite ZSM-5 are present in the IR spectra of samples S-1 to S-7. All samples showed vibration patterns at 950 – 1250 cm^{-1} and 420 – 500 cm^{-1}. The strongest vibration in the 950 – 1250 cm^{-1} region is assigned to a T-O stretching involving motion primarily associated with oxygen atoms. The next strongest band in the region of 420 – 500 cm^{-1} is assigned to a T-O bending mode. The presence of a double ring vibration at 550 cm^{-1} indicates the open structure characteristic of ZSM-5 framework structure.

Besides the main bands, samples S-6, S-7 and S-8 also showed a band at 620 cm^{-1}. This band corresponds to characteristic vibration of crystobalite of the RHA. From sample S-8 onward, the double ring band at 550 cm^{-1} for ZSM-5, was not detected,

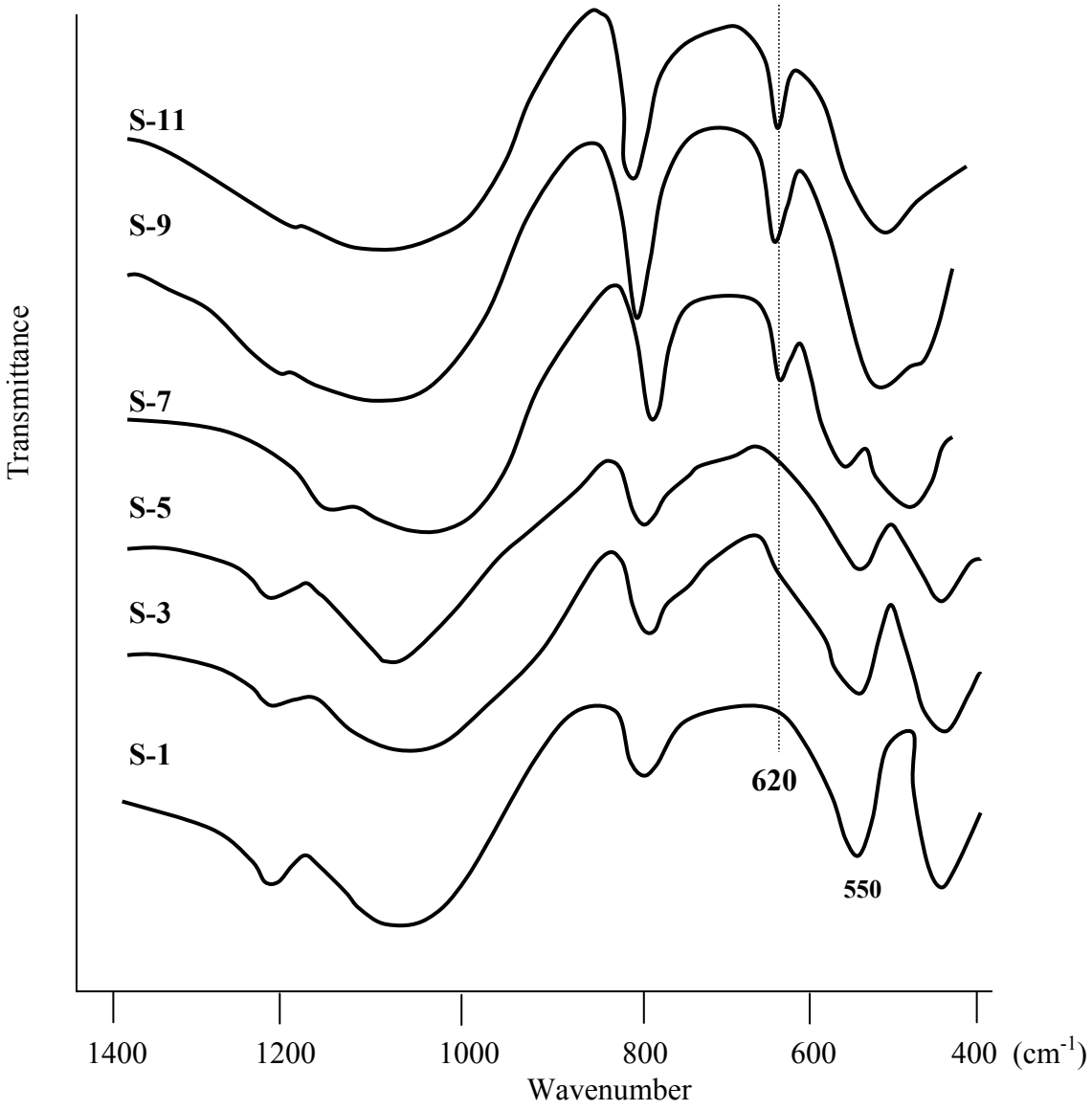

Figure 3: FTIR spectra of samples S-1, S-3, S-5, S-7, S-9 and S-11

indicating that the samples consist mostly of the starting RHA. However results from the XRD still showed the ZSM-5 phases as a minor constituent. Due to its small amount in the sample, the band is being overlapped by the broad band of bending vibration of the silica RHA which also vibrate at similar wavenumber.

In this study, samples with SiO_2/Al_2O_3 ratios of 30 or less, produced pure crystalline ZSM-5 indicating that all RHA has been transformed to ZSM-5 phase. When the silica to alumina ratio was increased up to 100 as in samples S-6 to S-8, the crystobalite phase of the starting RHA still exist in the sample. This showed that the amount of the initial SiO_2 was too high such that only part of the silica was used in the formation of ZSM-5. The failure to transform all RHA to ZSM-5 is due to the lack of alkalinity in the reaction mixtures which in this case was provided by the Na_2O and the template tetrapropylammonium cation. The alkali condition is necessary for the formation of any kind of zeolite including ZSM-5 as this will facilitate the dissolution of silica and alumina. Higher alkalinity will prolong the nucleation time and give more chances for silica to dissolve completely and later proceed to the formation of ZSM-5 framework with better crystallinity [16]. Apart from providing the alkalinity, the presence of the Na^+ and the TPA^+ cations also enhanced the crystallization rate. Without the Na^+, crystallization to the final ZSM-5 structure would proceed slowly [6].

Francisco [7] reported that when the silica to alumina ratio was made high, parameters such as the alkalinity and crystallization time need to be increased in order to transform all silica to ZSM-5. On the other hand, reducing the silica to alumina ratio in the initial gel, would facilitate the gel crystallization. Since the crystal formation of ZSM-5 in this study was allowed to form in 7 days, the presence of undissolved silica or RHA

in samples S-6 to S-8 indicated that the crystallization time was inadequate in order to dissolve all the silica to form pure ZSM-5. In addition to this, the lack of alkalinity in the initial reaction mixtures in these samples has resulted in the slow dissolution of the silica. The presence of Na^+ cation in the reaction mixture reduces the crystallization time and simultaneously increases the crystallization of ZSM-5. As such, it is suggested that the alkalinity and/or the crystallization time should be increased in order to ensure complete transformation of RHA to ZSM-5.

2. Effect of free alumina and low TPA^+

Another experiment was carried out in order to study the effect of the presence of alumina and the amount of TPA^+ cation in the initial gel compositions in the formation of ZSM-5. Comparison was made on samples S-9, S-10 and S-11 to that of sample S-1 which was taken as the reference sample. Sample S-9 was crystallized from initial gel composition without alumina while S-10 and S-11 were formed from the initial gel composition with less mole oxide ratio of TPA^+ cation compared to that of sample S-1. The concentration of alumina in the gel would influence the rate of crystallization of ZSM-5. When the alumina content of the gel is lowered when all the other factors remain unchanged, the rate of crystallization of ZSM-5 increased [6]. The apparent activation energies for ZSM-5 nucleation and for crystal growth are much lower in the absence of alumina and the induction period before crystals appeared is also shorter for the alumina-free system. For sample S-9 with free alumina in the reaction mixture, ZSM-5-like phase was also formed. The phase which is similar to ZSM-5 structure without aluminium is known as silicalite. However, only a small quantity of ZSM-5-like phase was produced and the rest of the sample contained unreacted RHA. This is in contrast with that of the

normal hydrothermal behavior of SiO_2 / Al_2O_3, in which lower reaction rates occurred, resulting in less ZSM-5-like phase formed within 7 days of crystallization. This finding is due to the slow dissolution of crystalline silica of the RHA by OH^- of the Na_2O in the absence of alumina. In this case the presence of small amount of alumina might be required to form aluminosilicate anions with the dissolved silica. This aluminosilicate anion is the precursor for the nucleation and crystal growth of the ZSM-5 [6] and its formation might help the dissolution of the rest of the silica.

The addition of template such as cation TPA^+ to the gel is to promote crystallization. The TPA^+ cations have been recognized as being able to form complexes with either silicate or aluminosilicate species by competing with the Na^+ ions for charge compensation of these silicates or aluminosilicate species [5]. These cations may stabilize the formation of certain subunits and then cause further replication of these primarily formed building units via a stereospecific hydrogen bond between the TPA^+ ions and oxygen anions of the silicates or aluminosilicates. Hence the presence of TPA^+ may be necessary for the formation of a particular structure or function as structure directing. This effect is now generally known as the templating effect in zeolite synthesis. For samples S-10 and S-11, in which the content of TPA^+ was reduced to 5 and 3 moles respectively, while other oxides remain the same, as in S-1, the same results were obtained as for sample S-9. Only a small quantity of ZSM-5 was produced. Due to the small quantity of ZSM-5 in the sample, the band at 550 cm^{-1} which is specific to the type of double ring vibration for ZSM-5 do not appear in the IR spectrum.

The amount of ZSM-5 that was formed greatly decreased with the decrease in the quantity of the template i.e. TPA^+ from 100% ZSM-5 crystallinity in S-1 to about 30 % in

S-10 and S-11 (Table 2). This showed that the effect of the amount of template is also crucial for the formation of enough secondary building units, SBUs [6] of ZSM-5 structure and proved that TPA^+ act as structure directing agents in the formation of ZSM-5 framework. Since the amount of TPA^+ cations has been reduced, the charge competition of silicate and alumina contributed by the TPA^+ was also reduced compared to Na^+. As a result, the subunits formed for the replication of structure formation of ZSM-5 was also reduced, resulting in the reduction of the amount of the ZSM-5 produced.

From the results, it is concluded that ZSM-5 structure is easily synthesized in the presence of TPA^+ cations and the rate of crystallization increased with increasing TPA^+ / SiO_2 ratio, at least up to 6. Decreasing the TPA^+ cations will reduce the crystallization rate resulting in a slow formation of ZSM-5 crystals, hence only a small amount of ZSM-5 were formed during the 7 days period.

Conclusion

Crystalline RHA has been proven to be active and can be utilized as an alternative silica source for the synthesis of zeolite ZSM-5. Zeolite ZSM-5 was successfully formed from crystalline RHA with initial molar composition of 5.4 – 10.0 Na_2O : 24.0 – 100.0 SiO_2 : 1.0 – 2.9 Al_2O_3 : 1800 – 3600 H_2O : 6-3 TPABr. However, only SiO_2 / Al_2O_3 ratios of 30 or less will produce pure ZSM-5. High silica to alumina ratio in the starting reaction mixture decreased the solubility of gel and reduced the crystallization rate for the formation of crystals. In order to transform all ash to ZSM-5 phase the alkalinity and time of crystallization need to be increased to ensure that all the silica is dissolved to form ZSM-5.

Acknowledgement:

Authors would like to thank the Ministry of Science and Environment for research fund under IRPA program, project no. 09-02-06-0057-SR0005/09-03.

References

1. Argauer, R.J. and Landolt, G.R. (1972) "Crystalline Zeolite ZSM-5 and Methods Of Preparing." U.S. Patent 3 702 886.

2. Szostak R., (1989) "Molecular Sieves: Principal of Synthesis and Identification", New York: Van Nostrand, Reinholg Catalysis Series

3. Bekkum H.V., Flanigen E.M. and Jansen J.C, (Eds), (1991), "Introduction to Zeolite Science and Practice." *Stud. Sur. Sci. Catal."* **58**, Netherlands: Elsevier

4. Chen, N.Y., William R.G. and Frank G.D. (1989) Shape selective Catalysis in Industrial Applications, Chemical Industries. Vol. 36, New York: Marcel Dekker Inc.

5. Davis M.E. (1998), "Zeolite-based Catalyst for Chemical Synthesis", *Microporous and Mesoporous Materials,* **21**, 21-27.

6. Barrer, R.M., (1982) *"*Hydrothermal Chemistry of Zeolites," London: Academic Press.

7. Fransisco J. M., Carmen M.L., Maria A. C., Caribary U. (1999). "Templat Free Synthesis and Catalytic Behaviour of Aluminium Rich MFI-Type Zeolites," *Applied Catalysis A: General,* **181**. 29 – 38.

8. Pan M., Lin Y.S, (2001), "Templat-free Secondary Growth Sythesis of MFI type Zeolite Membranes, "*Microporous and Mesoporous Materials",* **43,** 319-217

9 Wha Jung Kim, Myung Churl Lee, David T.Hayurst, (1998). *"*Synthesis of ZSM-5 at Low Temperature and Atmospheric Pressure in a Pilot-Scale Batch Reactor*",* *Microporous and Mesoporous Materials*. **26**, 133-141.

10 Coker E.N., Janson J.C, Francesco D.R., Francois F., Martens J.A., Jacobs P.A and Albert S.J., (2001), "ZSM-5 Synthesised on Space: Catalyst with Reduced External Surface Activity", *Microporous and Mesoporous Materials,***46,** 223-236

11 Rawtani A.V., Rao M.S. and Gokhale K.V.G.K, (1989) "Synthesis of ZSM-5 Zeolite Using Silica From Rice Husk Ash", *Ind. Eng. Chem*, **28,** 1411-1414

12. Ramli Z., Hamdan H., Endud S., Chinnappan S. M., Soon S.Y., Wong K. C., (2000) 'Sintesis dan Pencirian Zeolit Beta daripada Silika Sekam Padi' *Buletin Kimia,* Bil 1&2, 37-44

13. Hamdan H., Mohd Muhid M.N., Endud, S., Listiorini E., Ramli Z., (1997). "^{29}Si MAS NMR, XRD and FESEM Studies of Rice Husk Silica for the Synthesis of Zeolites". *J. Non-Crystal Solids*. **211**. 126-131.

14. Ramli, Z., Listiorini, E. and Hamdan, H. (1996) "Optimization and Reactivity study of silica in the synthesis of zeolites from Rice Husk." *Jurnal Teknologi* Issue:. 25, 27-36l

15. K. B. Pramod, M. S. Rao, K.V. G. K. Gokhale, (1981). "Synthesis of Mordenite Type Zeolite Using Silica from Rice Husk Ash", *Ind. Eng. Chem. Prod. Res. Dev.,* **20**, 721-726

16. Didik Prasetyoko (2001), "Sintesis Terus Zeolite Beta daripada Abu Sekam Padi dan Penggunaannya Sebagai Mangkin Heterogen Bagi Tindak Balas Friedel Craft", Universiti Teknologi Malaysia: MSc Thesis

17. Treacy, M. M. J., Higgins, J. B. and von Ballmoos, R. (1996). "Collection of Simulated XRD Powder Patterns for Zeolites", 3rd ed. Amsterdam: Elsevier

18. Flanigen E.M., Khatami H., and Szymanski H. A. (1971). "Infrared Structural Studies of Zeolite Frameworks", In: Robert F. Gould (Ed), *Advanced Chem. Series,* **101**, 201-227

Surface Acid Properties of Nb-Zeolite Beta Characterized By Infrared Spectroscopy and Temperature Programmed Desorption of Ammonia

Zainab Ramli, Marzita Abd Mazak and Farediah Ahmad
Department of Chemistry, Faculty of Science,
Universiti Teknologi Malaysia, 81310 UTM Skudai, Johor, Malaysia

Abstract : Zeolites are widely used as acid catalysts in organic reactions, such as isomerization, alkylation and acylation. In general, hydrogen form zeolite Beta (H-BEA) contains higher amount of Brönsted acid sites as compared to Lewis acid. In this study the surface acidity of zeolite Beta was modified by incorporating niobium oxides in order to increase the Lewis acidity of the catalyst. Different weight percentage of niobium (Nb) were incorporated into H-BEA (framework Si/Al = 11) by wet impregnation technique. The types and the amounts of acidities of the samples were determined by infrared technique (IR) using pyridine as probe base while the strength of the acid sites was measured by Temperature Programmed Desorption (TPD) of ammonia. IR results showed that all zeolite Beta and the modified sample contain both acidities with the amount of Brönsted were higher than Lewis acidity. The amount of Brönsted acid decreased with the increased percentage of Nb loadings. However the amounts of Lewis acid in H-BEA increased with Nb loading up to 2 %wt but decreased in 4 %wt Nb BEA samples. Ratios of the amount of Brönsted to Lewis acids showed that 4 %wt Nb on H-BEA sample has the lowest ratio (1.55) as compared to 2 %wt Nb BEA (1.78) and H-BEA itself (2.24) indicating that incorporated Nb has successfully increased the Lewis acidity of H-BEA samples with the optimum at 4 %wt Nb. TPD results showed that the strength and the amount of acid sites also increased after 2 %wt Nb loading and decreased after 4 %wt Nb loading.

Abstrak : Zeolit telah digunakan secara meluas sebagai mangkin asid dalam tindakbalas organic seperti pengisomeran, pengalkilan dan pengasilan. Secara umumnya, zeolit Beta dalam bentuk hidrogen (H-BEA) mempunyai lebih banyak tapak asid Brönsted berbanding Lewis. Dalam kajian ini , Keasidan zeolit Beta telah diubahsuai dengan memasukkan niobium oksida untuk meningkatkan jumlah asid Lewis didalam mangkin. Peratus berat niobium (Nb) yang berbeza telah dimasukkan kedalam H-BEA (Si/Al bingkaian = 11) dengan kaedah penepuan basah. Jenis dan jumlah keasidan sampel ditentukan oleh kaedah IR menggunakan piridin sebagai bes prob sementara kekuatan tapak asid diukur menggunakan TPD ammomia. Hasil IR menunjukkan semua zeolit Beta dan sampel terubahsuai mengandungi kedua-dua tapak asid dengan jumlah tapak asid Brönsted lebih tinggi dari Lewis. Jumlah asid Brönsted berkurang dengan pertambahan peratus berat muatan Nb. Walaubagaimanapun jumlah asid Lewis dalam H-BEA bertambah selepas dimuatkan dengan 2 %berat Nb dan berkurang selepas dimuatkan dengan 4 % berat Nb. Jumlah nisbah asid Brönsted kepada Lewis menunjukkan sampel 4 %wt Nb BEA mempunyai nisbah paling rendah (1.55) berbanding 2 %wt Nb BEA (1.78) dan H-BEA sendiri (2.24) menunjukkan kemasukan niobium telah berjaya meningkatkan keasidan Lewis dalam sample H-BEA dengan kadar optimum pada 4 %berat Nb. Hasil TPD menunjukkan kekuatan dan jumlah tapak asidjugabertambahselepas dimuatkan dengan 2 %niobium dan berkurang selepas dimuatkan dengan 4 % niobium.

Introduction

Zeolites possess acid sites on the surface which can catalysed many reactions such as alkylation, isomerization, amination, cracking and etc [1]. The acid sites in zeolites are linked to tetrahedral aluminium atoms in the framework of the zeolite. The framework alumimium atoms negatively charged and balanced by extraframework cations, represent potential active acid site [2]. Transitions metals in different oxidation states and coordinations can be introduced into different zeolite structures either as charge-neutralizing cations, supported metal clusters, complexes, or lattice cations.

The acidity of zeolite might be increased by using transition metal oxide as a supported such as niobium, vanadium, gallium and etc. There is little information about the introduction of niobia into zeolite lattices. Because niobia salts are very sensitive to moisture, the traditional methods for modification of zeolites, specifically slurrying in aqueous solution, cannot be applied. Therefore, a solid-state interaction between niobia and a zeolite was explored as a method for Nb incorporation to zeolites [3]. Chang et al [4] reported that a Nb-

containing ZSM-5 zeolite was prepared by the impregnation of H-ZSM-5 or Na-ZSM-5 with a freshly prepared aqueous solution of niobium oxalate.

In catalysis, niobium compounds can play various functions, as follows: promoter, support, solid acid catalyst or redox materials [5;6]. Among the niobium compounds, hydrated niobium pentoxide (niobic acid, $Nb_2O_5.\ nH_2O$) has revealed high catalytic activity, selectivity, and stability for acid catalyzed reactions. The surface acid strength of hydrated niobium oxide corresponds to the acid strength ($H_o \leq -5.6$) of 70% sulfuric acid. Thermal treatment of niobic acid generates surfaces containing both Lewis acidic and Brönsted acidic sites, the relative proportions of the two types of site being sensitive to pretreatment temperature. Infrared spectra of adsorbed pyridine established that the highest number of Brönsted sites occurred after heating at 373 K whereas heating at 573 K produced the highest number of Lewis sites [7]

Experimental

Zeolite Beta was synthesized using rice husk ash (RHA) as a silica sources and the ash is in the form of amorphous silica. The synthesis of zeolite beta was carried out hydrothermally at 150˚ C in a stainless steel autoclave for six days from mixtures containing amorphous silica from RHA, sodium aluminate (54% Al_2O_3; 41% w/w Na_2O, technical grade), tetraethylammonium hydroxide (40% solution in water, Fluka Chimika), sodium hydroxide (99%, Merck), based on method described by Didik [8]. The gel is prepared according to the following molar chemical composition:

$1.96Na_2O : 27SiO_2 : Al_2O_3 : 5TEA_2O : 240H_2O.$

The Na-form of zeolite Beta samples (Na-BEA) which contain Na cation was converted to the NH_4-form (NH_4-BEA) by ammonium cation. Ion exchange was done by using of ammonium nitrate solution (1M). The Na-BEA sample (5 g) was mixed with ammonium nitrate solution (1 M). The mixture was stirred for about 4 hours at 80˚ C. Then, zeolite was filtered and washed repeatedly with distillated water. The ammonium exchange was repeated three times. Finally, the protonated form (H-BEA) was obtained by calcining the NH_4-form at 550 ˚C for 4 hours.

Zeolite Beta was modified by introducing niobium oxide by wet impregnation method. Niobium (V) pentoxide ($C_{10}H_{25}NbO_5$) was used as the source of Nb species. Niobium (V) pentoxide was dissolved in 50 mL of 2-propanol, followed by the addition of 1 g of zeolite Beta in hydrogen form (H-BEA). The mixture was stirred for 3 hours at 80˚C. Then the mixture was heated at 60˚C overnight to vaporize the solvent. The impregnated samples thus obtained were washed thoroughly with distillated water and finally the samples were dried overnight at 100 ˚C. The amount of Niobium (V) pentoxide taken is calculated by using the following equations:

$$\text{Wt \% loading} = \frac{(\text{Wt.(Nb)})}{(\text{Wt.(Nb)}) + (\text{Wt.Zeo})} \times 100\% \qquad \text{(Eq 1.1)}$$

$$\text{Wt Nb (V) pento} = \frac{(\text{MW (Nb (V) pento) x Wt Nb}}{\text{AW Nb x Purity Nb (V) Etho}}$$

Wt.M = weight of metal (Nb)
Wt.Zeo = weight of zeolite
Wt Nb (V) Etho = weight of Niobium (V) Ethoxide taken
MW Nb (V) Etho = molecular weight of Niobium (V) Ethoxide
Wt Nb = weight of Niobium metal
AW Nb = atomic weight of Niobium
Purity Nb (V) Etho = Purity of Niobium (V) Ethoxide taken

The products obtained were characterized by XRD, UV-Vis DR, FTIR pyridine and TPD of ammonia.

Results and Discussion

X-ray Diffraction Pattern

Niobium oxide was incorporated into zeolite Beta (H-BEA) for the modification of the acidity properties. The X-ray diffractograms patterns of H-BEA, zeolite Beta with 2% wt of niobium loading (2 %wt Nb BEA) and zeolite Beta with 4% wt of niobium loading (4%wt Nb BEA) are presented in Figure 1. The XRD pattern of incorporated niobium zeolite Beta samples (2 %wt Nb BEA and 4 %wt Nb BEA) show similar profiles to the parent zeolite Beta (H-BEA). These results indicate that the whole structure of zeolite Beta is still intact even after the incorporation of niobium. The existence of niobium species on the zeolite surface could not be observed from the XRD diffractogram. This is due to the low percentage of niobium loading such that the niobium species dispersed on zeolite surface in monolayer coverage.

.

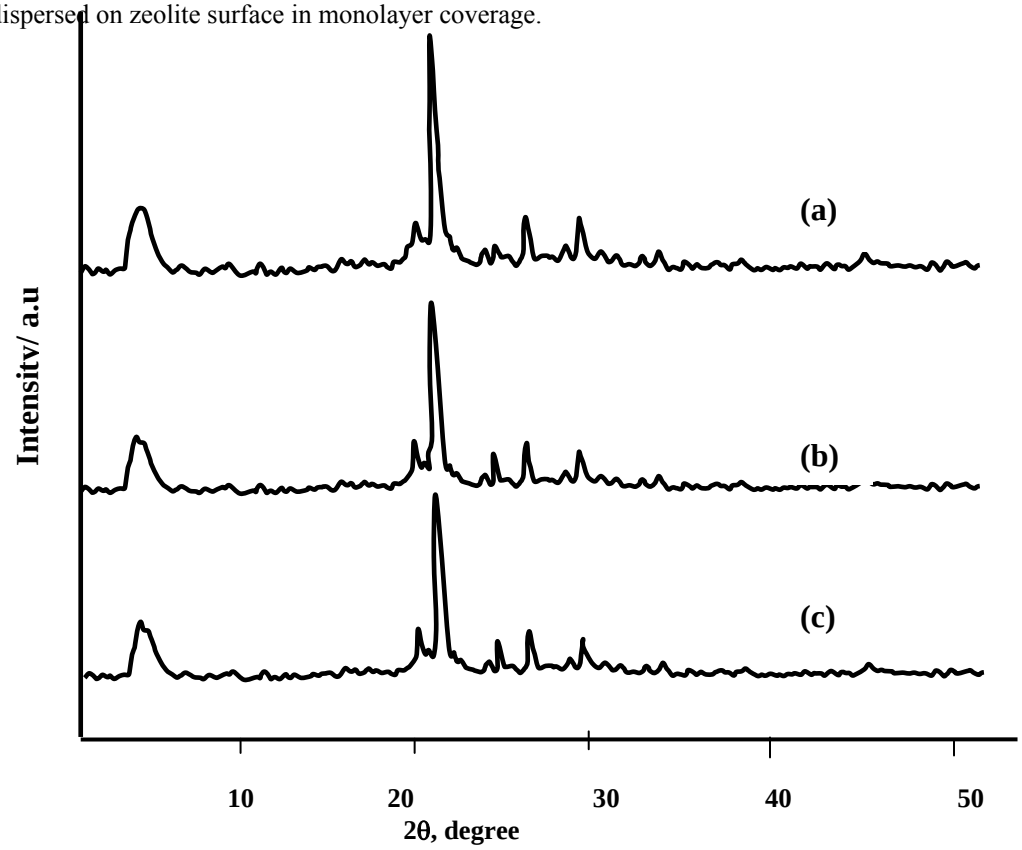

Figure 1: X-Ray diffractogram pattern of (a) zeolite Beta (H-BEA) (b) zeolite Beta with 2% wt of niobium loading (2 %wt Nb BEA) and (c) zeolite Beta with 4% wt of niobium loading (4 %wt Nb BEA).

The percentage of crystallinity of the samples is tabulated in Table 1. The crystallinity of 2 %wt Nb BEA sample decreased slightly compared to the parent zeolite Beta (H-BEA). Sample 4 %wt Nb BEA gave the lowest crystallinity compared to others. It is indicates that the crystallinity of niobium zeolite Beta sample decrease with the increasing of % wt of niobium loading. The decreasing of the crystallinity is due to the increasing of % wt of niobium loading up to 4% wt. The high content of niobium will increase the strength of niobic acid. This will reduce the crystallinity of the zeolite framework.

Ultra Violet Visible Diffuse Reflectance (UV-Vis DR)

UV-Vis DR spectroscopy has been extensively used to characterize the nature and coordination of metal oxide or metal in substituted molecular sieves [9]. The UV-Vis DR spectra of the samples are shown in Figure 2. The UV-Vis spectrum of the precursor niobic acid (Nb) sample exhibits a shoulder band at around 250 nm and a maximum band at around 290 nm. The band centered at at 250 nm was assigned to tetrahedral niobium linked to zeolite surface and the band at 290 nm was attributed to octahedral Nb_2O_5 [9]. It is indicates that the Nb precursor alone exist in two frameworks for the tetrahedral and octahedral structure.

Table 1: Crystallinity of zeolite Beta (BEA-11) and zeolite Beta with different % wt of niobium loading.

Sample	Wt of niobium loading (%)	Crystal content	% crystallinity of zeolite beta
H-BEA	-	BEA	100
2 %wt Nb BEA	2	BEA	92.7
4 %wt Nb BEA	4	BEA	62.9

The UV-Vis spectra of 2 %wt Nb BEA and 4 %wt Nb BEA display broad peaks with maximum bands at 254 nm and 243 nm respectively. No adsorption peak was observed at around 290 nm. The parent zeolite Beta (H-BEA) did not have any adsorption peak as expected. It indicated the presence of niobium species on zeolite Beta surface might be in the tetrahedral form. Besides, the band appear at around 250 nm could imply that the tetrahedral polymeric NbO_4. Tanaka *et al.* and Gao *et al* [10;11] have been reported that the single tetrahedral of niobium species appeared at around 220 nm. All the bands in the UV-Vis DR spectra for all samples were attributed to the charge transfer transitions O^{2-} to Nb^{5+} which can be associated to the energy gap between the O 2p valence band and the Nb 4d conduction band [12,13].

Close examination showed that the band at 243 nm in 2 %wt Nb BEA sample was shifted to higher wavelength at 254 nm in 4 %wt Nb BEA sample. It is noted that the niobium content was increased from 2% niobium loading (2 %wt Nb BEA sample) to 4% in 4 %wt Nb BEA sample. Similar results were reported by Damyanova *et al.* [14] and Mendes *et al.* [15] in which the position and width of the UV absorption bands of niobium-oxide species depend on the niobium content and the size of niobia crystallites. The decreased in Nb concentration leads to a blue shift of the charge transfer band, caused by decreasing of the size of niobium-oxide species. With decreasing of niobium loading, the ligand-metal charge transfers (LMCT) maximum peak shifts from higher wavelength to lower wavelength.

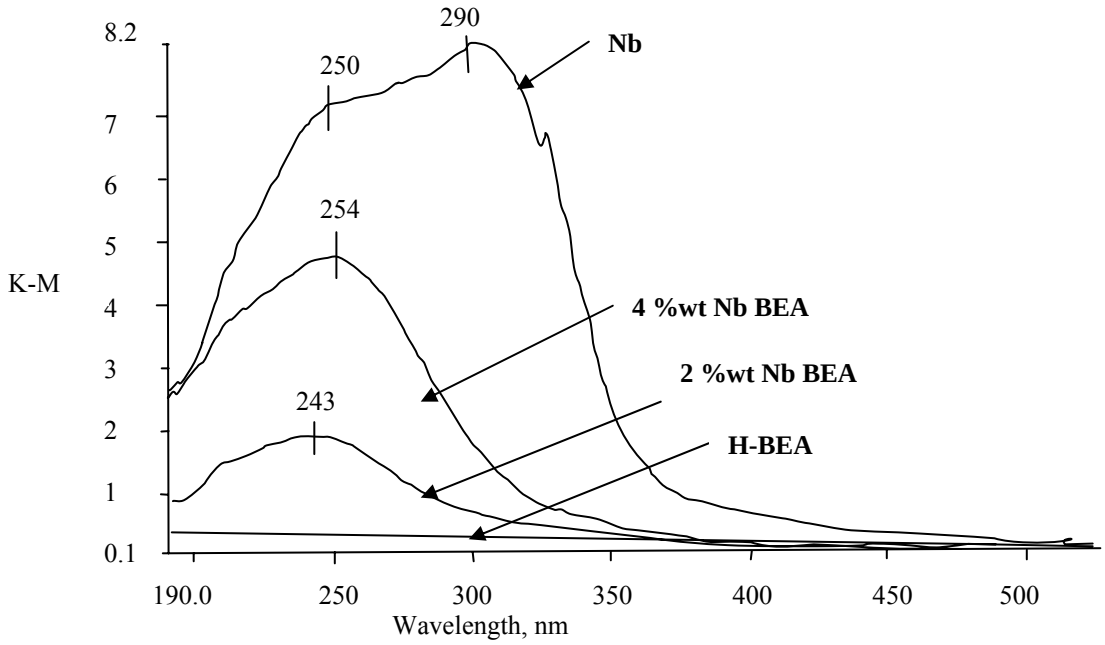

Figure 2: UV-Vis spectra of niobic acid (Nb) sample, zeolite Beta (H-BEA) and zeolite Beta with 2% wt of niobium loading (2 %wt Nb BEA) and zeolite Beta with 4% wt of niobium loading (4 %wt Nb BEA)

FTIR pyridine

The effect of niobium loading to zeolite Beta towards hydroxyl stretching region was also investigated using FTIR spectroscopy. Figure 3 shows IR spectra of H-BEA and H-BEA with niobium at different wt% loading which were recorded after heating under vacuum ($<10^{-2}$ mbar) at 400 °C for 16 hours. The IR spectra of zeolite Beta with niobium loading samples (2 %wt Nb BEA and 4 %wt Nb BEA) show similar pattern to that of the parent zeolite Beta (H-BEA). However, the intensity of the bridging hydroxyl band at around ~ 3600 cm^{-1} decreased after the samples loaded with niobium. The decreasing of the bridging hydroxyl bands, suggests that some of niobium species on the zeolite surface has reacted with the bridging hydroxyl groups in zeolite framework.

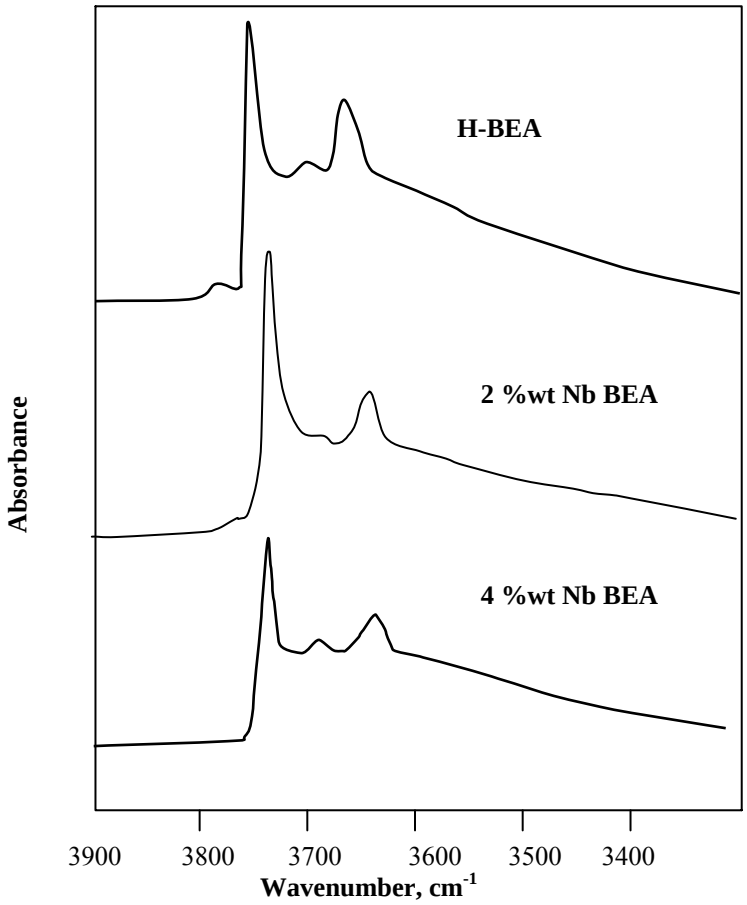

Figure 3: IR spectrum of hydroxyl groups of zeolite Beta (H-BEA) and zeolite Beta with different % wt of niobium loading at 400 ºC

Figure 4 exhibits the FTIR spectra for sample H-BEA, 2 %wt Nb BEA, 4 %wt Nb BEA and the niobic acid (Nb) as precursor after pyridine adsorption and desorption at 150 °C. The FTIR was recorded in the range between 1400 and 1700 cm^{-1}, where bands due to skeletal vibrations of the pyridine ring can be observed. The calculated amount of Brönsted and Lewis acid sites in all samples are summarized in Table 2. It is noted that 2 %wt Nb BEA samples has slightly higher Brönsted acid sites compared to the parent zeolite Beta (H-BEA). The finding suggests that niobium has contributed to the increase of Brönsted acidity in the sample of niobium zeolite Beta. This was proved by the appearance of Brönsted acid sites in the IR spectrum of Nb precursor.

The amount of Lewis acid sites also increased after niobium loading in 2 %wt Nb BEA sample. Similarly, the increase is expected as the IR spectrum for niobic acid shows higher Lewis acid sites [16]. However, an increase of niobium oxide content caused the decrease in the Brönsted as well as Lewis acid sites in 4 %wt Nb BEA samples. Besides the low crystallinity of the sample, the results may be due to coverage of niobium on the surface of zeolite Beta that affects the acidic property of the bulk sample [17]. Based on the finding from XRD, UV-Vis and acidity study, we proposed the models for the surface structure of zeolite Beta with niobium loading as shown in Figure 5. It is proposed that the niobium species on zeolite surface in tetrahedral form and possess polymeric NbO_4 [18].

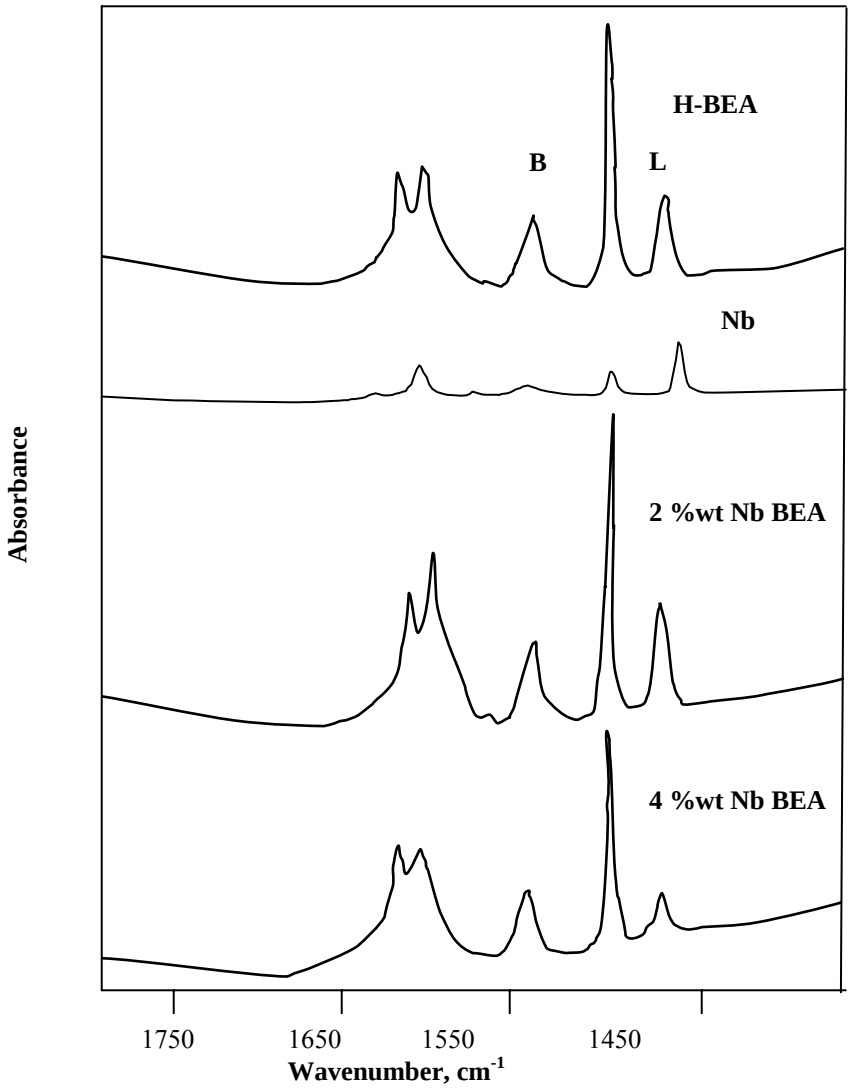

Figure 4: FTIR spectrum of zeolite Beta (H-BEA); niobic acid (Nb) and zeolite Beta with different % wt of niobium loading (2 %wt Nb BEA and 4 %wt Nb BEA) after pyridine desorption at 150 °C

Table 2: The amount of Brönsted and Lewis acid sites in zeolite Beta samples.

Sample	Acidity, mmole/g		Ratio of B/L
	Brönsted (B)	Lewis (L)	
H-BEA	1.30	0.58	2.24
Nb	0.10	0.15	0.69
2 %wt Nb BEA	1.39	0.78	1.78
4 %wt Nb BEA	0.59	0.38	1.55

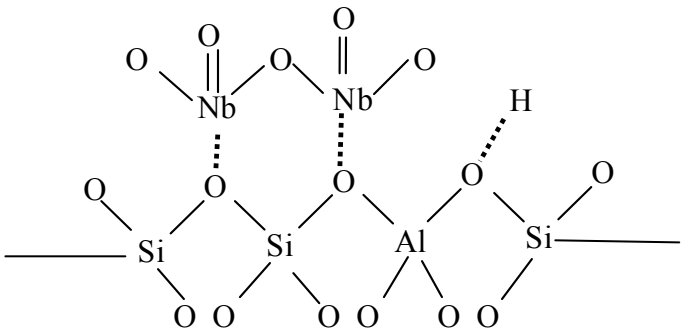

Figure 5: Proposed model for the surface structure of zeolite Beta with niobium loading

Temperature Programmed Desorption (TPD) of Ammonia

Figure 6 exhibits the TPD profiles of H-BEA, 2 %wt Nb BEA and 4 %wt Nb BEA samples. As shown in Figure 6, the TPD thermogram of H-BEA consists of two peaks, while the TPD thermogram of 2 %wt Nb BEA and 4 %wt Nb BEA exhibit three peaks. The profile of the TPD thermogram of 2 %wt Nb BEA shows the increasing of peak intensity and the peak shifted about 10 °C to higher temperatures. One may observed from the results that the amount of desorbed ammonia has increased in 2 %wt Nb BEA sample. The results were supported by FTIR pyridine finding in which the presence of niobium has contributed to the increase of the acid strength and the amount of acid sites in H-BEA sample. The shift of the peaks indicated that the sample of 2 %wt Nb BEA has a higher acid strength compared to the parent H-BEA.

However, sample 4 %wt Nb BEA gives very low peak signals compared to both H-BEA and 2 %wt Nb BEA samples. The result indicates that the 4 %wt Nb BEA sample gives the lowest amount of acid sites compared to H-BEA and 2 %wt Nb BEA sample. This is due to the increasing content of niobium which covered most of zeolite surface and consequently reduces the amount of acid sites. Similar observation occurs with the FTIR

pyridine results. In addition, sample 4 %wt Nb BEA also showed lower temperature peaks in both low and high temperature region compared to H-BEA and 2 %wt Nb BEA. This indicates that the sample 4 %wt Nb BEA has the lowest acid strength.

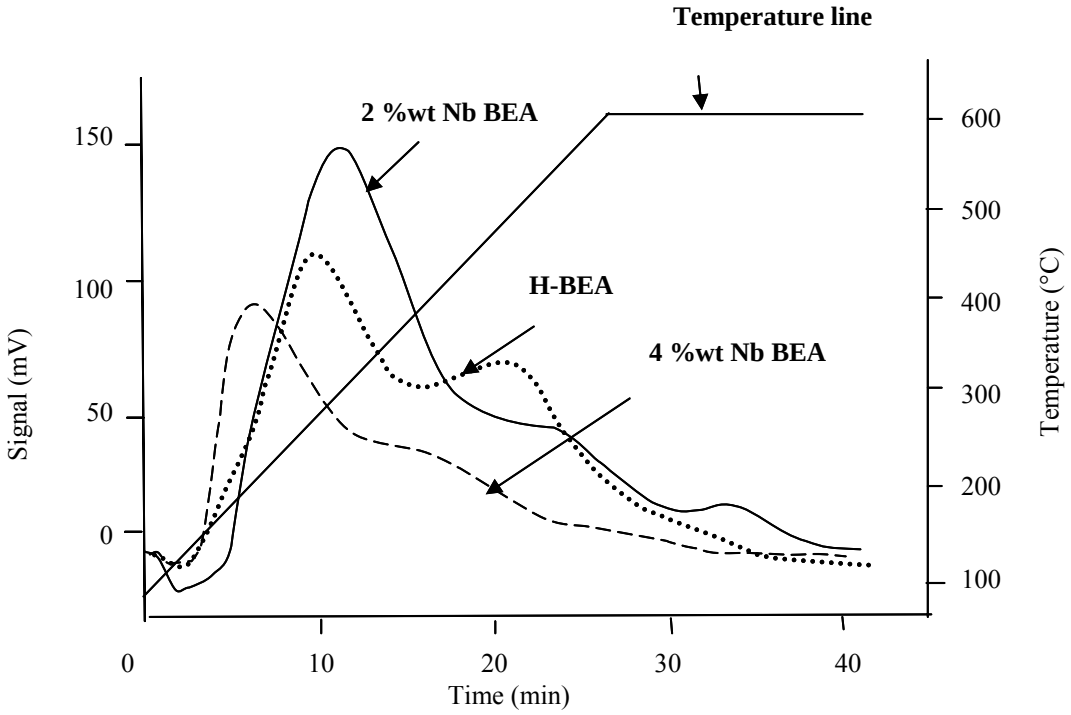

Figure 6: TPD of ammonia spectra of zeolite Beta (H-BEA) and zeolite Beta with different wt% of niobium loading (2 %wt Nb BEA and 4 %wt Nb BEA)

Table 3: Quantitative results of unmodified zeolite Beta (H-BEA) and modified zeolite Beta (2 %wt Nb BEA and 4 %wt Nb BEA)

Samples	Peak I (Low-temperature)		Peak II (High-temperature)		Peak II (High-temperature)	
	T (°C)	NH_3 desorbed (µmol/g)	T (°C)	NH_3 desorbed (µmol/g)	T (°C)	NH_3 desorbed (µmol/g)
H-BEA	253	3152	421	2037	-	-
2 %wt Nb BEA	301	5419	505	1581	600	153
4 %wt Nb BEA	199	1946	373	810	590	73

Conclusion

The crystallinity of zeolite Beta slightly decreased after incorporating with 2% wt niobium with markly decreased when niobium loading increased up to 4% wt. UV-Vis DR results showed that the niobium species in zeolite Beta samples are mainly in the tetrahedral coordination. The amount of Brönsted and Lewis acid sites in zeolite Beta increased after incorporated with niobium, with markly increased in Lewis acid sites after 2% wt niobium loading. This indicates that the niobium has contributed to the increase in the amount of Brönsted and Lewis acid sites in the sample. However the Brönsted and Lewis acid sites decreased after niobium loading increased up to 4% wt due to the low crystallinity of the sample. TPD results showed the strength and the amount of acid sites also increased after 2% wt niobium loading and decreased after 4% wt niobium loading.

Acknowledgement:

Authors would like to thank the Ministry of Science, Technology and Inovation, MOSTI, for research fund under IRPA program, project no. 09-02-06-0057 SR0005/09-03

References

1. Tanabe, T., and Hölderich, W. F. (1999). Industrial application of solid acid-base catalysts. *Applied Catalysis A: General.* 181: 399-434.
2. Barrer, R. M. (1982). *Hydrothermal Chemistry of Zeolites.* London: Academic Press
3. Nowak, I. and Ziolek, M. (1999). Niobium compounds: Preparation, Characterization, and Application in Heterogeneous catalysis. *American Chemical Society.* 99: 3603-3624.
4. Chang, Y. F., Somorjai, G. A., and Heinemann, H. (1995). An $^{18}O_2$ temperature-Programmed Isotope Exchange Study of Transition-Metal-Containing ZSM-5 Zeolites Used for Oxydehydrogenation of Ethane, *Journal of catalysis*. 154: 24-32
5. Tanabe, K., and Okazaki, S. (1995). Various reactions catalyzed by niobium compounds and materials. *Applied Catalysis A: General.* 133: 191-218.
6. Ziolek, M. (2003). Niobium-containing catalysts-the state of the art. *Catalysis today.* 78: 47-64.
7. Ahmad, I., Dines, T. J., Anderson, J. A., and Rochester, C. H. (1999). Fourier-transform infrared study of the adsorption of acetophenones on niobic acid. *Spectochimica Acta Part A.* 55: 397-409
8. Didik, P. (2001). *Pengoptimuman sintesis zeolite beta daripada abu sekam padi:pencirian dan tindakbalas pemangkinan Friedel-Crafts.* UTM. Tesis MSc.
9. Gallo, J. M.R., Paulino, I. S., and Schuchardt, U. (2004). Cyclooctene epoxidation using Nb-MCM-41 and Ti-MCM-41 synthesized at room temperature. *Applied Catalysis A: general.* 266**:** 223-227
10. Tanaka, T., Nojima, H., Yoshida, H., Nakagawa, H., Funabiki, T., and Yoshida, S. (1993). Preparation of highly dispersed niobium oxide on silica by equilibrium adsorption method. *Catalysis Today.*16: 297-307.
11. Gao, X., Wachs, I. E., Wong, M. S., and Ying, J. Y. (2001). Structural and Reactivity Properties of Nb-MCM-41: Comparison with That of Highly Dispersed Nb_2O_5/SiO_2 Catalysts. *Journal of Catalysis.* 203: 18-24.
12. Armaroli, T., Busca, G., Carlini, C., Giuttari, M., Galletti, A. M. R., and Sbrana, G. (2000). Acid sites characterization of niobium phosphate catalysts and their activity in fructose dehydration to 5-hydroxymethyl-2-furaldehyde. *Journal of Molecular CatalysisA: Chemical.* 151: 233-243.
13. Resini, C., Panizza, M., Raccoli, F., Fadda, M., Maria M, Carnasciali, Busca, G., Lopez, E. F., and Escribano, V. S. (2003). Oxidation of ethane and cyclohexane over vanadia-niobia-silica catalysts. *Applied Catalysis A: General.* 251**.** 29-38
14. Damyanova, S., Dimitrov, L., Petrov, L., Grange, P. (2003). Effect of niobium on the surface properties of Nb_2O_5-SiO_2-supported Mo catalysts. *.Applied Surface Science.* 214: 68-74
15. Mendes, F. M. T., Perez, C. A., Soares, R. R., Noronha, F. B., and Schmal, M. (2003). Ammonium complex of niobium as a precursor for the preparation of Nb_2O_5/Al_2O_3 catalysts. *Catalysis Today.* 78: 449-458.
16. Moraes, M., Pinto, W. D. S. F., Gonzalez, W. A., Carmo, L. M. P. M. Pastura, N.M.R., and Lachter, E. R. (1996). Benzylation of toluene and anisole by benzyl alcohol catalyzed by niobic acid: influence of pretreatment temperature in the catalytic activity of niobic acid. *Applied Catalysis A:General.* 138: L7-L12.
17. Francisco, M. S. P., Landers, R., and Gushikem, Y. (2004). Local order structure and surface acidity properties of a Nb_2O_5/SiO_2 mixed oxide prepared by the sol gel processing method. *Journal of Solid State chemistry.* 177: 2432-2439.
18. Yoshida, H., Tanake, T., Yoshida, T., Funabiki, T., and Yoshida, S. (1996). Control of the structure of niobium oxide species on silica by the equilibrium absorption method. *Catalysis Today.* 28: 79-89.

DELAMINATED ZEOLITE, ITQ-6 AS HETEROGENEOUS CATALYST FOR FRIEDEL CRAFTS ALKYLATION

Zainab Ramli, Noor Aishikin Mohd Yusoff and Halimaton Hamdan

Department of Chemistry, Faculty of Science, Universiti Teknologi Malaysia, 81310 UTM Skudai, Johor, Malaysia

Keywords: Mesoporous ITQ-6, Microporous FER, alkylation of resorcinol

Abstract: The ability of ITQ-6, a kind of mesoporous zeolitic material to replace microporous zeolite as catalyst has attracted particular attention. In this study, modification of a precursor of microporous ferrierite, PREFER to mesoporous material, ITQ-6 was carried out by delamination technique. The XRD results show that the crystalline phase of PREFER diminished for the sample after delamination. Porosity study of the ITQ-6 sample shows formation of homogeneous mesopores in the size between 3.5-4.0 nm. The acidity study indicates that ITQ-6 still contains appreciable amounts of Brönsted and Lewis acidities. Catalytic evaluation of the resulting material, ITQ-6 was carried out in the alkylation of resorcinol with methyl *tert*-butyl ether which gave 4-*tert*-butyl resorcinol and 4,6-*di*-*tert*-butyl resorcinol as main products. The conversion of resorcinol when using ITQ-6 was ten times higher than ferrierite, FER with similar selectivity of disubstituted product. It shows that the mesoporosity of ITQ-6 was responsible for the higher activity of the catalyst in the reaction.

Abstrak: Kebolehan ITQ-6 sejenis bahan zeolit berliang meso menggantikan zeolit berliang mikro sebagai mangkin telah menarik perhatian. Dalam kajian ini, pengubahsuaian bahan awal ferrierit berliang mikro, PREFER kepada bahan berliang meso ITQ-6 dilakukan melalui teknik penyahlaminan. Keputusan XRD menunjukkan yang fasa hablur PREFER musnah selepas proses penyahlaminan. Kajian keliangan terhadap sampel ITQ-6 menunjukkan pembentukan liang meso yang homogen dengan saiz liang antara 3.5-4.0 nm. Kajian keasidan menunjukkan yang ITQ-6 masih mengandungi keasidan Brönsted dan Lewis dengan amoun yang agak banyak. Kereaktifan bahan yang terhasil, ITQ-6 diuji dalam tindak balas pengalkilan resorsinol dengan metil *tert* butyl eter yang menghasilan 4-*tert*-butil resorsinol and 4,6-*di*-*tert*-butil resorsinol sebagai hasil utama. Pertukaran resorsinol apabila menggunakan ITQ-6 adalah sepuloh kali lebih tinggi daripada ferrierit, FER, dengan kepilihan yang sama bagi hasil dwitertukarganti. Ini menunjukkan yang ITQ-6 yang berliang meso bertanggungjawab ke atas kereaktifan mangkin dalam tindak balas.

Introduction

The Friedel Crafts alkylation of resorcinol with methyl *tert*-butyl ether or equivalent alkylating agents is known to give mono *tert*-butylated product (4-*tert*-butyl resorcinol) and further alkylation will lead to the formation of di-*tert*-butylated product (4,6-di-*tert*-butyl resorcinol) [1]. The products (butylated dihydroxybenzenes) are useful materials in the synthesis of antioxidants, polymer stabilizer and in the treatment of mitochondrial respiration ailments. Therefore this reaction has become industrially important.

Presently, Lewis acid type catalysts for aromatic alkylations include aluminum chloride, ferric chloride, and boron trifluoride. Those of the Bronsted-Lowry acid type are fluoride acid, sulfuric acid and phosphoric acid. However, these traditional catalysts have limitations such as environmental pollution hazards arising from the disposal of potential toxic wastes, reactor corrosion and difficulty in handling. In order to avoid these problems many efforts have been devoted in the search of solid acid and base catalysts more selective, safe, environment friendly, generable, reusable and which need not to be destroyed after reaction. Therefore acidic oxide catalysts of the silica alumina type especially zeolite and cation-exchange resins are becoming increasingly useful as heterogeneous catalysts.

Throughout the 1990s, environmentalism remains a foremost concern, with zeolite in the forefront as solutions to new challenges in the generation of "Green Chemistry". The versatility of zeolite has allowed its application particularly as heterogeneous catalyst in acid [2], base [3] and redox [4] reactions. Over a

wide range of solid acids, zeolites hold high acidities on their surface and have received much attention in industry [5] and organic synthesis [6]. Uses of zeolite in the Friedel-Crafts reactions were extensively been studied [7,8].

The productions of fine chemicals are frequently facing the problem of producing products much bulkier than reactants when using zeolite as catalyst. The products remain occluded in the zeolite blocking the pores and deactivating the catalyst. Efforts have been focused to prepare a catalyst which has the properties of zeolite with larger pores size.

Since the discovery of new method for modification of zeolite from micropore to mesopore through delamination [9], further research on it has enlarged the field of zeolites. Nowadays the research interest focus on characterization, the mechanism of the formation, and synthesis of new materials based on the zeolite synthesis concept and morphology control and technical application of modified mesopore zeolite.

The delaminated zeolite was proved to be active in the acetalization of phenylacetaldehyde with glycerol [10], epoxidation of 1-hexene [11] and hydroxyalkylation of 2-methoxynaphthalene with paraformaldehyde [12]. In addition, by using a type of delaminated zeolite known as ITQ-6 it opens an alternative route way in order to catalyze the reaction that involved bulky chemicals and products. Therefore a study on the ability of delaminated zeolite, ITQ-6 as catalyst in the Friedel Crafts alkylation was carried out in this work.

Experimental

Materials

The precursor of ferrierite type zeolite material was synthesized with the ratio of $10SiO_2$:$1Al_2O_3$:$15NH_4F$:5HF:10R:$100H_2O$ where R is the organic template (R=4-amino-2,2,6,6-tetramethylpiperidine) used following the method described by Schreyeck *et al.* [13]. The as-synthesised material denoted as PREFER (precursor of ferrierite).

ITQ-6 sample was prepared by swelling the laminar PREFER according to the procedure described by Concepcion *et al.* [14]. A portion of PREFER material was calcined at 550 ^oC to yield the formation of microporous FER type zeolite.

Catalytic reaction

The catalytic reactions were conducted batchwise in 25 mL round bottle flask equipped with a condenser and stirred well. In a typical run, 5 mmole of resorcinol, 15 mmole of methyl tert-butyl ether and 100 mg freshly activated at 200 ^oC catalyst were used. The reactor was introduced into the thermostated bath at 80 ^oC, 100 ^oC and 120 ^oC for 24 hours. The mixtures of the reaction were analyzed using gas chromatography (GC).

Apparatus and procedure

The extent of crystallization and phase purity was evaluated for all samples by recording X-ray diffractograms using Seimens 500 Kristalloflex with Cu Kα radiation, (λ = 1.54056 A^o, 40 kV, 40 mA) in the 2θ range of 2-40^o at ambient temperature. Scanning was carried out in the step interval 0.05^o with counting time of 1 second per step.

Framework vibration, surface hydroxyl groups and acid sites were determined using Perkin Elmer Spectrum One FTIR spectrometer. The framework was characterized using KBr technique. On the other hand for surface hydroxyl group and acid sites study, self supported disc was prepared and placed in a glass cell equipped with CaF_2 windows. Sample was heated at 400 ^oC under vacuum condition (P ~ 1 x 10^{-7} mbar) overnight. Surface hydroxyl groups were recorded at room temperature. For acidity study, the

sample was dehydrated at 400 °C under vacuum (P ~ 1 x 10^{-7} mbar). Adsorption of pyridine on dehydrated sample was carried out at room temperature followed by desorption under vacuum at 150 °C for 1 hour in order to determine the existence of the acid sites.

The specific surface area and the pore size distributions of samples were determined by BET technique using ASAP 2010 instrument.

Field Emission Scanning Electron Microscope (FESEM), Carl Zeiss Supra Series model was used to determine the morphology and crystal size of the samples.

Identifications of the reactants and desired products were carried out using GC, Model No: Agilent 6890N with Ultra 1 methyl siloxane capillary column (25 m length, 0.25 diameters with 0.2 μm wall thickness). Confirmation of the products was done by comparing the retention time of the authentic samples.

Results and Discussion

X-ray Diffraction (XRD)

ITQ-6 can be obtained through delamination process of layered zeolite ferrierite precursor. The PREFER sample was first swollen to form bulk material by intercalation of swelling agent, cetyltrimethylammonium bromide (CTABr) between the PREFER layers through ion exchange. This bulk material is assigned as preITQ-6. Then the preITQ-6 was delaminated through sonication to produce ITQ-6 followed by calcinations in order to remove the organic templates. This will lead to the formation of material called mesoporous ITQ-6. All the treatments done to the PREFER sample was monitored using XRD technique. ITQ-6 is formed by single layers organized in a "house of cards"-type structure, which is thermally stable and presents a well-defined and homogeneous external surface area. The schematic process of preparing ITQ-6 is illustrated in Figure 1.

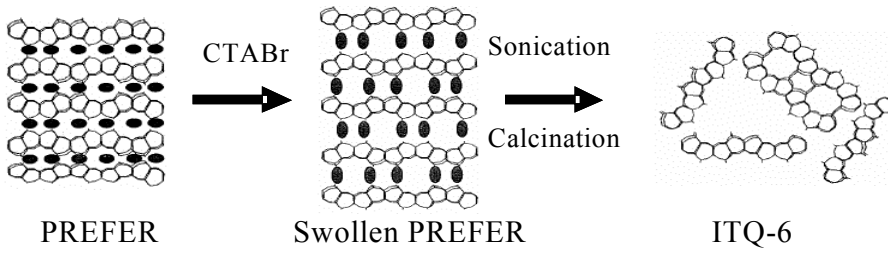

Figure 1: Scheme for preparing ITQ-6 material.

Figure 2 shows the X-ray diffractogram of PREFER samples after each treatment. As can be seen in Figure 2, the swollen material, preITQ-6 shows an increased in the d-basing of d_{200} plane in the range 1.31-3.00 nm compared to 1.30 nm for PREFER while the peaks corresponding to the individual layers decreased strongly. This indicates that the PREFER layers containing 4-amino-2,2,6,6-tetramethylpiperidine templates had been expanded in the present of CTABr as swelling agent. When the delamination was completed as in sample ITQ-6-bc, the XRD peaks of the sample are much broader and less intense than that of PREFER and preITQ-6. A sharp peak was observed at 2θ 6.8° indicating the presence of a small amount of PREFER that had not been swollen and delaminated.

Upon calcinations of the delaminated ITQ-6-bc sample, much broader and less intense peaks were observed in the X-ray diffractogram of ITQ-6 sample compared to the ITQ-6-bc sample. The X-ray diffractogram of ITQ-6 sample also shows a sharp peak at 2θ 9.4° which is due to the existence of FER

type zeolite due to the removal of templates in the delaminated ITQ-6-bc sample that contain a small amount of PREFER.

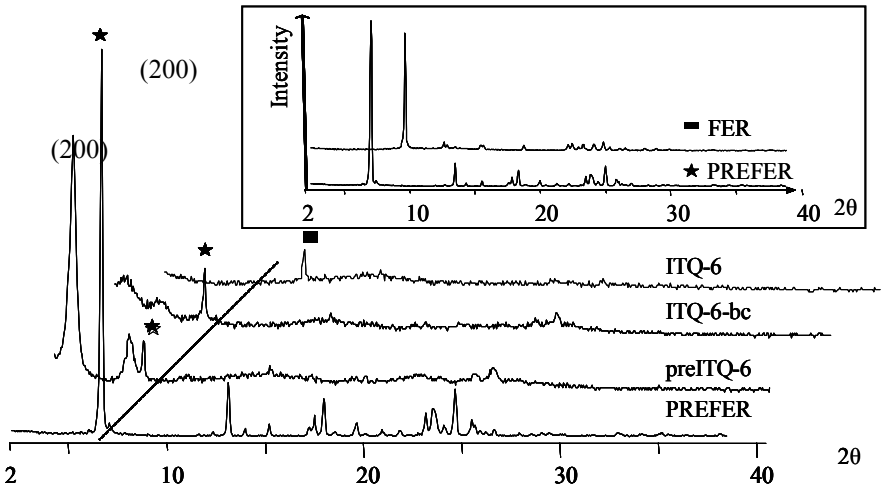

Figure 2 : X-ray diffractograms of PREFER samples after every treatments (insert shows XRD pattern of FER and PREFER)

Microporous FER type zeolite can be obtained through complete removal of template by calcination of PREFER material at 550 ^{o}C. During calcinations of two-dimensional sheets of PREFER, the condensation of the silanol groups and elimination of the organic template occur; this accompanied by a decrease of the interlayer spacing to form three-dimensional FER type material.

X-ray diffractogram of PREFER material and FER type zeolite (calcined PREFER) is presented in Figure 2 (small box). The XRD patterns of both samples are practically identical and characteristic of highly crystalline products accept for the peak at d_{200}.

Table 1 : Values of unit cell parameters for PREFER and FER type zeolite.

	a (Å)	**b (Å)**	**c (Å)**
PREFER	26.09	13.94	7.42
FER	18.68	13.99	7.49

As shown in Table 1 the values of the parameter *b* and *c* are unchanged, whereas the *a* parameter decreased drastically upon removal of templates by calcinations. Finally all these observation suggest that the structural changes leading from the PREFER structure to the FER type structure involved essentially the *a* axis.

Fourier Transform Infrared (FTIR)
Framework
The IR spectra of the ITQ-6 framework and hydroxyl group are presented in Figure 3. The framework of ITQ-6 was found to be similar to the amorphous silica and in agreement with X-ray diffractogram findings. The band at 430 cm^{-1} assigned for pore structure of ferrierite framework diminished and the intensity of the characteristic peaks of ferrierite framework at 721 cm^{-1} and 580 cm^{-1} decreased upon delamination process. It can be observed from the IR spectra that the strongest band corresponding to asymmetric stretching around 1080 cm^{-1} has becomes broaden.

Hydroxyl species and the acidity property

Acidity measurement, type of acid sites and hydroxyl groups in FER and ITQ-6 were characterized by infrared spectroscopy and pyridine molecule was used as probe base.

After the dehydration of FER type material at 400 °C, three bands were observed in the hydroxyl region of FER spectrum. The bands are assigned for vibration external terminal silanol (Si-OH) groups (3746 cm^{-1}), Al(OH) groups (3664 cm^{-1}) and bridging OH (Si-OH-Al) groups at (3598 cm^{-1}). IR spectrum of delaminated ITQ-6 material evacuated at 400 ^{o}C shows the formation of large amounts of silanol groups at 3742 cm^{-1} (Figure 3a) assigned to external silanol groups in accordance with the proposed structure. The total acidity results of the samples are summarized in the Table 2. Delaminated ITQ-6 appears to have both Brönsted and Lewis acid sites even after delamination process.

Table 2 : Acid sites of ITQ-6 measured by Adsorption Desorption of Pyridine at 150 ^{o}C

	Brönsted, 1545 cm^{-1} ($\mu moleg^{-1}$)	**Lewis,** 1454 cm^{-1} ($\mu moleg^{-1}$)
FER	3.12	1.09
ITQ-6	10.14	9.87

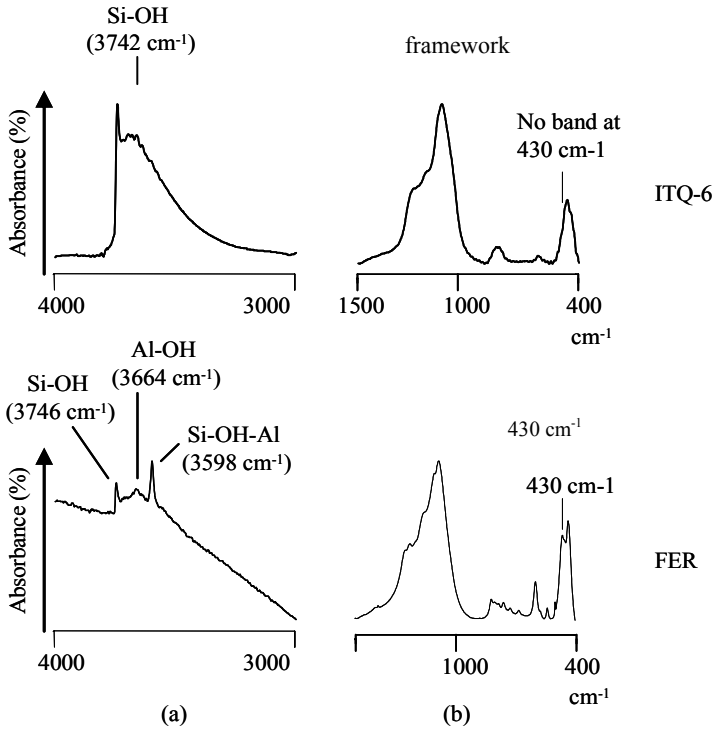

Figure 3 : FTIR spectra of ITQ-6 and FER samples (a) hydroxyl vibration (P = $\approx 10^{-7}$ mBar) and (b) framework structure.

Nitrogen adsorption

Figure 4 exhibits (a) nitrogen adsorption-desorption isotherms and (b) pore size distribution plot of ITQ-6 and FER samples. The ITQ-6 exhibits the adsorption-desorption isotherm of Type IV and hysteresis loop of Type H3 which characterized it as mesoporous material. Hysteresis loop of Type H3 in the range 0.40-1.00 shows that capillary condensation occurred in the slit shape pores with non-uniform size. This proved that the layered structure in the ITQ-6 material had destroyed. FER exhibits the adsorption-desorption isotherm of Type I with hysteresis loop of Type H4. This indicates the presence of micropores in the FER-type material. Since FER is having micropore type material, interaction between the solid and gas molecule was enhanced leading to high volume of nitrogen adsorbed at low relative pressure.

From the pore size distribution plot, ITQ-6 gives a sharp peak in the mesoporous region centered at Ca = 4 nm indicates a uniform pore size distribution. Whereas the FER sample shows non-uniform pore size distributions having micropores as dominant pore with meso and macropore exist on the external surface of the crystal.

Table 3 summarises the values obtained by applying the BET equation to the values of the nitrogen adsorption isotherm for ITQ-6. The micropore surface area, external surface area and micropore volume were determined from the 't-plot' by using Harkin-Jura equation. From the table it can be proved that the pore with meso size has been formed by delamination process of PREFER to ITQ-6 leads to material with higher external surface. ITQ-6 with higher external area is more accessible for bulk molecule to the acid sites compared to the micropore FER type material.

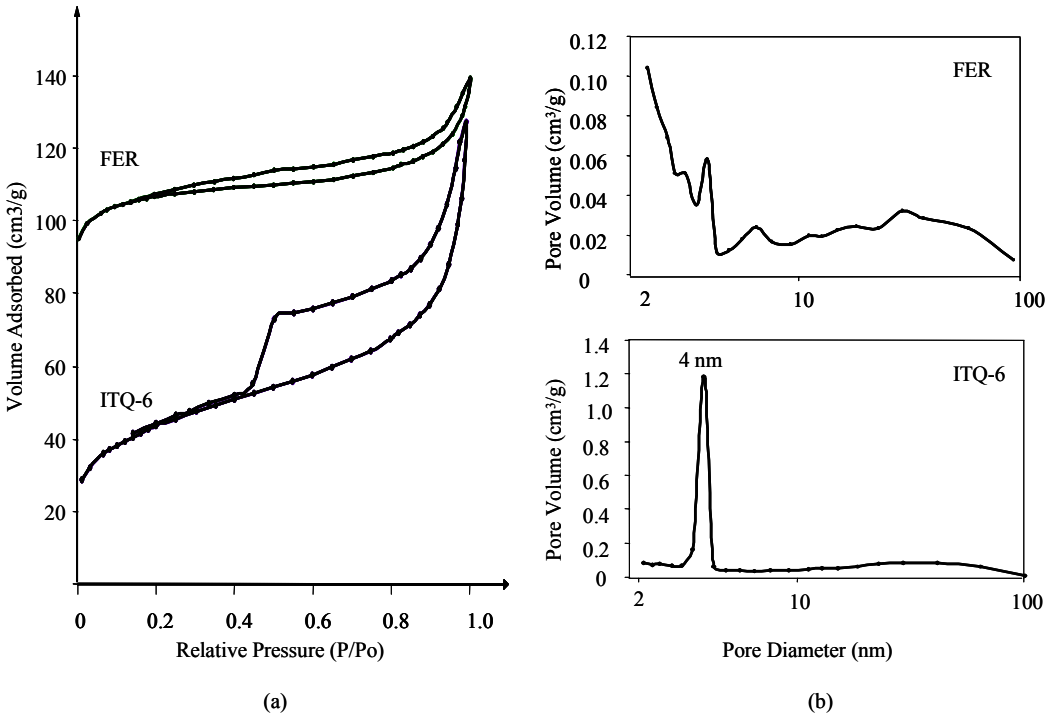

Figure 4 : (a) Nitrogen adsorption-desorption isotherm and (b) pore size distribution of ITQ-6 and FER

Table 3 : Specific surface areas, S (m^2g^{-1}) and micropore volume, V (cm^3g^{-1}) determined from nitrogen adsorption isotherm.

	S_{Total} (BET)	S_{Micro} (t-plot)	$S_{External}$ (t-plot)	V_{Micro} (t-plot)
ITQ-6	153.94	59.48	94.46	0.025
FER	290.17	260.78	29.39	0.120

Field Emission Scanning Electron Microscope (FESEM)

The morphologies of the PREFER, ITQ-6 and FER samples are shown in Figure 5. The crystals of PREFER and FER (Figures 5a and 5c) had a plate-like morphology with a very homogeneous distributions. The aggregates are made of very thin stacked crystals (about 60 x 10 x 0.5 μm).

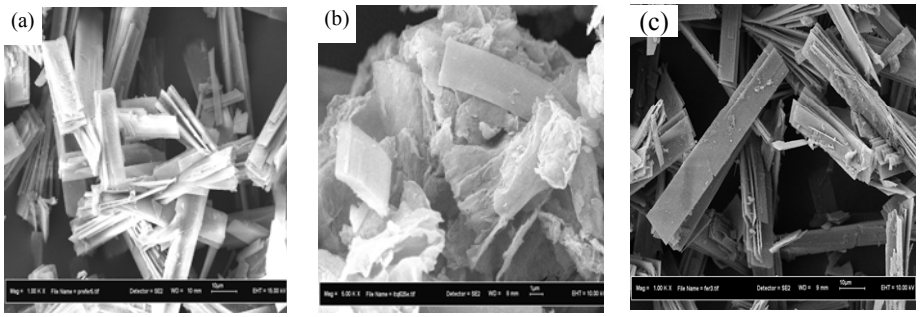

Figure 5 : FESEM micrographs of (a) PREFER (magnification1000x) (b) ITQ-6 (magnification5000x) and (c) FER (magnification 1000x)

.

The FESEM micrographs of ITQ-6 (Figure 5b) material clearly indicates that the crystal size and morphology of PREFER is strongly influenced by the delamination process. The plate-like crystal was destroyed upon the delamination process. There are no specific structure was observed in ITQ-6 micrographs. The plate-like crystals of FER is still present in the ITQ-6 material. This was proved by XRD of ITQ-6 where a sharp peak at 2θ 9.8^{o} indicates the present of small amount of crystal material in ITQ-6 sample.

Catalytic testing

The reaction was carried out by refluxing a mixture of methyl *tert* butyl ether and resorcinol using ITQ-6 and FER as catalysts. The reaction equation is shown in Eq. 1.

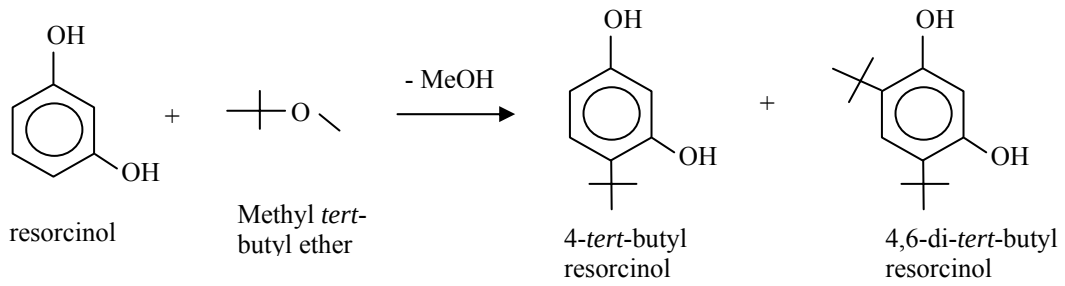

Eq. 1

The differences in the conversion of resorcinol, selective formation of 4-tert-butyl resorcinol and 4,6-di-tert-butyl resorcinol over both catalysts in the influence of temperature is shown in the Figures 6 and 7. The conversion of resorcinol increase from 11% to 55% as the reaction temperature increases from 80 ^{o}C to 120 ^{o}C. Basically, the selectivity of the products is not influenced by the reaction temperature. When the reaction was carried out at 120 ^{o}C, the selectivity of dialkylated product (bulkier molecule) show the highest selectivity compared with other temperature with high activity. Therefore as a comparison, FER was used as catalyst in order to study the effect of the pore size. The results show the activity of FER is much lower than ITQ-6. ITQ-6 was also found to have higher yield for both products compared to FER. This may be due to the pore restriction whereby the accessibility of the reactants to the active acid side is limited and the property of ITQ-6 which have higher external surface area compared to FER

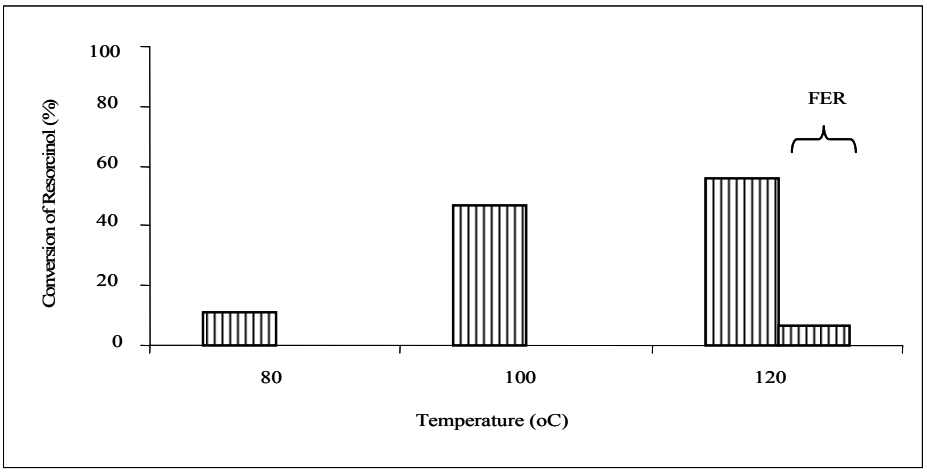

Figure 6 : Effect of reaction temperature on the conversion of resorcinol over ITQ-6 and FER

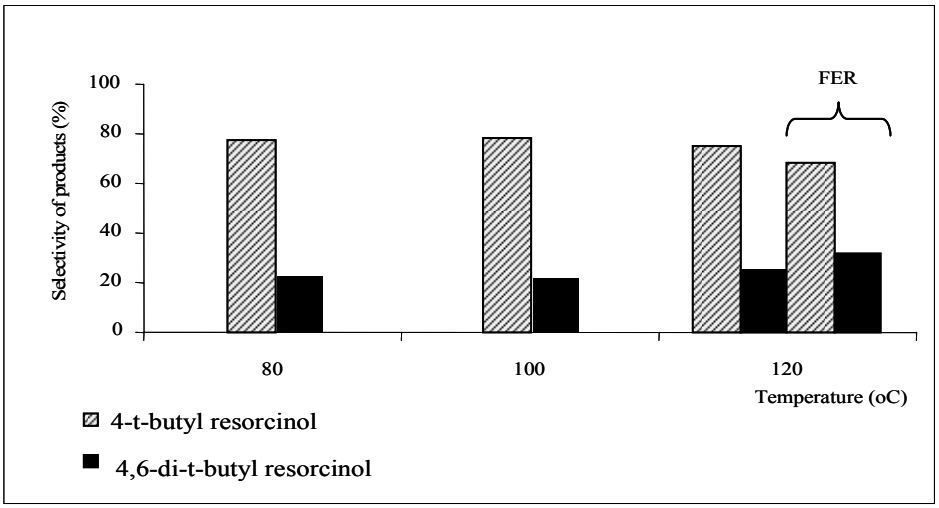

Figure 7 : Effect of reaction temperature on the products selectivity over ITQ-6 and FER

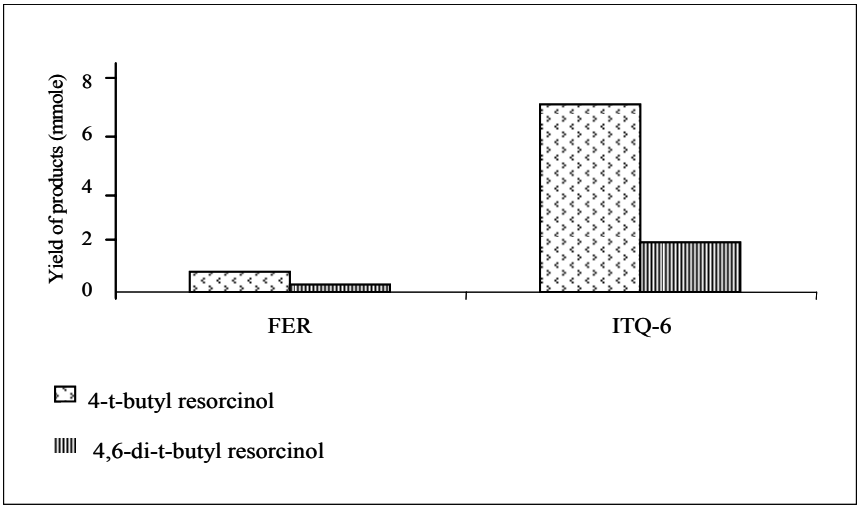

Figure 8 : Yield of products over ITQ-6 and FER

Conclusion

Delamination of layered PREFER material leads to the formation of new mesoporous zeolitic material known as ITQ-6. Modification of PREFER to the delaminated ITQ-6 can be done by intercalation of bulk molecule in this case CTABr between the layers followed by sonication of swollen material and calcinations to remove the organic templates. Besides its amorphous phase, ITQ6 is having mesopores size channel. The ITQ6 material also appears to have appreciable amount Brönsted and Lewis acid sites. The acidity of zeolite and mesopore size shown by ITQ-6 was proved to be active as heterogeneous acid catalyst for Friedel crafts alkylation.

Acknowledgements

The authors acknowledge the Malaysian Ministry of Science, Technology and Innovation for the financial support through IRPA funding 09-02-06-0057-SR005/09-06 and MARA for the scholarship funding.

References

[1] Sankarasubbier, N. and Murthy, K.V.V.S.B.S.R. 2001. Montmorillonite as a Versatile Solid Acid Catalyst for *tert*.-Butylation of Resorcinol. *Applied Catalysis A: General*. 213: 273-278.

[2] Jung, W. Y., Yoo, J. W., Lee, C. W., Jeong, H. C., Park Y. K. and Park S. E. 2000. *t*-Butylation of 1,2-dihydroxybenzene over Acidic Zeolites. *Catalysis Today.* 60: 255–261

[3] Arishtirova K., Kovacheva, P. and Vassilev, S. 2001. BaO/NaX Zeolite as a Basic Catalyst for oxidativemethylation of Toluene with Methane. *Applied Catalysis A: General.* 213: 197–202

[4] Javier P. R., Kumar, M. S. and Brückner, A. 2004. Reduction of N_2O with CO over FeMFI Zeolites: Influence of the Preparation Method on the Iron Species and Catalytic Behaviour. *Journal of Catalysis.* 223: 13-27

[5] Serrano, D. P., Aguado, J., Escola, J. M. and Rodríguez, J. M. 2005. Influence of Nanocrystalline HZSM-5 External Surface on the Catalytic Cracking of Polyolefins. *J. Anal. Appl. Pyrolysis* 74: 353–360

[6] Huang, Y., Meng, X., Dang, Z., Weng, S. and Zhang, C. 1995. Light Olefin Synthesis from Carbon Dioxide by Hydrogenation over $Fe_3(CO)_{12}$ Supported on ZSM-5 Zeolite Catalyst. *J. Chem. Soc., Chem. Commun.* 10:1025-1026

[7] Krishnan, A.V., Ojha, K. and Pradhan, N.C. Alkylation of Phenol with Tertiary Butyl Alcohol over Zeolites. *Organic Process Research & Development.* 2002. 6: 132-137

[8] Cheralathan, K.K, Kumar, I.S., Palanichamy, M. and Murugesan, V. Liquid Phase Alkylation of Phenol with 4-hydroxybutan-2-one in the Presence of Modified Zeolite Beta. *Applied Catalysis A*, 2003. 241: 247-260

[9] Corma, A., Fornes, V., Pergher, S. B., and Maesen, Th. L. M. and Buglass, J. G. (1998). Delaminated Zeolite Precursor as Selective Acidic Catalyst. *Nature.* 396: 353-356.

[10] Climent, M. J., Corma, A. and Velty, A. 2004. Synthesis of hyacinth, vanilla, and blossom orange fragrances: The benefit of using zeolites and delaminated zeolites as catalysts. *Applied Catalysis A: General*. 263: 155-161

[11] Corma, A., Diaz, U., Domine, M. E. and Fornés, V. 2000. New Aluminosilicate and Titanosilicate Delaminated Materials Active for Acid Catalysis, and Oxidation Reactions Using H_2O_2. *Journal American Chemical Society*. 122(12): 2804 - 2809;

[12] Corma, A., García, H. and Miralles, J. 2001. High activity layered zeolite ITQ-2 as catalyst for the hydroxyalkylation of 2-methoxynaphthalene and naphthalene with paraformaldehyde; Comparison of its performance with that conventional zeolites or mesoporous Al/MCM-41. *Microporous and Mesoporous Materials.* 43: 161-169.

[13] Schreyeck, L., Caullet, P., Mougenel, J. C., Guth, J. L. and Marler, B. 1996. PREFER: A New Layered (Alumino) Silicate Precursor Of FER-Type Zeolite. *Microporous Materials*. 6: 259-271.

[14] Concepción, P. López, C. Martínez, A. and Puntes, V. F. 2004. Characterization and catalytic properties of cobalt supported on delaminated ITQ-6 and ITQ-2 zeolites for the Fischer–Tropsch synthesis reaction. *Journal of Catalysis.* 228: 321–332

EFFECT OF $SiO_2\backslash Al_2O_3$ RATIOS TOWARDS THE ACIDITY AND ACTIVITY OF ZEOLITE BETA IN FRIEDEL-CRAFTS REACTION.

Marzita Abd Mazak, Farediah Ahmad and Zainab Ramli.

Department of Chemistry, Faculty of Science, University Teknologi Malaysia,, 81310 UTM Skudai, Johor.
Tel : +607-55334491 Fax: +607-5566162
Email: zarita_222@hotmail.com., zainab@.fs.kimia.utm.my

ABSTRACT

Zeolite beta is a potential heterogeneous catalyst in many applications such as in organic processes and petrochemical industries. Zeolite beta was prepared hydrothermally using rice husk ash as the silica source. The initial molar oxide ratios of SiO_2/Al_2O_3 of the gels were varied at 27,45 and 90. Transformation of the rice husk ash to zeolite beta and the changes in the crystallinity were monitored by XRD and FTIR. The XRD and FTIR results indicated that zeolite beta was formed from all SiO_2/Al_2O_3 ratios of the samples with high crystallinity and purity. The strength and the amount of acid sites in zeolite beta were determined by TPD. Analysis of the TPD results showed that the strength and the amount of acid sites decreased with increasing SiO_2/Al_2O_3 ratios of the zeolite beta samples. The reactivity of the zeolite beta samples was tested on the Friedel-Crafts acylation of resorcinol with acetic anhydride. All samples gave more than 90% conversion. Two products from the reaction were identified as 1,4-benzenedioldiacetate and 2,6-dihydroxyacetophenone. Selectivity of 1,4-benzenedioldiacetate increased from 85% to 91% while the selectivity of 2,6-dihydroxyacetophenone decreased from 15% to 9% with increasing SiO_2/Al_2O_3 ratios of zeolite beta.

1.0 Introduction

Zeolites have been widely studied for their applications as catalysts in the syntheses of organic and fine chemicals. The key opportunities for the use of zeolites as catalysts rely on their unique pores, which can control the selectivity of the reaction.[1] The use of zeolites and other solid acid catalysts in the manufacture of fine chemicals and chemical intermediates is gaining much more attention in recent years [2]. Solid acid catalysts such as zeolites [3] have been used in Friedel-Crafts acylation in which an active and selective heterogeneous catalyst could replace the more traditional homogeneous systems [1]. The Friedel-Crafts acylation reaction mechanism involves acylation either by an adduct of the catalyst and the acylating agent or by free acylium ions, depending on the reaction conditions. In heterogeneous zeolite-catalysed acylation, a similar mechanism is assumed to apply, in which the adduct is formed by the interaction of the surface acid sites with an acylating agent. In both cases, both acid Brönsted and Lewis are required in order for the reaction to proceed.

In this study, zeolite beta at different SiO_2/Al_2O_3 ratios has been used as catalyst in the Friedel-Crafts reaction of resorcinol with acetic anhydride, in which the product has potential antioxidant property. Since the reaction proceeds in the presence of both Lewis and Brönsted acid, the objective of this study is to prepare zeolite beta catalysts with different acid strength in terms of the amount of Lewis and Brönsted acid present and testing the reactivity of the catalysts in the Friedel Craft acylation of resorcinol with acetic anhydride.

2.0 Experimental

2.1 Synthesis of zeolite beta

Zeolite beta was synthesised using rice husk ash (RHA) as a silica source. The synthesis of zeolite beta was carried out hydrothermally from gel mixtures containing amorphous silica extracted from RHA, sodium aluminate (54% Al_2O_3; 41% w/w Na_2O, technical grade), tetraethylammonium hydroxide (40% solution in water, Fluka Chimika) and sodium hydroxide (99%, Merck), based on the method described by Didik *et al.* [4]. The gel was prepared according to the following molar chemical composition : $1.96Na_2O : 27SiO_2 :$

Al_2O_3 : $5TEA_2O$: $240H_2O$. In a typical preparation, 23.71g of tetraethylammonium hydroxide solution was dissolved in 4.6 g of water, followed by the addition of 1.21g of sodium aluminate. The mixture was stirred until a clear and viscous solution was formed. To this solution, 0.36 g of sodium hydroxide, which was dissolved in 9.00 g of water were added, followed by 11.10 g of RHA. The whole mixture was stirred vigorously for about two hours. The gel formed was then transferred into a stainless steel autoclave and kept in an air oven for crystallisation at 150 ˚C for 6 days. To stop the crystallization process, the autoclave was immersed in cold water. The solid product recovered by filtration was washed repeatedly with demineralised hot water until the pH of the filtrate was ~ 7.0. Finally, the product was dried at 100 ˚C in an air oven overnight and then calcined at 550˚ C for 16 h to remove the organic material occluded in the zeolite pores and to obtain the sodium form of the zeolite beta. The Na-form of zeolite beta obtained was converted to the NH_4-form by ion exchange using 1 M solution of ammonium nitrate at 80 ˚C for 4 h. The procedure was repeated three times. The protonated form was obtained by calcining the NH_4-form at 550 ˚C for 4 h and marked as H-BEA. The procedure was repeated for the preparation of zeolite beta with SiO_2/Al_2O_3 molar ratios of 45 & 90.

2.2 Characterization Techniques

Infrared spectroscopy is used to characterize the structure of zeolite beta which of the tetrahedra linked of SiO_4 or AlO_4 is in the mid-infrared region (300-1400 cm^{-1}). IR spectra were measured using Perkin Elmer 1600 FTIR spectrometer and KBr wafer technique. All spectra were measured with a 2 cm^{-1} resolution. The KBr wafer was made by mixing 0.25 mg of zeolite powder with 300 mg KBr powder and pressed under vacuum (10 tons). The pellet was then put in FTIR instrument to determine the characteristic peaks of zeolite beta. IR spectra were set in % transmittance and were taken between 1400-300 cm^{-1} at room temperature.

The samples were characterised by X-ray diffraction in order to confirm the structure of the zeolite and the preservation of the crystallinity of the zeolite. This method was based on the fact that every crystalline material has its own characteristic diffractogram. The sample was carefully ground to a fine powder, and then lightly pressed between two glass slides to get a thin layer. XRD patterns were acquired on a Siemens D5000 goniometer using CuKα radiation with $\lambda = 1.5406$ at 40kV and 10mA. X-ray diffractograms were scanned in the range of 2θ from 2˚ to 60˚ with step interval of 0.05˚ 2θ and a count time of 1s per step.

Temperature programmed of ammonia desorption technique is used to investigate the acidity of the catalyst. Ammonia desorption analysis was performed on the TPDRO 1100 Thermoquest equipment using 200 mg catalyst. Samples were first pretreated in a nitrogen flow (20 mL/min) at 110˚ C for 1 h. Desorption was done by heating the catalyst from 80 to 600 with a heating rate of 10˚ C/min. The amount of desorbing NH_3 was measured with a thermal conductivity detector. The TPD spectrum (derivative plot) was obtained from this curve by plotting the rate of ammonia desorption as a function of temperature.

2.3 Friedel-Crafts Acylation.

The zeolite -beta catalyst prepared at different SiO_2/Al_2O_3 ratios were activated at 773 K for 3 h. The activated catalyst (0.5g) was then added to a mixture of resorcinol (3.3 g, 30 mmol) and acetic anhydride (50 mmol) in a batch reactor with reflux and stirring in oil bath at 393K. The reaction was carried out within 1-24 hour. The reactants employed were resorcinol (99.0% from Merck), acetic anhydride (98.0% from Merck) and nitrogen as a diluent gas (99.9%). The liquid product was syringed out at interval times of 1, 2, 3, 4, 5, 20 and 24 h in order to determine the equilibrium of the reaction. The liquid product was analysed by gas chromatography (GC) with a Hewlett Packard 5890 series II instrument with FID using Ultra 1 column (diameter 0.25 mm, thickness 0.2 mm and length 30 m). About 0.1 mL sample was injected into the GC at the initial temperature of 50 ˚C for 1 min, followed by increasing the temperature at the rate of 10 ˚C/min to the final temperature of 250 ˚C where it was held for 30 min. For each sample, the analysis was carried out three times in order to ensure reproducibility of the analysis.

3.0 Results and Discussion

3.1 Catalysts Characterisation

Phase purity and crystallinity of the samples were determined by X-ray diffraction (XRD). Zeolite beta (BEA) have been synthesised using silica from rice husk ash (RHA). X-ray diffractogram of RHA shown in figure 1 indicates that the silica is in the amorphous form. The diffractogram patterns of the synthesized zeolite beta with varying SiO_2/ Al_2O_3 ratios are shown in figure1. The XRD pattern indicated that pure zeolite beta was formed from SiO_2/ Al_2O_3 ratios of 27, 45 and 90. All the samples have the XRD patterns typical of highly crystalline zeolite beta similar to the values reported by Wadlinger et al.[5] and Pariente et al.[6] which identified samples as zeolite Beta. XRD pattern of zeolite beta with SiO_2/ Al_2O_3 = 27, 45 and 90 ratios showed diffraction occurring at 2θ, 7.8˚, 16.5˚, 21.5˚, 22.5˚, 25.3˚, 26.9˚, 29.5˚, 43.5˚. Table 1 shows relative crystallinity of the synthesised zeolite beta indicating that the crystallinity increased with the increase of SiO_2/ Al_2O_3 ratios. The XRD patterns of synthesised and the sample after calcinations at 550˚C for 16 hours shows the crystallinity of calcined sample significantly decreasing after calcination at high temperature. The relative intensity of the XRD peaks decrease to about 71% after the removal of the template by calcination indicating that some part of the framework structure has collapsed. However the whole structure is still intact based on the presence of all the diffraction pattern in the XRD diffractograms of calcined samples.

IR spectra of various SiO_2/ Al_2O_3 ratios were recorded. Distinct vibrations appear in the regions between 1300-400 cm^{-1} which is assigned to the structural framework vibration of zeolite. Figure 2 shows IR spectra of Si-27, Si-45 and Si-90, showing similar pattern of IR spectra. Zeolite beta was characterised at wave numbers 1220,1172, 1075, 781, 601, 564, 517, 462 and 427 cm^{-1}[7]. IR spectra of silica RHA exhibit very strong bands at wave numbers 1103 cm^{-1}, 798 cm^{-1} and 470 cm^{-1} which correspond to the asymmetric stretching of tetrahedral SiO_4, symmetric stretching of SiO_4 tetrahedra and Si-O bending band vibrations, respectively. IR spectra of Si-27 indicated changing the asymmetric TO_4 (T=Si, Al) band at 1103 cm^{-1} with the band of RHA becoming sharper and shifted towards lower frequency at wave number 1075 cm^{-1}. This indicated the formation of Si-O-Al linkage of tetrahedral TO_4 framework. The band at 1220 cm^{-1} is assigned to the external asymmetric stretching vibration, which is sensitive to structure changes in zeolite beta, meanwhile the bands at 1075 cm^{-1} and 781 cm^{-1} are correspond to the asymmetric stretching and internal symmetric stretching of T-O tetrahedral vibration respectively, which are not sensitive to zeolite structure.

The bands at 564 and 517 cm^{-1} were assigned to double 6-ring (D6R) and double 4-ring (D4R) which is sensitive to zeolite structure [8]. Both bands relate to the crystallinity [6,9] of the zeolite beta. The 462 cm^{-1} band is assigned to T-O bending mode, which is not sensitive to zeolite structure, while the 427 cm^{-1} band is observed for T-O bending mode indicating the presence of pores structure [7]. As the of SiO_2/ Al_2O_3 ratios of the samples increased the internal asymmetric stretching at 1075 cm^{-1} band shifted towards higher wave numbers, which indicated the increase of silica content in zeolite framework [10]. IR spectra of the as-synthesized and the calcined zeolite beta showed peak at 1172 cm^{-1} assigned to the stretching vibration of template disappeared after calcinations. Calcination of Si-45 sample caused the asymmetric stretching of TO at 1078 cm^{-1} to shift towards higher frequency at 1086 cm^{-1}. The shifting of the frequency indicated that dealumination of Al framework has occurred.

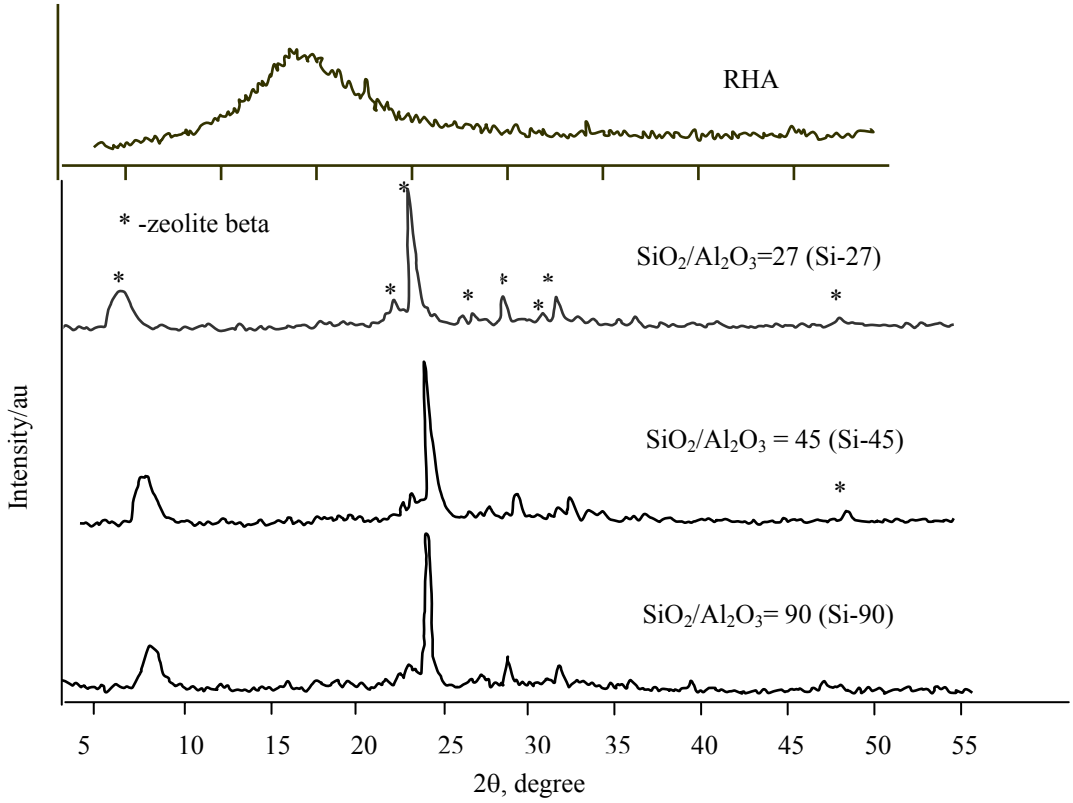

Fig 1: X-ray diffraction pattern of the as-synthesized zeolite beta at different SiO_2/Al_2O_3 ratios

Table 1: Crystal contents of zeolite beta at different SiO_2/Al_2O_3 ratios.

Samples	SiO_2/Al_2O_3 ratio	Crystal contents	BEA[(a)] crystallinity, %	Percentage of Zeolite beta
Si-27	27	BEA	94.3	100
Si-45	45	BEA	88.6	100
Si-90	90	BEA	100	100

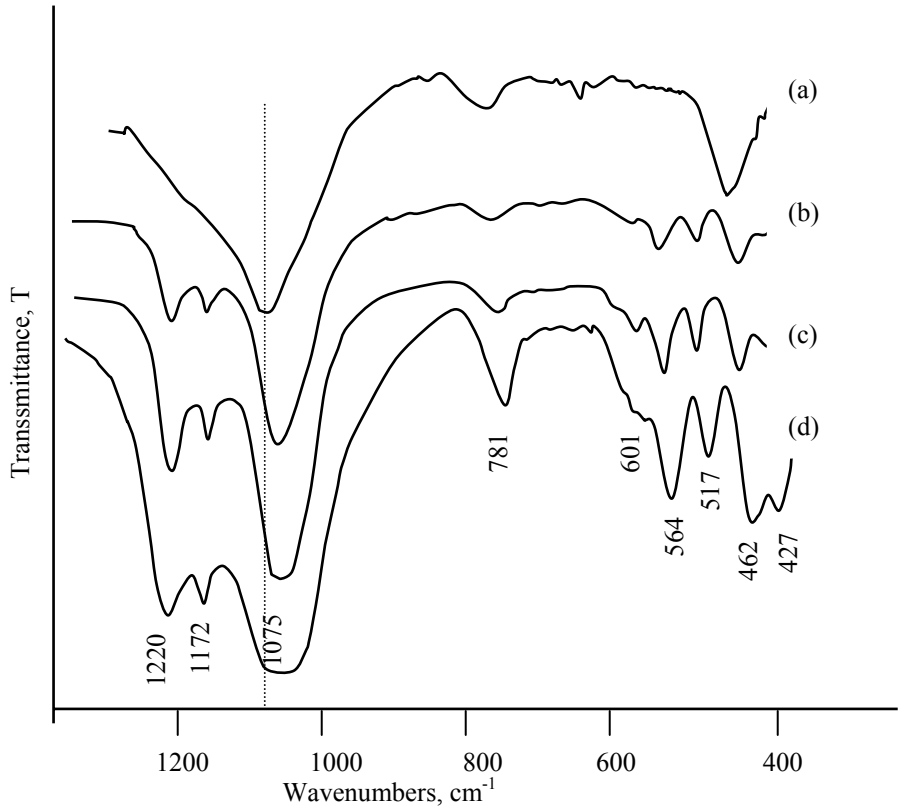

Fig 2: IR spectra of zeolite beta at different SiO_2/Al_2O_3 ratios [(a) rice husk ash (b) Si-27 (c) Si-45 (d) Si-90]

3.2 Acidity Study

Temperature programmed of ammonia desorption is used to estimate the acid property of the catalysts qualitative and quantitatively. The total amount of NH_3 desorbed relates to the number of acidic sites and from the desorption temperature, the strength of acidic sites is suggested. Figure 3 shows the TPD profiles for zeolite beta at different SiO_2/Al_2O_3 ratios. The thermogram of the samples presents two peaks, peak I and peak II. The results of NH_3-TPD of the catalysts are tabulated in Table 1. The amount of acid or acidity is expressed as moles of NH_3 desorbed per unit weight of the solid. Peak I relates to the hydroxyl group, which is low strength bonding and peak II relates to higher strength bonding of hydroxyl group to the NH_3 molecules. Results indicate that zeolite beta at SiO_2/Al_2O_3=27(Si-27) has the highest acid strength with the amount of acid site higher than zeolite beta at SiO_2/Al_2O_3 =45 and 90 (Si-45 and Si-90). From these results, it shows that an increase of SiO_2/Al_2O_3 ratios will decrease the amount and the strength of acid sites in zeolite beta.

Table 2 : The total amount of desorbed of zeolite beta at different SiO_2/Al_2O_3 ratios.Si-27, Si-45 and Si-90.

Sample	Peak I		Peak II	
	T (^oC)	NH_3 desorbed μmol\g	T (^oC)	NH_3 desorbed μmol\g
H-Si-27	257	3542	443.8	2462
H-Si-45	235	2428	437	2019
H-Si-90	152	1546	396	320

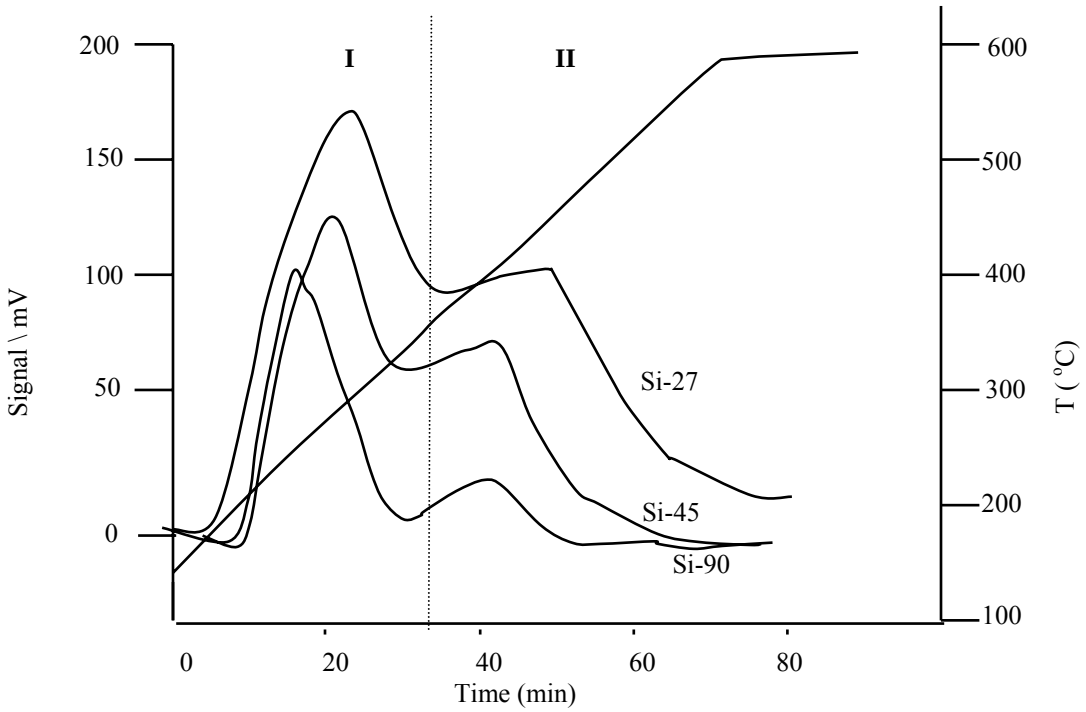

Fig 3: Ammonia TPD profiles of zeolite beta at different SiO_2/Al_2O_3 ratios.

3.3 Acylation Reaction of Resorcinol by Acetic Anhydride

Zeolite beta at different SiO_2/Al_2O_3 ratios was used as catalysts for Friedel-Crafts acylation of resorcinol with acetic anhydride. Figure 4 shows the conversion of resorcinol over zeolite beta at different SiO_2/Al_2O_3 ratios. It is observed that the reaction was very active in the presence of catalyst is which the conversion reached a maximum within 2 h of reaction time. After 1 hour of reaction time sample Si-27 (SiO_2/Al_2O_3 =27) gave about 99% conversion of resorcinol higher than zeolite beta at SiO_2/Al_2O_3 =45 and 90. Two main products from the reaction were identified as 1,4-benzenedioldiacetate and 2,6-dihydroxyacetophenone. Selectivity of 1,4-benzenedioldiacetate increased from 85% to 91% with the increase of SiO_2/Al_2O_3 ratios of zeolite beta.

On the other hand, product selectivity of 2,6-dihydroxyacetophenone decreased from 15% to 9% as the SiO_2/Al_2O_3 ratios of the zeolite beta increased.

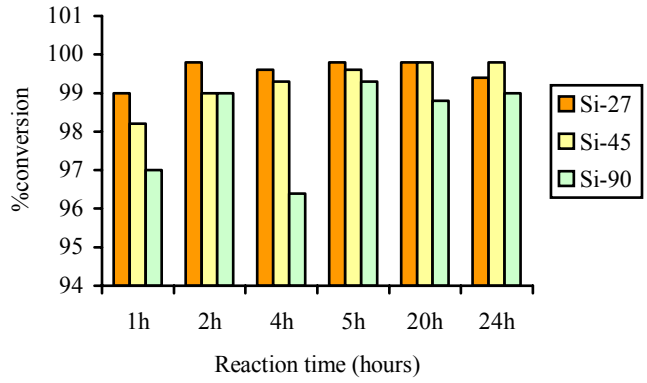

Fig 5: Effect of reaction time on conversion of resorcinol over zeolite beta catalyst at different SiO_2/Al_2O_3 ratios

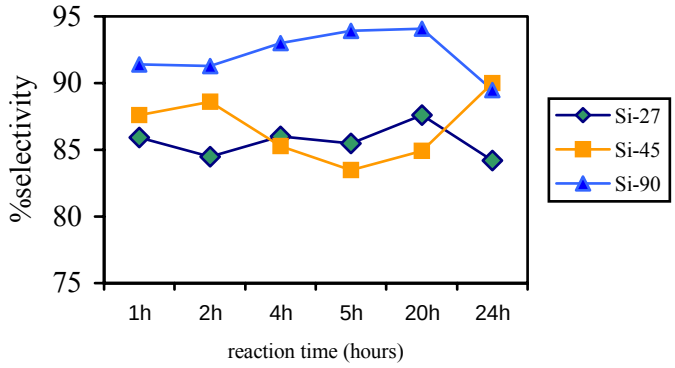

Fig 6 : Effect of reaction time on %selectivity of 1,4-benzenediol diacetate over zeolite beta at different SiO_2/Al_2O_3 ratios.

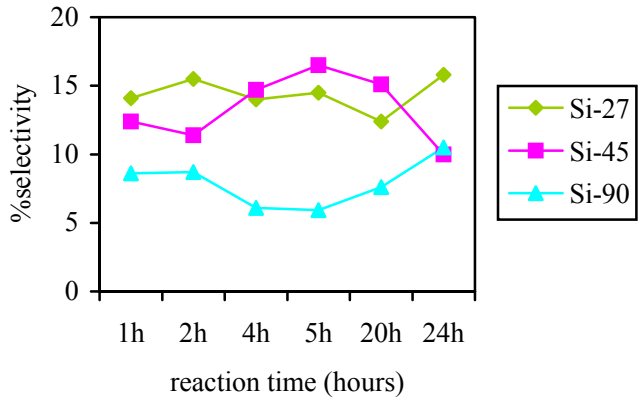

Fig 7 : Effect of reaction time on %selectivity 0f 2,6-dihydroxyacetophenone over zeolite beta at different SiO_2/Al_2O_3 ratios

4.0 Conclusion

RHA has proven to be an active silica source in the preparation of zeolite. Zeolite beta was successfully produced at the initial oxide molar ratios between 27-90 with high purity and crystallinity. Acidity study has shown that the strength and the amount of acid sites decrease with the increase of SiO_2/Al_2O_3 of zeolite beta as expected. This acidity relate to activity of the zeolite beta catalyst in which the Friedel-Crafts reaction show high activity in the presence of high acidity. In general all samples gave more than 90% conversion. Two main products from the reaction were identified as 1,4-benzenedioldiacetate and 2,6-dihydroxyacetophenone.

Acknowledgements

The authors wish to thank Universiti Teknologi Malaysia and Ministry of Science, Technology and Environment (MOSTE) for financial support under IRPA project no. 09-02-06-0057 SR0005/09-03

References

1. Gaare, K. and D Akporiaye. (1996). "Modified Zeolites as Catalysts in the Friedel-Crafts Acylation." *J. Mol. Cat. A.* **109**: 177-187.
2. Das, D., and S. Cheng.(2000). "Friedel-Crafts Acylation of 2-methoxy-Naphtalene over Zeolite Catalysts." *Applied. Catalysis A.* **201**: 159-168
3. Wang, Q.L., Y. Ma, W. Jiang, and B. Zeo. (1997). " Friedel-Crafts Acylation of Anisole over Zeolite Catalysts." *App. Cat. A* **165**: 199-206
4. Didik Prasetyoko(2001) "Pengoptimuman sintesis zeolite beta daripada abu sekam padi:pencirian dan tindakbalas pemangkinan Friedel-Crafts." Tesis MSc. UTM.
5. Wadlinger, R. L., Kerr, G. T. and Rosinski, E. J. (1967). "Synthesis Zeolite Beta." (U.S. Patent 3,308,069)
6. Pariente, J. P., Martens, J. A. and Jacobs, P. A. (1987). "Crystallization Mechanism of Zeolite Beta from TEA_2O, Na_2O, and K_2O Containing Silicate Gels." *Applied Catalysis A.* **31**. 35-64.
7. Eapen, M. J., Reddy, K. S. N. and Shiralkar, V. P. (1994). "Hydrothermal Crystallization of Zeolite Beta Using Tetraethylammonium Bromide." *Zeolites.* **14**. 295 – 302.
8. Martens, J. A., Perez-Pariente, J., Sastre E., Corma, A. and Jacobs, P. A., *Appl. Catal.*, 45 (1998) 85.
9. Flanigen, E. M. (1976). "Structural Analysis by Infrared Spectroscopy in Zeolite Chemistry and Catalysis." In Rabo, J. A., "Zeolite Chemistry and Catalysis." *ACS Monograph.* **171**. 80 – 117.

Gallium Impregnated Zeolite Beta Catalysts for Friedel-Crafts Alkylation of Resorcinol

Zainab Ramli*, Aiman Najati Akmar Rahman, and Farediah Ahmad
Department of Chemistry, Faculty of Science, Universiti Teknologi of Malaysia, 81310 UTM Skudai, Johor, Malaysia.
Email: zainab@kimia.fs.utm.my Tel.: +607 5534491 Fax: +607 5566162

Incorporation of gallium into zeolite beta via impregnation is done in order to modify the physicochemical and acidic property of the zeolite to obtain high selectivity and yield [1] in Friedel-Crafts alkylation of resorcinol. The reaction requires the presence of both Bronsted and Lewis acid catalyst to proceed at a convenient rate. The reaction products are antioxidant which found a wide variety of application in industries [2]. The XRD results showed that monolayer coverage of GaO occurs at ca.7.3 wt% which correspond well with the catalytic results that gave the maximum selectivity for the monosubstituted resorcinol after 8 wt% Ga loading. Bronsted acidity decreased with the increase Ga loading and becomes constant after 5 wt% loading, while Lewis acidity increased with the increase of Ga loading. Results shows the activity of the catalysts depends on the Bronsted acidity but the presence of GaO in monolayer coverage zeolite beta suppressed the external Bronsted acid sites which then responsible for the 100% selectivity of the product.

Experimental

Ga containing zeolite beta were prepared by impregnation of $Ga(NO_3)_3$ in water on H-BEA using method described by Choudhary et al[3]. The resulting sample was denoted as XGa/H-BEA (X is the percentage of Ga). Samples were characterized by XRD and acidity study was done using pyridine as probe molecule and monitored by FTIR spectrometer. Catalytic activity of the catalysts in the alkylation of resorcinol with MTBE was performed at 80°C for duration of 24 hrs.

Results and discussion

The XRD patterns for all XGa/H-BEA samples (Figure 1) show the structure of zeolite beta is still maintained even after high loading of Ga without the appearance of crystal phases of Ga_2O_3. In general the crystallinity was found to decrease with higher amount of Ga loading due to the concentration of zeolite beta decreased as the Ga loading increased.

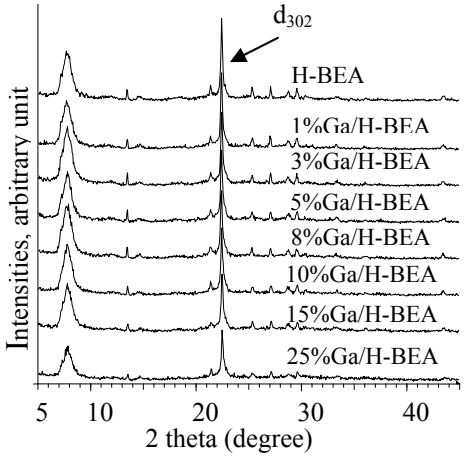

Figure 1 : XRD pattern of samples

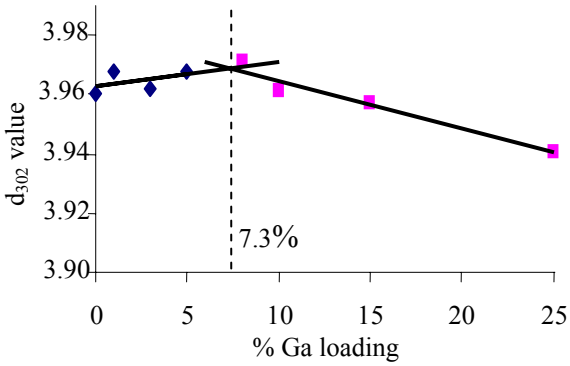

Figure 2 : Graph of d_{302} value of peak $2\theta = 22.3^o$ vs loading amount of Ga on the samples

The monolayer coverage of Ga-O on zeolite beta was determined by XRD by plotting the d_{302} value of the peak at $2\theta = 22.3^o$ vs loading amount of Ga on the samples (Figure 2). A line with positive gradient was found for low amount of Ga loading, while for higher amount of Ga loadings, a line with negative

gradient was obtained. The interception of these two lines occurs at the value of 7.3 wt% showing the percentage of monolayer coverage of Ga on zeolite beta.

The types of acid sites were measured by FTIR using pyridine as probe molecule. The spectra were monitored at room temperature after evacuation at 150^{o}C for 1hr. In the region of pyridine, all samples show similar peaks at 1455 cm^{-1} and 1545 cm^{-1}. The peak at 1455 cm^{-1} relates to pyridine bound coordinatively with Lewis acid sites while peak at 1545 cm^{-1} is contributed to pyridine interacting with Bronsted acid sites. The presence of these peaks for all samples indicates that all samples contain both Lewis and Bronsted acid sites [4] which are suitable as catalyst for Friedel-Crafts reaction. The amount of Bronsted and Lewis acid sites in samples was calculated, and plotted as graph (Figure 3). An increment of Lewis acid sites occurs for samples with percentage of Ga loading more than the monolayer coverage (> 5wt% Ga) whereas amount of Bronsted acid sites remain constant for sample after 5 wt% of Ga loading.

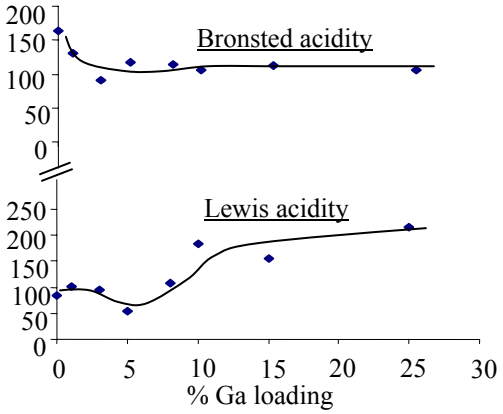

Figure 3 : Graphs of the amount of Bronsted and Lewis acid sites (μmole gram^{-1}) vs loading amount of Ga

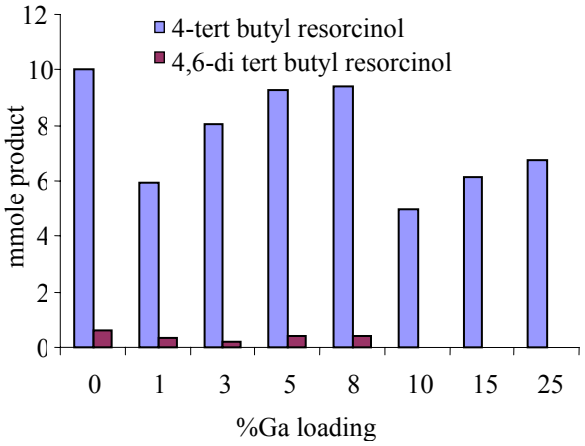

Figure 4 : Yield of products

Based on the catalytic activity of samples in Friedel-Crafts alkylation of resorcinol (Figure 4) all samples were found active as catalyst in this reaction giving 4-tert butyl resorcinol and 4,6-di tert butyl resorcinol [2,5] as major and minor products respectively. Catalytic activity responded well with the Bronsted acid findings, as the optimum yield of main product is achieved for samples after approximately 5-8 wt% of Ga loading. However, product decreased after 8 wt% Ga loading as supported by XRD analysis and lost of disubstituted product (4,6-di tert butyl resorcinol), giving 100% selectivity of 4-tert-butyl resorcinol. We suggest the Lewis acidity might be responsible for the 100% selectivity of monobutylated resorcinol obtained for samples > 8 wt% Ga..

References

[1] K.J. Chao, S.P. Sheu, L. Lin, M.J. Genet, and M.H Feng . Zeolites. 18 (1997) 18

[2] B. M. Devassy, S.B. Halligudi, S.P. Elangovan, S. Ernst, M. Hartmann and F. Lefebvre. Journal of Molecular Catalysis A: Chemical, 210 (2004) 113

[3] V.R. Choudhary and S.K. Jana. Applied Catalysis A, 224 (2002) 51

[4] V.I. Parvulescu, L. Frunza, G. Catana, R. Russu, and V. Parvulescu. Applied Catalysis A, 121 (1995) 69

[5] S. Narayanan and K.V.V.S.B.S.R. Murthy. Applied Catalysis A. 213 (2001) 273

Acknowledgements

Universiti Teknologi Malaysia
MOSTI Malaysia, IRPA : Project No : 09-02-06-0057 SR0005/09-03

PENGGUNAAN TEKNIK KROMATOGRAFI DAN SPEKTROSKOPI RESONANS SPIN ELEKTRON (ESR) BAGI ANALISIS HASIL DAN PENENTUAN SIFAT ANTIOKSIDA HASIL DALAM PENGALKILAN FRIEDEL-CRAFTS *P*-KRESOL.

Aiman Najati Akmar Rahman, Zainab Ramli dan Abdul Rahim Yacob

Jabatan Kimia, Fakulti Sains, Universiti Teknologi Malaysia, 83100 Skudai, Johor.

Keywords : Gas chromatography (GC), Electron Spin Resonance (ESR), antioxidant, Friedel-Crafts, zeolite beta

Abstrak : Tindak balas Friedel-Crafts merupakan tindak balas yang penting dalam proses industri terutamanya bagi menghasilkan bahan farmaseutikal, bahan pewangi, bahan penambah dan juga antioksida. Dalam kajian ini, pengalkilan Friedel Crafts *p*-kresol dengan *tert*-butanol telah dilakukan meggunakan zeolit beta sebagai mangkin, bagi menghasilkan bahan antioksida. Hasil tindak balas dipisahkan menggunakan teknik kromatografi gas – pengesan pengionan nyalaa (GC-FID), pengecaman komponen bagi hasil tindak balas menggunakan teknik kromatografi gas-spektrometri jisim (GC-MS) menunjukkan hasil utama adalah 2-*tert*-butil-*p*-kresol. Analisis kuantitatif GC mendapati peratus pertukaran reaktan, peratus kepilihan hasil dan peratus hasil tindak balas pengalkilan *p*-kresol adalah sebanyak 22.38%, 96.65% dan 21.63% masing-masing. Kajian sifat antioksida hasil tindak balas Friedel Crafts *p*-kresol dilakukan dengan menindakbalaskan hasil tindak balas dengan 1,1-difenil-2-pikril-hidrazil (DPPH) dan kehadiran radikal bebas diukur menggunakan spektroskopi resonans elektron (ESR). Perbandingan kekuatan hasil tindak balas yang mengandungi 2-*tert*-butil-*p*-kresol memberikan aktiviti antioksida 7 kali lebih tinggi berbanding reaktan asalnya *p*-kresol. Keupayaan bertindak balas bagi setiap 1 uL sampel dengan kepekatan DPPH ialah 0.44 mM DPPH/1μL hasil tindak balas pengalkilan berbanding 0.06 mM DPPH/1 μL *p*-kresol.

Abstract : Friedel-Crafts reactions occur in acid catalysed condition. In this study, zeolite beta is used as heterogeneous catalyst for the Friedel-Crafts alkylation reaction of *p*-cresol. All reaction products were analyzed using GC and were identified using GCMS. The alkylation of *p*-cresol with *tert*-butanol was performed at 110 ^{o}C produces 2-*tert*-butyl-*p*-cresol as major product. The reaction gives reactant conversion of 22.38 %, aelectivity of 96.65 % and yield of 21.63 % respectively.The *p*-cresol alkylation reaction gives more than 95 % selectivity of 2-*tert*-butyl-*p*-cresol. Study of the antioxidant properties of the Friedel-Crafts reaction product was conducted by reacting the sample with 1,1-diphenyl-2-pycryl-hydrazil (DPPH) radical and the activity was measured using the Electron Spin Resonance (ESR) method. Comparison of the antioxidant strength of the alkylation product and its starting reactant, *p*-cresol shows that the sample containing 2-*tert*-butyl-*p*-cresol is 7 times higher in antioxidant strength which is 0.44 mM DPPH/1 μL of alkylation sample as compared to the initial reactant, *p*-cresol which only gives 0.06 mM DPPH/1 μL of *p*-cresol.

Pengenalan

Antioksida merupakan bahan yang boleh meneutralkan atau melambatkan kesan pengoksidaan yang disebabkan oleh tindak balas berantai oleh radikal bebas. Radikal bebas menyebabkan proses pengoksidaan bahan yang mengandungi lipid seperti makanan, bahan kosmetik dan bahan farmaseutikal, di mana proses autopengoksidaan lipid oleh radikal bebas menyebabkan kerosakan terhadap kualiti bahan tersebut [1]. Fenomena ini boleh dielakkan atau dilambatkan melalui penggunaan antioksida sintetik atau semulajadi. tert-butil hidroksi toluena (BHT) dan tert-butil hidroksi anisol (BHA) merupakan 2 jenis

antioksida sintetik yang lazim digunakan dalam bahan kosmetik dan makanan. Bahan yang mempunyai struktur molekul menyerupai fenol mempunyai potensi sebagai antioksida kerana radikal yang terhasil daripadanya mrupakan spesies yang stabil dan dapat menghentikan proses pengoksidaan berantai [2]. Penghasilan antioksida melalui pengalkilan Friedel-Crafts fenol dan terbitannya seperti kresol, resorsinol, katekol, 4-metoksifenol bagi menghasilkan antioksida sintetik telah dilaporkan sebelum ini [3-6].

Tindak balas pengalkilan Friedel-Crafts berlaku dalam keadaan mangkin berasid yang homogen atau heterogen. Zeolit merupakan bahan yang popular sebagai mangkin kerana memiliki sifat yang mempunyai kepilihan tinggi tehadap hasil tindak balas, mudah dipisahkan dari hasil tindak balas, aktiviti pemangkinan yang tinggi, stabil secara kimia dan terma, boleh digunakan semula, mesra alam dan tidak menyebabkan masalah hakisan (pengaratan) [7]). Dalam kajian ini, tindak balas Friedel-Crafts p-kresol bermangkinkan zeolit beta dipilih sebagai satu cara bagi menghasilkan antioksida.

Penggunaan kromatografi gas bagi analisis kuantitatif memberikan beberapa kelebihan kerana fasa bergerak gas mempunyai kelikatan yang rendah dan membolehkan penggunaan turus yang panjang seterusnya menghasilkan kecekapan pemisahan yang tinggi. Kelebihan ini menyebabkan ia lazim digunakan bagi analisis hasil tindak balas bagi tujuan ujian aktiviti pemangkinan di mana analisis dilakukan bagi membolehkan pemisahan komponen-komponen di dalam suatu campuran hasil tindak balas serta serta penilaian aktiviti pemangkinan berdasarkan amaun reaktan dan hasil tindak balas yang terkandung dalam satu campuran. Teknik GC dilaporkan sebagai teknik yang lazim digunakan bagi tujuan ujian aktiviti pemangkinan tindak balas Friedel-Crafts yang melibatkan sebatian aromatik [8-12]. Penggunaan GC dengan pengesan pengionan nyala (GC-FID) merupakan kaedah yang sesuai bagi analisis sebatian organik. Kaedah piawai dalaman yang digunakan dalam kajian ini adalah merupakan kaedah di mana amaun tertentu bahan piawai ditambah ke dalam satu siri larutan analit dengan kepekatan yang berlainan. Daripada hasil penyuntikan larutan–larutan tersebut, kelok kalibrasi dihasilkan bagi menentukan kuantiti kepekatan analit dalam sampel. Analisis kuantitatif yang dilakukan adalah menentukan peratus pertukaran reaktan, peratus kepilihan hasil, dan peratus hasil.

Lazimnya, pengujian sifat antioksida dilakukan menggunakan teknik kolorimetri, chemiluminescence dan menggunakan spektrofotometer UV-VIS [13-15]. Dalam kajian ini, resonans spin elektron (ESR) digunakan bagi ujian aktiviti antioksida sampel yang dihasilkan berdasarkan teknik peneutralan radikal 1,1-difenil-2-pikril-hidrazil (DPPH) sebagai teknik yang lebih spesifik dan sensitif bagi mengesan keupayaan sifat antioksida sampel terhadap radikal DPPH [16].

Eksperimen

Bahan kimia

Bahan kimia yang digunakan dalam penyelidikan ini ialah *p*-kresol (Merck, 98.0 %), *tert*–butanol (Merck, 99.5 %), asetik anhidrida (BDH, 99 %) dan zeolit (SiO_2/Al_2O = 25, CP814E, Zeolyst International) sebagai mangkin bagi tindak balas pengalkilan *p*-kresol.Bagi teknik analisis GC pula, 2-propanol (J.T Baker, 100.0 % asai oleh GC) digunakan sebagai pelarut dan toluena (Merck, 99.5 %) sebagai piawai dalaman. Bagi teknik pengujian sifat antioksida menggunakan spektroskopi ESR, bahan kimia yang

digunakan ialah 1,1-difenil-2-pikril-hidrazil, DPPH (Sigma,Aldrich, 90.0 %) dan pelarut etanol (Chemtech, 95.0 %). Air suling, metanol (Fisher, ACS grade) dan asid nitrik (Merck, 65 %) digunakan sebagai bahan pencuci alat radas.

Tindak balas pengalkilan p-kresol

Zeolit beta (0.5 gram) dalam bentuk ammonium diaktifkan dengan melakukan pemanasan dalam relau silinder pada suhu 500 ^{o}C selama 3 jam. *p*-kresol (30 mmol, 3.15 mL) dan *tert*-butanol (30 mmol, 2.85 mL) dipipet dan dimasukkan ke dalam autoklaf keluli 150 mL dan ditambah dengan mangkin zeolit beta yang telah diaktifkan. Autoklaf dimasukkan ke dalam ketuhar pada suhu 110 ^{o}C selama 24 jam dan tindak balas berlaku tanpa pengadukan. Pensampelan hasil dilakukan sebelum penambahan mangkin, 5 minit selepas mangkin ditambah, dan apabila tindak balas berakhir iaitu pada masa 24 jam dengan menggunakan mikropipet dan disimpan dalam botol sampel.

Analisis Hasil Tindak balas Menggunakan GC

Kaedah piawai dalaman digunakan dalam analisis ini di mana toluena dipilih sebagai piawai dalaman dan 2-propanol sebagai pelarut. Satu siri piawai *p*-kresol dengan kepekatan 1, 3, 5, 7, dan 10 M serta toluena dengan kepekatan 10 M disediakan bagi menghasilkan graf kalibrasi *p*-kresol/toluena melawan kepekatan *p*-kresol, M. Bagi analisis sampel, sebanyak 100 µL piawai dalaman ditambah kepada 100 µL sampel. Analisis sampel GC Hewlett Packard GC 5890 Series II dengan pengesan pengionan nyala (FID) dengan turus Carbowax (diameter 0.25 mm, tebal selaput tipis 0.2 µm dan panjang 30 m) suhu teraturcara dilakukan dengan isipadu suntikan 0.2 µL, suhu awal ketuhar 50 ^{o}C dengan masa awal 5 minit, kadar peningkatan suhu 15 ^{o}C per minit suhu akhir ketuhar 200 ^{o}C dan masa akhir selama 15 minit.Pengenalpastian hasil dilakukan menggunakan alat kromatografi gas-spektrometer jisim.

Peratus pertukaran, % A

$$\%\ A = \frac{A_{awal} - A_{akhir}}{A_{awal}} \times 100 \qquad \text{Persamaan 1.1}$$

Peratus selektiviti hasil, % B

$$\%\ B = \frac{B}{B_{jumlah\ hasil}} \times 100 \qquad \text{Persamaan 1.2}$$

Peratus hasil, % C

$$\%\ C = \frac{A_{awal} - A_{akhir}}{A_{awal}} \times \frac{B}{B_{jumlah\ hasil}} \times 100 \qquad \text{Persamaan 1.3}$$

Dengan,

A awal = keluasan *p*-kresol awal
A akhir = keluasan *p*-kresol akhir
B = keluasan 2-*tert*-butil *p*-kresol
B jumlah = keluasan seluruh hasil tindak balas (tidak termasuk reaktan)

Analisis kuantitatif bagi ujian aktiviti pemangkinan bagi menegetahui peratus pertukaran reaktan, peratus kepilihan hasil dan peratus hasil dikira berdasarkan persamaan 1.1, 1.2 dan 1.3 masing-masing.

Pengujian sifat antioksida hasil tindak balas menggunakan radikal DPPH
Aktiviti antioksida sampel hasil tindak balas pengalkilan *p*-kresol dan sampel tulen *p*-kresol diuji dengan menggunakan kaedah pemencilan 1,1-difenil-2-pikril-hidrazil (DPPH) yang merupakan radikal bebas yang stabil, menggunakan kaedah spektroskopi resonans spin elektron (ESR). Satu siri larutan piawai DPPH dalam etanol disediakan dengan kepekatan 2, 4, 6, 8 dan 10 mM bagi menghasilkan graf kalibrasi ketinggian isyarat ESR,cm melawan kepekatan DPPH, mM. Campuran tindak balas mengandungi 120 µL sampel dan 120 µL larutan DPPH dalam etanol bagi setiap kepekatan DPPH 2, 4, 6, 8 dan 10 mM. Analisis menggunakan spektrometer ESR model JEOL-JES FA 100 dilakukan menggunakan parameter berikut : modulasi frekuensi, 100 kHz; amplitud, 20; pusat medan, 322.167 mT; kuasa, 0.998 mW, frekuensi gelombang mikro, 9020.429 MHz; dan masa sapuan, 30 saat. Campuran dianalisis selepas 30 saat pengadukan.

Keputusan dan perbincangan

Penyediaan Graf Kalibrasi Piawai p-kresol bagi Tindak balas Friedel-Crafts
Hasil tindak balas dianalisis menggunakan kromatografi gas teknik piawai dalaman. Toluena telah dipilih sebagai piawai dalaman kerana mempunyai struktur yang hampir sama dengan *p*-kresol, manakala isopropanol digunakan sebagai pelarut dalam kromatografi gas kerana sifatnya yang mudah meruap. Kuantiti setiap sebatian yang dapat dikenalpasti melalui pemisahan oleh kromatografi gas dilakukan dengan membandingkan luas puncak piawai dalaman dengan reaktan (*p*-kresol). Rajah 1 menunjukkan graf piawai dalaman bagi nisbah luas puncak *p*-kresol/toluena melawan kepekatan *p*-kresol, M. Daripada graf ini, diperolehi satu garis lurus dengan kecerunan yang positif. Graf ini digunakan bagi mendapatkan kepekatan *p*-kresol dalam tindak balas dan bagi mengira peratus pertukaran *p*-kresol pada masa–masa tertentu. Kromatogaram GC hasil pemisahan tindak balas pengalkilan *p*-kresol mengandungi piawai dalaman, dengan kehadiran puncak toluena pada t_R = 7.9 minit dan pelarut isopropanol pada 5.4 minit.

Analisis hasil tindak balas pengalkilan p-kresol
Pengalkilan *p*-kresol oleh *tert*-butanol memberikan hasil utama 2-*tert*-butil-*p*-kresol dan hasil lain iaitu 2,6-di-*tert*-butil-*p*-kresol dan eter. Tindak balas ini merupakan contoh bagi mekanisme penukargantian elektrofilik, di mana karbokation *tert*-butil terbentuk oleh penukargantian *tert*-butanol dan gelang aromatik seperti yang ditunjukkan oleh persamaan 1.4. Kromatogram memberikan lima puncak utama pada masa penahanan, t_R = 2.4, 5.4, 7.9, 22.6 dan 25.4 minit. Puncak bagi reaktan adalah pada 2.4 minit dan 22.6 minit iaitu *tert*-butanol dan *p*-kresol masing-masing. Puncak pada masa penahanan 25.4 minit merupakan hasil utama yang dikenalpasti melalui GC-MS sebagai 2-*tert*-butil-*p*-kresol yang berada dalam kedudukan orto terhadap kumpulan hidroksi. Secara organik, kumpulan hidroksi

merupakan pengarah orto dan para, tetapi disebabkan kedudukan para pada gelang telah dilindungi oleh kumpulan metil, maka hanya isomer orto yang terbentuk dalam tindak balas ini. Pada t_R di antara 22.0 – 26.0 minit terdapat dua puncak kecil dilabel sebagai D yang mungkin merupakan 2,6-di-*tert*-butil-*p*-kresol dan eter yang mempunyai struktur hampir sama dengan hasil utama. Devassy *et al*. telah melaporkan penghasilan eter dan 2-6-di-*tert*-butil-*p*-kresol dalam tindakbalas pengalkilan *p*-kresol dengan *tert*-butanol menggunakan mangkin asid heteropoli berpenyokong zirkonia [17]. Walaubagaimanapun, kedua-dua puncak memberikan luas yang sangat kecil menyebabkan kepilihan hasil terhadap 2-*tert*-butil-*p*-kresol menghampiri 100 %. Ini disebabkan saiz molekul 2-6-di-*tert*-butil-*p*-kresol dan eter adalah lebih besar untuk menembusi liang zeolit beta yaang mempunyi diameter 7 Å sehingga menyebabkan hasil cenderung kepada pembentukan 2-*tert*-butil-*p*-kresol. Peratus pertukaran, kepilihan hasil dan peratus hasil tindak balas dikira menggunakan persamaan 1.1,1.2 dan 1.3.

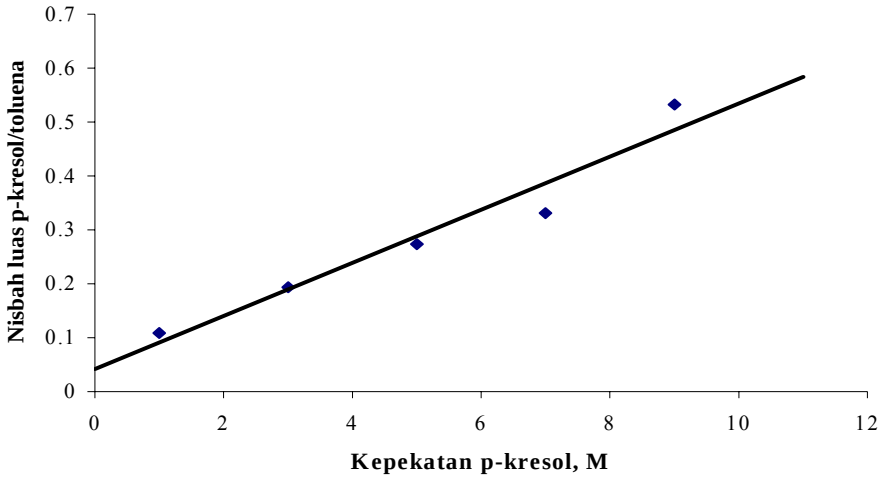

Rajah 1 : Graf kalibrasi piawai dalaman nisbah luas *p*-kresol/ toluena dibandingkan dengan kepekatan *p*-kresol.

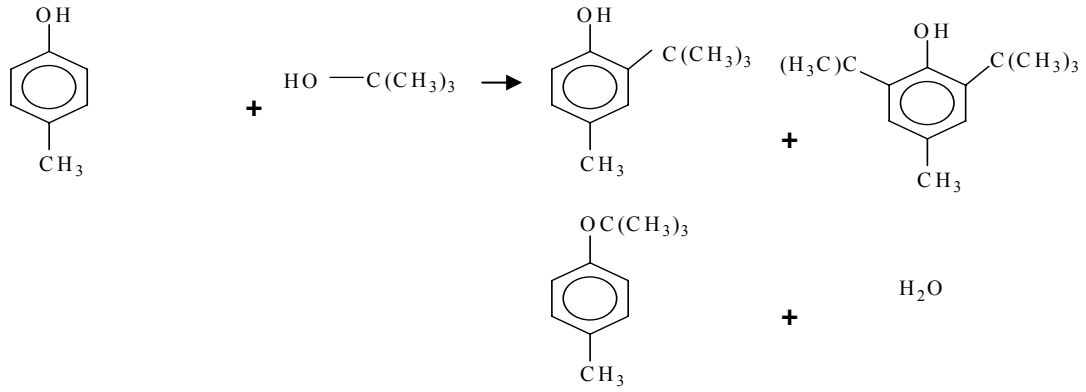

Persamaan 1.4 : Persamaan tindak balas pengalkilan *p*-kresol dengan *tert*-butanol [17].

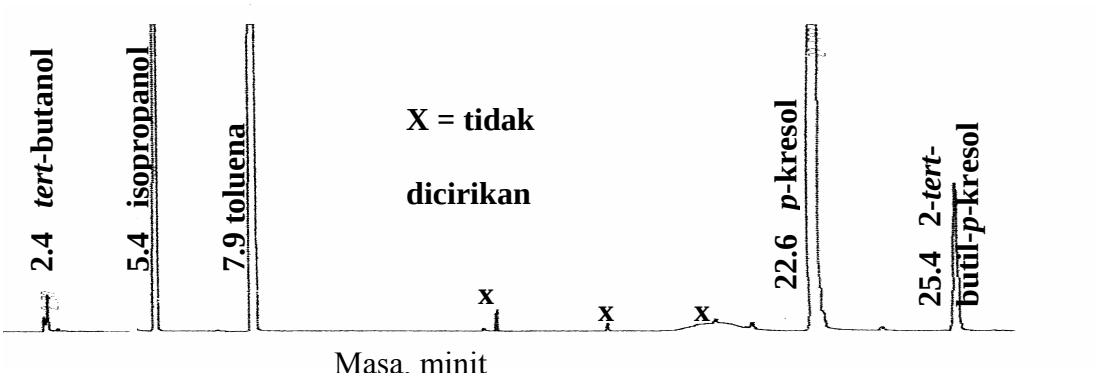

Rajah 3 : Kromatogram GC hasil tindak balas pengalkilan *p*-kresol yang mengandungi piawai dalaman.

Jadual 1: Peratus pertukaran, kepilihan dan hasil bagi tindak balas pengalkilan *p*-kresol tanpa mangkin dengan mangkin zeolit beta**.**

Tindak balas	Peratus,%		
	Pertukaran	Kepilihan	Hasil
Tanpa mangkin	8.90	34.10	3.00
Mangkin zeolit beta	22.38	96.65	21.63

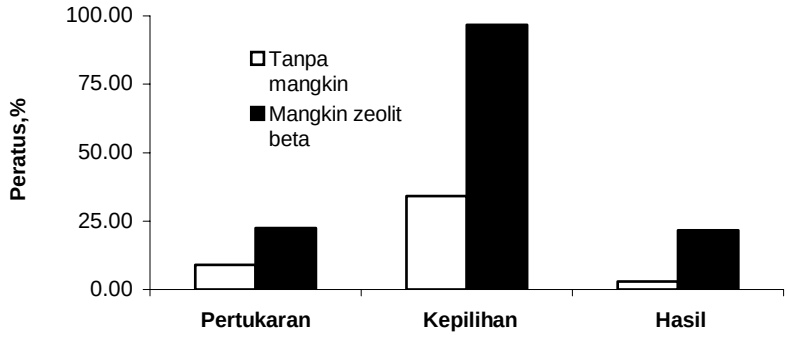

Rajah 4: Peratus pertukaran, kepilihan dan hasil bagi tindak balas pengalkilan *p*-kresol tanpa mangkin dan dengan mangkin zeolit beta**.**

Pengujian sifat antioksida sampel pengalkilan p-kresol menggunakan radikal DPPH.

Radikal 1,1-difenil-2-pikril-hidrazil (DPPH) digunakan untuk menguji sifat antioksida sampel hasil tindak balas pengalkilan Friedel-Crafts ini dan reaktan asalnya iaitu *p*-kresol. Radikal DPPH merupakan satu radikal bebas yang stabil mengandungi satu elektron tidak berpasangan dalam strukturnya. Sifat antioksida sampel diuji berdasarkan kebolehannya membentuk (DPPH)**:**H. secara pendermaan elektron dengan meneutralkan elektron tidak berpasangan pada radikal DPPH [18]. Aktiviti antioksida sampel terhadap radikal DPPH diukur berdasarkan pengurangan ketinggian isyarat ESR DPPH dalam larutan etanol menggunakan instrumen elektron spin resonans (ESR).

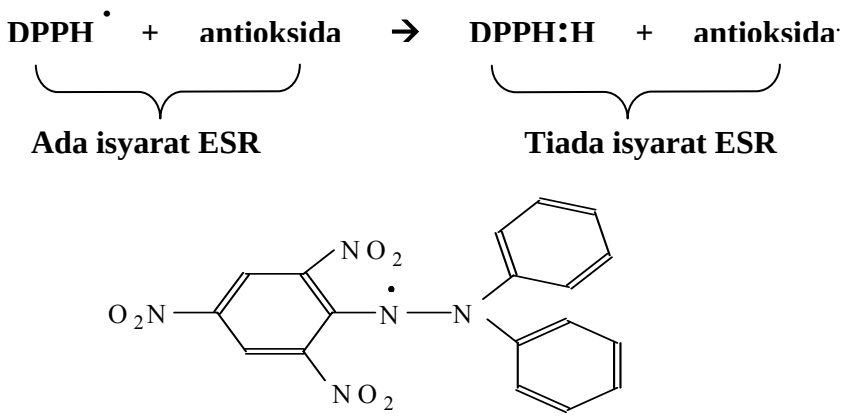

Rajah 5 : Struktur radikal 1,1-difenil-2-pikril-hidrazil (DPPH).

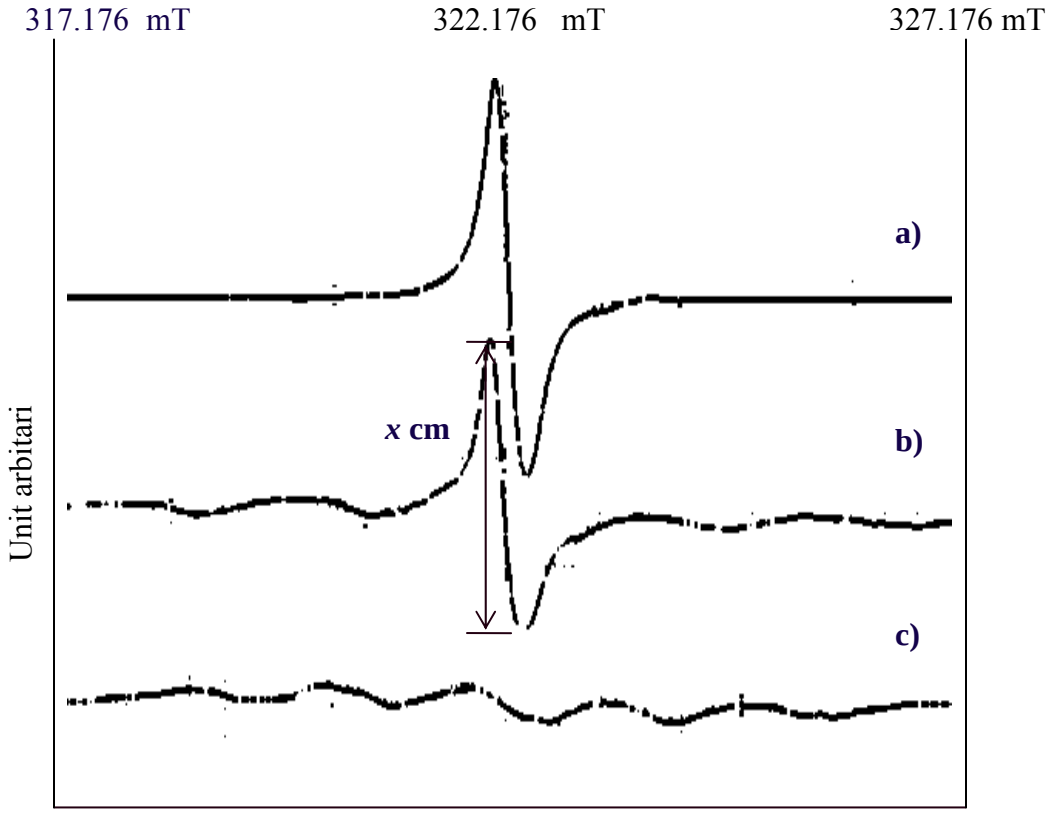

Rajah 6: Spektrum ESR (a) pepejal DPPH tulen (b) 10 mMDPPH dalam etanol (c) 10 mM DPPH dalam etanol yang mengandungi hasil pengalkilan.

Rajah 6(a) menunjukkan spektrum ESR DPPH tulen dalam keadaan pepejal, di mana kehadiran puncak disebabkan oleh kehadiran elektron tidak berpasangan pada radikal DPPH tersebut. Rajah 6(b) pula menujukkan spektrum DPPH dalam 10 mM pelarut etanol, di mana puncak DPPH dalam keadaan pepejal masih wujud menunjukkan fasa pepejal DPPH masih lagi terdapat dalam larutan tersebut. Spektrum ini menghasilkan hanya lima puncak berdasarkan aturan 2nI + 1, (n = bilangan atom nitrogen, I = spin nukeus bagi atom nitrogen, I =1, bagi ^{14}N). secara amnya, nukleus spin I memecahkan spektrum kepada 2nI + 1 garis hiperhalus. Spektrum menunjukkan elektron berada di antara 2 atom nitrogen yang terdapat dalam radikal tersebut. Julat ketinggian yang diberikan tanda ***x*** merupakan ketinggian isyarat ESR yang diukur bagi menentukan aktiviti antioksida.

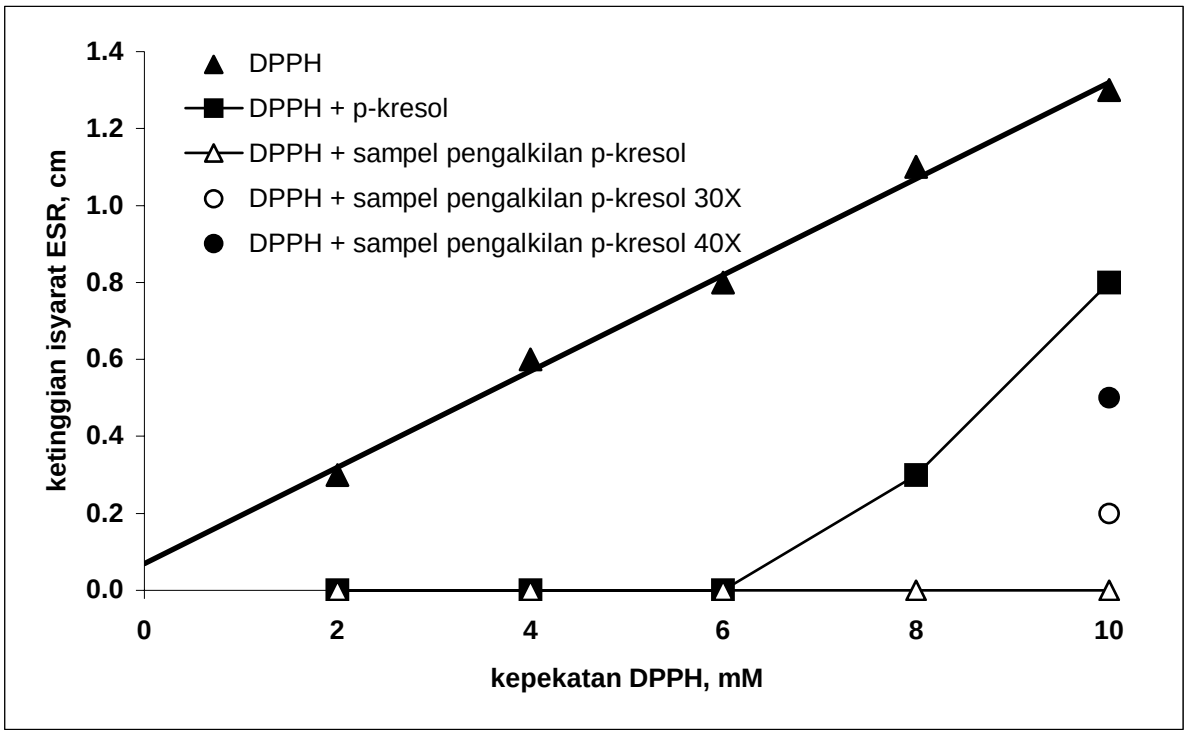

Rajah 7 : Graf ujian antioksida sampel pada kepekatan 2-10 mM DPPH

Jadual 2 : Peratus DPPH yang bertindak balas dengan sampel bagi setiap kepekatan DPPH

Kepekatan DPPH, mM	% DPPH bertindak balas	
	p-kresol	hasil pengalkilan *p*-kresol
2	100	100
4	100	100
6	100	100
8	72.7	100
10	38.5	100

Jadual 3 : Peratus DPPH yang bertindak balas dengan sampel penglkilan yang dicairkan pada kepekatan 10 mM

Kepekatan DPPH, mM	% DPPH bertindak balas bagi hasil pengalkilan p-kresol	
	30 kali pencairan sampel	40 kali pencairan sampel
10	84.61	61.54

Bagi menentukan kepekatan radikal DPPH yang bertindak balas dengan sampel antioksida, satu graf ketinggian isyarat ESR, cm melawan kepekatan DPPH telah diplot berdasarkan 2,4,6,8 dan 10 mM DPPH, seterusnya peratus DPPH yang bertindak balas dikira. Melalui jadual 2, didapati, keupayaan antioksida sampel hasil pengalkilan *p*-kresol adalah lebih baik berbanding reaktan asalnya. Ini dapat dilihat berdasarkan rajah 7, di mana sampel hasil pengalkilan *p*-kresol dapat bertindak balas dengan 100 % DPPH berpekepekatan 10 mM, berbanding sampel *p*-kresol yang berjaya bertindak balas dengan hanya 38.5 % DPPH pada kepekatan yang sama. Secara teorinya, struktur molekul dapat menerangkan keupayaan antioksida sampel yang mengandungi 2-*tert*-butil-*p*-kresol dan *p*-kresol. 2-*tert*-butil-*p*-kresol mengandungi kumpulan alkil pada kedudukan orto gelang, kumpulan alkil merupakan kumpulan penderma elektron. Kehadiran kumpulan penderma elektron pada gelang aromatik berhampiran kumpulan hidroksi menyebabkan struktur yang terhasil daripada tindak balas dengan DPPH adalah lebih stabil, memudahkan lagi tindak balas berlaku berbanding sampel tulen *p*-kresol, ini menjadikan sampel pengalkilan sebagai antioksida yang lebih baik.

Kesimpulan

Daripada ujikaji, didapati tindak balas pengalkilan *p*-kresol dengan *tert*-butanol bermangkinkan zeolit beta memberikan peratus kepilihan hasil yang tinggi menghampiri 100 %. Analisis kuantitatif hasil tindak balas menggunakan teknik kromatografi gas piawai dalaman memberikan peratus pertukaran reaktan, peratus kepilihan hasil dan peatus hasil bagi tindak balas ini sebanyak 22.38 %, 96.65 %, 21.63 % masing-masing. Pengecaman hasil tindak balas menggunakan GC-MS menunjukkan hasil utama bagi merupakan 2-*tert*-butil-*p*-kresol. Kajian antioksida terhadap sampel pengalkilan *p*-kresol menunjukkan sampel pengalkilan *p*-kresol merupakan antioksida yang 7 kali lebih baik berbanding reaktan asalnya, *p*-kresol sendiri. 1 µL sampel pengalkilan berupaya bertindak balas dengan 0.44 mM DPPH berbanding 1 µL *p*-kresol yang hanya mampu bertindak balas dengan 0.06 mM DPPH.

Penghargaan

1. Jabatan Kimia, Fakulti Sains, UTM.
2. Ibnu Sina Institute for Fundamental Science Studies, UTM.
3. MOSTE, IRPA : No Projek: 09-02-06-0057 SR0005/09-03

Rujukan

1. V.Louli ,N.Ragoussis,K.Magoulas (2004). "Recovery of phenolic antioxidants from wine industry by-products". *Bioresource Technology* .**9** .201 –208
2. V. Bondet, W. Brand-Williams and C.Berset (1997). " Kinetics And Mechanism of Antioxidant Activity using the DPPH Free Radical Method". *Academic Press*. **30**.609-615
3. Ganapati D.Yadav, Nirav S. Doshi (2002). "Alkylation of Phenol with methyl-tert-butyl ether and tert-butanol over Solid Acids: Efficacies of Clay-Based Catalysts.*Applied Catalysis A General*.**236**. 129-147
4. Sankarasubbier Narayanan *, K.V.V.S.B.S.R. Murthy (2001). "Montmorillonite as a versatile solid acid catalyst for *ter*t.-butylation of resorcinol ". *Applied Catalysis A: General* .**213**. 273–278
5. Jung Whan Yoo a , Chul Wee Lee a , Sang-Eon Park , Jaejung Ko (1999). "Alkylation of catechol with t-butyl alcohol over acidic zeolites". *Applied Catalysis A: General* .**187**. 225–232
6. Ganapati D. Yadav, M.S.M Mujeebur Raahuman (2003). "Efficacy of solid acids in the synthesis of butylated hydroxy anisoles by alkylation of 4-methoxyphenol with MTBE". *Applied Catalysis A:General.* **253**.113-123
7. Krishnan, A.V. Keka Ojha and C. Pradhan, Narayan (2002). "Alkylation of Phenol with Tertiary Butyl Alcohol over Zeolites". *Organic Process Research & Development*. **6** . 132-137
8. Kanakkampalayam Krishnan Cheralathan, Inguva Sudarsan Kumar, Muthiahpillai Palanichamy, Velayutham Murugesan (2003). " Liquid Phase Alkylation of Phenol with 4-hydroxybutan-2-one in the presence of Modified Zeolite Beta". *Applied Catalysis A: General*. **241**. 247-260
9. Vogt, A. Kouwenhoven, H.W. and Prins, R (1994). "Fries Rearrangement over Zeolitic Catalysts". *Applied Catalysis A: General*. **123**.37-49
10. Emil Dumitriu and Vasile Hulea (2003). "Effects of Channel Strucure and Acid Properties of Large Pore Zeolites in the Liquid-phase tert-butylation of Phenol". *Journal of Catalysis*. **218**. 249-257
11. Maurizio Lenarda, Massimo Da Ros, Manuela Casagrande, Loretta Storaro, Renzo Ganzerla (2002). "Post-synthethic Thermal and Chemical Treatments of H-BEA Zeolite: Effects on the Catalytic Activity". *Inorganica Chimica Acta*. **349**. 195-202
12. Jung Whan Yoo, Chun Wee Lee, Sang Eon Park, Jaejung Ko (1999). "Alkylation of catechol with ter-butyl alcohol over Acidic Zeolites". *Applied Catalysis A: General*. **187**. 225-232.
13. Irene Parejo, Carles Codina, Christos Petrakis, Panagiotis Kefalas (2000). "Evaluation of Scavenging Activity Assesed by Co(II)/EDTA-induced luminol chemiluminescence and DPPH (2,2-diphenyl-1-picrylhydrazil) Free Radical Assay". *Journal of Pharmacological and Toxicological Methods*. **44**. 507-512
14. Ahmet Cakir, Ahmet Mavi, Ali Yildirim, Mehmet Emin Duru, Mansur Harmandar, Cavit Kazaz (2003). "Isolation and Characterization of Antioxidant Phenolic Compounds from the Aerial Parts of *Hypericum hyssopifolium* L. by Activity Guided Fractionation". *Journal of Ethno-Pharmacology*. **87**. 73-83
15. T.Kulisic, A.Radonic, V.Katalinic, M.Milos (2003). "Use of Different Methods for Testing Antioxidative Activity of Oregano Essential Oil". *Food Chemistry*. Article In Press
16. Hiroyuki Ukeda, Yukiko Adachi, Masayoshi Sawamura (2002). "Flow injection Analysis of DPph Radical Based on Electron Spin Resonance". *Talanta*. **58**. 1279-1283
17. Devassy Biju, M. Shanbhag, G.V.Lefebvre, F. and Halligudi, S.B (2003). "Alkylation of *p*-cresol with *tert*-butanol Catalyzed by Heteropoly Acid Supported on Zirconia Catalyst". *Journal of Molecular Catalysis*. Science Direct. In Press.
18. Zhu – Qiu Jin and Xiu Chen (1998). "A Simple Reproducible Model of Free Radical Injured Isolated Heart Induced by, 1,1-difenil-2-pikril-hidrazil (DPPH)". *Journal of Pharmacological And Toxicological Methods*. **39**. 63-70.

Reactivity of Modified Zeolite Beta Catalyst In The Friedel Crafts Alkylation Of Resorcinol With *Tert*-Butanol

INTRODUCTION

Friedel-Crafts Alkylation

Friedel-Crafts alkylations are very well established reaction in organic synthesis. For example butylation of dihydroxybenzenes is an industrially important reaction as the products of this reaction; butylhydroxybenzenes are useful materials in the synthesis of antioxidants, polymer stabilizers and in the treatment of mitochondrial respiration ailments (Narayanan and Murthy, 2001). In the Friedel-Crafts alkylation of aromatic compounds, a hydrogen atom or other substituent group of an aromatic nucleus is replaced by an alkyl group through the interaction of an alkylating agent in the presence of catalysts. The most frequently used alkylating agent are alkyl halides, alkenes and alcohols although aldehydes, ketones and various other reagents have also been used (Olah, 1973).

This reaction typically needs homogeneous catalysts containing a lot of acid sites. Generally, a conventional Lewis acid catalyst such as $AlCl_3$, BF_3 and $TiCl_4$ was widely used in an industrial process. Besides that, mineral acid such as sulfuric acid, phosphoric acid, hydrogen fluoride and aqueous citric acid have also been used as catalysts. However, Lewis acids must be used in higher than stoichiometric amounts and the catalysts must be destroyed at the end of the reaction with a significant production of undesirable wastes. Thus, it is highly desirable to develop new processes that can reduce the environmental and economic problems associated with the classical Friedel-Crafts alkylation catalysts (Aguilar *et al*., 2000). Finally, reactions are not always clean and may lead to a mixture of products. Figure 2.10 shows the mechanisme of alkylation of benzene with *tert*-butyl chloride as an alkylating agent with $AlCl_3$ as Lewis acid catalysts (Wade, 2003).

The use of recoverable and regenerable solid acid catalysts such as zeolites, phosphotungstic acid ($H_3PW_{12}O_{40}$) supported on SiO_2 in the form of cerium salt (Castro *et al*., 1998), mesoporous molecular sieves such as MCM-41 (Gunnewegh *et al*., 1996; Zhao *et al*., 2003) and clay such as montmorillonite (Narayanan and Murthy, 2001; Yadav and Doshi, 2003) can overcome many problems of these types. The use of this heterogeneous catalyst is due

to the high selectivity of yield, good in separation and the recyclable of the catalyst. Narayanan and Murthy, (2001) reported the catalytic activity of different solid acid catalysts such as zeolites Y, HZSM-5, alumina, MCM-41 and montmorillonite on catalyzed Friedel-Crafts alkylation of resorcinol with *tert*-butanol. Modified montmorillonite was found to be active catalysts in the reaction. Armengol *et al.* (1995) reported the alkylation of benzene and toluene with cinnamyl alcohol. The reaction was carried out in the presence of a series of acid Y faujasites and with different framework Si to Al ratio. Zhang *et al.* (1998) have studied the alkylation of phenol by *tert*-butyl alcohol catalysed by zeolite H-Beta. The catalytic properties of zeolite Beta in the *tert*-butylation of phenol are best in the reaction temperature ranges from 378-458 K. Medium acid sites on zeolite Hβ are advantageous to produce *ρ-tert*-butylphenol and that of strong acid sites are helpful for the formation of 2,4-di-*tert*-butylphenol, while weak acid sites are effective in producing *o-tert*-butylphenol.

Zeolites Beta is one of the zeolite types which are currently being widely studied for their application in the synthesis of organic and fine chemicals. Zeolite Beta has proven to be a reactive catalysts in many organic processes such as alkylation, (Cheralathan *et al*., 2003; Chiu *et al*., 2004; Shi *et al.*, 2002; Barthel *et al*., 2001; Halgeri and Das, 1999; Mitra *et al*., 1997; Algarra *et al.*, 1995; Nivarthy *et al*., 1998) acylation (Escola and Davis, 2001; Casagrande *et al*., 2000; Das and Cheng, 2000; Kim *et al.,* 2000) and various hydrocarbon reactions (Absil *et al*., 1998).

The key opportunity for the use of zeolites Beta as catalyst relies on their unique pores, which can control the selectivity of the reaction. Furthermore, zeolite Beta has a high Si/Al ratio, large pore, high acid strength and thermal stability (Pariente *et al*., 1987; Meier *et al.*, 1996). It is well known that zeolite Beta has both Brönsted and Lewis acid sites. Due to the acid property, zeolite Beta can be catalyzed Friedel-Crafts reaction. Narayanan and Sultana (1998) have proposed the reaction mechanism of aniline alkylation with ethanol over zeolites which was catalyzed by Brönsted acid site. It has been reported that both Brönsted and Lewis acid sites or either one of their can catalyzed the alkylation of aniline over solid acid catalysts at different condition (Narayanan and Deshpande, 1995; 2000).

The application of zeolite Beta catalyst to the Friedel-Crafts alkylation of aromatic compounds has been described in the literatures. Alkylation of benzene with propylene is an industrially important reaction for the production of isopropyl benzene, an intermediate for

the production of acetone and phenol and the reaction was catalysed by zeolite Beta (Han *et al*., 2003). Zeolite Beta was reported by Barthel *et al*. (2001) to show high selectivity as a catalyst in the hydroxyalkylation of anisole with chloral. Shi *et al.* (2002) have studied the alkylation of benzene with ethylene to ethylbenzene over zeolite Beta catalysts. The results showed that high pressure operating conditions, including the supercritical fluid operation, may be harmful to the catalyst structure, and the operation in the vapor-liquid state near the critical point may cause heavy destruction to the catalyst.

The influence of the concentration of acid sites for isobutene or *n*-butene alkylation on zeolite Beta with varying degrees of Na^+ ion exchanged was reported by Nivarthy *et al.* (1998). All catalysts studied showed complete conversion of *n*-butene over a significant time-on-stream. Isooctanes were the dominating products over H-BEA, while the importance of di- and multiple alkylation increased with increasing Na^+ concentration in the zeolite. Halgeri and Das (1999) have studied the novel catalytic aspects of zeolite Beta for alkyl aromatic transformation. Zeolite Beta was found to be selective for cymenes and diisopropyl benzene formations and zeolite Beta appears to be quite promising candidate for several commercial applications. Mitra *et al.* (1997) have also been studied the alkylation of aromatics on zeolite Beta. The alkylation of benzene with isobutanol gave a mixture of secondary butyl benzene and isobutyl benzene instead of tertiary butyl benzene which is usually obtained.

Friedel-Crafts alkylation of dihydroxybenzene is an industrially important reaction to produce fine chemicals. The product butylhydroxybenzenes in particular are useful materials in the synthesis of antioxidants, polymer stabilizers and in the treatment of mitochondrial respiration ailments. Butylhydroxybenzenes such as butylated hydroxyanisole (BHA) and butylated hydroxytoluene (BHT) are commercial synthetic antioxidants. BHA and BHT are the most widely used antioxidants in the food industry, especially for oils and also known to increase the storage life of fatty food materials (Rehman and Salariya, 2006). These synthetic antioxidants are highly active and cheap. They are colourless, odourless and tasteless, but they are generally active only at low temperature (Zhang *et al*., 2004).

Resorcinol is an example of a derivative of hydroxybenzene and the product from the alkylation of resorcinol also has an antioxidant property. Alkylation of resorcinol has been studied using *tert*-butanol, (Biju *et al*., 2004; Narayanan and Murthy, 2001) ethyl

acetoacetate, propynoic acid and propenoic acid (Gunnewegh *et al*., 1996) as an alkylating agents. Most of the information in connection with the Friedel-Crafts alkylation of dihydroxybenzenes such as resorcinol was using mineral acids such as sulfuric acid, phosphoric acid and aqueous citric acid as catalysts. Narayanan and Murthy (2001) was first reported the use of solid acid catalysts for the *tert*-butylation of resorcinol. The liquid phase alkylation of resorcinol with *tert*-butyl alcohol was carried out over HZSM-5, HY, HM, MCM, alumina, montmorillonite-K10 and modified montmorillonite-K10. The major products of this reaction are 4-*tert*-butylresorcinol and 4,6-di-*tert*-butylresorcinol. Biju *et al.* (2004) described the alkylation of resorcinol with *tert*-butanol, carried out using zirconia supported phosphotungstic acid as catalyst in liquid phase conditions which resulted in the formation of different products found in the liquid phase. The different products obtained were the results of different pathways corresponding to the transformation of O-alkylated products into C-alkylated products as shown in Figure 1. Such rearrangements occurred on heating or by contact with acid catalysts. It is clear from the reaction scheme that resorcinol mono *tert*-butyl ether is a primary product while 4-*tert*-butylresorcinol can be a primary and/or a secondary product depending on the kinetics of the butylation reaction.

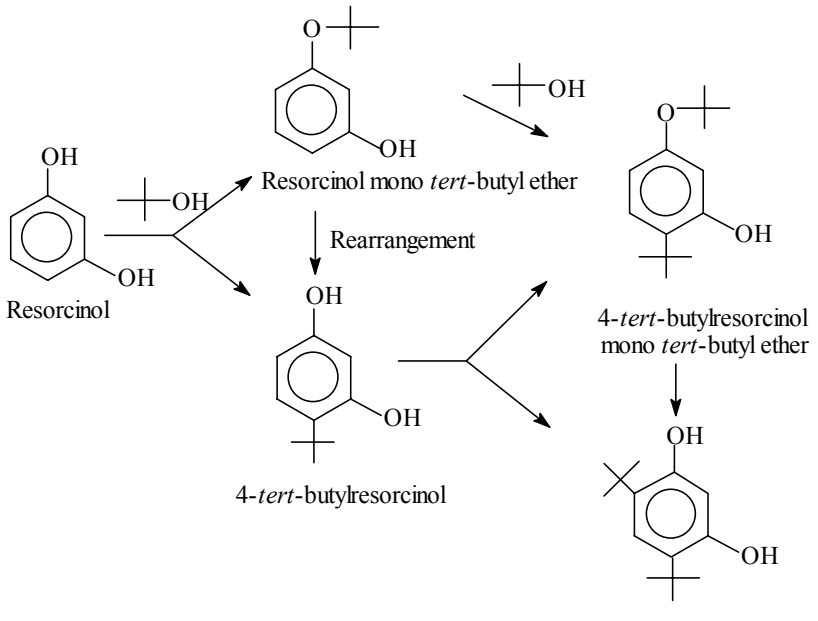

Figure 1: The formation of different products in Friedel-Crafts alkylation of resorcinol with *tert*-butanol (Biju *et al*., 2004)

Antioxidant

An antioxidant is a compound which can donates a nonpair electron and neutralizes the effect of an oxidation. Human body cells use electrons to get energy and molecules loss

electrons and free radicals appear (Bergman *et al.,* 2003). These radicals are very unstable and react rapidly with the other groups or substances in the body, leading to cell or tissue injury (Je *et al.,* 2004). Free radicals are generally very destructive for lipids and lipid-soluble substances in foods, leading to the formation of-flavours and undesirable chemical compounds, as well as destructive for human body cells, by interfering in metabolic reactions (Louli *et al.,* 2004). Free radicals in human body can destroy DNA structure and caused aging and diseases such as cancer, atherosclerosis, gastric ulcers, pulmonary dysfunction and several other diseases. Antioxidants, which scavenge free radicals, are known to possess an important role in preventing these free radicals induced diseases (Ukeda *et al.,* 2002).

Antioxidant properties are among the first links between chemical reactions and biological activity and have been extensively studied for the past 10 years. Many synthetic antioxidants with benzene derivatives such as butylated hydroxylanisole (BHA) and butylated hydroxytoluene (BHT) are well known to possess this activity (Trouillas *et al.,* 2003). In the present study, we will investigate the free radical scavenging activity of butylated resorcinol which relate to its antioxidative activities. The antioxidative activities of samples will be evaluated on the basis of their abilities to scavenge 1,1-diphenyl-2-picrylhydrazyl (DPPH) radical to form (DPPH)**:**H. The free radical signals can be detected by Electron Spin Resonance (ESR) technique.

EXPERIMENTAL

Synthesis of Zeolite Beta

Zeolite Beta was synthesized using rice husk ash (RHA) as a silica source and the ash is in the form of amorphous silica. The synthesis of zeolite beta was carried out hydrothermally at 150°C in a stainless steel autoclave for six days from mixtures containing amorphous silica from RHA, sodium aluminate, tetraethylammonium hydroxide, sodium hydroxide based on the method described by Didik (2001). The gel was prepared according to the following molar chemical composition:

$$1.96\ Na_2O : 27\ SiO_2 : Al_2O_3 : 5\ TEA_2O : 240\ H_2O.$$

The gel mixture was stirred vigorously for about two hours. The gel formed was then transferred into a stainless steel autoclave and kept in an air oven for crystallization at 150°C for 6 days. To stop the crystallization process after 6 days, the autoclave was immersed in

cold water. The solid product recovered by filtration was washed repeatedly with demineralized hot water until the pH of the filtrate was ~ 7.0. Finally, the product was dried at 100°C in an air oven overnight. The solid product marked as Si-27 which means the sample was synthesized from the gel mixture having $SiO_2/Al_2O_3 = 27$.

The Si-27 sample was calcined at 550°C for 16 hours to remove the organic material occluded in the zeolite pores and to obtain the sodium form of the zeolite Beta. The calcination temperature was increased slowly from room temperature to 550°C at a heating rate of 1°C/min. The sample obtained after calcination was named as Si-27cal.

Modification of Zeolite Beta

Zeolite Beta was modified to optimize the acidity of the zeolite Beta and to increase the catalytic efficiency. In this research, zeolite Beta was modified by two methods;

(i) preparation of zeolite Beta at different SiO_2/Al_2O_3 ratio of the initial gel

(ii) impregnation of niobium(V) ethoxide into zeolite Beta samples.

Preparation of Zeolite Beta at Different SiO_2/Al_2O_3 Ratio

To investigate the effect of framework Si/Al towards catalytic activity, zeolite Beta was synthesized at a different SiO_2/Al_2O_3 molar ratio of initial gel composition. Zeolite Beta with SiO_2/Al_2O_3= 45 and 90 (Si-45 and Si-90) was synthesized by using the same method as synthesized Si-27 sample. Table 1 listed the different oxides mole ratios of the initial gel containing silica, water, sodium hydroxide, alumina and organic template. All the samples were characterized by XRD to confirm the phase of crystal growth in the samples. The samples obtained were referred to Si-27, Si-45 and Si-90 in which the number was referred to the SiO_2/Al_2O_3 ratio of the initial gel.

Table 1: Ratio of gel oxides mixture in the preparation of zeolite beta based on the mole oxides.

Sample name	SiO_2/Al_2O_3 ratio	Na_2O	Al_2O_3	SiO_2	TEA_2O	H_2O
Si-27	27	1.96	1	27	5	240
Si-45	45	4.00	1	45	10	480
Si-90	90	8.00	1	90	20	800

The Na-form of zeolite Beta sample (Na-BEA) which contains Na cation was converted to the NH_4-form (NH_4-BEA) by ammonium cation. Ion exchange was done by using ammonium nitrate solution (1 M). The Na-BEA samples (5 g) were mixed with ammonium nitrate solution (1 M). The mixture was stirred for about 4 hours at 80°C. Then, zeolite was filtered and washed repeatedly with distillated water. The ammonium exchange was repeated three times. Finally, the protonated form (H-BEA) was obtained by calcining the NH_4-form at 550ºC for 4 hours.

Impregnation with Niobium(V) ethoxide

Niobium oxide was introduced into zeolite Beta by wet impregnation method. Niobium(V) ethoxide ($Nb(OC_2H_5)_5$) was used as the source of Nb species. Appropriate amount of niobium(V) ethoxide to obtain 1, 2 and 4 wt% Nb were dissolved in 50 mL of 2-propanol separately , followed by the addition of 1 g of H-BEA. The mixtures were stirred for 3 hours at 80°C. Then the mixtures were heated at 60°C overnight to vaporize the solvent. The impregnated samples thus obtained were washed thoroughly with distillated water and finally the samples were dried overnight at 100°C. Finally, niobium-zeolite Beta sample was calcined at 400°C for 3 hours. The samples obtained were denoted as 1Nb-Beta, 2Nb-Beta and 4Nb-Beta with the number referred to the wt% of Nb impregnated.

Catalytic Test: Butylation of Resorcinol over Zeolite Beta Catalysts

All zeolite beta catalysts were activated before putting in the reaction mixtures to eliminate the adsorbed water and organic templates from the zeolite channels. The activation of catalysts was carried out in a tube furnace. Zeolite beta sample (0.4 g) was placed in a sintered quartz tube and heated at 400ºC for 3 hours. Zeolite Beta was calcined at 400ºC because at 500ºC Brönsted sites were nearly removed completely from the surface and the number of Lewis acid sites was greatly reduced (Ahmad *et al.,* 1999).

All reactions were carried out using glass batch reactor. The activated catalyst (0.4 g) was immediately placed in a 50 mL two necked round bottle flask equipped with a reflux condenser containing a mixture of resorcinol (1.0 g) and *tert*-butanol (7.16 g). The reaction was stirred and heated at 80 ºC for 24 hours. The round bottle flask was placed into an oil bath with a magnetic stirrer as shown in Figure 3.1. . The liquid product was syringed out at the interval time of 0.25, 0.5, 1, 2, 3, 4, 5, 6, 7, 8, 20, 24 hours in order to determine the

equilibrium of the reaction. The liquid product obtained was separated from catalysts and placed in glass vials for further characterization using GC and GCMS.

Toluene was used as an internal standard (IS) in the analyses with 2-propanol as the solvent. A standard series of resorcinol at 2, 4, 6, 8, 10, 12 and 14 M and one standard stock solution of toluene (10 M) were prepared to make a calibration graph of the ratio of area of resorcinol/toluene (IS) versus the concentration of resorcinol. Internal standard (100 μL) was added to 100 μL reaction product. Then, about 1 μL of the solution was injected into the GC at the initial temperature of 50ºC for 8 min, followed by increasing the temperature at the rate of 12ºC/min to the final temperature of 280ºC where it was held for 10 min.

Identification of the alkylation products in the liquid yield was characterized by GC-MS using Agilent 6890N-5973 Network Mass Selective Detector model equipped with HP-5MS column (30 m x 0.251 mm x 0.25 μm), diffusion pump and turbomolecular pump. Sample was analyzed with splitless method. Helium gas was used as the carrier gas. The oven-programmed setup is shown in Table 2

Table 2: The oven-programmed setup for GC-MS

Ramp	Rate, °C/min	Next, °C	Hold, min	Run time, min
Initial	-	50	3	3
Ramp 1	10	210	10	31
Post	-	-	-	34

Antioxidant Testing

The antioxidant activity of the Friedel-Crafts alkylation product was assessed on the basis of the scavenging activity of the stable 1,1-diphenyl-2picrylhydrazyl (DPPH) free radical using ESR spectroscopy. A standard series of DPPH in ethanol solution with different concentration at 0.5, 2, 4, 6, 8 and 10 mM was prepared to make a calibration graph of the ESR signal, cm versus the concentration of DPPH in ethanol solution, mM. 10 μL DPPH was added to the same volume of each samples at different concentration of DPPH in ethanol solution (0.5, 2, 4, 6, 8 and 10 mM) After mixing vigorously for 10 s, the solutions were then transferred into a quartz capillary tube and fitted into the cavity of the electron spin resonance (ESR) spectrometer. The spin adduct was measured after 2 mins.

Measurement conditions: central field 322.167 mT, modulation frequency 100 kHz, power 0.998 mW, amplitude 0.1 x 200 and sweep time 30 s.

RESULTS AND DISCUSSION

Catalytic Activity of Zeolite Beta in Friedel-Crafts Alkylation

Friedel-Crafts reaction of resorcinol with *tert*-butanol was chosen in order to study the catalytic activity of zeolite Beta synthesized from RHA. Catalytic activity was investigated through the effect of reaction time and reaction temperature towards the yield of reaction. The studies on the effect of Si/Al ratio of zeolite Beta framework and the effect of niobium loading to zeolite beta towards the activity of the catalysts in the Friedel-Crafts alkylation were also investigated. The product of the reaction was analysed by gas chromatography (GC) with toluene as the internal standard. Figure 4.19 shows the chromatogram of the products of Friedel-Crafts reaction, catalysed by zeolite Beta at 80ºC for 8 hours. The chromatogram shows peak at retention time, t_R =1.36, 2.28, 14.07, 16.29, 17.71 minutes. The determination of the area of each compound was carried out by GC analysis.

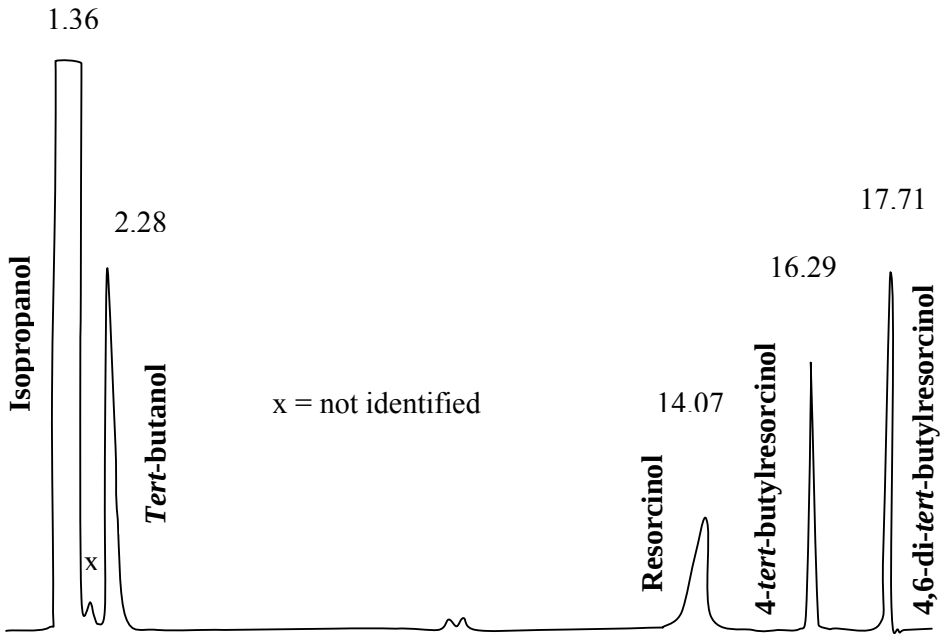

Figure 2: Chromatogram for the alkylation of resorcinol with *tert*-butanol reaction at 80ºC for 8 h catalyzed by BEA-11

Similar retention time (t_R) was observed for the product of the reaction which was catalyzed by zeolite Beta at different Si/Al ratio. The results indicated that products of the alkylation consists similar compounds, but the conversion of resorcinol and the selectivity of the products were different. The peak at t_R = 1.36 was attributed to isopropanol as a solvent, peaks at t_R = 2.28 and 14.07 were assigned to the reactants i.e *tert*-butanol and resorcinol, respectively. Peaks at t_R = 16.29 and 17.71 were identified as 4-*tert*-butylresorcinol and 4,6-di-*tert*-butylresorcinol. The major product was identified as 4,6-di-*tert*-butylresorcinol, while 4-*tert*-butylresorcinol was the minor one.

Based on the area of resorcinol and the area of toluene obtained from the GC analysis, the calibration graph of the standard of the area resorcinol/toluene at different concentration of resorcinol (mmole/mL) was plotted as shown in Figure 3. The graph shows linear line with positive slope. The calibration graph was plotted to obtain the concentration of resorcinol in the reaction, subsequently the conversion of resorcinol was calculated based on this concentrations. The percentage of conversion of resorcinol, selectivity and yield of the products were calculated based on the following equations:

$$\% \text{ Conversion} = \frac{C_{initial} - C_{final}}{C_{initial}} \times 100 \quad \textbf{(1)}$$

Where: $C_{initial}$ = Concentration of initial resorcinol
C_{final} = Concentration of final resorcinol

$$\% \text{ Selectivity} = \frac{\text{Area of X}}{\text{Area of total product}} \times 100 \quad \textbf{(2)}$$

X = 4,6-di-*tert*-butylresorcinol or 4-*tert*-butylresorcinol

$$\% \text{ Yield} = \frac{\%\text{Conversion} \times \%\text{ Selectivity}}{100} \quad \textbf{(3)}$$

Optimizations of Reaction Condition

(a) Effect of Reaction Time

The influence of time on the alkylation of resorcinol with *tert*-butanol over BEA-11 catalysts and without the catalyst is depicted in Figure 4. The reaction was carried out at 80ºC whereby the sample was syringed out at the interval of 0.25, 0.5, 1.0, 2.0, 3.0, 4.0, 5.0, 6.0, 7.0, 8.0, 20, 22 and 24 hours. The alkylation of resorcinol in the presence of catalyst

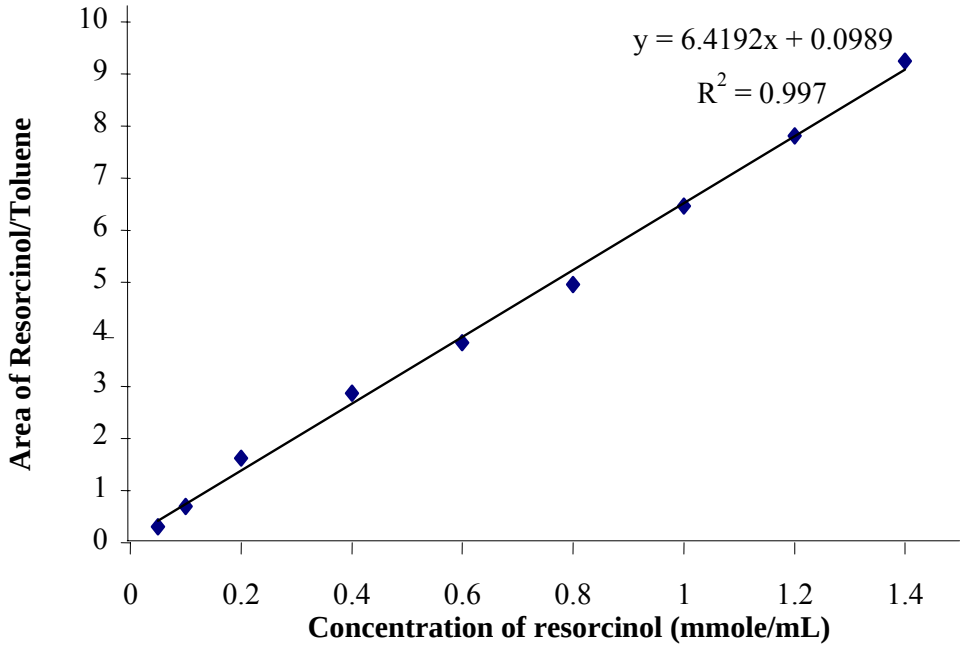

Figure 3: Standard calibration graph for the area of resorcinol/toluene versus the concentration of resorcinol (mmole/ mL)

proceeded faster with 95 % conversion in 8 hours, whereas only 24 % conversion of resorcinol without the catalyst for the same period of time. This proved that Friedel-Crafts alkylation of resorcinol needs catalyst in order to obtain the product in a shorter time. However the conversions of resorcinol in the presence of catalysts decrease to 40 % when the reaction prolong to 20 hours. In this case, the reverse reaction might have occurred since the reaction reached equilibrium within 7 to 8 hours.

Figure 5 shows the changes in the conversion and the selectivity of both products. The conversion increased steadily up to 6 hours with 90 % conversion in which the reaction started to reach equilibrium. The products was formed as early as 0.25 hours in which 4-*tert*-butylresorcinol was formed to be higher in selectivity (69 %) compared to 4,6-di-*tert*-butylresorcinol (31 %). With the extended of reaction time, the selectivity of 4-*tert*-butylresorcinol was found to decrease whereas 4,6-di-*tert*-butylresorcinol increased. This observation suggests that 4-*tert*-butylresorcinol has changed to 4,6-di-*tert*-butylresorcinol during the reaction and also suggest that most of 4,6-di-*tert*-butylresorcinol was probably being formed from 4-*tert*-butylresorcinol.

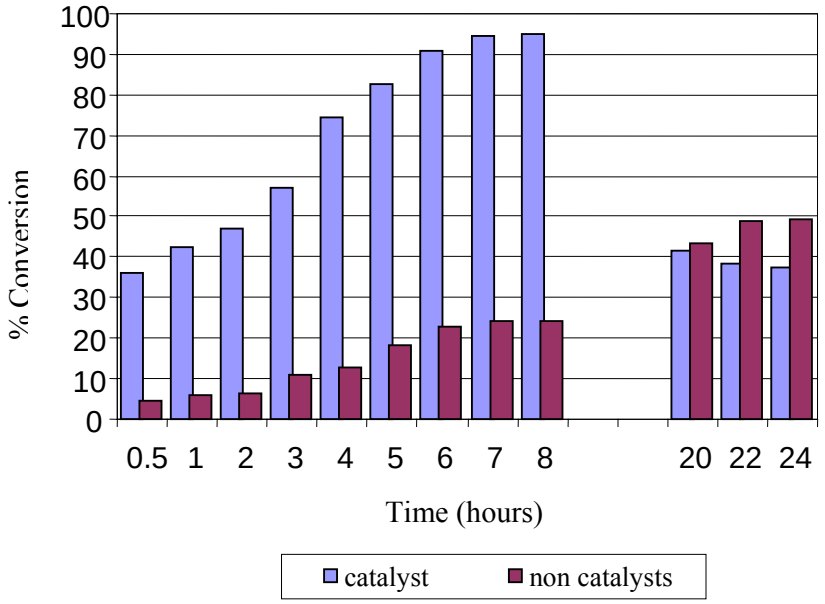

Figure 4.: The conversion of resorcinol in alkylation reaction; catalyst and non catalysts

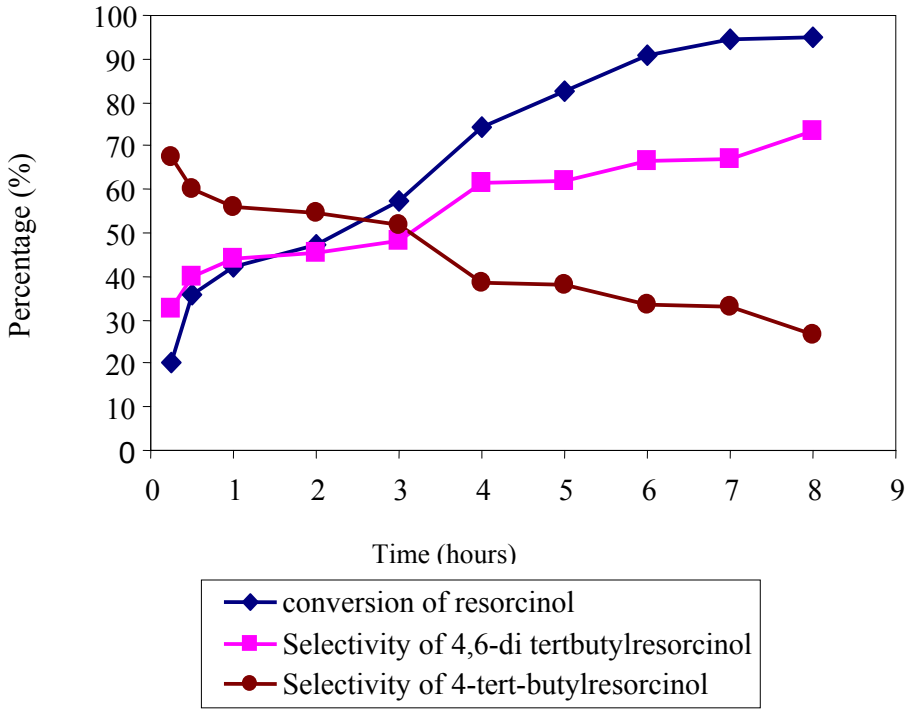

Figure 5: Alkylation of resorcinol with *tert*-butanol catalysed by BEA-11: Effect of reaction time

Figure 6 illustrates the effect of reaction time towards % yield of 4,6-di-*tert*-butylresorcinol. The percentage yield was calculated based on Equation 4.6. In the initial period the percentage yield of 4,6-di-*tert*-butylresorcinol increased constantly within 0.5 hours of reaction whereby reached equilibrium at 5 hours. The highest yield of 4,6-di-*tert*-butylresorcinol obtained was 73 % at 8 hours.

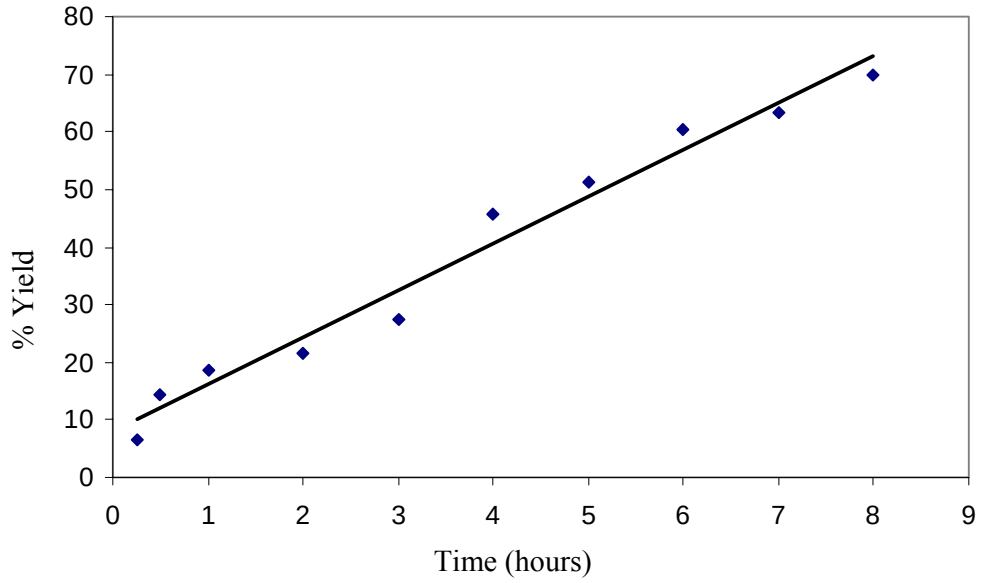

Figure 6: Effect of reaction time on the yield of 4,6-di-*tert*-butylresorcinol

(b) Effect of Reaction Temperature

Figure 7 represents the effect of reaction temperatures for alkylation of resorcinol over H-BEA-11 catalysts. The reaction was tested at room temperature, 60, 80, and 100°C within 8 hours. It showed that the conversion of resorcinol at room temperature was very low indicating that BEA-11 is not active as catalysts at this temperature. The conversion of resorcinol increased slightly at 60°C but reached to maximum at 80°C. However, the conversion of resorcinol was decreased 70 % to 25 % when the temperature was further increased to 100°C. The effects of temperature on the % yield of 4,6-di-*tert*-butylresorcinol at 8 hours reaction is clearly illustrated in Figure 8. It cleared showed the % yield of 4,6-di-*tert*-butylresorcinol was the highest at 80°C. This indicates that the optimum reaction temperature for Friedel-Crafts alkylation of resorcinol with *tert*-butanol is 80°C.

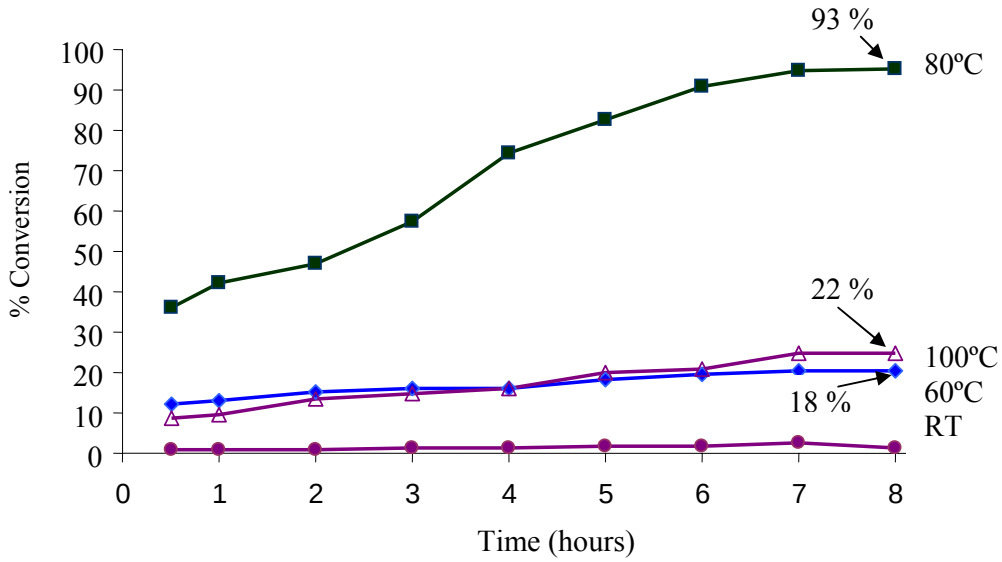

Figure 7: Influence of reaction temperatures on the conversion of resorcinol over BEA-11

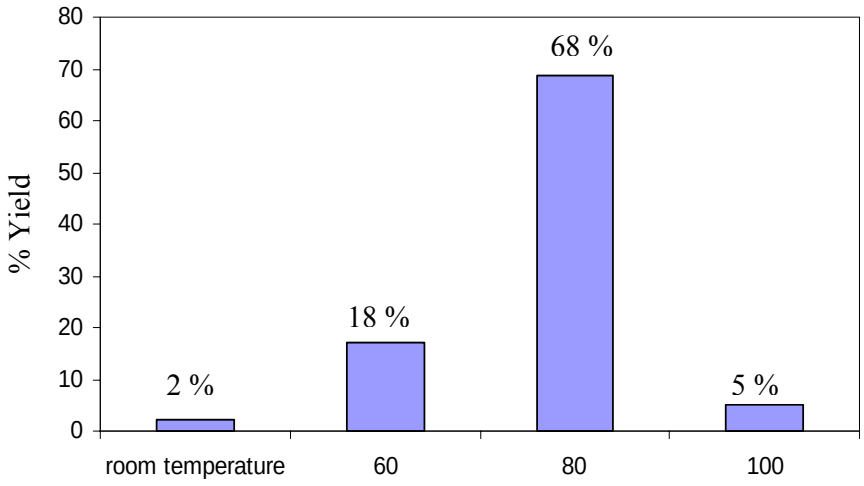

Figure 8: Influence of reaction temperatures on the yield of 4,6-di-*tert*-butylresorcinol at 8 hours reaction time over BEA-11

(c) Effect of Different Si/Al Ratio of Zeolite Beta Catalyst

The alkylation of resorcinol with *tert*-butanol was carried out in the presence of a difference Si/Al ratios zeolite Beta catalysts. This is to study the effect of Si/Al ratios towards the activity of the reaction. The reaction was performed at optimum temperature, 80°C within 8 hours of reaction time. The conversion of resorcinol over various Si/Al ratios of zeolite Beta catalysts are shown in Figure 9. In general, the percentage of conversion decreased with the increasing of Si/Al ratio of zeolite Beta samples. BEA-11 catalysts gave the highest conversion (95 %) followed by BEA-19 with 70 % and lastly BEA 21 only gave 64 % conversion. The conversion in terms of catalytic activity decreased in the order BEA-11 > BEA-19 > BEA-21. Similarly, the selectivity of the 4,6-di-*tert*-butylresorcinol showed a good correlation with Si/Al ratios of zeolite Beta catalyst, in which the selectivity decreased relatively with the increasing of Si/Al ratios (Table 3).

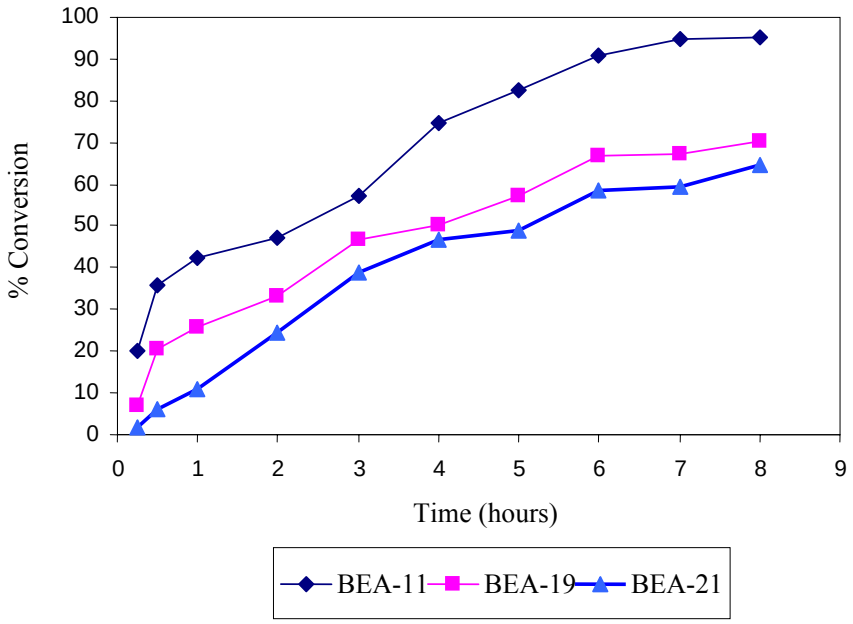

Figure 9: Conversion of resorcinol versus reaction time over different Si/Al ratios of zeolite Beta catalyst

Figure 10 shows the correlation between the selectivity and the yield of 4,6-di-*tert*-butylresorcinol with the amount of Brönsted and Lewis acid sites at different Si/Al ratios of zeolite Beta. It clearly showed that the yield and the selectivity of 4,6-di-*tert*-butylresorcinol increased with the increased of Brönsted acid site in zeolite Beta samples. However the amount of Lewis acid sites did not affect to the selectivity and the yield of

Table 3: Selectivity of 4,6- di-*tert*-butylresorcinol and 4-*tert*-butylresorcinol with different Si/Al ratios of zeolite Beta catalyst

Sample	Si/Al ratio	% Selectivity of 4,6-di-*tert*-butylresorcinol	% Selectivity of 4-*tert*-butylresorcinol
BEA-11	11	81.31	18.69
BEA-19	19	78.44	21.56
BEA-21	21	56.7	43.30

4,6-di-*tert*-butylresorcinol significantly. It is suggested that the enrichment of Brönsted acid sites in catalysts is responsible for the enhancement of the catalyst activity in producing the highest amount of the alkylation products. In addition, TPD of ammonia results showed BEA-11 has a highest amount of acid sites followed by BEA-19 and BEA-21 (refer Table 4.8). It indicated the yield and the selectivity of of 4,6-di-*tert*-butylresorcinol increased with the increased of amount of acid sites. Overall, the activity of zeolite Beta catalyst with Si/Al = 11 (BEA-11) gave the highest catalytic activity compared to zeolite Beta with Si/Al = 19 (BEA-19) and Si/Al = 21 (BEA-21) ratios. This activity can be related to the acid property of the catalysts obtained from the FTIR pyridine adsorption in which the BEA-11 has the highest amount of Brönsted acid sites and also having the highest crystallinity compared to other catalysts.

Table 4 shows the correlation between the catalytic performances with the surface area and crystallinity of zeolite Beta at different Si/Al ratios. BEA-11 with the highest crystallinity and surface area gave the highest % yield of 4,6-di-*tert*-butylresorcinol followed by BEA-19 and BEA-21. It indicated that the yield of 4,6-di-*tert*-butylresorcinol increased with the increased of crystallinity and surface area of the sample. In this case, the high crystallinity and surface area provided more active acid sites consequently increase % yield of the product

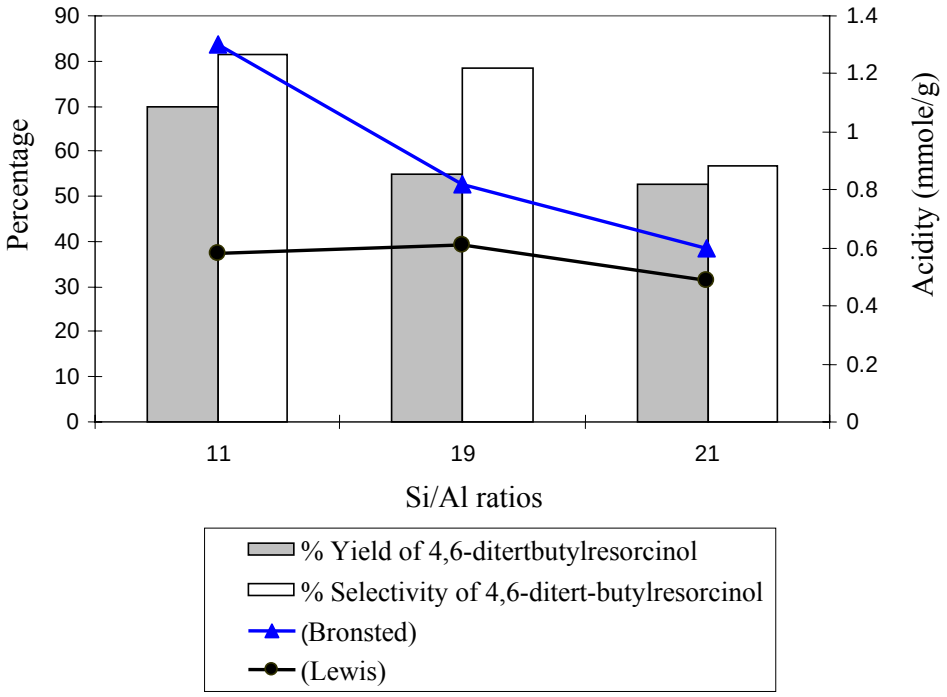

Figure 10: The correlation between the selectivity and the yield of 4,6-di-*tert*-butylresorcinol with the amount of Brönsted and Lewis acid sites at different Si/Al ratios of zeolite Beta

Table 4: The correlation between the catalytic performances with the surface area and crytallinity of zeolite Beta at different Si/Al ratios

Samples	% Crystallinity	Surface Area BET, m^2/g	% Yield of 4,6-di-*tert*-butylresorcinol
BEA-11	100	528.85	70.0
BEA-19	80.7	482.64	56.0
BEA-21	67.6	428.87	54.0

(d) Effect of Zeolite Beta With Niobium Loading

The modified zeolite Beta with niobium was tested as catalyst in the Friedel-Crafts alkylation of resorcinol. Figure 11 depict the conversion of resorcinol over zeolite Beta with niobium loading (2Nb-BEA-11 sample) and without niobium loading (BEA-11 sample) catalysts. It was observed that the conversion of resorcinol on 2Nb-BEA-11 catalysts

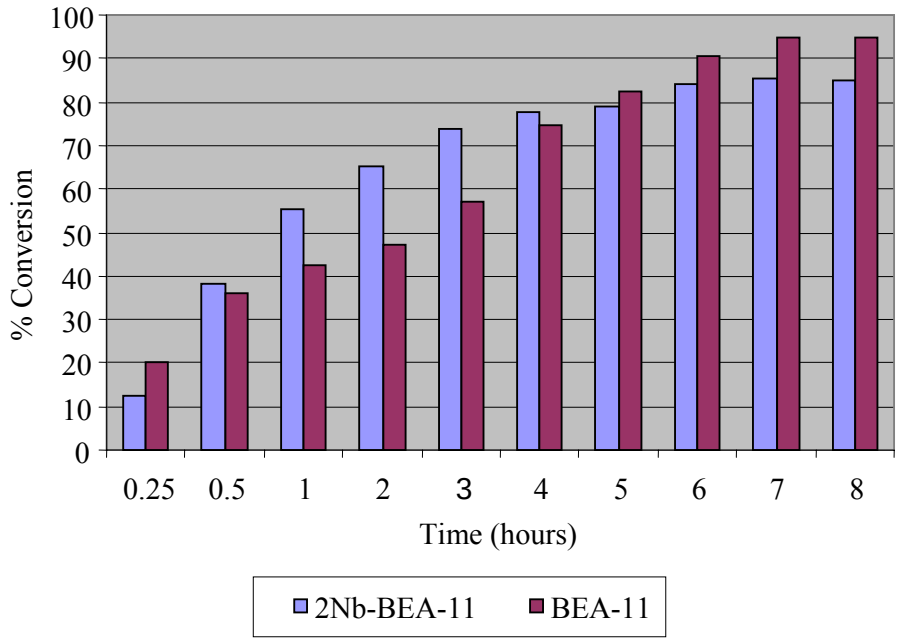

Figure 11: The conversion of resorcinol for alkylation reaction catalyzed by zeolite Beta with niobium loading (2Nb-BEA-11) and zeolite Beta without niobium loading (BEA-11)

relatively higher than the parent BEA-11 within 0.5 to 4 hours of reaction time. The conversion of resorcinol reached equilibrium state at 4 hours on 2Nb-BEA-11 whereas the conversion of resorcinol on BEA-11 increased slower and reached equilibrium after 6 hours. However the conversion on BEA-11 catalysts was slightly higher than 2Nb-BEA-11 catalysts within 5 to 8 hours of reaction period. These finding suggested that the presence of niobium has slightly increased the activity of the catalyst in term of increasing the rate of reaction.

Figure 12 displays the correlation between the selectivity and the yield of 4,6-di-*tert*-butylresorcinol with the amount of Bronsted and Lewis acid sites in 2Nb-BEA-11 and BEA-11 catalysts. It is showed that the selectivity and the yield of 4,6-di-*tert*-butylresorcinol increased with the increasing of the amounts of Brönsted and Lewis acid sites in 2Nb-BEA-11 catalysts. It is also noted that the 2Nb-BEA-11 catalysts gave 100 % selectivity for the major product 4,6-di-*tert*-butylresorcinol. Meanwhile, BEA-11 sample gave only 78 % selectivity for 4,6-di-*tert*-butylresorcinol and 4-*tert*-butylresorcinol is can still be detached of about 22 % selectivity. These finding suggested that the enrichment of Brönsted acid sites in

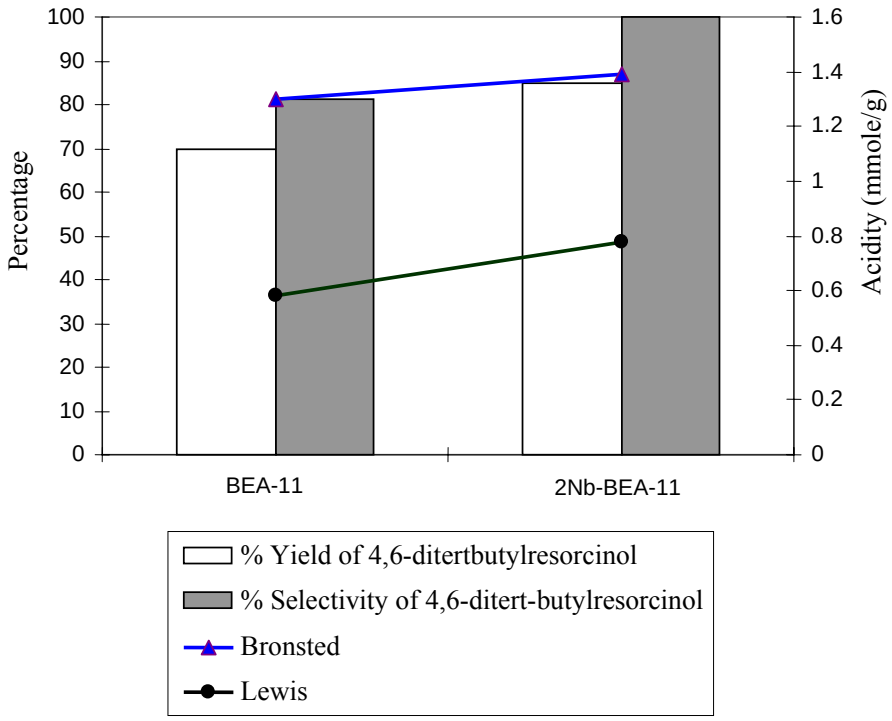

Figure 12: The correlation between the selectivity and the yield of 4,6-di-*tert*-butylresorcinol with the amount of Brönsted and Lewis acid sites in BEA-11 and 2Nb-BEA-11 samples at 8 hours reaction time.

niobium zeolite Beta (2Nb-BEA-11) will enhance the selectivity for 4,6-di-*tert*-butylresorcinol. This finding was supported by unpublished results by Aiman (2005) in which the selectivity for 4,6-di-*tert*-butylresorcinol increased with the increased of Brönsted acid sites suggested that the alkylation of resorcinol with *tert*-butanol is catalyzed by Brönsted acid sites.

(e) Influence of Catalyst Acidity Towards Catalytic Activity.

Zeolite Beta used as a catalyst in this study consists of two types of acidic sites; Brönsted and Lewis acid sites as shown from the FTIR pyridine study. However, it had been proposed that only the very strong Brönsted acid site was more active in alkylation (Feller *et al.,* 2004; Diaz-Mendoza *et al*., 1998). Based on the acidity study, all zeolite Beta samples have higher Brönsted acid than Lewis acid sites. The amount of Brönsted acid sites increased with the

decrease of Si/Al ratios of the zeolite Beta framework. Meanwhile the amount of Lewis acid sites does not shown any correlation with the Si/Al ratios.

The alkylation of resorcinol with *tert*-butanol catalyzed by various H-Beta at different Si/Al ratios in this study reveals that the conversion of resorcinol increased with the decreasing of Si/Al ratios of zeolite Beta. The increasing of the conversion is parallel with the increasing of Brönsted acid sites in the samples. As shown in Figure 10, the calculated amount of the selectivity and the yield of the major product are also influenced by the amount of Brönsted acid sites that exist in zeolite Beta framework. It is noted that the enrichment of Brönsted acid sites in the catalysts is responsible for the higher percentage yields of the products for the Friedel-Crafts alkylation. Similarly, the selectivity of 4,6-di-*tert*-butylresorcinol also shows a good correlation with Si/Al ratios, in which the selectivity decreased relatively with the increasing of Si/Al ratios (see Table 4).

Based on the acidity study, zeolite Beta with niobium loading (2Nb-BEA-11) shows the higher amount of Brönsted and Lewis acid sites compared to zeolite Beta alone (BEA-11). In this case the increase in the acidity must be contributed by niobium oxide. This is due to the acid property of the niobic acid possess both Bronsted and Lewis acid sites. As shown in Figure 12, the presence of niobium in zeolite Beta, 2Nb-BEA-11 gave 100 % selectivity for 4,6-di-*tert*-butylresorcinol whereas BEA-11 alone gave both 4,6-di-*tert*-butylresorcinol (78 % selectivity) and 4-*tert*-butylresorcinol (22 % selectivity). These findings suggest that zeolite Beta with niobium loading (2Nb-BEA-11) is more selective than zeolite Beta alone (BEA-11). The correlation between the selectivity and the yield of the products with the amount of Brönsted acid sites shows the enhancement of Brönsted acid sites in 2Nb-BEA-11 sample; consequently increase the selectivity up to 100 %. This finding suggests that the alkylation of resorcinol with *tert*-butanol is catalyzed by Brönsted acid sites. Besides, the nature of niobium itself as an active and good metal oxides catalysts for many reactions might be responsible for the increase in selectivity of 4,6-di-*tert*-butylresorcinol.

In this study, sample 2Nb-BEA-11 is identified as the most active catalyst and gave a better catalytic performance in term of the selectivity and the yield of 4,6-di-*tert*-butylresorcinol compared to BEA-11 alone.

Proposed Reaction Mechanism

Based on the results obtained, the reaction mechanism of the alkylation of resorcinol over zeolite Beta catalysts was proposed. The outline of the mechanism is shown in Figure 13. Based on the catalytic activity study; the conversion of resorcinol increased with the increased of Brönsted acid sites in the sample. In addition, the selectivity and the yield of 4,6-di-*tert*-butylresorcinol is increased with the increased of Brönsted acid sites in all samples. Meanwhile, the Lewis acid sites did not significantly effect the selectivity and the yield of 4,6-di-*tert*-butylresorcinol. This finding also supported by unpublished result by Aiman (2005) in which the selectivity of 4,6-di-*tert*-butylresorcinol is increased with the increasing of Brönsted acid site in gallium-zeolite Beta catalyst. Therefore, it is suggested that the reaction was catalyzed by Brönsted acid site as shown in Figure 4.30 (Narayanan and Deshpande, 1995; Narayanan and Sultana, 1998; Narayanan and Deshpande, 2000).

The mechanism involved the electrophilic aromatic substitution. The reaction is divided inti three stages. The first stage is the formation of an electrophile; the Bronsted acid-base reaction of *tert*-butanol with zeolite to form *tert*-butyl cation or an electrophile. The second step is the addition of the electrophile by using two π electron from the aromatic ring to generate a carbocation which is resonance stabilized. The final step is the removal of a proton by the zeolite anion from the carbon bearing the electrophile to restore the aromatic of resorcinol. The product analysis revealed that 4-*tert*-butylresorcinol and 4,6-di-*tert*-butylresorcinol were formed indicated that butylation took place selectively at 4 and 6, positions of resorcinol.

Antioxidant Property of Butylated Resorcinol

Friedel-Crafts alkylation of resorcinol with *tert*-butanol produces butylated resorcinols (4-*tert*-butylresorcinol and 4,6-di-*tert*-butylresorcinol) which are expected to have antioxidant property. 1,1-Diphenyl-2-picryl-hydrazyl (DPPH), a stable free radical has been used for detecting antioxidant activity in the samples. The DPPH contains an odd electron in its structure (Figure 14). The antioxidative activities of the Friedel-Crafts alkylation products and the starting material, resorcinol were evaluated on the basis of their abilities to scavenge DPPH radical to form (DPPH)**:**H.(Equation 4) (Jin and Chen, 1998). The free radical signals can be detected by Electron Spin Resonance (ESR) technique

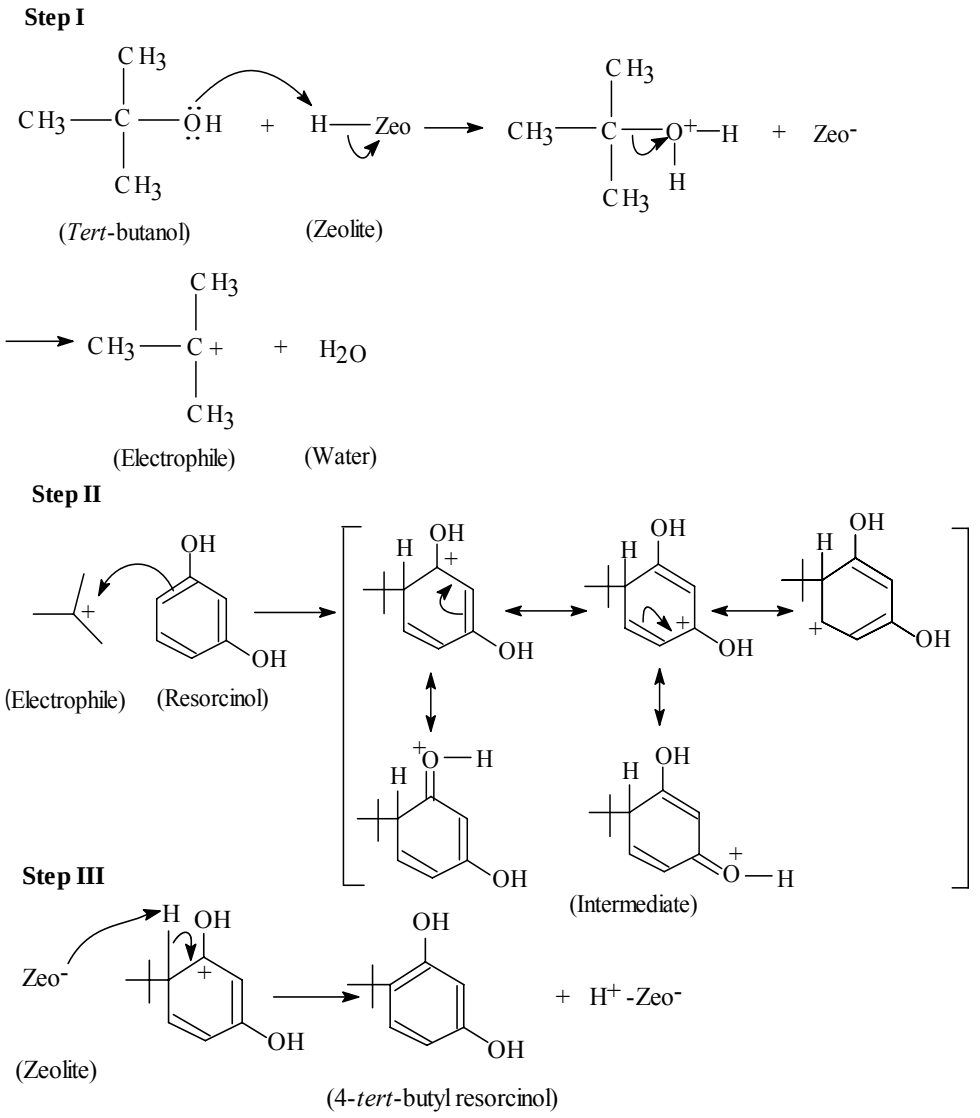

4,6-di-*tert*-butylresorcinol was obtained from 4-*tert*-butylresorcinol as shown below

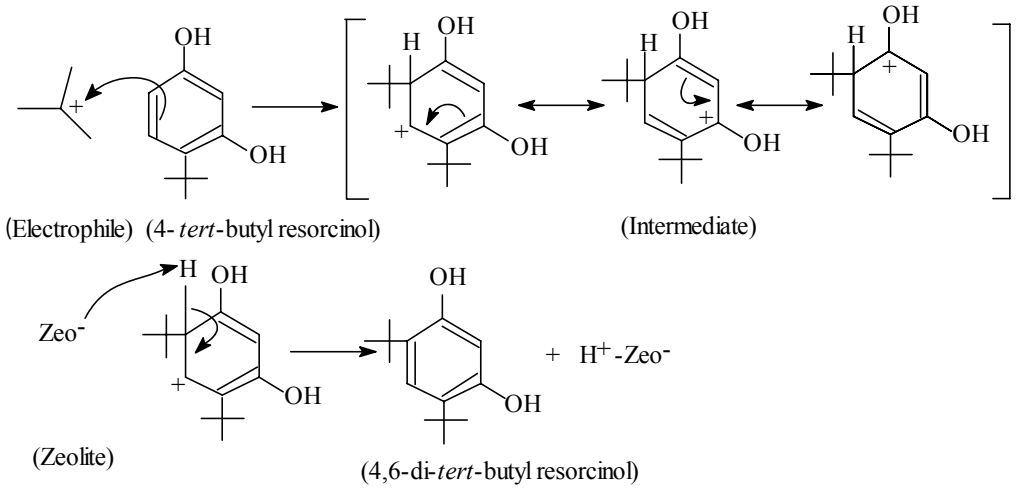

Figure 13: Proposed reaction mechanism of the alkylation of resorcinol with *tert*-butanol over zeolite Beta catalysts

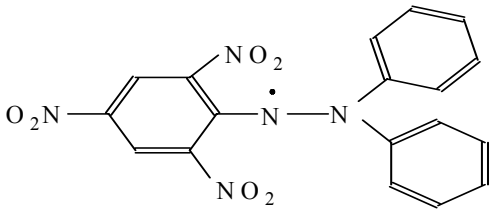

Figure 14: Chemical structure of 1,1-diphenyl-2-picryl-hydrazyl ($DPPH^{\bullet}$)

$$DPPH^{\bullet} + \text{Antioxidant} \rightarrow DPPH{:}H + \text{Antioxidant}^{\bullet} \qquad \textbf{(4)}$$

ESR signal **No ESR signal**

The radical of DPPH gives typical ESR spectra shown in Figure 15 (a, b and c). The spectrum of the DPPH radical (a) shows peaks indicating the existence of an odd electron. The ESR spectrum of DPPH in ethanol (b) shows five peak based on (2nI + 1) equation, where n = number of nitrogen atom, I = nucleus spin of nitrogen atom (I = l for ^{14}N). The spectrum indicates that the electron is located between two nitrogen atoms in the DPPH radical as shown in Figure 4.31. There is no ESR signal after DPPH has completely reacted with butylated resorcinols as shown in spectrum (d).

The antioxidant activity of the samples towards DPPH was measured based on the intensity of ESR signals of DPPH in ethanol solution. The symbol of ***x*** represents the height of ESR signals which is measured to determine the antioxidative activities. In this study, the products of Friedel-Crafts alkylation are referred to as butylated resorcinol.

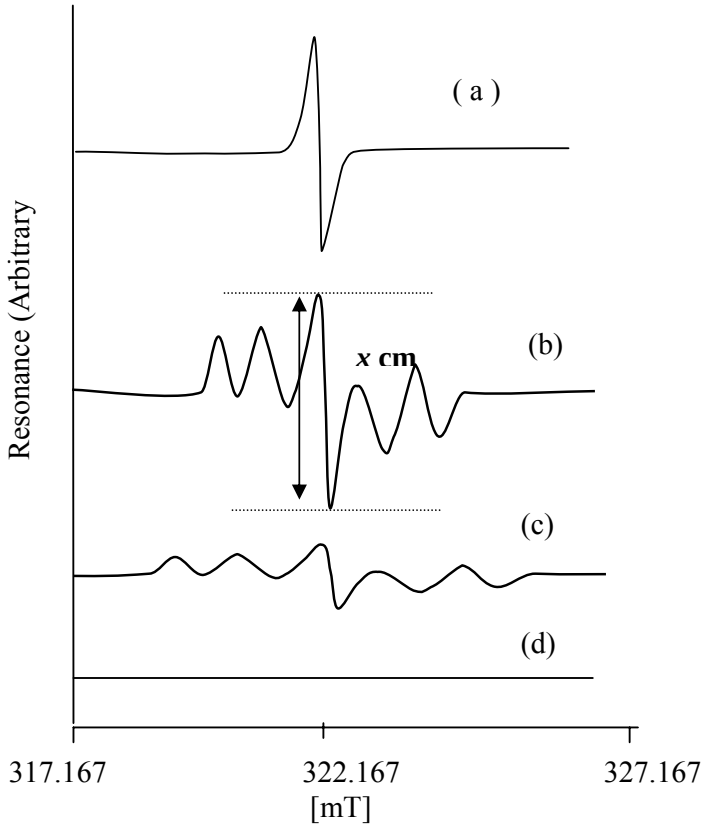

Figure 15: ESR spectra of (a) DPPH free radical (solid state) (b) DPPH radical in ethanol solution of 10 mM (c) DPPH radical in an ethanol solution of 10 mM after reacted with butylated resorcinol, g=2.00178 (d) DPPH completely reacted with butylated resorcinol

In this study, the strength of the antioxidant was determined by the detecting the disappearance of the ESR signal when the DPPH was reacted with the test sample (butylated resorcinol). Different concentration of DPPH in ethanol solution (10 μL) was added to both samples (resorcinol and butylated resorcinol). From the data obtained from ESR analysis, the straight line representing the intensities of ESR signals of DPPH, DPPH with resorcinol and DPPH with butylated resorcinol are shown in Figure 4.33. The data showed that the optimum concentration of DPPH reacted completely with resorcinol and butylated resorcinol at 1.5 mM and 6 mM respectively. It indicated that the butylated resorcinol has a stronger antioxidant four fold than the starting material, resorcinol. However when the concentration of DPPH is increased to 8 mM, the ESR signals of butylated sample started to appear and slightly increased at 10 mM. The percentage of the reacted DPPH can be calculated from

the graph by using Equation 4.8, for example at 6 mM, the DPPH is 100 % reacted with butylated resorcinol sample while only 62.6 % DPPH reacted with resorcinol. The percentage of reacted DPPH was calculated by using the following equation:

$$\% \text{ DPPH reacted} = \frac{X-Y}{X} \times 100 \qquad \textbf{(58)}$$

X = ESR signal of initial DPPH

Y = ESR signals of sample after reacted with DPPH, resorcinol and butylated resorcinol

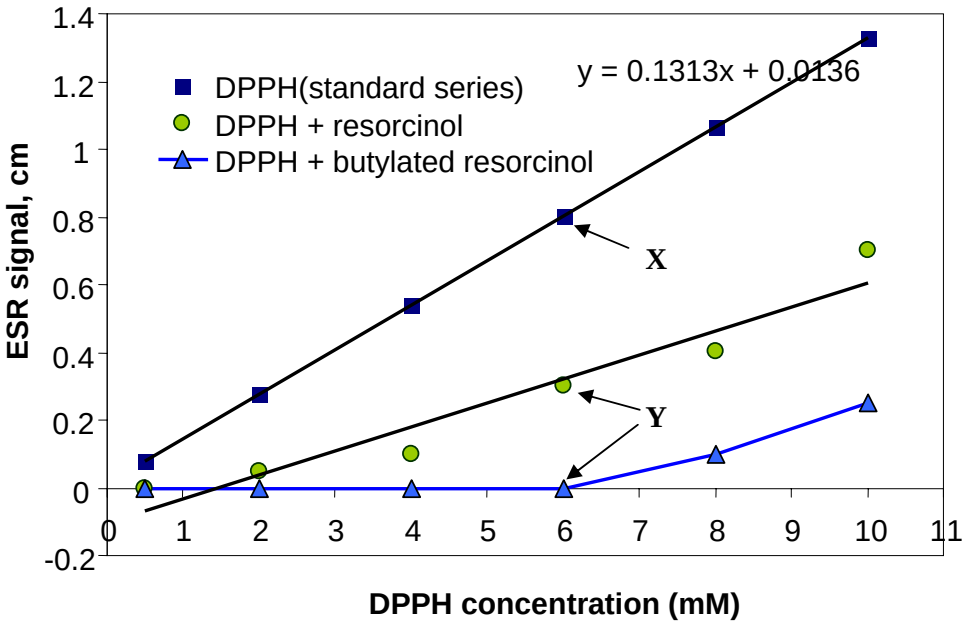

Figure 4.33: Graph of ESR signals of DPPH (standard series), DPPH after reacted with resorcinol and DPPH after reacted with butylated resorcinol at different concentration

CONCLUSIONS

The catalytic activity study of zeolite Beta at different Si/Al ratios was tested in Friedel-Crafts alkylation of resorcinol with *tert*-butanol. The optimum reaction condition was found to be at 80°C of reaction temperature and at 8 hours of reaction time. The alkylation of resorcinol over zeolite Beta at different Si/Al ratios produced 4,6-di-*tert*-butylresorcinol as the main product and 4-*tert*-butylresorcinol as the side product. The formation of dialkylated

product (4,6-di-*tert*-butylresorcinol) from the monoalkylated product (4-*tert*-butylresorcinol) increased with increase of reaction time. In general, the activity of zeolite Beta catalyst increased with the decreased in Si/Al ratios in zeolite Beta samples. Zeolite Beta with Si/Al =11 ratio gave the highest conversion (95 %) followed by zeolite Beta with Si/Al =19 ratio with 70 % and lastly zeolite Beta with Si/Al = 21 ratio which only gave 64 %. Similarly, zeolite Beta with Si/Al =11 ratio gave the highest selectivity of 4,6-di-*tert*-butylresorcinol (81 %) followed by Zeolite Beta with Si/Al =19 ratio (78 %) and Zeolite Beta with Si/Al = 21 ratio (56 %). The conversion of resorcinol and the selectivity of 4,6-di-*tert*-butylresorcinol increased with the increase of Brönsted acid sites while there has no correlation between the conversions of resorcinol and the selectivity of 4,6-di-*tert*-butylresorcinol with the amount of Lewis acid sites. This finding indicated that the activity of the zeolite Beta catalysts is largely relates to the Brönsted acid sites. Besides, the catalytic performance increased with the increased of the crystallinity and the surface area of the zeolite Beta at different Si/Al ratios.

The activity of modified zeolite Beta with Nb loading gave slightly lower conversion than the parent zeolite Beta but higher selectivity of 4,6-di-*tert*-butylresorcinol. The conversion of resorcinol in zeolite Beta sample with 2 wt% niobium loading are more active and reached equilibrium faster than the parent zeolite Beta. This finding indicates that the presence of niobium has slightly increased the activity of the catalyst in term of increasing the rate of reaction. In addition, the selectivity of 4,6-di-*tert*-butylresorcinol has increased to 100 % in zeolite Beta samples with 2 % w/w niobium loading from 78 % in the parent zeolite Beta. In this study, zeolite Beta with 2 % w/w niobium loading was identified as the most active catalyst and has a potential to be selective catalysts in the Friedel-Crafts alkylation of resorcinol. Comparison of the antioxidant strength between the alkylation product and its starting reactant, resorcinol showed that the alkylation product containing butylated resorcinol has 4 times stronger antioxidant property than the reactant resorcinol

References:

Aguilar.J., Corma A., Melo F.V., Sastre E.,(2000) "Alkylation of biphenyl with propylene using acid catalysts', *Catalysis Today* 55.225-232

Bergman, Margalit, Perelman, Alexander, Dubinsky, Zyx, Grossman, Shlomo (2003). "Scavenging of Reactive Oxygen Species by a Novel Glucurinated Flavonoid Antioxidant Isolated and Purified from Spinach". Phytochemistry. 62. 753-762

Das D. and Cheng S. (2000). Friedel-Crafts acylation of 2-methoxynaphtalene over zeolite catalysts. *Applied Catalysis A: General.* 201. 159-168

De Castro, C., Primo, J., and Corma, A. (1998). "Heteropolyacids and Large Pore Zeolites as Catalysts in Acylation Reactions Using Unsaturated Organic acids as Acylating Agents." *J. Mol Cat A.*134. 215-222

Escola J. M. and Davis M. E. (2001). Acylation of biphenyl with acetic anhydride and carboxylic acids over zeolite catalysts. *Applied Catalysis A: General.* 214. 111-120

Ganapati D. Yadav, Nirav S. Doshi (2003). "Alkylation of aniline with methyl-tert-butyl ether (MTBE) and tert-butanol over solid acids: product distribution and kinetics". *Journal of Molecular Catalysis A: Chemical* 194. 195-209

Gunnewegh, E.A., Gopie, S.S., and Bekkum, H. Van. (1996). "H MCM-41 Type Molecular Sieves as Catalysts for Friedel-Crafts Acylation of 2-metoxynaphtalene." *J. Mol. Cat. A* 106.151-158

Je, Jae-Young., Park, Pyo-Jam, Kim, Se-Kwon (2004). "Free radical scavenging properties of hetero-chitooligosaccharides using an ESR spectroscopy." *Food and Chemical Toxicology*. 42. 1-7

Loulin V., Ragoussis, N., Magoulas, K. (2004). "Recovery of phenolic antioxidants from wine industry by-products." *Bioresource Technology*. 92. 201-208.

Narayanan, Sankarasubbier., K.V.V.S.B.S.R. Murthy. (2001). "Montmorillonite as a versatile solid acid catalyst for Tert-butylation of resorcinol". Applied Catalysis A: General 213.273-278

Olah, G.A. (1973). "Friedel-Crafts Chemistry." New York: John Wiley and sons

Trouillas, P., Calliste, C.A., Allais, D.P., Simon, A., Marfak, A., Christine Delage, Jean –Luc Duroux. (2003) Antioxidant, anti-inflammatory and antiproliferative properties of sixteen water plant extracts used in the Limousin countryside as herbal teas". *Journal Food Chemistry.* 80 399-407

Ukeda, Hiroyuki, Adachi, Yukiko., Sawamura, Masayoshi. (2002). "Flow injection analysis of DPPH radical based on electron spin resonance." *Talanta.* 58. 1279-1283

Wade JR., L.G. (2003). "Organic Chemistry". 5th Edition. New Jersey. Prentice Hall, Pearson Education Inc.742-749

Zhao, X.S., Lu, Max G.q., Song, C. (2003). "Immobilization of aluminum chloride on MCM-41 as a new catalyst system for liquid-phase isopropylation of naphthalene". *Journal of Molecular Catalysis A: Chemical* 191.67-74

Aiman Najati Akhmar Rahman (2007) MSc. Thesis. UTM

Title of thesis : Gallium Impregnated Zeolite Beta Catalysts for Friedel-Crafts Alkylation of Resorcinol

Name : Aiman Najati Akhmar Rahman

ABSTRACT

Gallium containing zeolites constitute a very interesting class of solid acid from catalytic standpoints. In this study, acidity of zeolite Beta was modified by varying the SiO_2/Al_2O_3 ratio and by the incorporation of gallium *via* direct and post synthesis methods to obtain high selectivity and yield in Friedel-Crafts alkylation of resorcinol which proceeds in the presence of acid catalysts. Zeolite beta with different framework Si/Al ratios were successfully synthesized. XRD, FTIR and ^{29}Si NMR analyses indicated that the synthesized zeolite Beta with different silica content increased in order of initial SiO_2/Al_2O_3 ratios 25 < 45 < 100, but the crystallinity increased in order of SiO_2/Al_2O_3 ratios 45 > 100 > 25. The amount of Brønsted acid sites studied by FTIR pyridine adsorption followed the order of the crystallinity of the samples. Catalytic activity of zeolite samples were evaluated in the butylation of resorcinol which produced 4-*tert*-butylresorcinol and 4, 6-di-*tert*-butylresorcinol as the major and minor products respectively. The yield of the product increased with the increased amount of Brønsted acid sites in modified zeolite Beta catalysts while the selectivity of the product was in reverse order. Incorporation of gallium into zeolite Beta framework by direct synthesis to produce gallosilicate Beta was successful and proved by XRD, FTIR and surface hydroxyl studies. The crystallinity and surface area of gallosilicate Beta decreased significantly after continuous treatment to obtain hydrogen form sample, giving low amount of Brønsted acid sites but high amount of Lewis acid sites. This results in the low yield of 4-*tert*-butyl resorcinol (30.3 %) but higher product selectivity of more than 95%. Incorporation of gallium by impregnation of 1 – 25 wt% of Ga loading led to a monolayer coverage occured at 7.3 – 7.5 wt% of Ga loading. Samples of low amount of gallium loading (1 – 5 wt %) showed decrease in the amount of Brønsted acid sites while sample at high amount of Ga loading (≥ 8 wt %) showed increased in the amount of Lewis acid sites. In general, the catalytic activity of gallium impregnated samples increase with the increase of Ga loading. Sample at 8 wt% Ga loading showed the optimum resorcinol conversion and 4-*tert*-butylresorcinol yield of 63.0% and 60.3% respectively, while the selectivity was 95.8%. Lewis acid sites found in prominent amount in 8 wt% Ga impregnated sample is responsible along with Brønsted acid sites in obtaining the optimum yield and conversion in Friedel-Crafts alkylation of resorcinol. Approximately 100% selectivity of 4-*tert*-butyl resorcinol was achieved for sample ≥10 wt% of Ga loaded in zeolite Beta. Ga incrporated zeolite Beta by both direct and post synthesis methods was found to give increase amount of Lewis acid sites in the zeolite Beta catalysts.

Marzita Abd Mazak (2006) MSc. Thesis. UTM

Title of thesis : Modified Zeolite Beta as Catalysts in Friedel-Crafts Alkylation of Resorcinol

Name : Marzita Abd Mazak

ABSTRACT

Zeolites are widely used as acid catalysts for the synthesis of fine chemicals in industrial processes. One such process is Friedel-Crafts alkylation which proceeds in the presence of acid catalysts. In this research, the acid property of zeolite Beta was studied in order to increase its activity in the Friedel-Crafts alkylation of resorcinol with *tert*-butanol. Zeolite Beta was chosen as catalysts in the Friedel-Crafts alkylation because it possesses large pore and high acid strength. Zeolite Beta was modified by varying the SiO_2/Al_2O_3 ratios of the initial gel and introducing niobium oxide into zeolite Beta samples. All samples were characterized by XRD, FTIR, N_2 adsorption, UV-Vis DR and ^{29}Si MAS NMR. XRD results showed all samples gave highly pure zeolite Beta phase. ^{29}Si MAS NMR showed that the zeolite Beta samples with initial SiO_2/Al_2O_3 ratios = 27, 45 and 90 result in the zeolite Beta having Si/Al framework ratios of 11, 21 and 19 respectively. The crystallinity of zeolite Beta is slightly decreased after the introduction of niobium oxide into the samples. UV-Vis DR results showed that the niobium species in zeolite Beta samples are mainly in the tetrahedral form. Acidity study of the catalysts was measured by FTIR pyridine adsorption and TPD of ammonia. FTIR pyridine showed that the amount of Brönsted acid sites in zeolite Beta samples increased in the order of framework Si/Al ratios = 21 < 19 < 11 and also increased after 2 % wt Nb loading but decreased after 4 % Nb loading. Meanwhile the Lewis acid site did not showed any correlation to the Si/Al ratios of zeolite Beta but increased after incorporated with niobium. TPD results showed that the amount of acid sites in zeolite Beta samples decreased while the acid strength increased with the increased of Si/Al ratios of zeolite Beta framework. The strength and the amount of acid sites also increased after 2 % wt Nb loading and decreased after 4 % wt Nb loading. All catalysts were tested in Friedel-Crafts alkylation of resorcinol with *tert*-butanol. GC analysis showed the alkylation of resorcinol over zeolite Beta at different Si/Al ratios produced 4,6-di-*tert*-butylresorcinol (main product) and 4-*tert*-butylresorcinol. The conversion decreased in the order, zeolite Beta with Si/Al = 11 (95 %) > 19 (70 %) > 21 (64 %) and the selectivity of 4,6-di-*tert*-butylresorcinol also decreased in the order Si/Al= 11 (81 %) > 19 (78 %) > 21 (56 %). Zeolite Beta sample with Nb loading has successfully produced 4,6-di-*tert*-butylresorcinol with 100 % selectivity. ESR analysis showed that the alkylation product containing butylated resorcinol is 4 times stronger antioxidant than the resorcinol itself.

Title of Thesis : Synthesis of zeolite Ferrierite from Rice Husk Ash, Characterization and Activity Towards Friedel Crafts Acylation of Anisole with propyl anhydride.

Name : Hasliza binti Bahruji

ABSTRACT

Rice husk ash (RHA) consisting more than 90% of amorphous silica obtained under controlled burning of rice husk was directly used in the synthesis of ferrierite type-zeolite. The synthesis was performed under hydrothermal condition in the presence of different organic templates, oxides compositions and at various crystallization periods. Solid products obtained from the synthesis were characterized by XRD, FTIR, ^{29}Si MAS NMR, N_2 adsorption and SEM techniques. Results showed that pure ferrierite can be formed from the initial molar oxide ratios in the range of 1.31 – 1.5 Na_2O : Al_2O_3 : 10 – 30 SiO_2 : 4 – 10.0 template : 410 H_2O with only pyrrolidine (Py) as the organic template. In general, quartz was obtained at higher SiO_2/Al_2O_3 and lower Py/Al_2O_3 ratios. The crystal phase changes from ferrierite to analcime and lastly to quartz, with increasing SiO_2/Py ratios. RHA was directly transformed to ferrierite phase within one day and reached equilibrium after 4 days crystallization. The acidity study of the H-ferrierite samples at different SiO_2/Al_2O_3 ratios (12, 20 and 30) using IR-pyridine adsorption method showed the increase of acid sites with the decrease of SiO_2/Al_2O_3 ratios in ferrierite framework. In each case, the Brønsted acid sites is higher than Lewis acid sites. The catalytic activity of ferrierite at different SiO_2/Al_2O_3 ratios towards Friedel-Crafts reaction between anisole and acid anhydrides was investigated. Results from the catalytic activity showed that only *p*-methoxypropiophenone and propionic acid was produced as the main product and side product respectively when propionic acid was used as acylating agent. The optimum temperature for the reaction was 120^{o}C and ferrierite catalyst with SiO_2/Al_2O_3 ratio 12 gave the highest conversion of anisole (66 %) and the selectivity of the main product (80 %). When acetic anhydride was employed as acylating agent, the conversion of anisole (55 %) and the selectivity of desired product (98 %) showed a higher percentage as compared with propionic anhydride. In both cases, the main product obtained is in *para* orientations with higher selectivity proved that H-ferrierite is a selective catalyst for the production of *para* orientation products.

Title of thesis : Pengalkilan dan Pengasilan Friedel-Crafts p-kresol Bermangkinkan Zeolite Beta Bagi Menghasilkan Zeolit Beta Bagi Menghasilkan Antioksida

Name : Aiman Najati Akhmar Rahman

ABSTRAK

Tindak balas pengalkilan dan pengasilan Friedel-Crafts berlaku dalam keadaan mangkin berasid yang homogen atau heterogen. Dalam kajian ini, pengalkilan dan pengasilan Friedel-Crafts *p*-kresol yang dimangkinkan oleh zeolit beta telah dilakukan. Pengalkilan *p*-kresol dilakukan pada suhu 110 ^{o}C selama 24 jam dengan membandingkan keadaan tindak balas yang dilakukan pada tekanan atmosfera dengan tindak balas yang dilakukan pada tekanan tinggi. Semua hasil tindak balas dianalisis menggunakan GC dan dikenalpasti dengan GC-MS. Hasil pengalkilan *p*-kresol dengan *tert*-butanol pada tekanan atmosfera dan tekanan tinggi menghasilkan 2-*tert*-butil-*p*-kresol Tindak balas pada tekanan tinggi memberikan peratus pertukaran dan peratus hasil yang lebih tinggi daripada tindak balas pada tekanan atmosfera dengan peratus pertukaran dan peratus hasil 22.38 % dan 21.63 % dan peratus kepilihan hasil yang sangat tinggi mencapai 95 %. Tindak balas pengasilan *p*-kresol dengan asetik anhidrida pada tekanan atmosfera pada suhu 120 ^{o}C dan masa 48 jam memberikan peratus kepilihan dan hasil iaitu 2-hidroksi-5-metil-asetofenon yang sangat rendah iaitu 4.3% dan 1.7 % masing-masing. Ini menujukkan zeolit beta adalah tidak aktif dalam menghasilkan keton aromatik dalam tindak balas ini. Kajian sifat antioksida bahan dilakukan dengan menindakbalaskan hasil tindak balas pengalkilan dan *p*-kresol dengan 1,1-difenil-2-pikril-hidrazil (DPPH) serta diukur menggunakan ESR Perbandingan kekuatan sampel yang mengandungi 2-*tert*-butil-p-kresol memberikan aktiviti antioksida yang lebih tinggi melalui keupayaan bertindak balas dengan kepekatan DPPH 7 kali lebih tinggi berbanding reaktan asalnya,iaitu 0.44 mM DPPH/1μL sampel hasil pengalkilan berbanding 0.06 mM DPPH/1 μL *p*-kresol.

Title of thesis : Siliceous Zeolite Beta: Synthesis, Characterization and Its Activities in Friedel-Crafts Acylation of Anisole

Name : Kwek Siang Sing

ABSTRACT

Zeolite Beta is one of the synthetic zeolite, which draws much attraction because of its unique characteristics and well recognized as an interesting catalyst for chemical synthesis due to its high thermal and chemical stability, strong acid sites, hydrophobicity and large pore size. In this study, siliceous zeolite Beta was synthesized by using the different silica sources with an initial molar composition of 202 SiO_2: Al_2O_3: 109 TEAOH: 3154 H_2O. The siliceous zeolite Beta was also synthesized by increasing the SiO_2/Al_2O_3 ratio from 200 to 6400. The gel solution was hydrothermally treated at 140^oC for 6 days at static condition. The resulting solid products were characterized by using XRD and FTIR. The percentages yields of zeolite Beta obtained from the experiments decreases with the increases of SiO_2/Al_2O_3 ratios. Acidity of siliceous zeolite Beta was tested in Friedel-Crafts reaction of anisole by propionic anhydride, which can be catalyzed by either Lewis acid or Brønsted acid. Low Si/Al ratios of zeolite usually contain higher Brønsted acid sites and favour more conversion of anisole. Products identified by gas chromatography showed that p-methoxypropiophenone was the main product with propionic acid as the side product. The resulting zeolite Beta with $SiO_2/Al_2O_3 > 200$ gave the same conversion of anisole (80%) and the same selectivity ($\cong$ 60%), indicating that the samples has same amount of acidity because of the samples has similar framework Si/Al ratio. It indicated that siliceous zeolite Beta are not obtained as expected from the initial molar SiO_2/Al_2O_3 alone. However, the high selectivity shown by the siliceous zeolite Beta indicated these samples are a good catalyst for the chosen Friedel-Crafts reaction.

Jasmie Bin Marutai (2005). Thesis Projek Sarjana Muda. UTM

Title of thesis : Sintesis Zeolit Ferrierit daripada Abu Sekan Padi Sebagai Mangkin Asid Dalam Tindak Balas Pengalkilan Friedel Crafts Katekol

Name : Jasmie Bin Marutai

ABSTRAK

Zeolit adalah mangkin heterogen yang penting dan banyak digunakan dalam bidang industri. Dalam kajian ini, abu sekam padi (RHA) yang mengandungi >90% silika digunakan untuk mensintesis zeolit ferrierit dan seterusnya digunakan sebagai mangkin dalam tindak balas pengalkilan Friedel Crafts katekol. Sintesis ferrierit dilakukan secara hidroterma dengan pemanasan selama 8 hari dalam aotuklaf dengan menggunakan pirolidin sebagai templat organik. Hasil pepejal yang diperolehi dicirikan dengan menggunakan kaedah FTIR dan XRD. Keputusan menunjukkan zeolit ferrrierit telah berjaya disintesis dan dikenalpasti sebagai ferrierit yang bercampur dengan zeolit analsim. Kebolehan ferrierit sebagai mangkin diuji dalam tindak balas pengalkilan Friedel Crafts katekol dengan tert-butanol yang dilakukan pada suhu 100^{o}C selama 24 jam pada dua keadaan iaitu pada tekanan atmosfera dan tekanan tinggi. Hasil yang diperolehi dicirikan dengan menggunakan GC dan dikenalpasti dengan GC-MS. Pengalkilan katekol dan tert-butanol pada kedua-dua keadaan menghasilkan 4-tert-butil-katekol sebagai hasil utama. Pada tekanan tinggi, peratus pertukaran dan peratus hasil yang diperolehi adalah tinggi iaitu sebanyak 19.71% pertukaran, 80.13% kepilihan dan 15.79% hasil berbanding pada tekanan atmosfera iaitu 10.52% pertukaran, 87.92% kepilihan, 9.25% hasil. Hasil kajian yang diperolehi ini menunjukkan bahawa ferrierit berupaya bertindak sebagai mangkin yang selektif dengan peratus kepilihan yang tinggi.

Title of thesis : Sintesis Zeolite Beta daripada Abu Sekam Padi Sebagai Mangkin Asid dalam Tindak Balas Pengalkilan Friedel-Crafts

Name : Nurhidayah Binti Deris

ABSTRAK

Zeolit Beta adalah bahan makroliang 3-dimensi yang mempunyai tapak asid Bronsted dan Lewis, sesuai dijadikan sebagai mangkin selektif dalam tindak balas Friedel-Crafts. Zeolit Beta daripada abu sekam padi telah disintesis dengan SiO_2/Al_2O_3 25. Kewujudan ikatan TO_4 dalam zeolit ditentukan dengan spektroskopi FTIR. Kaedah XRD digunakan untuk menentukan kehabluran dan fasa zeolit Beta di samping keamatan hablur yang terhasil. Keaktifan zeolit Beta sebagai mangkin heterogen dikaji dalam tindak balas pengalkilan Friedel-Crafts katekol dengan tert-butanol. Tindak balas ini dikaji berdasarkan kesan suhu dan sistem liang bagi zeolit Beta dan ferrerit. Hasil tindak balas melalui pemisahan oleh kromatografi gas memberikan 4-tert-butil-katekol sebagai hasil utama. Peratus hasil ini meningkat dengan pertambahan suhu. Peratus kepilihan dan pertukaran juga meningkat dengan pertambahan suhu tindak balas. Perbandingan antara zeolit Beta dan ferrerit menunjukkan zeolit Beta lebih selektif kerana saiz liangnya yang lebih besar (~7 Å) berbanding ferrerit (~5 Å). Zeolit Beta yang disintesis juga menunjukkan kecekapan sebagai mangkin asid yang hampir sama dengan mangkin Beta komersial.

Available online at www.sciencedirect.com
SCIENCE DIRECT
Journal of Molecular Catalysis A: Chemical 241 (2005) 118–125
JOURNAL OF MOLECULAR CATALYSIS A: CHEMICAL
www.elsevier.com/locate/molcata

TS-1 loaded with sulfated zirconia as bifunctional oxidative and acidic catalyst for transformation of 1-octene to 1,2-octanediol

Didik Prasetyoko [a], Zainab Ramli [a], Salasiah Endud [a], Hadi Nur [b,*]

[a] *Department of Chemistry, Faculty of Science, Universiti Teknologi Malaysia, 81310 UTM Skudai, Johor, Malaysia*
[b] *Ibnu Sina Institute for Fundamental Science Studies, Universiti Teknologi Malaysia, 81310 UTM Skudai, Johor, Malaysia*

Received 11 January 2005; received in revised form 24 June 2005; accepted 29 June 2005
Available online 15 August 2005

Abstract

Titanium silicalite (TS-1) loaded with sulfated zirconia as bifunctional oxidative and acidic catalyst has been synthesized at various loadings of zirconium (2–20 wt%). Structure and properties of the samples were characterized by X-ray diffraction (XRD), temperature programmed reduction (TPR), Fourier transform infrared (FTIR) and UV–vis diffuse reflectance (UV–vis DR) spectroscopy techniques. The monolayer dispersion capacity of zirconium on the TS-1 was found to be 0.65 Zr^{4+} nm^{-2} TS-1. The UV–vis DR spectroscopy showed that the tetrahedral coordination of the titanium was observed in all samples, while octahedral zirconium was only observed in the samples containing high amount of zirconium loading (10, 15 and 20 wt%). The TPR profiles suggested that the zirconium structure impregnated on the surface of TS-1 with high amount of zirconium loading (15 and 20 wt%) have a similar structure to sulfated zirconia calcined at 500 °C. Adsorption of pyridine onto the samples indicated that Brönsted acid sites are only present in samples with high sulfated zirconia loading, i.e. 15 and 20 wt%. As analyzed by XRD, the formation of Brönsted acid sites is due to the presence of disulfate species on the surface of TS-1. It has been demonstrated that samples with 15 and 20 wt% loadings of sulfated zirconia showed activity towards consecutive transformation of 1-octene to 1,2-octanediol through the formation of 1,2-epoxyoctane using aqueous hydrogen peroxide.

Keywords: Bifunctional catalyst; TS-1; 1-Octene; Sulfated zirconia; Epoxidation; Hydrolysis

1. Introduction

A large segment of the modern chemical industry is based on selective catalytic oxidation processes [1]. More than 60% of the chemicals and intermediates synthesized via catalytic processes are the products of oxidation. Most of the oxidation processes are being carried out in the gas and liquid phases. Catalytic oxidation in the liquid phase is widely used in bulk chemicals manufacture and are becoming increasingly important in the synthesis of fine chemicals [2]. Over the last decade, titanium silicalite (TS-1) which was first synthesized by Taramasso et al. [3] in 1983 has shown excellent catalytic activity in organic oxidation reactions using hydrogen peroxide as oxidant under mild conditions. In alkenes epoxidation, many works have been done to enhance the epoxide selectivity due to the industrial importance of epoxides in the synthesis of organic and pharmaceutical materials. The ability of TS-1 to catalyze a wide variety of oxidation transformations including alkenes epoxidation with 30% aqueous hydrogen peroxide has led to extensive research worldwide on the synthesis of related heterogeneous catalysts for liquid-phase oxidation [4]. The major side product of the epoxidation reaction using H_2O_2 is diols. It has been known that the formation of diols from epoxides is catalyzed by Brönsted acid sites. On the other hand, diols are attractive feedstocks for the fine chemical industry. At present, diols are manufactured industrially via a two-step sequence consisting of epoxidation of an olefin, followed by hydrolysis of the resulting epoxides.

Much attention has been paid to sulfated zirconia recently due to its significant catalytic activity in many hydrocarbon

* Corresponding author. Tel.: +607 5536061; fax: +607 5536080.
E-mail address: hadi@kimia.fs.utm.my (H. Nur).

1381-1169/$ – see front matter © 2005 Elsevier B.V. All rights reserved.
doi:10.1016/j.molcata.2005.06.070

conversions, such as isomerization, alkylation, acylation, esterification, etherification, condensation, nitration and cyclization [5–9]. It was shown that the catalytic activity of the sulfated zirconia is related mainly to its acid properties. Some authors have reported that the catalysts contain both Brönsted and Lewis acid sites which are responsible for the activity. Several studies have been done on the structure and activity of zirconia-loaded silica, alumina and mesoporous molecular sieves [10–15]. However, the preparation of sulfated zirconia loaded on a strong oxidative support as bifunctional oxidative and acidic catalyst, for the consecutive reaction of alkenes to diols through the formation of epoxides have never been reported. In this study, TS-1 loaded with sulfated zirconia has been synthesized and used as bifunctional oxidative and acidic catalyst in which the Ti atoms in TS-1 acts as oxidative acid sites while sulfated zirconia deposited on the surface of TS-1 acts as Brönsted acid sites. The effect of zirconium loading on the structure and properties of the catalysts was investigated. The catalytic activity was examined in the consecutive transformation of 1-octene to 1,2-octanediol through the formation of 1,2-epoxyoctane using aqueous hydrogen peroxide as oxidant.

2. Experimental

2.1. Preparation of sample

TS-1 containing 1 mol% of titanium was prepared according to a procedure described earlier [3,16]. TS-1 loaded with sulfated zirconia (SZ) was prepared by the wet impregnation method. The TS-1 was added into a solution of zirconium sulfate hydrate [$Zr(SO_4)_2{\cdot}4H_2O$] in water. The mixture was stirred at room temperature for 3 h, followed by evaporation of the solvent at 100 °C. The solid was dried at 100 °C for 24 h and calcined at 500 °C for 7 h. The resulting sample was denoted as *X*SZ/TS-1, in which *X* is the percentage of zirconium in the sample. For control, bare sulfated zirconia (SZ500) was prepared by drying of $Zr(SO_4)_2{\cdot}4H_2O$ at 100 °C for 3 days followed by calcination at 500 °C for 7 h. Table 1 summarizes the zirconium contents of the samples and their treatment after impregnation with $Zr(SO_4)_2$.

Table 1
Zirconium content of the samples[a]

Sample	Zr (wt%)
TS-1	0[b]
2SZ/TS-1	1.8[c]
5SZ/TS-1	5.1[c]
10SZ/TS-1	9.9[c]
15SZ/TS-1	15.5[c]
20SZ/TS-1	20.3[c]

[a] After the impregnation of $Zr(SO_4)_2$, the sample was dried at 100 °C for 24 h and calcined.
[b] The sample was calcined at 550 °C for 5 h.
[c] The sample was calcined at 500 °C for 7 h.

2.2. Characterization

All samples were characterized by powder X-ray diffraction (XRD) for crystallinity and phase content of the solid materials, using a Bruker Advance D8 difractometer with the Cu Kα (λ = 1.5405 Å) radiation as the diffracted monochromatic beam at 40 kV and 40 mA. The pattern was scanned in the 2θ ranges between 20° and 40° at a step 0.020° and step time 1 s. UV–vis DR spectra were recorded under ambient conditions using a Perkin-Elmer Lambda 900 UV/VIS/NIR spectrometer. The spectra were monitored in the range of 190–600 nm. Temperature programmed reduction (TPR) experiments were performed using a TPDRO 1100 Thermo Quest CE instrument. The sample (0.05 g) was pre-treated in a nitrogen flow at the rate of 30 ml min^{-1} at 500 °C for 1 h and cooled down to 100 °C. The reduction analysis was performed by heating the sample from 100 up to 900 °C at a rate of 10 °C min^{-1} in a flowing mixture of 5% hydrogen in nitrogen H_2/N_2 at the rate of 25 ml min^{-1}. Infrared (IR) spectra of the samples were collected on a Shimadzu Fourier Transform Infrared (FTIR) spectrometer, with a spectral resolution of 2 cm^{-1}, scans 10 s, at temperature 20 °C. For acidity evaluation, the wafer of the sample (10–12 mg) was prepared and locked in the cell equipped with CaF_2 windows and evacuated at 400 °C under vacuum condition for 4 h. Infrared spectra of the sample were recorded at room temperature in the hydroxyl region of 4000–3000 cm^{-1} and pyridine vibration region at 1700–1300 cm^{-1}.

2.3. Catalytic testing

The catalyst performance was tested in the epoxidation of 1-octene using aqueous H_2O_2 (30%) as oxidant. The reaction mixture containing 1-octene (8 mmol), H_2O_2 (15 mmol) and acetone (10 g) as solvent was put in a round bottom flask equipped with a condenser. The catalyst (0.05 g) was then added to the solution. The reaction was carried out in an oil bath under stirring at 70 °C. The products of the reaction were analyzed by a Hewlett-Packard 6890 N gas chromatograph using an Ultra-1 column and a Hewlett-Packard GC-MSD instrument using an HP5 column.

3. Results and discussion

3.1. X-ray diffraction

Fig. 1 shows the XRD patterns of the SZ500 and SZ/TS-1 samples. It is shown that no diffraction lines for tetragonal or monoclinic phases of zirconia are observed indicating that the SZ is highly dispersed on the surface of TS-1. It is found that the MFI structure of TS-1 was maintained after the sulfated zirconia (SZ) loading. However, the XRD peak intensities of TS-1 decreased when the loading amount of the SZ was increased. This might be due to the decrease in the percentage

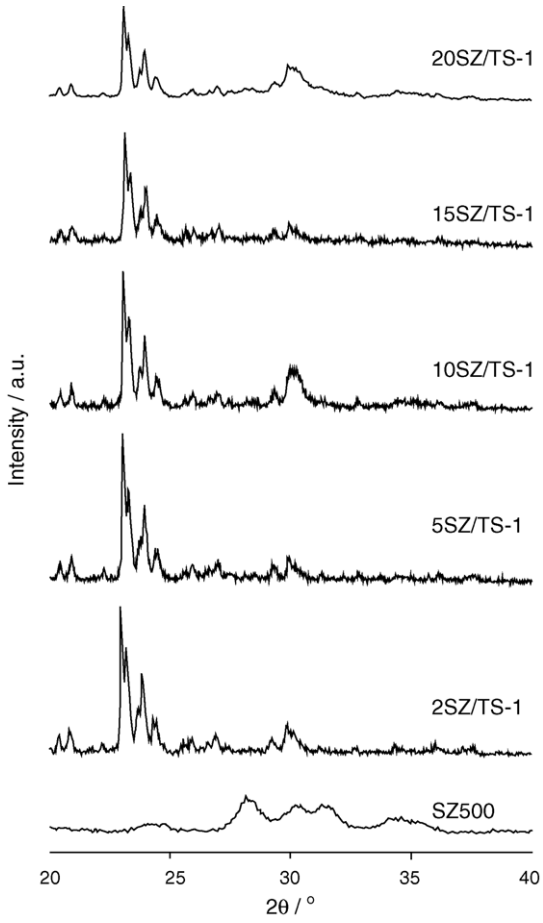

Fig. 1. XRD pattern of the TS-1 loaded with sulfated zirconia.

amount of TS-1 in the samples as the loading amount of the SZ increased.

The monolayer coverage of ZrO_2 can be determined from the plot of the diffraction line intensity of TS-1 at $2\theta = 23^\circ$ versus loading amount of zirconium on the samples as shown in Fig. 2. The diffraction line intensities of 2SZ/TS-1 and 5SZ/TS-1 were similar to those of the parent TS-1 and are significantly lower for 10SZ/TS-1, 15SZ/TS-1 and 20SZ/TS-1. Hence, a horizontal line was found for low SZ loadings and another straight line with a tangent can be drawn for higher SZ loadings. The interception of the two lines was found at 6 wt% of SZ loading which is equal to 0.65 Zr^{4+} nm^{-2} TS-1. This value corresponds to monolayer dispersion capacity of zirconium on the TS-1.

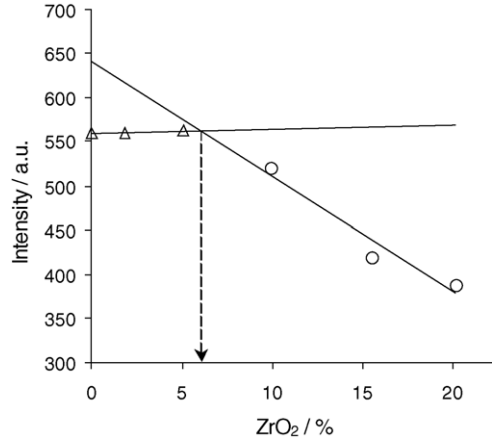

Fig. 2. The graph of peak intensity of TS-1 at $2\theta = 23^\circ$ vs. loading amount of zirconium on the s TS-1 loaded with sulfated zirconia.

3.2. Infrared spectroscopy

The infrared spectra of zeolite lattice vibration between 1400 and 400 cm^{-1} are depicted in Fig. 3. According to Flanigen [17], the absorption bands at around 1100, 800 and 450 cm^{-1} are lattice modes associated with internal linkages in SiO_4 (or AlO_4) tetrahedral and are insensitive to structural changes. The absorption bands at around 1230 and 547 cm^{-1} are characteristic of the MFI type zeolite structure and are sensitive to structure changes. All samples showed a band at around 970 cm^{-1}. The vibrational modes at around this frequency may be the result of several contributions, i.e. the asymmetric stretching modes of Si–O–Ti linkages, terminal Si–O stretching of SiOH–(HO)Ti "defective sites" and titanyl [Ti=O] vibrations. However, this band can be attributed to the titanium in the framework, since silicalite,

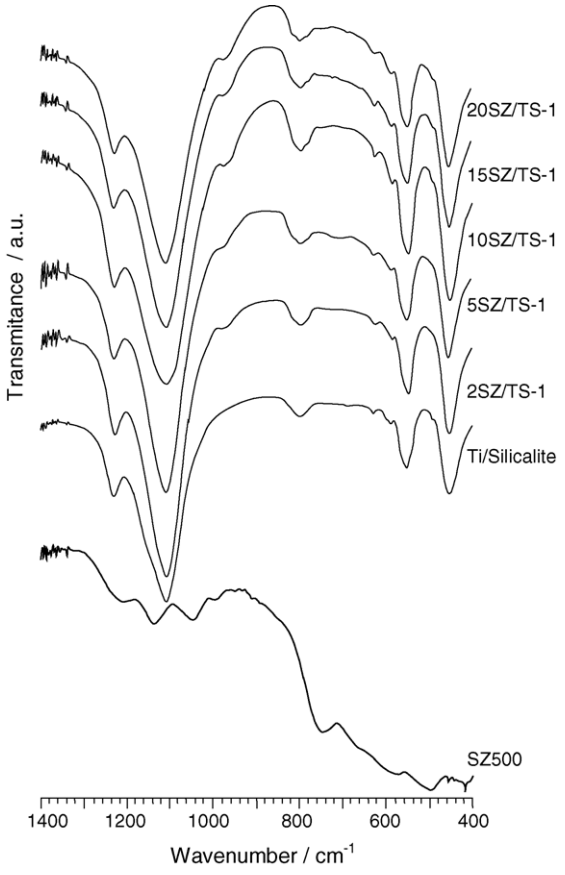

Fig. 3. Infrared spectra of TS-1 loaded with sulfated zirconia.

a Ti-free zeolite, did not show any band at around this frequency [18–21]. In addition, impregnation of silicalite with Ti (sample Ti/silicalite) gave rise to no band around 970 cm^{-1}. Therefore, it is concluded that the TS-1 sample contains Si–O–Ti connections. There is no band shifting or additional band observed after impregnation of zirconium sulfate on TS-1. This finding suggests that both the MFI structure and titanium framework were still maintained after loading of SZ.

3.3. UV–vis diffuse reflectance spectroscopy

As shown in Fig. 4, an absorption band at around 210 nm was observed in the spectra of SZ/TS-1. This band is attributed to ligand-to-metal charge transfer not only associated with isolated Ti^{4+} framework sites (between O^{2-} and the central Ti(IV) atoms) in tetrahedral coordination but also with isolated Zr^{4+}. This is supported by the fact that the impregnation of HZSM-5, a Ti-free aluminosilicalite, with zirconium sulfate (5SZ/HZSM-5) also showed a band at around 210 nm. The second band at lower energy of about 230 nm is attributed to zirconium species in an octahedral coordination [3,22].

Fig. 4 displays UV–vis DR spectra of SZ500 and SZ/TS-1 catalysts. The UV–vis DR spectrum of SZ500 indicates the existence of a shoulder band at around 210 nm and a sharp band centered at 230 nm. A single absorption band at 210 nm was observed in the spectrum of SZ/TS-1 containing low amounts of zirconium (2, 5 and 10 wt%), while a band at 225 nm was observed in the case of 15SZ/TS-1 and 20SZ/TS-1. The decrease in intensity of the band at 210 nm with an increase in SZ loading (up to 15 wt%) suggests that tetrahedral titanium species in the TS-1 was covered by SZ. This implies that as the amount of SZ loading increases, concentration of tetrahedral titanium species decreases.

Octahedral zirconium species, which corresponds to the peak at 230 nm, starts to appear in 10SZ/TS-1, being significantly high at higher SZ loading (Fig. 4). This finding indicates that not only SZ/TS-1 contains tetrahedral Ti but also agglomerated SZ at high zirconium loading.

3.4. Temperature programmed reduction

The TPR profiles for SZ500 and SZ/TS-1 after calcination at 500 °C are shown in Fig. 5. There is no peak of hydrogen consumed for sulfate-free zirconia, indicating that reduction did not occur in the sample. The SZ500 showed broad and sharp peaks with high intensities, starting at 500 °C and peaking at 700–720 °C and 750 °C. Similar TPR profiles with lower reduction temperatures can be observed for 15SZ/TS-1 and 20SZ/TS-1. The TPR profiles of 2SZ/TS-1, 5SZ/TS-1 and 10SZ/TS-1 showed a broad signal at reduction temperature of 500–700 °C. It is observed that both the signal intensity and reduction temperature decreased as SZ loading decreased.

According to Xu and Sachtler [23], the high temperature TPR peaks are assigned to the reduction of sulfate species in the sample to form sulfur dioxide and water. Besides sulfur dioxide, hydrogen sulfide was also evolved during treatment of sulfated zirconia with hydrogen in helium at high temperature [24]. Meanwhile, Bobricheva et al. [25] and Vera et al. [26] suggested that the peak at temperature range of

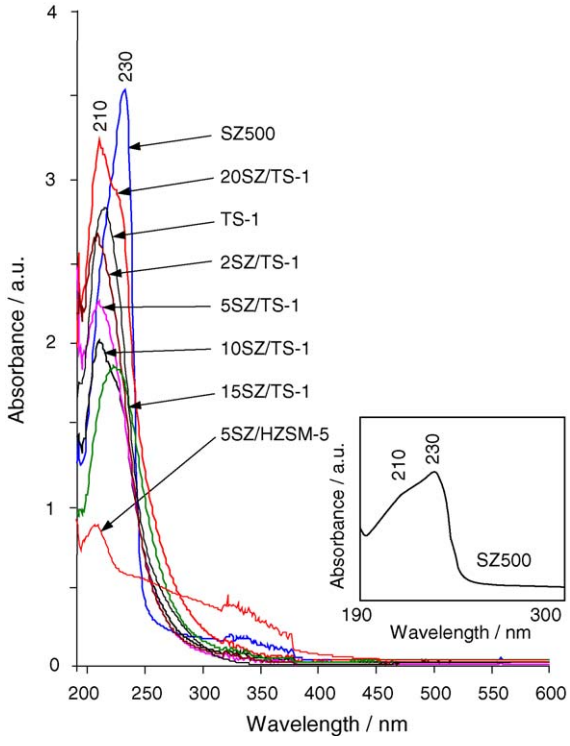

Fig. 4. UV–vis diffuse reflectance spectra of TS-1 loaded with sulfated zirconia.

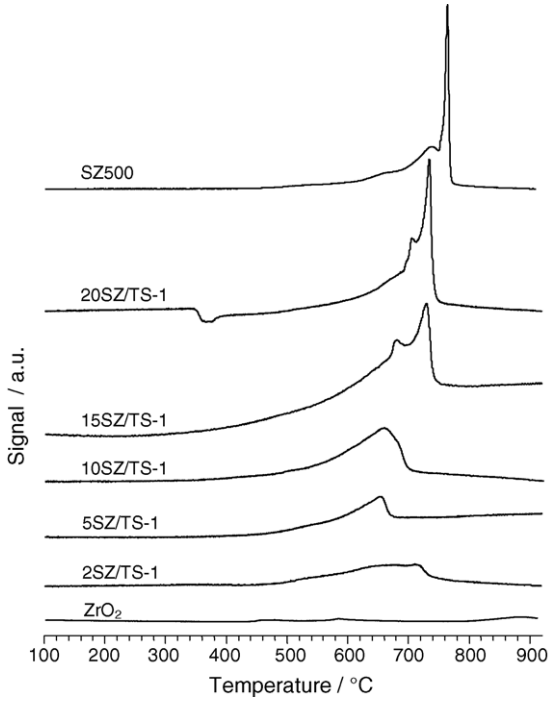

Fig. 5. TPR profiles of TS-1 loaded with sulfated zirconia.

500–600 °C is attributed to a surface process of lattice oxygen elimination (formation of anionic vacancies) and the reduction of Zr^{4+} to Zr^{3+} on the surface of zirconia sulfate during the hydrogenation process. It suggests that release of sulfate from the surface of sulfated zirconia occurs during these processes. Therefore, it can be concluded that all the TPR peaks at low and high reduction temperatures are attributed to desorption of sulfate species. Furthermore, TPR profiles of 15SZ/TS-1 and 20SZ/TS-1 are similar to those of SZ500, suggesting that there is no difference in the molecular structure of SZ between these samples.

3.5. Acidity

Fig. 6a shows the FTIR spectra of the SZ/TS-1 samples after evacuation at 400 °C for 4 h under vacuum. In the region of hydroxyl groups, the peak at 3745 cm^{-1}, which is assigned as silanol hydroxyl groups, can be clearly observed for samples with low loading amount of the SZ (2SZ/TS-1 and 5SZ/TS-1). This band was diminished at higher SZ loading (10-20SZ/TS-1), suggesting the SZ is located in the space/sites previously occupied by silanol groups. It is also possible that SZ contains hydroxyl groups since the peak at around 3550 cm^{-1} corresponds to the hydrogen bonding between the hydroxyl groups (see Fig. 9).

The FTIR spectra of the SZ/TS-1 samples in the sulfate region are shown in Fig. 6a. It is shown that the spectra of

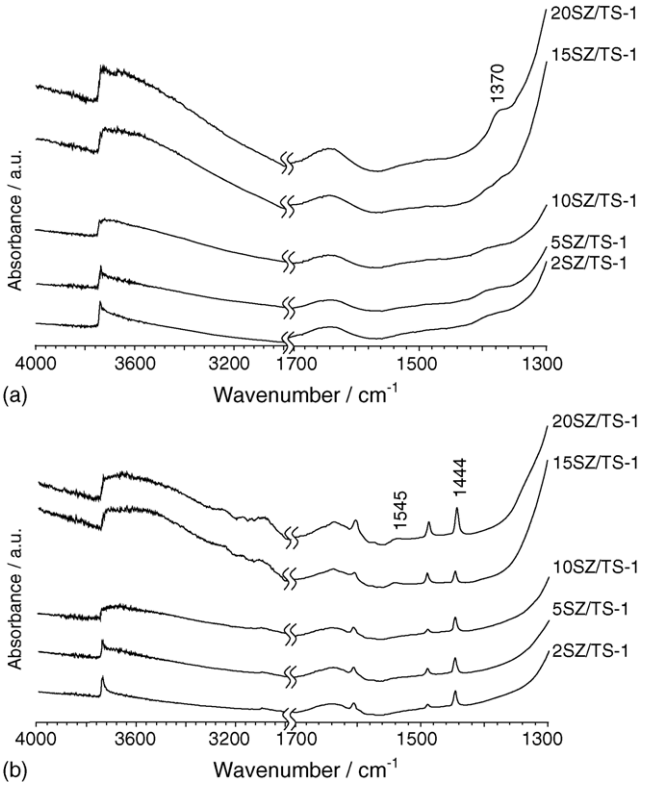

Fig. 6. FTIR spectra of the samples: (a) after evacuation at 400 °C for 4 h in vacuum, (b) after pyridine adsorption and evacuation at 150 °C for 1 h.

2SZ/TS-1, 5SZ/TS-1 and 10SZ/TS-1 are similar. The spectra of 15SZ/TS-1 and 20SZ/TS-1 showed an additional peak at 1370 cm^{-1} which is assigned to $\nu_{S=O}$ asymmetric vibration [27]. It is clearly observed that the intensity of the peak was significantly high in 20SZ/TS-1 suggesting an increase in the amount of sulfate with an increase in SZ loading.

It is interesting to relate the surface coverage obtained from XRD with the $\nu_{S=O}$ asymmetric peak at 1370 cm^{-1} which appeared on the spectra of samples. It has been calculated from the XRD data that the monolayer dispersion of zirconium is 0.65 Zr^{4+} nm^{-2} TS-1. It is revealed that the $\nu_{S=O}$ asymmetric peak only starts to appear in the spectrum of 15SZ/TS-1 although 10SZ/TS-1 has the zirconium content almost double compared to the amount of zirconium monolayer dispersion capacity calculated from the XRD data which is 1.12 Zr^{4+} nm^{-2} TS-1. It can be suggested that the $\nu_{S=O}$ asymmetric band only becomes detectable in SZ/TS-1 that contains a double layer of SZ.

The acidity of the SZ/TS-1 catalysts was monitored by FTIR using pyridine as a probe molecule (see Fig. 6b). There were no significant changes in the hydroxyl region of the spectra of the samples after pyridine adsorption compared to that before pyridine adsorption. The presence of silanol peak after pyridine adsorption indicates that the silanol groups do not react with pyridine, indicating that the silanol groups are not acidic. The peaks at 1608 and 1444 cm^{-1} in the spectra of 2SZ/TS-1, 5SZ/TS-1 and 10SZ/TS-1 are attributed to adsorbed pyridine bound coordinatively with Lewis acid sites. The spectra of 15SZ/TS-1 and 20SZ/TS-1 showed the additional absorption bands at 1640 and 1545 cm^{-1} which correspond to pyridine interacting with Brönsted acid sites. The disappearance of the $\nu_{S=O}$ asymmetric peak after the adsorption of pyridine is due to the reduction of the bond order of S=O from a highly covalent double-bond character to a lesser double–bond character; the shift of the band to a lower wavenumber was observed when a basic pyridine molecule was adsorbed on the catalysts [28].

The acidity study also indicates that SZ is responsible for the formation of Brönsted acid sites. In addition, it proves that Brönsted acid sites are present only in the samples containing double layer of zirconium, whereas samples with monolayer of zirconium do not show Brönsted acidity. Since the Brönsted acidity is only found in the sample containing octahedral zirconium (see UV–vis spectra of 15SZ/TS-1 and 20SZ-TS-1 in Fig. 4), it can be concluded that the sulfate species are bonded with octahedral zirconium and not with tetrahedral zirconium. This conclusion is supported by the model proposed by Clearfield et al. [29].

3.6. Catalytic activity

The catalytic properties of the SZ/TS-1 samples were studied in the catalytic epoxidation of 1-octene using H_2O_2 as oxidant in acetone as solvent at 70 °C. The same reactions were carried out over a mechanical mixture of TS-1 and

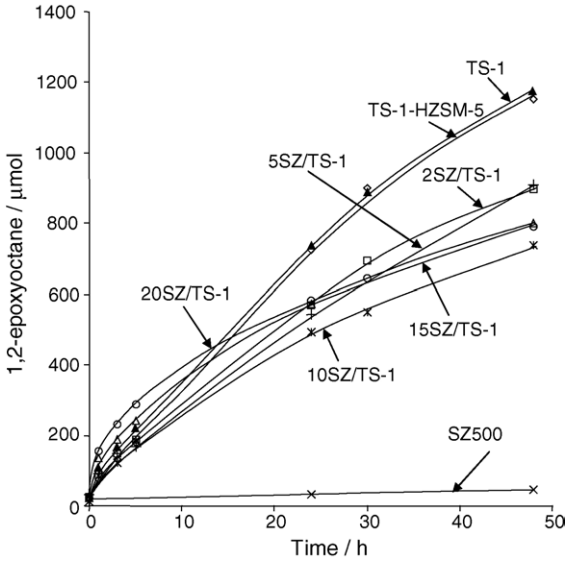

Fig. 7. The oxidation rate of 1-octene to 1,2-epoxyoctane using TS-1 loaded with sulfated zirconia with aqueous H_2O_2 as oxidant. All reactions were carried out in acetone as solvent at 70 °C.

HZSM-5 zeolite (TS-1-HZSM-5) for comparison. The amount of HZSM-5 was adjusted to match the amount of Brönsted acid in 20SZ/TS-1. As analyzed by pyridine adsorption, the concentration of Brönsted acid of HZSM-5 was 0.5 mmol g^{-1}. Theoretically, the epoxidation reaction of alkene to epoxide and the hydrolysis of epoxide to form diol are catalyzed by oxidative and acidic sites, respectively.

Fig. 7 shows the oxidation rate of 1-octene to 1,2-epoxyoctane using TS-1 loaded with sulfated zirconia using aqueous H_2O_2 as oxidant. At the beginning, the initial reaction rate of the catalysts with low zirconium loading (2SZ/TS-1, 5SZ/TS-1 and 10SZ/TS-1) was similar to that of TS-1 and TS-1-HZSM-5, whereas catalysts with high zirconium loading (15SZ/TS-1 and 20SZ/TS-1) showed considerably higher activities. However, at longer reaction time, TS-1 and TS-1-HZSM-5 showed the highest activity among the SZ/TS-1 catalysts (see Fig. 7). Meanwhile, SZ500 was totally inactive toward epoxidation. It was also observed that the catalytic activity of TS-1 was similar to that of TS-1-HZSM-5 suggesting that the epoxidation of 1-octene was not affected by HZSM-5. In order to evaluate H_2O_2 selectivity, the reaction was carried out with a similar molar amount of 1-octene and H_2O_2. It is observed that the yield of 1,2-epoxyoctane decreased with decreasing H_2O_2 after 24 h of reaction time under stirring condition compared to the system containing large excess of H_2O_2 (15 mmol) against 1-octene (8 mmol). The decrease in the molar amount of H_2O_2 and 1,2-epoxyoctane were similar (ca. 15%). This finding indicates that it is necessary to use excess amount of H_2O_2 in order to compensate the decomposition of H_2O_2 during the reaction.

As shown in Fig. 7, at the initial stage, the 15SZ/TS-1 and 20SZ/TS-1 catalysts had similar activities towards the formation of 1,2-epoxyoctane. The characterization results described in Sections 3.3 and 3.5 showed that both samples contain octahedral zirconium, sulfate species and Brönsted acid sites. In order to confirm the effect of sulfate species on enhancement of the catalytic activity, the epoxidation reaction was carried out using TS-1 containing 20 wt% of the sulfate-free zirconia. The result clearly showed that its reaction rate is similar to that of TS-1. Addition of HZSM-5, an acid catalyst, also shows insignificant change in the reaction rate. The structure of zirconium species present in the samples did not influence the catalytic activity of the parent catalyst either, since SZ500 is inactive as catalyst. Based on the above considerations, one concludes that enhancement of the epoxidation activity is not affected by the presence of the double layer of zirconium, the Brönsted acid sites or the octahedral zirconium. This suggests that the enhancement of the catalytic activity at the initial reaction rate could be attributed to the sulfate-bonded zirconia species present on the surface of TS-1 loaded with high amount of sulfated zirconia. The possible explanation for this phenomenon is described in the following paragraph.

It has been proposed that oxo-titanium species (superoxo- and hydroperoxo-titanium) are the reactive sites for olefin epoxidation reaction using H_2O_2 catalyzed by TS-1 [30,31]. The reactive oxo-titanium species in TS-1 was generated by interaction of tetrahedral titanium in TS-1 with aqueous H_2O_2 adducts. Therefore, the increase of epoxidation reaction rates in SZ/TS-1 catalysts can be explained by the rates of the formation of the reactive oxo-titanium species. The sulfate present on the surface of SZ/TS-1 probably can increase the adsorption rate of aqueous H_2O_2 onto TS-1. Consequently, the rate of the formation of oxo-titanium species increases and accordingly the production of epoxides is also increased. Meanwhile, a decrease in the activity of SZ/TS-1 samples that was observed at prolonged reaction time is probably due to the lower diffusion rate of 1-octene to the active sites inside the pore of TS-1.

The hydrolysis rate of 1,2-epoxyoctane to 1,2-octanediol using TS-1 loaded with sulfated zirconia using aqueous H_2O_2 as oxidant is shown in Fig. 8. Generally, TS-1, 15SZ/TS-1, 20SZ/TS-1 and TS-1-HZSM-5 were found to be active in the hydrolysis of 1,2-epoxyoctane although their activities are lower when compared with 20SZ/TS-1 and 15SZ/TS-1. Considering that SZ/TS-1 catalysts contain Brönsted acid sites, one expects that they are responsible for the hydrolysis of 1,2-epoxyoctane. Since the amount of Brönsted acid of 20SZ/TS-1 was higher than that of 15SZ/TS-1, its activity to hydrolyze 1,2-epoxyoctane was evidently higher as expected. It is noted that the amount of Brönsted acid in the TS-1-HZSM-5 was adjusted to be similar to that found in 20SZ/TS-1. However, the rate of the formation of 1,2-octanediol (up to 48 h) on the TS-1-HZSM-5 system was much lower and comparable with that on the low loading of SZ/TS-1 and TS-1. This indicates that highly active bifunctional oxidative and acidic catalyst may be prepared by deposition of SZ on the surface of TS-1 and cannot be achieved by mechanical mixing of TS-1 with HZSM-5.

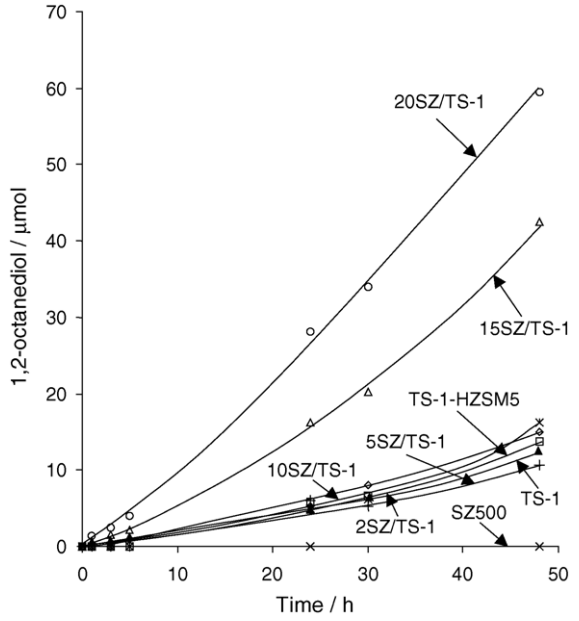

Fig. 8. The oxidation rate of hydrolysis of 1,2-epoxyoctane using TS-1 loaded with sulfated zirconia. All reactions were carried out in acetone as solvent at 70 °C.

Since the size of Zr^{4+} (ca. 0.1 nm), the source of SZ sites, is smaller than the size of the pore entrance of TS-1 (0.5 nm), the Zr species should be attached to the internal and external surfaces. As described in Section 3.5, it is possible that the SZ is located in a place where the silanol groups of TS-1 were previously positioned. Based on this consideration, it seems that SZ is effectively located close to Ti active sites, since the epoxide immediately reacts with SZ acid active site to hydrolyze the epoxide. This consecutive reaction is more difficult to occur efficiently over the TS-1-HZSM-5 catalytic system since the epoxide must diffuse to acid sites of HZSM-5 which are predominantly located in its pore. On the basis of these results, a model of the bifunctional oxidative and acidic catalytic system for consecutive reaction of 1-octene to 1,2-octanediol is proposed (see Fig. 9).

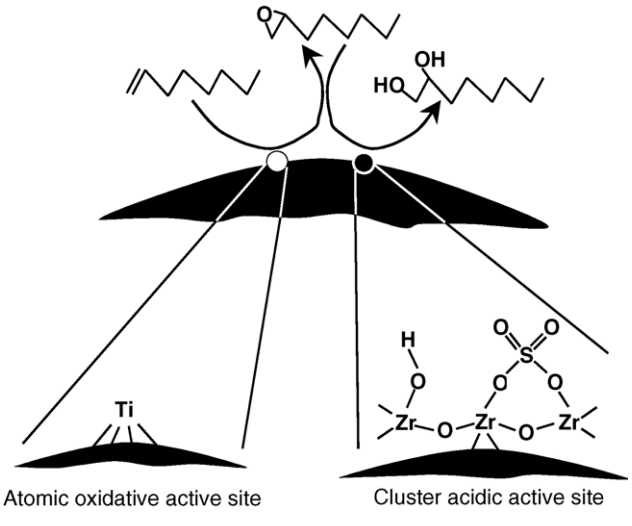

Fig. 9. Proposed model of TS-1 loaded with sulfated zirconia as bifunctional catalyst for consecutive transformation of 1-octene to 1,2-octanediol through the formation of 1,2-epoxyoctane.

4. Conclusion

Bifunctional oxidative and acidic catalysts have been successfully prepared by the dispersion of sulfated zirconia on the TS-1 at high zirconium loading up to double layer zirconium, i.e. 1.3 Zr^{4+} nm^{-2} TS-1. The catalysts have oxidative site due to titanium located in the framework of silicalite, while octahedral zirconium containing sulfate as Brönsted acidic sites. It has been demonstrated that samples with 15 and 20 wt% loadings of sulfated zirconia have shown the activity toward the consecutive transformation of 1-octene to 1,2-octanediol through the formation of 1,2-epoxyoctane using aqueous hydrogen peroxide.

Acknowledgement

We gratefully acknowledge funding from The Ministry of Science Technology and Innovation Malaysia (MOSTI), under IRPA grant no. 09-02-06-0057 SR0005/09-03.

References

[1] G. Centi, F. Cavani, F. Trifiro, in: M.V. Twigg, M.S. Spencer (Eds.), Fundamental and Applied Catalysis, Kluwer Academic Press, New York, 2001, p. 7.
[2] R.A. Sheldon, J. Dakka, Catal. Today 19 (1994) 215.
[3] M. Taramasso, G. Perego, B. Notari, US Patents No. 4,410,501 (1983).
[4] C. Perego, A. Carati, P. Ingallina, M.A. Mantegazza, G. Bellussi, Appl. Catal. A: Gen. 221 (2001) 63.
[5] M. Hino, S. Kobayashi, K. Arata, J. Am. Chem. Soc. 101 (1979) 6439.
[6] E.J. Hollstein, J.T. Wei, C.Y. Hsu, US Patent No. 4,918,041 (1990).
[7] B.H. Davis, R.A. Keogh, R. Srinivasan, Catal. Today 20 (1994) 219.
[8] C.Y. Hsu, V.K. Patel, D.H. Vahlsing, J.T. Wei, H.K. Myers Jr., US Patent 5,019,671 (1991).
[9] G.D. Yadav, J.J. Nair, Microporous Mesoporous Mater. 33 (1999) 1.
[10] S. Damyanova, P. Grange, B.J. Delmony, J. Catal. 168 (1997) 421.
[11] Y.Y. Huang, B.Y. Zhao, Y.C. Xie, Appl. Catal. A: Gen. 173 (1998) 27.
[12] T. Lei, J.S. Xu, Y. Tang, W.M. Hua, Z. Gao, Appl. Catal. A: Gen. 192 (2000) 181.
[13] C.L. Chen, C. Tao, L. Soofin, P. Hong, C.J. Bhongale, C.Y. Mou, Microporous Mesoporous Mater. 50 (2001) 201.
[14] I.J. Dijs, J.W. Geus, L.W. Jenneskens, J. Phys. Chem. B 107 (2003) 13403.
[15] J.R. Sohn, D.H. Seo, Catal. Today 87 (2003) 219.
[16] A.J.H.P. van der Pol, A.J. Verduyn, J.H.C. van Hooff, Appl. Catal. A: Gen. 92 (1992) 113.
[17] E.M. Flanigen, in: J.A. Rabo (Ed.), Zeolite Chemistry and Catalysis, vol. 171, ACS Monograph, 1976, p. 80.
[18] K.S. Smirnov, B. van de Graaf, Microporous Mater. 7 (1996) 133.
[19] E. Astorino, J.B. Peri, R.J. Willey, G. Busca, J. Catal. 157 (1995) 482.

[20] G. Ricchiardi, A. Damin, S. Bordiga, C. Lamberti, G. Spano, F. Rivetti, A. Zecchina, J. Am. Chem. Soc. 123 (2001) 11409.
[21] S. Bordiga, A. Damin, F. Bonino, A. Zecchina, G. Spano, F. Rivetti, V. Bolis, C. Prestipino, C. Lamberti, J. Phys. Chem. B 106 (2002) 9892.
[22] B. Rakshe, V. Ramaswamy, S.G. Hegde, R. Vetrivel, A.V. Ramaswamy, Catal. Lett. 45 (1997) 41.
[23] B.Q. Xu, W.M.H. Sachtler, J. Catal. 167 (1997) 224.
[24] R. Srinivasan, R.A. Keogh, D.R. Milburn, B.H. Davis, J. Catal. 153 (1995) 123.
[25] I.V. Bobricheva, I.A. Stavitsky, V.K. Yermolaev, N.S. Kotsarenko, V.P. Shmachkova, D.I. Kochubey, Catal. Lett. 56 (1998) 23.
[26] C.R. Vera, C.L. Pieck, K. Shimizu, J.M. Parera, Appl. Catal. A: Gen. 230 (2002) 137.
[27] D.J. Rosenberg, B. Bachiller-Baeza, T.J. Dines, J.A. Anderson, J. Phys. Chem. B 107 (2003) 6526.
[28] J.R. Sohn, W.C. Park, Appl. Catal. A: Gen. 239 (2003) 269.
[29] A. Clearfield, G.P.D. Serrette, A.H. Khazi-Syed, Catal. Today 20 (1994) 295.
[30] D. Srinivas, P. Manikandan, S.C. Laha, R. Kumar, P. Ratnasamy, J. Catal. 217 (2003) 160.
[31] F. Bonino, A. Damin, G. Ricchiardi, M. Ricci, G. Spano, R. D'Aloisio, A. Zecchina, C. Lamberti, C. Prestipino, S. Bordiga, J. Phys. Chem. B 108 (2004) 3573.

BIFUNCTIONAL Nb/Ti-MCM-41 CATALYST IN OXIDATIVE ACIDIC REACTION OF CYCLOHEXENE TO DIOL

Zainab Ramli, Mazidah Abdul Shukor and Didik Prasetyoko

Dept. of Chemistry, Faculty of Science, Universiti Teknologi Malaysia, 81310 UTM Skudai, Johor D.T.

Keywords: bifunctional catalyst, Nb/TiMCM-41, oxidative-acidic, diol

Abstract: Bifunctional oxidative and acidic catalyst was prepared by incorporating titanium ion (Ti^{4+}) and niobic acid in mesoporous molecular sieves MCM-41 structure. The catalyst is active both in oxidation, and acid-catalyzed reaction of olefin to diol. Nb/Ti-MCM-41 catalyst was prepared by first synthesizing Ti-MCM-41 by hydrothermal method, followed by subsequent impregnation of niobic acid (Nb) into Ti-MCM-41 at various %wt Nb loading. The framework structure of Ti-MCM-41 collapsed after incorporation of Nb but the tetrahedral form of Ti^{4+} still maintained with octahedral Nb species. Both Brønsted and Lewis acid sites are present in all Nb/Ti-MCM-41 samples. The formation of cyclohexanediol in the epoxidation of cyclohexene proved the bifunctional oxidative and acidic catalyst through the formation of cyclohexane oxide. The yield increased with the increase amount of the Brønsted acid sites provided by niobium species.

Abstrak: Mangkin dwifungsi oksidatif berasid disediakan dengan memasukkan ion titanium (Ti^{4+}) dan asid niobik dalam struktur penapis molekul mesoliang MCM-41. Mangkin aktif dalam kedua-dua tindak balas bermangkinkan pengoksidaan dan asid bagi olefin kepada diol. Mangkin Nb/Ti-MCM-41 disediakan bermula dengan mensintesis Ti-MCM-41 secara hidroterma, diikuti dengan pengisitepuan asid niobik (Nb) ke dalam Ti-MCM-41 pada berbagai % berat muatan Nb. Struktur bingkaian Ti-MCM-41 didapati runtuh selepas kemasukan Nb tetapi struktur tetrahedron Ti^{4+} masih kekal dengan spesies octahedron Nb. Kedua-dua tapak asid Brønsted dan Lewis hadir dalam semua sampel Nb/Ti-MVM-41. Pembentukan sikloheksandiol dalam pengepoksidaan sikloheksena membuktikan mangkin adalah dwifungsi oksidatif berasid melalui pembentukan sikloheksan oksida. Hasil bertambah dengan pertambahan tapak asid Brønsted yang disediakan oleh spesies niobium.

Introduction

Mesoporous molecular sieves (MMS) have attracted a great deal of world-wide attention among researches in the fields of inorganic synthesis, functional materials, and heterogeneous catalysis, due to their regular pore structure, uniform pore diameter and high surface area[1,2]. One of the interesting fields in development of catalyst is the creation of two active sites in a single material catalyst, called bifunctional catalyst. The bifunctional catalyst in this study is active both in oxidation and acid-catalyzed reactions. Didik *et al*. [3-6] has reported the activity of bifunctional catalysts prepared by incorporation of sulphate, zirconia, niobium on TS-1 molecular sieve, on the epoxidation of 1-octene to its respective diol. The niobium incorporated TS-1, Nb/TS-1 catalyst [6] was found to be the most active catalyst in which the diol yield depends on the amount of incorporated niobium.

However the same catalyst when applied in epoxidation of cyclohexene did not yield any desired product. The reason might be due to the microporosity of TS-1 being medium pore class molecular sieve having pore size of ~ 5Å. To prove that the activity of Nb/TS-1 as the bifunctional oxidative-acidic catalyst was hindered by pore restriction, we chose MCM-41 with the pore size in mesoporous range as the support for niobium species. In this study, Ti-MCM-41 (TM) and Nb/Ti-MCM-41 (Nb/TM) samples were prepared and characterized using XRD, FTIR and UV-Vis DR. Acidity was measured by FTIR using pyridine as probe molecule. The catalysts prepared are tested in the epoxidation reaction of cyclohexene.

Experimental

Synthesis of Ti-MCM-41 and Nb/Ti-MCM-41

Ti-MCM-41 (TM) was prepared by direct hydrothermal following method described by Blasco et al.[7] Tetraethylorthosilicate,(TEOS) was placed into a teflon beaker and stirred.

Tetraethylorthotitanate(TEOT) in isopropyl alcohol was added dropwise into the TEOS. The temperature of the mixture was raised to 35 ^{o}C and mixed homogeneously for half an hour followed by cooling to 0 ^{o}C (solution A). The tetramethyammonium hydroxide (TMAOH) was dissolved in water, followed by the addition of cetyltrimethylammonium bromide (CTMABr). The mixture was stirred for half an hour and then was also cooled to 0 ^{o}C (solution B). Solution B was added slowly to the solution A with stirring at 0 ^{o}C. The resulting gel with the oxide ratio 0.03Ti:1Si: 63.81H_2O: 0.39TMAOH: 1.02CTMABr was heated between 80 – 90 ^{o}C for 4 hours. Water was added and the gel was placed into PTFE bottle and heated at 98 ^{o}C in oven for 3 days. The solid was filtered and washed using hot water until the filtrate becomes neutral. Finally, the solid obtained was dried at 110^{o}C overnight and calcined at 500 °C. Sample Nb/Ti-MCM-41 (Nb/TM) was prepared by impregnation technique using $Nb(OC_2H_5)_5$ as Nb precursor. Dried TM and calculated amount of $Nb(OC_2H_5)_5$ was mixed in n-hexane. The mixture was stirred for 3 hrs. The solid was recovered by evaporating the n-hexane at 80 ^{o}C followed by addition of HNO_3 in distilled water and aged overnight. Finally, the solid was heated at 120^{o}C until dried.

Characterizations and Acidity Measurement

Characterization by XRD for identification of the crystalline phases of the samples was done using a Bruker Advance D8 Difractometer with the Cu Kα (λ = 1.5405 Å) scanned in the 2θ range of 1.5 – 12^{o} at a step time 1 sec. The IR spectra of samples were collected on a Perkin Elmer FTIR using KBr pellet method. The framework spectra were recorded in the region of 1500-400 cm^{-1}. The geometry structure of Ti and Nb species in the samples were monitored by UV-Vis Diffuse Reflectance, recorded at ambient conditions on a Perkin Elmer Lambda 900 UV/VIS/NIR spectrometer in the wavenumber range 190-600 nm.

For acidity study, the sample was made a 13mm disc. The sample was first heated at 400^{o}C in vacuum conditions overnight. Before pyridine adsorption, the IR of the dehydrated samples was taken. Pyridine was then adsorbed for 5 seconds, continued by desorption at 150 ^{o}C for an hour. The IR spectra of the samples were taken at room temperature.

Catalytic testing

The catalysts performance was tested in the epoxidation of the cyclohexene using hydrogen peroxide as oxidant. The reaction mixture containing cyclohexene (10 mmol), H_2O_2 (10 mmol) in acetonitrile (10 g) and cyclohexene (1.0 mmol) were placed in a 25 cm^3 round bottom flask equipped with a magnetic stirrer and condenser. An amount of 0.05 g catalyst was added into the solution. The reaction was carried out in oil bath at 70 ^{o}C with continuous stirring. The aliquots were sampled out at regular time intervals and analyzed with GC-FID using Ultra 1 methyl siloxane capillary column (25 m length, 0.25 mm diameters with 0.2 μm wall thickness).

Results and Discussion

Characterization of the catalysts

The phase crystallinity of the samples is characterized by XRD. The diffractograms of Ti-MCM-41 (TM) and niobium incorporated TM samples (Nb/TM) are presented in Figure 1. The XRD of Ti-MCM-41 (TM) shows 3 diffraction lines with different intensities. The most intense peak relative to the (100) plane is usually taken as a measure for the crystallinity [4] or the highly ordered of the synthesized TM. Thus the intense d_{100} peak indicates that the Ti-MCM-41 is highly ordered mesoporous material. However the peak was very much reduced in intensity and shifted to higher 2θ upon incorporation of Nb on TM. The XRD patterns of Nb/TM samples does not shows any significant diffraction line, indicating that after impregnation of Nb species on TM, the MCM-41 framework structure has collapsed.

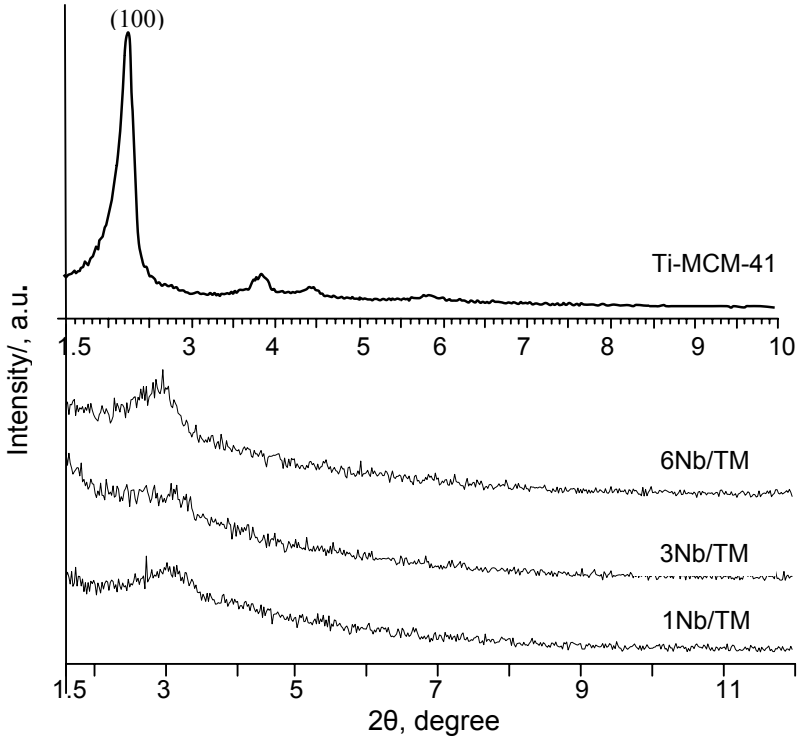

Figure 1: XRD of TM and Nb/TM samples at 1,3 and 6 %wt Nb loading

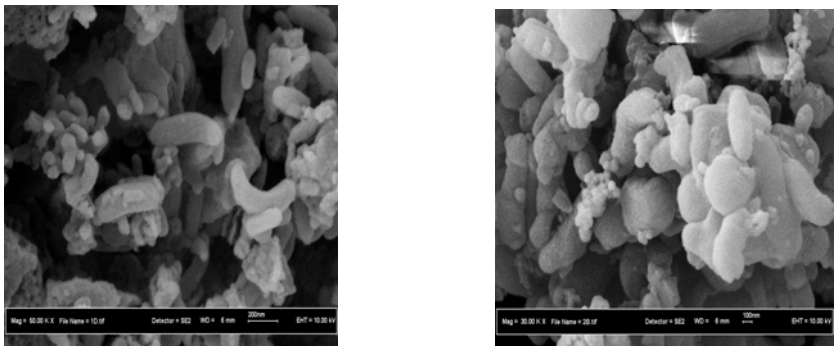

(a) (b)

Figure 2: FESEM micrographs of samples (a) TM and –magnification 50,000x (b) Nb/TM-magnification 30,000x

Field Emission SEM (FESEM) was applied to study the surface morphology of the samples. FESEM micrographs of TM and Nb/TM sample are shown in Figure 2. "Worm" type of morphology and irregular shape particle was observed from the TM and Nb/TM samples. The sample after impregnation (Nb/TM) showed that the worm type has coagulated and agglomerated thus, the particles became larger.

IR cannot ascertain the presence of framework Ti in the TM sample as the band assign for TiO_4 at ca. 970 cm^{-1} [8] overlapping with Si-O band of silanol group which usually present in MCM-41 sample. However its present can be confirmed by UV-Vis DR. UV-Vis DR spectra of TM sample shows in

Figure 3. It exhibits a single sharp absorption band at 226 nm, assigned to the ligand to metal charge transfer involving isolated titanium atom in the tetrahedral coordination [9]. For Nb/TM samples, a band appears at 226 nm-236 nm showing that the samples have retained the tetrahedral form of Ti. This is important to maintain the oxidative sites in the Nb/TM catalyst which only active when Ti^{4+} is in the form of tetrahedral. A shoulder band around 260 nm in Nb/TM samples is assigned to the octahedral Nb species [7]. The intensity of this band increased as the niobium content in the samples increased.

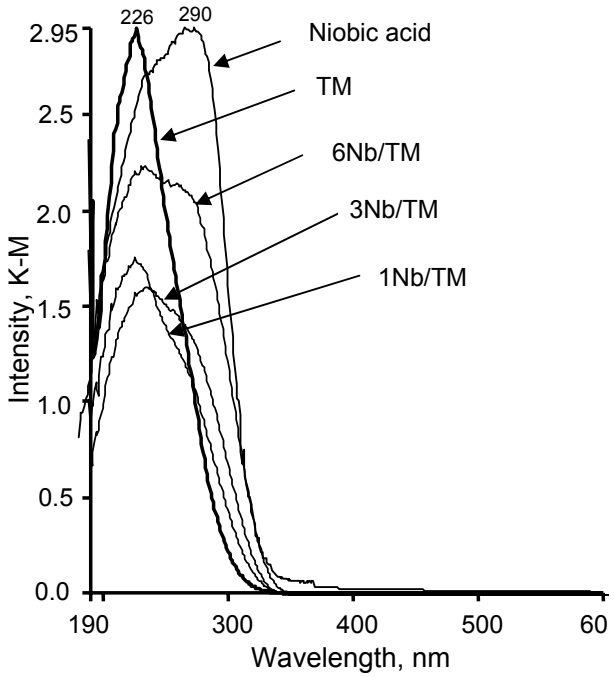

Figure 3: UV-Vis DR spectra of TM and Nb/TM samples

Acidity Study

Surface acidity of the samples was carried by pyridine adsorption at room temperature on the dehydrated samples at 400 ^{o}C under vacuum and monitored by IR spectroscopy. The type and the amount of the acid sites can be determined using this method. The IR spectra of the TM and Nb/TM samples after evacuation at 400^{o}C show a single peak at *ca*. 3740 cm^{-1} in the hydroxyl region with quite high intensity. This peak is assigned for terminal silanol groups. The presence of silanol groups is a characteristic of MCM-41 sample.

IR spectra in the pyridine region of the samples after pyridine adsorption and desorption at 150 °C are shown in Figure 4. All samples showed peaks at around 1545 cm^{-1}, 1490 cm^{-1} and 1447 cm^{-1} which were due to the Brønsted, Brønsted-Lewis mixture and Lewis sites, respectively. These results showed that Brønsted and Lewis acid sites are present in all samples. The amount of Brønsted acids increased with the increasing Nb loading on the TM. Table 1 listed the amount of Brønsted acid sites calculated on the basis of area under the peak at ca 1540 cm^{-1}. This finding indicates that Nb plays a role in the formation of Brønsted acid sites

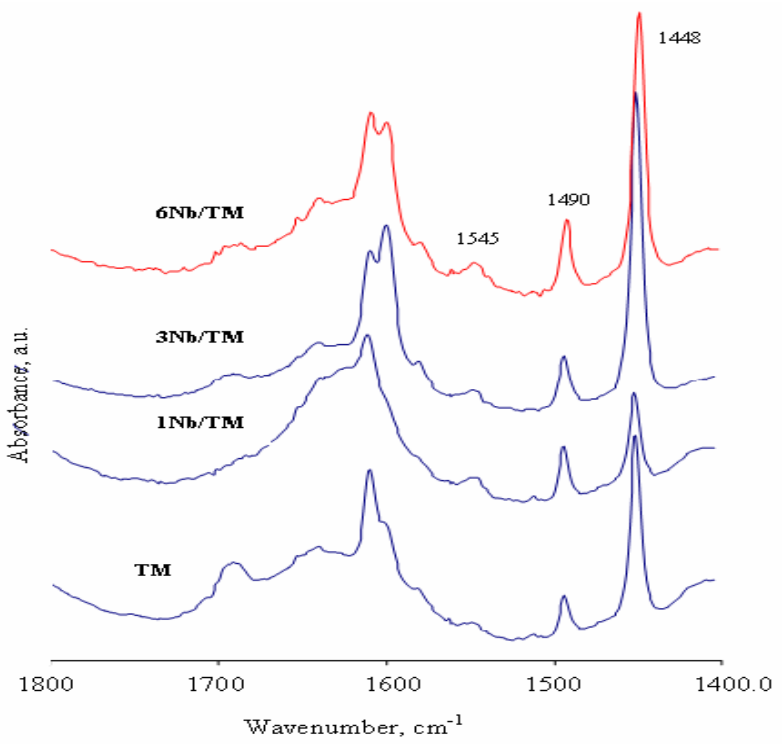

Figure 4: IR spectra of the TM and Nb/TM samples in pyridine vibration region

Catalytic activity

Catalyst performance was investigated in the epoxidation of cyclohexene. Figure 5 shows the products of cyclohexene epoxidative-acidic reaction catalysed by the TM and Nb/TM samples while Table 1 listed the catalytic performance of the TM and Nb/TM samples in relation with the Brønsted acidity and the turn over frequency (TOF). All samples showed activity toward the formation of products, i.e. cyclohexane oxide, cyclohexenone, cyclohexenol and cyclohexanediol. However, in the absence of Nb, no cyclohexanediol was formed in the reaction catalyzed by TM sample while the amount of cyclohexanediol formed increased with the increase of Nb loading on Nb/TM samples. However, data from the turn over frequency (TOF) in Table 1 showed that sample 3Nb/TM gave higher value than sample 6Nb/TM while the sample 1Nb/TM gave the lowest TOF. It is suggested that the Brønsted acid sites in sample 3Nb/TM is more effective compared to other samples. This might be due to the presence of less polymerized niobium oxides species in sample 3Nb/TM as compared to sample 6Nb/TM as observed by UV-Vis DR spectroscopy.

On the other hand, in term of selectivity of cyclohexanediol, high selectivity is observed on sample containing high amount of Brønsted acid sites i.e. sample 6Nb/TM. All TM containing Nb samples showed activity toward the formation of cyclohexanediol with sample 6Nb/TM gave higher yield of cyclohexanediol compared to samples 3Nb/TM and 1Nb/TM. The yield of cyclohexanediol increased due to the increase amount of Brønsted acid present in the catalysts as demonstrated by pyridine adsorption study. From the catalytic testing, it has been proven that the yield of cyclohexanediol increased when using the catalyst with high amount of Nb loading. Based on these findings it is suggested that the formation of cyclohexanediol is catalyzed by Brønsted acid sites

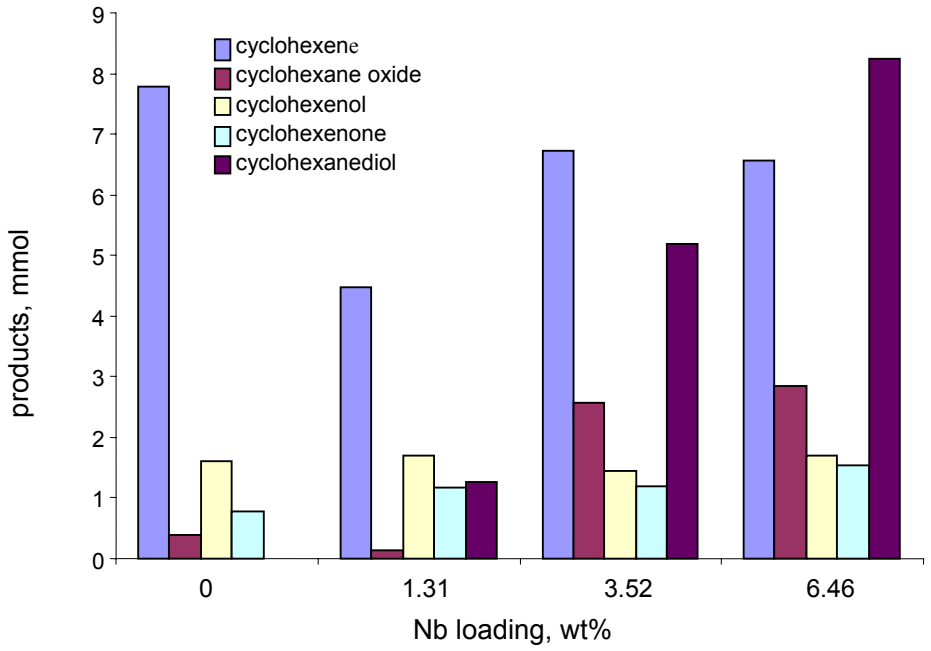

Figure 5 : Histogram showing products from the epoxidative-acidic reaction of cyclohexene catalysed by TM and Nb/TM samples.

Table 1: Catalytic activity of TM and Nb/TM samples

Sample	Conversion (%)	Brønsted ($\mu molg^{-1}$)	Diol (mmol)	TOF (h^{-1})	Selectivity (%)
TM	2	1.39	-	-	-
1Nb/TM	5.2	4.46	1.27	271	29.66
3Nb/TM	3	6.52	5.19	758	49.76
6Nb/TM	3.2	11.09	8.25	708	57.53

Conclusion

The bifunctional catalyst has successfully been synthesized in the Ti-MCM41 containing niobium. It was proven by characterizations, acidity measurement and catalytic testing on the epoxidation of cyclohexene. Acidity study has confirmed the presence of Brønsted and Lewis acid sites. The amount of Brønsted increased as the amount of niobium increased. The main product from the epoxidation reaction of cyclohexene by the catalysts is cyclohexanediol proved the bifunctional oxidative acidic function of the catalyst. The yield of cyclohexanediol increased with the increasing amount of Nb loading.

Acknowledgement

Authors would like to thank the Malaysian Ministry of Science, Technology and Innovation (MOSTI) for funding under IRPA project No. 09-02-06-0057 SR0005/09-03

REFERENCES

[1]. Nowak, I. Ziolek, M. (2005). "Effect of Texture and Structure on the Catalytic Activity of Mesoporous Niobosilicates for the Oxidation of Cyclohexene". *Micropor. Mesopor. Mater.* **78**. 281-288.

[2]. Nowak, I. Kilos, B. Ziolek, M. Lewandowska, A. (2003). "Epoxidation of Cyclohexenon Nb-containing Meso and Macroporous Maetrials". *Catal. Today*. **78**. 487-498.

[3]. Didik Prasetyoko, Salasiah Endud, Zainab Ramli and Hadi Nur (2005). "Enhancement of Catalytic Activity of Titanosilicalite-1 – Sulfated Zirconia Combination Towards Epoxidation of 1-Octene with Aqueous Hydrogen Peroxide". *Reaction Kinetics and Catalysis Letters.* **86**(1): 83-89,

[4]. Hadi Nur, Didik Prasetyoko, Salasiah Endud, and Zainab Ramli. (2004) "Sulfation: a Simple Method to Enhance the Catalytic Activity of TS-1 in Epoxidation of 1-Octene with Aqueous Hydrogen Peroxide". *Catalysis Communications.* **5**: 725-728,.

[5]**.** Didik Prasetyoko, Zainab Ramli, Salasiah Endud, and Hadi Nur. (2005) "Structural and Superacidity Study of Bifunctional Catalyst, Sulfated-Titanium/TS-1". *Malaysian Journal of Chemistry*. **7**(1): 011-018.

[6]. D. Prasetyoko. Zainab Ramli. Salasiah Endud. H. Nur. (2005). "Preparation and Characterization of Bifunctional Oxidative and Acidic Catalysts Nb_2O_5/TS-1 for Synthesis of Diols". *Mater. Chem. Phys*. **93**. 443-449.

[7] Blasco, T. Corma, A. Navarro, M.T. Pèrez Pariente, J. (1995). "Synthesis, Characterization, and Catalytic Activity of Ti-MCM-41 Structures". *J. Catal*. **156**. 65-74.

[8] Zecchina, A. Bordiga, S. Spoto, Lamberti, C, Ricchiardi, G.., Scarano, D., Petrini, G. Leofanti, G. Mantegazza, M. (1996). Structural characterization of Ti centres in Ti-silicalite and reaction mechanism in cyclohexanone ammoximation. *Catal Today*. **32**: 97-106

[9] Yu, Jiangqiang. Feng, Zhaochi. Xu, Lei. Li, Meijun. Xin, Qin. Liu, Zhongmin. Li, Can. (2001). "Ti-MCM-41 Synthesized from Colloidal Silica and Titanium Trichloride: Synthesis, Characterization and Catalysis". *Chem. Mater*. **13**. 994-998.

Jointly published by
Akadémiai Kiadó, Budapest
and Springer, Dordrecht

React.Kinet.Catal.Lett.
Vol. 86, No. 1, 83-89
(2005)

RKCL4659

ENHANCEMENT OF CATALYTIC ACTIVITY OF TITANOSILICALITE-1 – SULFATED ZIRCONIA COMBINATION TOWARDS EPOXIDATION OF 1-OCTENE WITH AQUEOUS HYDROGEN PEROXIDE

Didik Prasetyoko[a], Zainab Ramli [a], Salasiah Endud[a] and Hadi Nur[b,*]

[a]Department of Chemistry, Faculty of Science, Universiti Teknologi Malaysia,
81310 UTM Skudai, Johor, Malaysia

[b]Ibnu Sina Institute for Fundamental Science Studies, Universiti Teknologi Malaysia,
81310 UTM Skudai, Johor, Malaysia

Received September 28, 2004
In revised form January 31, 2005
Accepted February 18, 2005

Abstract

Titanosilicalite-1 (TS-1) in combination with sulfated zirconia efficiently catalyzes the epoxidation of 1-octene with aqueous hydrogen peroxide. The presence of both octahedral zirconium and sulfate species in the catalysts enhances the epoxidation rates.

Keywords: Titanosilicalite-1, sulfated zirconia, epoxidation

INTRODUCTION

Epoxides are becoming important useful commercial products in the area of petrochemical and fine chemical industries. Many efforts have been made to facilitate the production of epoxides, which include the use of catalysts in the production processes. The breakthrough was achieved by Taramasso in 1983 who reported the preparation and catalytic activity of titanosilicalite-1 (TS-1) [1]. TS-1 represents an important change since it has shown interesting catalytic properties in alkene epoxidations with hydrogen peroxide as the oxidant. Compared to the traditional oxidation reactions, H_2O_2 as the oxidant in all the oxidations catalyzed by TS-1 has the advantage of producing environmentally

* Corresponding author. E-mail: hadi@kimia.fs.utm.my

0133-1736/2005/US$ 20.00.

benign water as its by-product. It has been applied to catalytic oxidation of different organic substrates, for example, epoxidation of olefins, hydroxylation of aromatics, amoximation of cyclohexanol and oxidation of alcohols [2,3]. It exhibits an excellent catalytic reactivity and selectivity in different oxidations attributed to coordination of the catalytic oxidation property in titanium and shape selectivity effects in ZSM-5 structure. However, development of the catalysts in order to increase its catalytic activity towards epoxides is still in progress, such as in catalyst preparation and modification [3,4]. Meanwhile, zirconia-silica composite prepared by sol-gel method and zirconia supported on the silica aerosil have been shown to be an active catalyst in the epoxidation of 1-octene using *t*-butyl hydroperoxide (TBHP) as oxidant [5,6]. Its activity is related with the structure of zirconium in the materials, i.e. coordinatively unsaturated configuration. We now demonstrate that the catalytic activity of TS-1 towards the epoxidation of 1-octene with aqueous hydrogen peroxide can be enhanced by deposition of sulfated zirconia on the surface of TS-1.

EXPERIMENTAL

TS-1 containing 1% mol of titanium was prepared according to a procedure described earlier by Taramasso *et al*. [1]. Zirconium sulfate containing TS-1 was prepared by wet impregnation method. The TS-1 was added into a solution of zirconium sulfate hydrate [$Zr(SO_4)_2 \cdot 4H_2O$] in water. The mixture was stirred at room temperature for 3 h, followed by evaporation of the solvent at 100^{o}C. The solid was then dried at 100^{o}C for 24 h and calcined at 500^{o}C for 7 h. The resulting sample was denoted as *X*ZS/TS-1, in which *X* was the percentage of zirconium in the sample. For comparison, unsulfated zirconia impregnated TS-1 (sample 20Zr/TS-1, Zr=20 wt.%) was prepared by impregnation of TS-1 with zirconium isopropoxide from its hexane solution at room temperature. Then, the zirconium isopropoxide was hydrolyzed followed by drying at 100^{o}C and calcination at 500^{o}C for 7 h. Sample ZS500 was prepared by drying of zirconium sulfate hydrate at 100^{o}C for 3 days followed by calcination at 500^{o}C for 7 h.

All samples were characterized by powder X-ray diffraction (XRD) for crystallinity and phase content of the solid materials, using Bruker Advance D8 Diffractometer with the CuKα (λ=1.5405 Å) radiation as the diffracted monochromatic beam at 40 kV and 40 mA. Infrared (IR) spectra of the samples were collected on a Shimadzu Fourier Transform Infrared, with a spectral resolution of 2 cm^{-1}, scanned every 10 s at 20^{o}C. For the acidity study, the wafer of the sample (10-12 mg) was prepared and locked in the cell equipped with CaF_2 windows, and evacuated at 400^{o}C under vacuum for 4 h. Pyridine was adsorbed at room temperature. Diffuse reflectance UV-visible (UV-vis DR)

spectra were recorded under ambient conditions on a Perkin Elmer Lambda 900 UV/VIS/NIR spectrometer. The spectra were monitored in the 190 – 600 nm range and Kubelka-Munk axis.

The catalysts performance was tested in the epoxidation of 1-octene using hydrogen peroxide (30%) as an oxidizing agent. The reaction mixture, i.e. 8 mmol of 1-octene, 15 mmol of H_2O_2 in 10 gram acetone as solvent and 0.8 mmol of cyclooctane as an internal standard were put in the round bottom flask equipped with a condenser. An amount of 0.05 g catalyst was then added into the solution. The reaction was carried out in an oil bath with stirring at 70^{o}C. The products of the reaction were analyzed by Hewlett Packard Model 6890N gas chromatograph using Ultra-1 column and Hewlett Packard GC-MSD using HP5 column.

RESULTS AND DISCUSSION

Zirconium sulfate (ZS) at various contents was dispersed on TS-1. The XRD pattern of all the ZS/TS-1 samples showed that diffraction lines for tetrahedral or monoclinic phases of zirconia were not observed, which indicated that the ZS was highly dispersed on the surface of the TS-1. It is found that the MFI structure of TS-1 was still maintained after ZS loading (data not shown). However, the XRD peak intensities of TS-1 decreased as the loading amount of the ZS increased. This might be due to the decrease in the percentage amount of the TS-1 in the samples as the loading amount of the ZS increased. The monolayer coverage of zirconium can be determined from the graph of the diffraction line intensity of TS-1 at $2\theta=23^o$ *vs.* loading amount of zirconium on the samples. The diffraction lines of samples 2ZS/TS-1 and 5ZS/TS-1 showed similar intensities compared to the parent TS-1, while samples 10ZS/TS-1, 15ZS/TS-1 and 20ZS/TS-1 showed lower intensities. Hence, a horizontal line was found for low ZS loading and another straight line can be drawn for higher ZS loading. The intercept of the two lines occurred at the value 0.65 Zr^{4+}/nm^2 TS-1, which is equal to 6 wt.%. This value corresponds to the value for monolayer dispersion capacity of zirconium on the TS-1.

Figure 1a shows the IR spectra of the ZS/TS-1 samples after evacuation at 400^{o}C for 4 h in vacuum. In the region of hydroxyl groups (4000-3000 cm^{-1}), the peak of silanol groups at 3745 cm^{-1} still can be observed for samples with low loading amount of the ZS (2ZS/TS-1 and 5ZS/TS-1). However, the peak disappeared for samples with higher ZS loading (10-20ZS/TS-1). This finding suggests that the monolayer coverage of the ZS on the TS-1 is in the range of 5 to 10 wt.% of zirconium (0.57 to 1.12 Zr^{4+}/nm^2 TS-1), in which all silanol groups or surface of TS-1 have been covered with ZS with the maximum amount of 1.12 Zr^{4+}/nm^2 TS-1. The FTIR spectra of the ZS/TS-1 samples in the

ranges of 1700 – 1300 cm^{-1} (Fig. 1b) show that samples 2ZS/TS-1, 5ZS/TS-1, and 10ZS/TS-1 exhibit a similar pattern, without the peak assigned for sulfate vibration. However, samples 15ZS/TS-1 and 20ZS/TS-1 showed additional peaks at 1370 cm^{-1}, assigned for asymmetric $\nu_{S=O}$, confirming the presence of sulfate species [7]. In addition, the intensity of this peak was significantly higher in sample 20ZS/TS-1, in which the amount of sulfate increased as ZS loading increased.

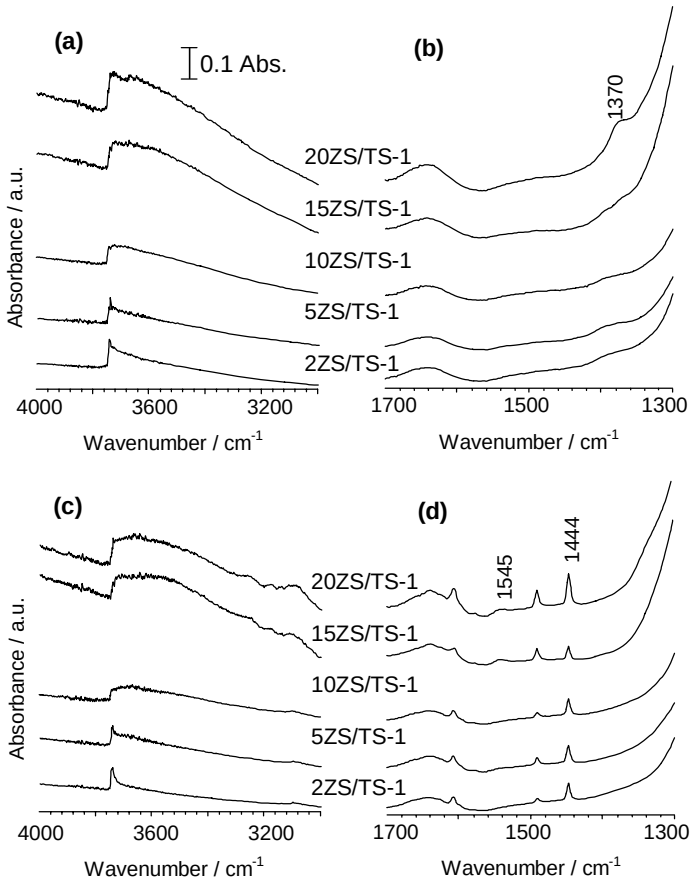

Fig. 1. FTIR spectra of the samples: (a, b) after evacuation at 400°C for 4 h in vacuum, (c, d) after pyridine adsorption and evacuation at 150°C for 1 h

It is interesting to relate the surface coverage of zirconium sulfate from the XRD finding with that of the IR spectroscopy. The XRD data found that the monolayer dispersion was 0.65 Zr^{4+}/nm^2 TS-1, while IR data had shown that the asymmetric $\nu_{S=O}$ appeared on sample 15ZS/TS-1 (1.76 Zr^{4+}/nm^2 TS-1), but not for sample 10ZS/TS-1 (1.12 Zr^{4+}/nm^2 TS-1). At the value of 1.12 Zr^{4+}/nm^2 TS-1, the asymmetric $\nu_{S=O}$ did not appear although this sample had almost double the zirconium content compared to the amount of zirconium monolayer dispersion capacity obtained from the XRD data *i.e.* 0.65 Zr^{4+}/nm^2 TS-1. The asymmetric $\nu_{S=O}$ only started to appear in samples at 1.76 Zr^{4+}/nm^2 TS-1, which contained more zirconium than that of double monolayer capacity. It can be suggested that the second layer coverage will be formed after the formation of monolayer on the solid support. Therefore, it can be proposed that the asymmetric $\nu_{S=O}$ started to appear on samples of ZS/TS-1 that contained double layer of ZS which was equal to 1.3 Zr^{4+}/nm^2 TS-1.

The spectra of the sample after pyridine adsorption in the region of hydroxyl groups are shown in Fig. 1c. There were no significant changes of the spectra as compared to that before pyridine adsorption. The silanol peak was still present after pyridine adsorption, indicating that the silanol groups did not react with pyridine. It is therefore concluded that the silanol groups are not acidic. In the regions of pyridine and sulfate as displayed in Fig. 1d, samples 2ZS/TS-1, 5ZS/TS-1 and 10ZS/TS-1 showed similar peaks at 1608 and 1444 cm^{-1}. These bands appeared when adsorbed pyridine bound coordinatively with Lewis acid sites in which these samples have similar amount of Lewis acid sites. These results indicated that zirconium was not responsible for the formation of Lewis acid sites. Meanwhile, samples 15ZS/TS-1 and 20ZS/TS-1 showed the absorption bands at 1640 and 1545 cm^{-1}, which corresponded to pyridine interacting with the Brönsted acid sites, beside bands at 1608 and 1444 cm^{-1} characteristic for Lewis acid sites. In addition, the peak for asymmetric $\nu_{S=O}$ disappeared after the adsorption of pyridine, indicating that the S=O was bound to pyridine. This finding suggests that the S=O acted as an active acid site. It also indicates that ZS was responsible for the formation of Brönsted acid sites and they were only present in samples containing a double layer of zirconium, whereas samples with a monolayer of zirconium did not show Brönsted acid sites. It is therefore concluded that sulfate can only bond with zirconia at the double layer of zirconium.

The UV-Vis DR spectrum of sample ZS500 indicated the existence of a shoulder band at around 210 nm and a sharp band centered at 230 nm (data not shown). A single absorption band at 210 nm can be observed on samples ZS/TS-1 containing low amount of zirconium (2, 5 and 10 wt.%), while a band at 225 nm was observed on samples 15ZS/TS-1 and 20ZS/TS-1. The band at around 210 nm is assigned for zirconium or titanium with tetrahedral coordination. The second band at lower energy at about 230 nm is attributable

to zirconium species in an octahedral coordination. The IR and UV-Vis DR data showed that both sulfate and octahedral zirconium species can only be observed on the samples containing double layer zirconium. From these, we can conclude that sulfate species bonded with the octahedral zirconium species and not with tetrahedral zirconium species. Clearfield *et al.* [8] have proposed a model that allowed for the formation of Brönsted acid sites on sulfated zirconia containing octahedral zirconium species after heating at 300°C.

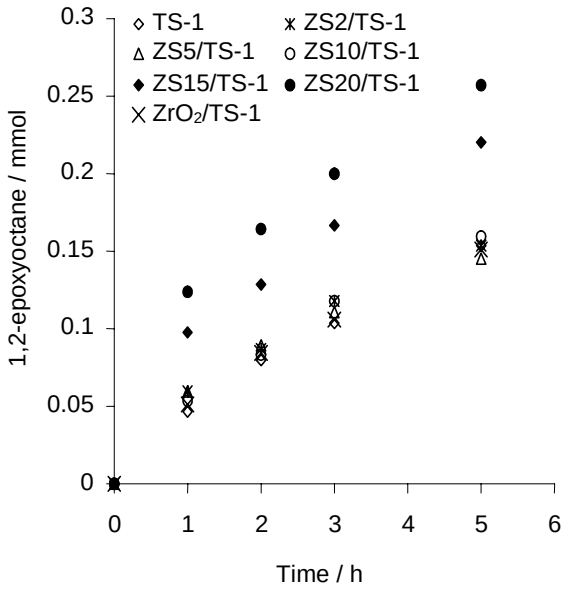

Fig. 2. The yield of 1,2-epoxyoctane on the epoxidation of 1-octene using various modified titanosilicalite-1 samples. All reactions were carried out at 70°C in acetone as solvent

All samples were tested as catalysts in 1-octene epoxidation using H_2O_2 as oxidant at 70°C. Figure 2 shows the rate of the formation of 1,2-epoxyoctane over various ZS/TS-1 samples. It can be seen that samples with low zirconium loading (2ZS/TS-1, 5ZS/TS-1 and 10ZS/TS-1) did not show any significant changes to the rate of reactions towards the formation of 1,2-epoxyoctane compared with TS-1 and ZrO_2/TS-1. However, remarkably higher activities were shown by samples at higher zirconium loading, ZS15/TS-1 and ZS20/TS-1. In addition, the 1,2-octanediol as by-product was observed, due to Brönsted acid sites present in the samples. This lowered the selectivity towards 1,2-epoxyoctane.

To determine the factor that influenced the enhancement of the catalyst activities, several experiments have been conducted. Higher activities were observed on samples ZS15/TS-1 and ZS20/TS-1. The characterization results showed that both samples contained high zirconium loading, Brönsted acid sites, octahedral zirconium, and sulfate species. However, from the catalytic testing, it was shown that the TS-1 containing high loading of zirconium without sulfate species (sample ZrO_2/TS-1) showed similar reaction rates with TS-1 itself, while the addition of HZSM-5 zeolite that contained Brönsted acid sites did not show significant changes of reaction rates. The structures of zirconium species present in the samples also did not influence the catalytic activity of the parent catalyst. When ZS500 was used as a catalyst without TS-1, no epoxidation product was obtained. Thus, high zirconium loading, Brönsted acid sites, octahedral zirconium containing ZS/TS-1, and ZS were not directly contributing to the enhancement of the catalytic activity. Therefore, it is suggested that the enhancement of its catalytic activity can be attributed to the sulfate-bonded zirconia species present in the surface of TS-1.

For olefin epoxidation reaction using H_2O_2 catalyzed by TS-1, the reactive sites are oxo-titanium species (superoxo- and hydroperoxo-titanium) [9]. The reactive oxo-titanium species in TS-1 were generated by the interaction of tetrahedral titanium (tetrapodal or tripodal) in TS-1 with aqueous H_2O_2 adducts. It was also reported that solvent acetone retarded the formation of oxo-titanium species [9]. Therefore, in this study, the increase of epoxidation reaction rates using ZS/TS-1 catalysts can be explained by the rates of the formation of the reactive oxo-titanium species. It is known that TS-1 has hydrophobic properties, while ZS has hydrophilic properties. The sulfate present on the surface of ZS/TS-1 probably can increase the adsorption rate of aqueous H_2O_2 into TS-1. Consequently, the rate of the formation of oxo-titanium species increased and accordingly the production of epoxides are also increased.

REFERENCES

1. M. Taramasso, G. Perego, B. Notari: *U.S. Patents,* No. 4,410,501 (1983).
2. E.J. Hollstein, J.T. Wei, C.Y. Hsu: *U.S. Patent,* 4,918,041 (1990).
3. C. Perego, A. Carati, P. Ingallina, M.A. Mantegazza, G. Bellussi: *Appl. Catal. A: General*, **221**, 63 (2001).
4. M.C. Capel-Sanchez, J.M. Campos-Martin, J.L.G. Fierro: *Appl. Catal. A: General*, **246**, 69 (2003).
5. S. Imamura, T. Yamashita, K. Utani, H. Kanai, K. Hamada: *React. Kinec. Catal. Lett.*, **72**, 11 (2001).
6. H. Kanai, Y. Okumura, K. Utani, K. Hamada, S. Imamura: *Catal. Lett.*, **76**, 3 (2001).
7. D.J. Rosenberg, B. Bachiller-Baeza, T. J. Dines, J.A. Anderson: *J. Phys. Chem. B.*, **107,** 6526 (2003).
8. A. Clearfield, G.P.D. Serrette, A.H. Khazi-Syed: *Catal. Today,* **20**, 295 (1994).
9. D. Srinivas, P. Manikandan, S.C. Laha, R. Kumar, P. Ratnasamy: *J. Catal.*, **217**, 160 (2003).

Available online at www.sciencedirect.com
SCIENCE DIRECT®
Materials Chemistry and Physics 93 (2005) 443–449
MATERIALS CHEMISTRY AND PHYSICS
www.elsevier.com/locate/matchemphys

Preparation and characterization of bifunctional oxidative and acidic catalysts Nb_2O_5/TS-1 for synthesis of diols

Didik Prasetyoko [a,*], Zainab Ramli [a], Salasiah Endud [a], Hadi Nur [b]

[a] *Department of Chemistry, Faculty of Science, Universiti Teknologi Malaysia, 81310 UTM Skudai, Johor, Malaysia*
[b] *Ibnu Sina Institute for Fundamental Science Studies, Universiti Teknologi Malaysia, 81310 UTM Skudai, Johor, Malaysia*

Received 31 March 2004; received in revised form 24 March 2005; accepted 26 March 2005

Abstract

Bifunctional oxidative and acidic catalyst was prepared by incorporation of titanium ion (Ti^{4+}) and niobic acid in zeolite molecular-sieve. The catalysts being active both in oxidation reactions due to the presence of tetrahedral Ti^{4+}, and acid-catalyzed reactions due to the presence of niobic acid. Nb/TS-1 was prepared by hydrothermal synthesis of TS-1, calcination in air and subsequent impregnation of niobium into TS-1. The sample was characterized by XRD, FTIR, UV–vis DR, TPR and pyridine adsorption techniques. The XRD analysis of Nb/TS-1 revealed that the MFI structure of the TS-1 support was found to be intact upon incorporation of niobium. The infrared spectra showed that the tetrahedral titanium in the TS-1 is still remained after impregnation with niobium while based on the UV–vis DR result, the niobium species are in the octahedral structure. On the basis TPR and infrared of hydroxyl groups results, it is concluded that niobium species interacted with the silanols on the surface of TS-1. Pyridine adsorption study shows both Brønsted and Lewis acid sites are present in Nb/TS-1. The catalytic results in the transformation of 1-octene to 1,2-octanediol through the formation of 1,2-epoxyoctane by using Nb/TS-1 indicate that the production of epoxide and diol was correlated with the presence of oxidative and Brønsted acidic sites in the catalyst.

Keywords: Bifunctional catalyst; Oxidative site; Acidic site; Microporous materials

1. Introduction

Development of efficient catalysts is a challenge in catalysis research. One of the interesting fields is the creation of two active sites in a single material catalyst, so-called bifunctional catalysts. The catalysts are potentially active for consecutive processes. Bifunctional oxidative and acid catalysts have been prepared by incorporation of trivalent metal ions (Al^{3+}, B^{3+}, Fe^{3+}, Ga^{3+}) and titanium ion (Ti^{4+}) together in the framework of zeolites [1]. The catalysts being active both in the oxidation and acid-catalyzed reactions [2]. In a previous study, van Bekkum and co-workers [3] have demonstrated that bifunctional Ti–Al-beta zeolites can lead to acid-catalyzed consecutive reactions. The catalysts were active in epoxidation of alkenes to produce epoxide and diol. However, it is difficult to control the number of oxidative site together with acidic sites due to some competition between titanium and aluminium to become isomorphously substitute in the framework of zeolites. In order to overcome such problem, a new catalyst system has been designed.

This work focuses on the enhancement of the catalytic performance of bifunctional oxidative and acidic catalysts by incorporation of titanium and niobium into zeolite molecular-sieve. Titanium silicalite (TS-1) molecular-sieves have attracted much attention during the last decade because of their interesting catalytic properties in oxidation reactions [2–6]. Niobium has been loaded on the surface of TS-1 to introduce acidity. The surface acid strength of hydrated niobium oxide, namely niobic acid ($Nb_2O_5 \cdot nH_2O$) corresponds to the acid strength ($H_0 \leq -5.6$) of 70% sulfuric acid and exhibits high catalytic activity, selectivity and stability for acid-catalyzed reactions [7,8].

In this paper, we reported the preparation and characterization of bifunctional oxidative and acidic catalyst, Nb/TS-1. Silicalite and TS-1 were prepared by direct hydrothermal syn-

* Corresponding author. Tel.: +60 75534530; fax: +60 75566162.
E-mail address: dramadhani@yahoo.com (D. Prasetyoko).

0254-0584/$ – see front matter © 2005 Elsevier B.V. All rights reserved.
doi:10.1016/j.matchemphys.2005.03.030

thesis method, whereas Ti/silicalite and Nb/TS-1 were prepared by impregnation of titanium in silicalite and niobium in the TS-1, respectively. By impregnation method, the titanium or niobium position was made to be in octahedral structure located as the extra-framework of silicalite or TS-1. The structure and properties of the catalysts were characterized with various techniques, such as X-ray diffraction (XRD), infrared (FTIR) and UV–vis DR spectroscopies, Temperature programmed reduction (TPR) and pyridine adsorption techniques. The catalytic activity of Nb/TS-1 in the epoxidation of 1-octene was significantly improved in comparison with TS-1.

2. Experimental

2.1. Preparation of samples

TS-1 was prepared according to a procedure described in the literature [4] with slight modification [9], using tetraethyl orthosilicates (Merck, 98%), tetraethyl orthotitanate, TEOT (Merck, 95%) in isopropyl alcohol, tetrapropylammonium hydroxide (Merck, 20% TPAOH in water), and distilled water. The gel was charged into a 150 ml autoclave and heated at 175 °C under static condition. The material was recovered after 4 days by centrifugation and washed with excess distilled water. A white powder was obtained after drying in air at 100 °C overnight. Silicalite was synthesized by using the same procedure without the addition of TEOT. The calcination of sample to remove of the template was carried out in air at 550 °C for 5 h with temperature rate 1° min^{-1}. Ti/silicalite (1 wt.%) were prepared by impregnation technique using TEOT as a precursor. About 0.99 g of silicalite was added into the solution of TEOT (0.0502 g) in isopropanol (50 ml) with stirring. The mixture was stirred for 4 h at 80 °C. The solid was recovered by slowly evaporating the alcohol at 80 °C. The solid material was then calcined in air at 550 °C for 5 h. Here, the prepared silicalite and silicalite loaded with titanium oxide are denoted SIL and Ti/SIL, respectively.

Sample Nb/TS-1, TS-1 loaded with niobium oxide, was prepared by impregnation technique using niobium ethoxide $Nb(OC_2H_5)_5$ (Aldrich, 99.95%) precursor. TS-1 was dried in oven at 200 °C for 24 h. After that, the necessary amount of niobium ethoxide was dissolved in *n*-hexane (Aldrich, >99%) to obtain the desired metal loading, and the required quantity of pre-dried of TS-1 was immediately added to the clear solution with stirring. The mixture was stirred at room temperature for 3 h. The solid was recovered by evaporating the *n*-hexane at 80 °C. The acid hydrolysis was performed by addition of 20 ml solution of 0.5 M HNO_3 in distilled water and aged overnight, followed by heating at 120 °C until dryness. The solid was then washed with distilled water for three times and finally dried at 200 °C for 24 h.

For comparison on the presence of Nb species, experiments were carried out to obtain niobium oxide and niobic acid. Niobic acid was prepared by hydrolysis of niobium ethoxide using neutral hydrolysis method, followed by calcination at 200 °C. The hydrolyzed niobium ethoxide is denoted NBA. Niobium oxide was also prepared by calcination of ammonium niobium oxalate at 550 °C for 3 h. The prepared particles were labeled NBO.

Titanium oxide was prepared by hydrolysis of titanium(IV) tetraethoxide (TEOT) at room temperature. The white solid was recovered by filtration, washing with water and drying at 100 °C overnight. Finally, the solid was calcined at 550 °C for 5 h. The thus-prepared particles were labeled TIO. Table 1 summarizes the chemical composition of all the above samples and preparation methods.

Table 1
Chemical compositions of the samples and preparation method

Sample	Code	Nb/(Nb + TS-1) (wt.%)	Methods
Titanium silicalite	TS-1	0.81 (gel)[a]	Direct synthesis
Silicalite	SIL	–	Direct synthesis
Ti/silicalite	Ti/SIL	1.0[b]	Impregnation
$Nb_2O_5{\cdot}nH_2O$/TS-1	Nb/TS-1	3.4	Impregnation and hydrolysis
Nb_2O_5	NBO	100	Calcination
$Nb_2O_5{\cdot}nH_2O$	NBA	100	Hydrolysis
TiO_2	TIO	–	Hydrolysis and calcination

[a] %Ti = Ti/(Ti + Si) in the initial gel.
[b] %Ti = Ti/TS-1, wt.%.

2.2. Characterizations

All molecular-sieves were characterized by powder X-ray diffraction (XRD) for identification of the crystalline phases in the catalysts using a Bruker Avance D8 diffractometer with the Cu Kα (λ = 1.5405 Å) radiation as the diffracted monochromatic beam at 40 kV and 40 mA. Typically, powder samples were ground and spread into a sample holder and then analyzed. The pattern was scanned in the 2θ range of 5–50° at a step 0.020° and step time 1 s. Infrared (IR) spectra of the samples were collected on a Perkin Elmer Fourier Transform Infrared (FTIR) spectrophotometer, with a spectral resolution of 2 cm^{-1}, at temperature 20 °C by KBr pellet method. The framework spectra were recorded in the region of 1400–400 cm^{-1}. UV–visible diffuse reflectance (UV–vis DR) spectra were recorded at ambient condition on a Perkin Elmer Lambda 900 UV/VIS/NIR spectrometer. Temperature programmed reduction (TPR) experiments were performed using TPDRO 1100 Thermo Quest CE Instrument as follows. The sample (typically about 0.05 g) was pre-treated in nitrogen at a flow rate of 30 cm^3 min^{-1} at 200 °C for 1 h and cooled down to 100 °C. The reduction analysis was performed by heating the sample from 100 up to 1000 °C at a rate of 10 °C min^{-1} and held for 5 min at 1000 °C with flowing mixture of 5% hydrogen in nitrogen (H_2/N_2) at the rate of 40 cm^3 min^{-1}. For hydroxyl groups and acidity study, about 10 mg of the sample was pressed at 2–5 tonnes for a minute to obtain a 13 mm disk. The sample was introduced in the

infrared cell with calcium fluorite, CaF_2 windows. The sample was heated at 200 °C in vacuum condition for 16 h. The infrared spectra were collected at room temperature using Shimadzu 2000 FTIR spectrometer at 2 cm^{-1} resolutions. The types of acid sites were examined using pyridine as a probe molecule. Pyridine was adsorbed at room temperature for a minute, continued by desorption at 150 °C for an hour. The infrared spectra were monitored at room temperature.

2.3. Catalytic test

The catalyst performance was tested in the epoxidation of the 1-octene using hydrogen peroxide as oxidant. The reaction mixture, i.e. 8 mmol of 1-octene (Sigma, 99%), 15 mmol of H_2O_2 in H_2O (Scharlau, 35% extra pure) in 10 g acetone (J.T. Baker) as solvent and 0.8 mmol of cyclooctane (Fluka, >99%) as an internal standard were placed in a 25 cm^3 round bottom flask equipped with a magnetic stirrer and condenser. An amount 0.05 g catalyst was then added in the solution. The reaction was carried out in oil bath with stirring at 70 °C. The aliquots were sampled at regular time intervals. The products of the reaction were analyzed with an HP 6890N GC using Ultra-1 column and HP GC-MSD using HP5 column.

3. Results and discussion

3.1. Solid characterizations

Fig. 1 shows the XRD patterns of the samples tabulated in Table 1. The XRD pattern of TIO sample indicated that the structure of TiO_2 was rutile. There is no diffraction line was observed on the XRD pattern from sample NBA prepared by hydrolysis of niobium pentoxide, suggesting that niobic acid is fully amorphous. On the other hand, sample NBO, niobium oxide prepared by calcination of ammonium niobium oxalate at 550 °C shows splitting of the diffraction line around $2\theta = 29°$, indicating that the sample is crystalline niobium oxide phase (T-Nb_2O_5) with orthorhombic structure [10].

The XRD patterns of TS-1, SIL, Ti/SIL and Nb/TS-1 samples revealed that the sample contained framework structures of the MFI type zeolite [11]. For sample Nb/TS-1, the structure of TS-1 is not strongly affected by the presence of impregnated niobium. The XRD patterns show that no diffraction line assigned for crystalline phase of the niobium oxide present. This indicated that niobium was well dispersed on the TS-1. This also suggested that the niobium is present in the form of amorphous niobium oxide hydrate, since it was prepared by hydrolysis of niobium ethoxide and not calcined at temperature higher than 400 °C. In addition, the peak intensity of TS-1 is drastically decreased up to 60% after impregnation of 3.4 wt.% of niobium on the TS-1. It is suggested that niobium is either located on the surface of TS-1 or covering the surface of TS-1. Since the estimated molecular size of $Nb(OEt)_5$ (ca. 1.1 nm), the source of Nb sites, is larger than the size pore-entrance of TS-1 (ca. 0.6 nm), they should be attached to the external surface of TS-1.

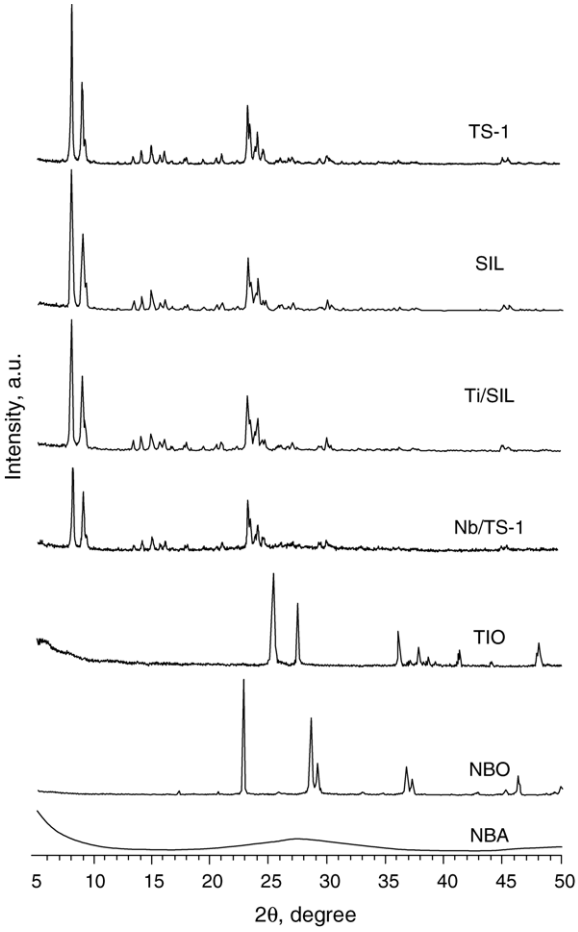

Fig. 1. XRD pattern of the samples.

The infrared spectra of the samples in the lattice vibration region between 1400 and 400 cm^{-1} are depicted in Fig. 2. Sample NBA shows a major strong band centered at 586 cm^{-1} and a shoulder band at 933 cm^{-1}. This spectrum is consistent with the skeletal vibration previously reported for amorphous niobic acid [12]. The spectrum of crystalline phase of niobium oxide (sample NBO) exhibits two strong bands at 615 and 850 cm^{-1}. The broad band at higher frequency ca. >850 cm^{-1} is associated with the stretching mode of terminal Nb=O bonds (niobyl species), while the band around 600 cm^{-1} can be assigned to the stretching of longer bridging Nb–O–Nb bonds. Samples TS-1, SIL, Ti/SIL and Nb/TS-1 showed similar bands. According to Flanigen [13], the absorption bands at around 1100, 800 and 450 cm^{-1} were three lattice modes associated with internal linkages in tetrahedral SiO_4 (or AlO_4) and are insensitive to structure changes. The absorption bands at about 1225 and 547 cm^{-1} are characteristic of MFI-type zeolite associated with the particular structural assembly of the tetrahedral and are sensitive to structure changes.

It is already known that the infrared spectrum of titanium silicalite, TS-1 is characterized by an absorption band at

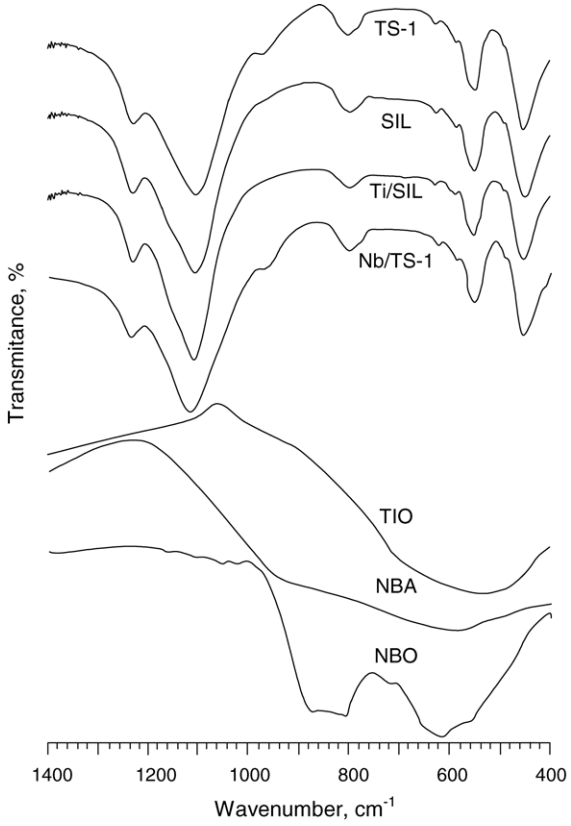

Fig. 2. FTIR spectra of the samples.

around 960 cm^{-1} [6,14–16]. However, the vibrational modes at around this frequency may be the result of several contributions i.e. the asymmetric stretching modes of Si–O–Ti linkages [14–16], terminal Si–O stretching of SiOH–(HO)Ti "defective sites" and titanyl [Ti=O] vibrations. Our TS-1 sample shows a weak band at 977 cm^{-1}. This band can be attributed to the titanium in the framework, since silicalite (SIL sample; contains only silica without addition of any titanium) does not show any band at around this frequency. Furthermore, sample Ti/SIL (titanium oxide loaded silicalite, 1 wt.% of Ti) also does not show the band around 960 cm^{-1}. It is concluded that the TS-1 sample contains Si–O–Ti connections. No additional bands appeared after impregnation of titanium in the SIL sample.

A small band at around 970 cm^{-1} assigned to the titanium ions in the tetrahedral structure is still present after impregnation of niobium (sample Nb/TS-1). No additional band after impregnation of niobium into the TS-1 can be observed. This finding shows that impregnation of niobium has not effected the MFI structure of TS-1 significantly. Infrared spectroscopy technique also cannot detect the presence of niobic acid in the sample Nb/TS-1, due to low vibration intensity of pure niobic acid itself as compared to TS-1.

The nature and coordination of metal oxide or metal in substituted molecular-sieves can be characterized by UV–vis DR spectroscopy technique. Fig. 3 shows the UV–vis spectra of the samples. The UV–vis spectrum of NBA sample exhibits a maximum band around 295 nm and a shoulder band around 243 nm. This main band (295 nm) attributed to the charge transfer transitions O^{2-} to Nb^{5+}, which can be associated to the energy gap between the O 2p-valence band and the Nb 4d-conductance band [12]. For TIO sample, the main band at around 340 nm and a strong band at 240 nm are observed, both assigned to the octahedral Ti (Oh). Silicalite (MFI sample) shows two bands at around 213 and 240 nm with very low intensity (0.05) (spectrum was magnified four times). These bands are not assigned to the coordination of titanium or niobium with oxygen due to their low intensity and the sample contains silicon only without any addition of titanium or niobium. For the TS-1 sample, only a single strong band at 215 nm was observed. This band is attributed to ligand-to-metal charge transfer associated with isolated Ti^{4+} framework sites (between O^{2-} and the central Ti(IV) atoms) in tetrahedral coordination, Td. The band characteristic of octahedral extra-framework titanium was not observed, while Ti/SIL sample shows a broad band at 240 nm attributed to extra-framework titanium oxide suggesting that impregnation of titanium only produce some extra-framework titanium species. Impregnation of niobium on the TS-1 (sample Nb/TS-1) shows a strong band at about 240 nm assigned to octahedral niobium species. Meanwhile, the band characteristic for tetrahedral titanium at about 215 nm cannot be observed due to the overlapping of this band with the band of niobium oxide that has remarkably higher intensity.

Fig. 4 shows the TPR profiles of the samples. Sample NBA prepared by hydrolysis of niobium ethoxide then calcined at 200 °C exhibited three regions of hydrogen consumption, i.e. a negative peak at around 550 °C and positive peaks at around 875 °C and at a higher temperature above 1000 °C. The negative peak can be attributed to CO or CO_2 formation due to carbon residue from the niobium ethoxide that is not

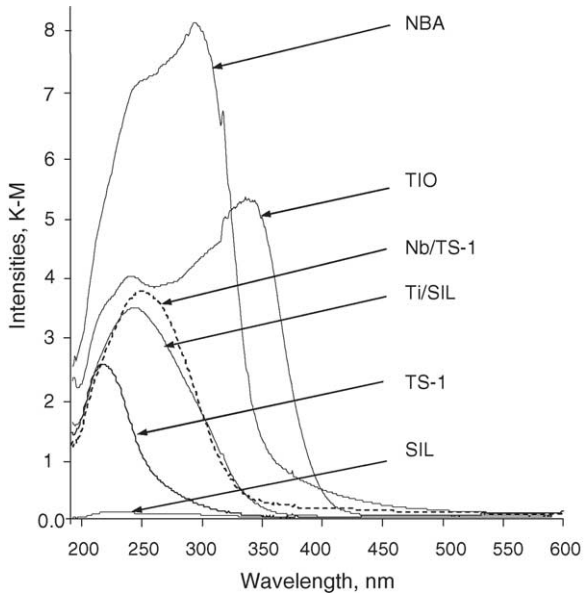

Fig. 3. UV-diffuse reflectance spectra of the samples.

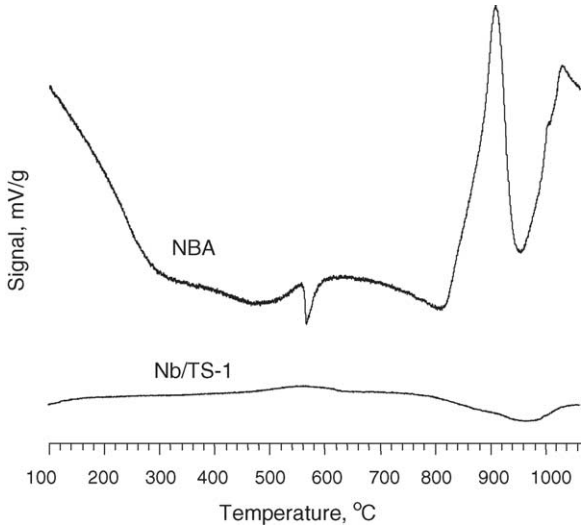

Fig. 4. TPR profiles of the samples.

fully hydrolyzed. The first positive peak was attributed to the reduction of Nb^{5+} to Nb^{4+} in the form of Nb_2O_5 to NbO_2 [8,17], while for reduction of NbO_2 to lower oxidation state of niobium, NbO needed higher reduction temperature.

Sample Nb/TS-1 does not show any significant peak in this reduction temperature range, although the sample contains niobium. This finding is explained to be due to several factors. Low amount of niobium loading results in high dispersion of niobium on the surface of TS-1 that cause high interaction between niobium and TS-1. Pereira et al. [17] found that high dispersions promote intimate contact between the niobium and the silica surface, Nb–O–Si bonding in relation to Nb–O–Nb bonding prevailing. It also can be explained based on the electronegativity concept that the presence of silicon in the coordination sphere of niobium should increase the electronic density niobium. Thus the reduction of niobium from Nb^{5+} to Nb^{4+} was more difficult to occur. Recently, Mendes et al. [18] found that 20 wt.% of niobium supported on Al_2O_3 did not show any hydrogen uptake as indication of the interaction of niobium with Al_2O_3.

The hydroxyl groups and acidity of the samples were monitored by infrared technique. The wafer sample was put in the glass cell and evacuated at 200 °C for 16 h under vacuum. The infrared spectra were recorded at room temperature. Fig. 5 shows the infrared spectra of the samples TS-1, NBA, NBO and Nb/TS-1 after evacuation at 200 °C. TS-1 shows a sharp peak at around 3743 cm^{-1} characteristic of hydroxyl silanol groups. Niobic acid (sample NBA) shows a small peak at around 3700 cm^{-1} and a broad peak centered at around 3400 cm^{-1} that can be assigned to hydroxyl stretching mode of free Nb–O–H groups and hydroxyl with hydrogen bonding, respectively [12]. On the other hand, crystalline niobium oxide does not show any peak in the region of hydroxyl groups indicating that crystalline niobium oxide does not contain any hydroxyl groups. A different finding was reported recently by Braga et al. [19] for niobium oxide calcined at 800 °C.

The peak at 3743 cm^{-1} disappeared as niobium was loaded on the TS-1. A small peak at 3733 cm^{-1} and broad peak centered at around 3530 cm^{-1} were observed in Nb/TS-1 sample. Meanwhile, a mechanical mixture of 20% NBA in TS-1 only shows a peak similar to that of TS-1 at around 3744 cm^{-1} assigned for silanol hydroxyl groups. Although this mixture contains 20 wt.% of NBA, however, no peak at around 3700 cm^{-1} assigned for Nb–O–H can be observed. It suggests that the amount of hydroxyl groups of Nb–OH in the sample NBA is much lower than the amount of silanol groups of TS-1. For samples Nb/TS-1, a drastic decrease of silanol species present on the surface of TS-1 indicates that there is strong interaction between niobium and TS-1 (niobium bonded with –O–Si, replaced hydrogen atom of silanol species in the TS-1). Since niobic acid does not show any peak in this region, the result clearly suggests that niobium species covered of the surface of TS-1. Therefore, deposition of niobium oxide species on TS-1 consumes surface Si–OH groups of TS-1, as consequently the silanol groups decreased.

The types of acid sites in the samples were monitored by pyridine adsorption. Pyridine was adsorbed at room temperature after evacuation of the sample at 200 °C for 16 h in vacuum. The infrared spectra were collected after evacuation at 150 °C for an hour. Fig. 6 shows the infrared spectra of the samples in the pyridine region. Sample NBO does not shows any peak which indicates that crystalline niobium oxide has no acidity. Sample NBA shows the peaks at 1636, 1609, 1575, 1540, 1489 and 1448 cm^{-1}. The peaks at around 1540 and 1448 cm^{-1} are due to Brønsted and Lewis acid sites,

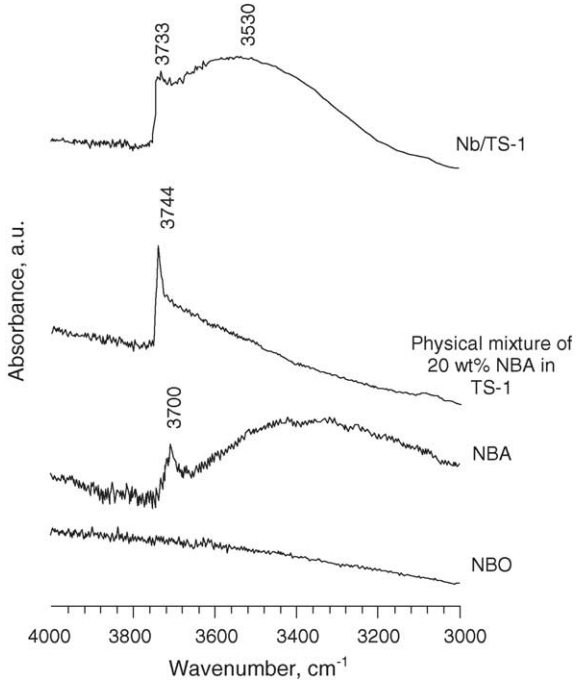

Fig. 5. FTIR spectra of the samples in the hydroxyls region, after evacuation under vacuum at 200 °C for 16 h.

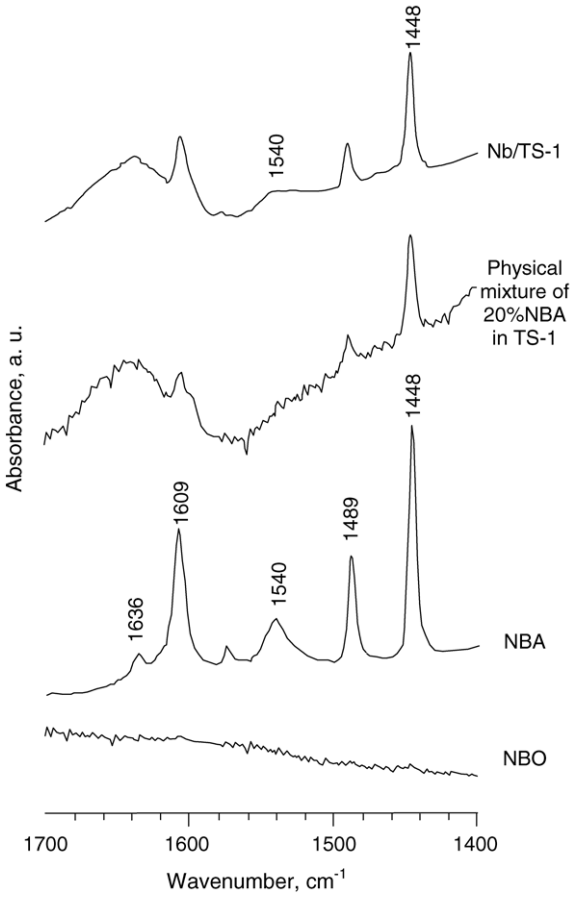

Fig. 6. FTIR spectra of the samples after evacuation under vacuum at 200 °C for 16 h followed by pyridine adsorption at room temperature and evacuation at 150 °C for an hour, in the pyridine regions.

respectively. Similar finding has been reported by Morais et al. [20] for niobic acid. Niobium oxide containing TS-1 (sample Nb/TS-1) show the peaks similar to that of sample NBA. However, the intensity of the characteristic peaks for Brønsted and Lewis acid sites at around 1540 and 1448 cm^{-1} is lower than that of sample NBA. Jehng and Wachs [21] have reported the evidence of both Brønsted and Lewis acid sites in niobium oxide supported on silica, while Mendes et al. [18] only found Lewis acid sites in the silica supported niobic acid. On the contrary, in this study, a mechanical mixture of niobic acid and TS-1 only shows the peaks at around 1608, 1489 and 1447 cm^{-1}, which are similar to those of sample TS-1.

3.2. Catalytic activity

The bifunctional catalyst Nb/TS-1 was tested in the epoxidation of 1-octene with aqueous H_2O_2 in acetone at 70 °C. Samples NBO and NBA showed no noticeable activity toward the formation of 1,2-epoxyoctane, consequently, there is no 1,2-octanediol observed from these reactions. TS-1 shows their activity toward the formation of 1,2-octanediol. However, Nb/TS-1 showed remarkable higher activity (four times higher in yield and selectivity for 1,2-octanediol) compared to TS-1. It suggested that TS-1 and Nb/TS-1 catalysts in this study contain Brønsted acid sites, since it is well known that the formation of 1,2-octanediol is catalyzed by Brønsted acid sites. However, from the pyridine adsorption studies, only Brønsted acid sites were observed on Nb/TS-1. It is suggested that the Brønsted acid sites might not have originated from the TS-1 catalyst itself, but rather formed during the reaction in the presence of water from the reaction mixtures. Meanwhile, the higher yield observed on Nb/TS-1 is due to the higher amount of Brønsted acid sites, which is responsible in this reaction. In addition, the induction time of the formation of 1,2-octanediol in TS-1 and Nb/TS-1 is observed after reaction for 24 and 3 h, respectively, indicating the higher reactivity of Nb/TS-1 catalyst. The titanium and niobium concentrations of the used Nb/TS-1 catalyst was determined by infrared and UV–vis DR spectroscopies. It is found that no leaching of titanium and niobium has been observed as analyzed by infrared and UV–vis DR spectroscopies, respectively.

4. Conclusion

Bifunctional oxidative and acidic catalysts was successfully synthesized by impregnation of niobic acid on the surface of TS-1(Nb/TS-1). It is demonstrated that the tetrahedral titanium species and niobic acid act as oxidative and acidic active sites, respectively. The catalytic results in the transformation of 1-octene to 1,2-octanediol through the formation of 1,2-epoxyoctane by using Nb/TS-1 indicate that the production of epoxide and diol was correlated with the presence of oxidative and Brønsted acidic sites in the catalyst.

Acknowledgements

We gratefully acknowledge funding from The Ministry of Science Technology and Innovation Malaysia, under IRPA grant no. 09-02-06-0057 SR0005/09-03.

References

[1] D. Trong On, S.V. Nguyen, V. Hulea, E. Dumitriu, S. Kaliaguine, Micropor. Mesopor. Mater. 57 (2003) 169.
[2] J.C. van der Waal, H. van, Bekkum, J. Mol. Catal. A: Chem. 124 (1997) 137.
[3] J.C. van der Waal, M.S. Rigutto, H. van Bekkum, Appl. Catal. A: Gen. 167 (1998) 331.
[4] M. Taramasso, G. Perego, B. Notari, US Patent 4,410,501 (1983).
[5] M.G. Clerici, P. Ingallina, US Patent 5,221,795 (1993).
[6] E. Duprey, P. Beaunier, M.A. Springuel-Huet, F.B. Verduraz, J. Fraissard, J.M. Manoli, J.M. Brĭegeault, J. Catal. 165 (1997) 22.
[7] S. Okazaki, Iizuka, T. Kado, US Patent 4,652,544 (1987).
[8] I. Nowak, M. Ziolek, Chem. Rev. 99 (1999) 3603.
[9] A.J.H.P. van der Pol, J.H.C. van Hooff, Appl. Catal. A: Gen. 92 (1992) 113.

[10] E.I. Ko, J.G. Weissman, Catal. Today 8 (1990) 27.
[11] M.M.J. Treacy, J.B. Higgins, R. von Ballmoos, Collection of Simulated XRD Powder Patterns for Zeolites, Elsevier, Amsterdam, 1996.
[12] T. Armaroli, G. Busca, C. Carlini, M. Giuttari, A.M.R. Galletti, G. Sbrana, J. Mol. Catal. A: Chem. 151 (2000) 233.
[13] E.M. Flanigen, in: J.A. Rabo (Ed.), Zeolite Chemistry and Catalysis, American Chemical Society, Washington, 1976, p. 80.
[14] D.R.C. Huybrechts, P.L. Buskens, P.A. Jacobs, J. Mol. Catal. 71 (1992) 129.
[15] E. Astorino, J.B. Peri, R.J. Willey, G. Busca, J. Catal. 157 (1995) 482.
[16] K.S. Smirnov, B. van de Graaf, Micropor. Mater. 7 (1996) 133.
[17] E.B. Pereira, M.M. Pereira, Y.L. Lam, C.A.C. Perez, M. Schmal, Appl. Catal. A: Gen. 197 (2000) 99.
[18] F.M.T. Mendes, C.A. Perez, R.R. Soares, F.B. Noronha, M. Schmal, Catal. Today 78 (2003) 449.
[19] V.S. Braga, J.A. Dias, S.C.L. Dias, J.L. de Macedo, Chem. Mater. 17 (2005) 690.
[20] M. Morais, E.F. Torres, L.M.P.M. Carmo, N.M.R. Pastura, W.A. Gonzalez, A.C.B. dos Santos, E.R. Lachter, Catal. Today 28 (1996) 17.
[21] J.M. Jehng, I.E. Wachs, Catal. Today 8 (1990) 37.

Malaysian Journal of Chemistry, 2005, Vol. 7, No. 1, 011 - 018

Structural and Superacidity Study of Bifunctional Catalyst, Sulfated-Titanium/TS-1

Didik Prasetyoko, Zainab Ramli (*), Salasiah Endud and Hadi Nur
Department of Chemistry, Faculty of Sciences,
Universiti Teknologi Malaysia, Skudai,
Johor Bahru, Malaysia.

Abstract : Bifunctional oxidative and acidic catalysts are prepared in this study. The sulfated titanium silicalite is prepared by first, synthesizing the titanium silicalite (TS-1) having oxidative properties, followed by the deposition of titanium on the surface of TS-1, and finally, treatment of the solid with sulfuric acid. The structure of the solid samples are characterized by XRD, FTIR, and UV-Vis DR spectroscopy techniques, while the strength and the type of acid site are monitored by Hammet indicator and pyridine adsorption method, respectively. The results show that the MFI structure of TS-1 is maintained even after the treatment with sulfuric acid. However, a part of the tetrahedral titanium framework of the TS-1 has been expelled from the framework and becomes non-framework octahedral titanium after contacting with sulfuric acid. The acidity study by Hammet indicator indicates that sample possesses superacidic property, measured by Hammet indicator 2,4-dinitrobenzene (pKa = -14.52), in which the acid type is Lewis, from the pyridine adsorption.

Abstrak : Mangkin dwifungsi pengoksidaan dan asid telah disediakan. Titanium silicalite bersulfat disediakan dengan mensintesis titanium silicalite (TS-1) dahulu yang mempunyai tapak pengoksidan, diikuti oleh penambahan titanium di atas permukaan TS-1, dan akhir sekali, pepejal dirawat dengan asid sulfuric. Struktur pepejal dicirikan dengan menggunakan kaedah XRD, FTIR, dan UV-Vis DR spektroskopi, sementara kekuatan dan jenis tapak asid dicirikan dengan kaedah penunjuk Hammet dan penjerapan piridina. Hasil pencirian menunjukkan bahawa struktur MFI daripada TS-1 masih utuh selepas sampel dirawat dengan asid sulfuric. Bagaimanapun, sebahagian titanium bingkaian dalam struktur tetrahedron daripada TS-1 telah terkeluar dan berubah menjadi oktahedron titanium luar bingkaian setelah tindak balas dengan asid sulfuric. Kajian keasidan dengan penunjuk Hammet menunjukkan bahawa sampel mempunyai sifat superasid, mengikut penunjuk Hammet 2,4-dinitrobenzena (pKa = -14.52). Penjerapan piridina menunjukkan bahawa sampel mempunyai tapak asid daripada jenis asid Lewis.

Key words*: superacidity, bifunctional catalyst, sulfated TS-1, Hammet indicator.*

Received : 17.03.04 ; accepted : 21.02.05

Introduction

One of the interesting fields in the area of catalysis is the creation of two active sites in a catalyst, the so-called bifunctional catalyst. One of the challenges is to design a highly functionalized catalyst by combination of oxidative and acidic sites for subsequent oxidation and acidic catalytic reactions. Bifunctional oxidative and acid catalysts have been prepared by incorporation of trivalent metal ions (Al^{3+}, B^{3+}, Fe^{3+}, Ga^{3+}) and titanium ion (Ti^{4+}) together in the framework of zeolites [1]. The catalysts are active both in the oxidation reactions and in acid catalyzed reactions [1,2

Titanium silicalite (TS-1) molecular-sieves have been paid much attention during the last decade because of its interesting catalytic properties in many oxidation reactions. This catalyst has very promising properties in the oxidation to produce fine chemicals. TS-1 is microporous crystalline molecular sieve having titanium (Ti) and silicon (Si) in the framework, which was first reported in 1983 [3]. It has MFI structure, obtained by substituting titanium for partial silicon in the framework (tetrahedrally coordinated titanium atoms in a silicalite structure). TS-1 having similar structure to ZSM-5 is only containing Si and Ti in the tetrahedral structure, without any Al in the framework. As a result, the framework has no charge and consequently no Brønsted acidity can be observed from TS-1 sample [4].

It has been known that sulfate addition is widely used to enhance the surface acidity of the solid catalysts, known as solid superacid catalysts. The acidity of the solid superacid is stronger than that of 100% sulfuric acid, that is $H_0 \leq -12$. Some sulfated metal oxides and mixed metal oxides, such as SO_4^{2-}/ZrO_2, SO_4^{2-}/SnO_2, SO_4^{2-}/TiO_2, SO_4^{2-}/Fe_2O_3, SO_4^{2-}/SiO_2-TiO_2, and SO_4^{2-}/SiO_2-ZrO_2 possessed superacidity properties [5-14]. Sulfated metal oxides have also been impregnated onto silica, alumina, and porous materials [15-24]. The strong acid properties are related to the sulfate ions. The types of acid sites and some structural model have been presented and reported as either Lewis or Bronsted acids. These solid superacid has been applied as acid catalysts in the reactions such as

isomerization, cracking, alkylation, acylation, and esterification [9-14, 19-24].

Here, we studied the structure and acidity of bifunctional oxidative and acidic catalysts, prepared by treatment of the TS-1 microporous materials with sulfate ion. The tetrahedral titanium in the TS-1 acts as an oxidative site, while the acid site is created by the addition of sulfate ion. The structure and properties of catalysts are characterized using XRD, FTIR and UV-Vis DR spectroscopies. The acid strength of the solids is measured by Hammet indicators technique, while the type of acid is determined by pyridine adsorption which is monitored by FTIR technique.

Experimental

Preparation of sample

TS-1 (2% of Titanium, %mol) was prepared according to a procedure described earlier [3, 25], using reagents i.e. tetraethyl orthosilicates (Merck, 98%), tetraethylorthotitanate (Merck, 95%) in isopropyl alcohol, tetrapropylammonium hydroxide (Merck, 20% TPAOH in water), and distilled water. The hydrothermal crystallization was carried out at 175^{o}C under static condition in the stainless steel autoclave for 4 days.

Sulfated TS-1 was prepared by impregnation method as follows: About 1 g of TS-1 was added into 25 ml of H_2SO_4 0.5 M under vigorous stirring at 80^{o}C for 3 hrs. After evaporation of water, the solid was dried at 100^{o}C for 24 hrs. The solid sample was then calcined at 550^{o}C for 3 hrs. The sample was denoted as SO_4/TS-1.

Sulfated titanium TS-1 was prepared by impregnation of titanium on TS-1 using tetraethylorthotitanate, TEOT as precursor, followed by hydrolysis using water, and finally titanium TS-1 was treated with sulfate ion. For 1wt.% of Ti loaded TS-1, pre-dried of as-synthesized TS-1 sample (0.83 g) was added into the solution of TEOT (0.073 g, Merck, 95%) in isopropanol (10 ml, Merck, 98%). The mixture was stirred at room temperature for 3 hrs, followed by evaporation of the solvent at 80^{o}C. The hydrolysis of TEOT in the surface of TS-1 was performed in the neutral condition by adding 10 ml of water, with stirring at room temperature for 24 hrs. The solid was dried at 100^{o}C for 24 hrs (Ti/TS-1). The Ti/TS-1 was added slowly into the sulfuric acid solution (10 ml, 0.5 M, Merck, 99%), and stirred at room temperature for 1 hr. The solid was separated from the liquid by centrifugation, followed by washing with water until neutral pH. Finally, the solid was dried at 100^{o}C for 24 hrs and calcined at 550^{o}C for 5 hrs. The resulting sample was denoted as SO_4^{2-}-Ti/TS-1. Table 1 summarizes the chemical composition of the samples and the preparation method.

Characterization

The solid structure was determined by using XRD, infrared and UV-Vis DR spectroscopy techniques. All molecular-sieves were characterized by powder X-ray diffraction (XRD) for the crystallinity and phase content of the solid materials using a Bruker Advance D8 Difractometer with the Cu Kα (λ=1.5405 Å) radiation as the diffracted monochromatic beam at 40 kV and 40 mA. The sample was scanned in the 2θ range between 5^o to 50^o at a step 0.020^o and step time 1s (scanning speed of 1.2^o/min). Infrared (IR) spectra of the samples were collected on a Perkin Elmer Fourier Transform Infrared (FTIR), with a spectral resolution of 2 cm^{-1}, scans 10 s, at temperature 20^{o}C by KBr pellet method. The framework spectra were recorded in the region of 1400 – 400 cm^{-1}.Diffuse reflectance UV-visible (UV-vis DR) spectra were recorded under ambient conditions on a Perkin Elmer Lambda 900 UV/VIS/NIR spectrometer. The acid strength of the solids were measured by Hammet indicators. The sample (0.05 g) was heated under nitrogen flow (40 cc/min) at 400^{o}C for 15 minutes and cooled down to 200^{o}C. The sample was taken out and added into the solution of benzene (Merck, 99%) containing Hammet indicators immediately and the color of indicator with different pKa were observed. The types of acid sites were characterized by absorbed base probe molecule. The wafer of the sample (10-

Table 1 : Initial titanium compositions and properties of the samples

Sample	Titanium (*)		Intensity,	Titanium (#)	
	Td, %wt	Oh, %wt	Cps (XRD)	Td, %	λ, nm
H-ZSM-5	-	-	-	-	-
TS-1	2	-	2400	100	208
SO_4/TS-1	2		2380	51	228
SO_4-Ti/TS-1	2	1.7	2254	67	215

(*) Composition of titanium in the initial mixture

(#) Based on UV-Vis DR data

12 mg) was locked in the cell equipped with CaF_2 windows, and evacuated at 400°C under vacuum condition for 4 hrs. Pyridine as probe molecule was introduced into the evacuated sample at room temperature. Infrared spectra of the sample were monitored at room temperature after desorption of pyridine at 150°C for 1 hr.

Results and discussion

Structure characterization

XRD was used to characterize the structure and the crystallinity of the samples. Figure 1 shows the XRD patterns of the samples, while Table 1 shows the highest peak of each sample, at 2θ = 7.9°. Generally, all samples show similar XRD pattern characteristic of MFI structure type of zeolite. Introduction of SO_4^{2-} anions into the TS-1 and titanium impregnated TS-1 (SO_4^{2-}/TS-1 and SO_4^{2}-Ti/TS-1 samples) has insignificant effect to crystallinity of the sample, with less than 1% changes. In addition, no significant peaks shifting can be observed in all TS-1 treated samples. This finding suggests that the MFI structure of TS-1 is maintained after the introduction of SO_4^{2-} and SO_4^{2-}-Ti. Figure 2 shows FTIR spectra of the samples. TS-1 sample show five peaks at *ca.* 1230, 1100, 800, 550 and 450 cm^{-1}, characteristic for MFI type of zeolites [26]. A peak at *ca.* 970 cm^{-1} is observed which is characteristic for titanium with tetrahedral structure [27, 28]. The analogues sample of TS-1, the silicalite MFI containing only silica in the framework does not show any band at around this frequency. In addition, the impregnated Ti on silicalite (1wt.% of Ti) also does not show the band around 970 cm^{-1}, i.e. no additional band appears after the impregnation of titanium. Impregnation of SO_4^{2-} and SO_4^{2-}-Ti into the TS-1 shows that all the characteristic peaks vibration for TS-1 is maintained with good intensities. However, the peak intensity for the tetrahedral titanium at *ca.* 970 cm^{-1} decreased after impregnation with SO_4^{2} or SO_4^{2-}-Ti on TS-1, indicating that the amount of

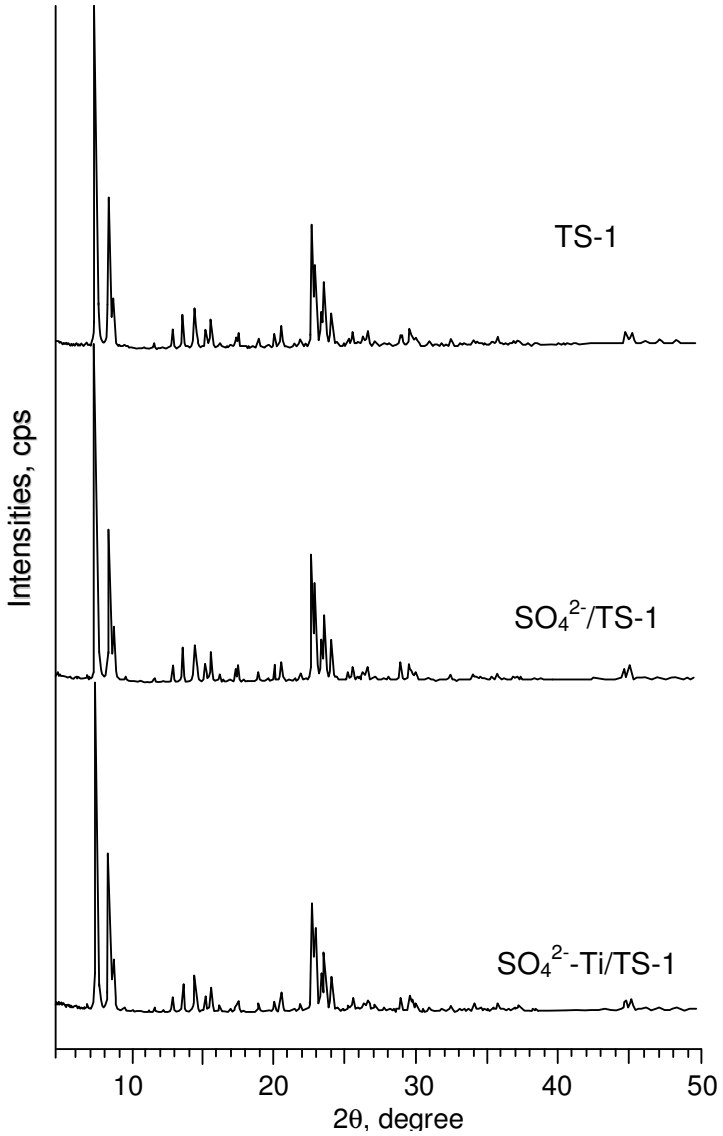

Figure 1 :. XRD pattern of the samples

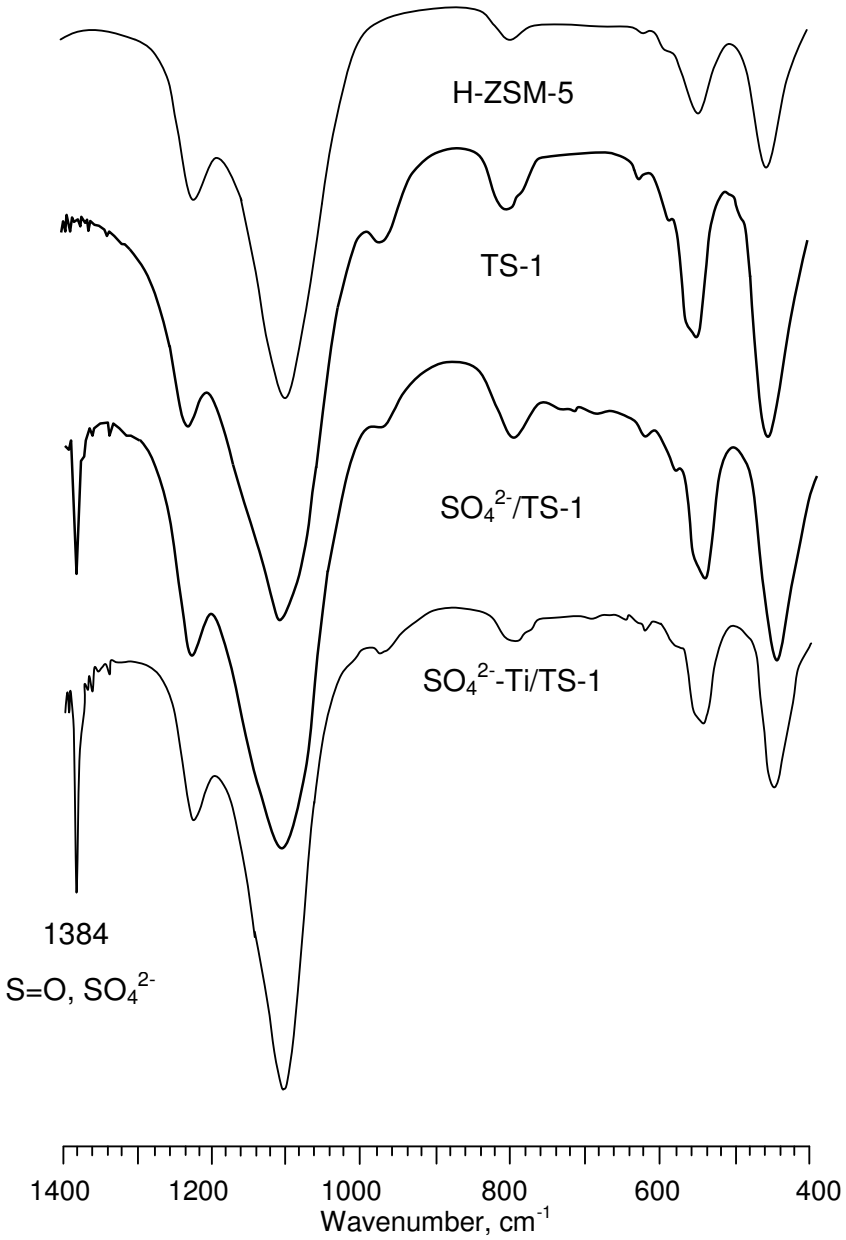

Figure 2 : FTIR spectra of the samples

tetrahedral titanium has decreased. In addition, a new peak at *ca.* 1384 cm^{-1} is observed, which corresponds to the asymmetric stretching vibration of the covalent S=O for SO_4^{2-} ion. This peak is considered as characteristic band of SO_4^{2-} on promoted superacid [6, 14]. This finding indicates that the MFI structure of TS-1 sample is not collapsed after the treatment with sulfuric acid in order to introduce the SO_4^{2-} anions. This observation can be seen in samples SO_4^{2-}/TS-1 and SO_4^{2-}-Ti/TS-1.

UV-Vis DR spectroscopy was used to monitor the titanium structure in the samples. The ultraviolet peak position of the Ti ion depends essentially on its coordination and on the size of extra-framework TiO_2 particles whenever present in the sample. The band in the range of 190-220 nm is attributed to a charge transfer of the tetrahedral titanium (Td) sites between O^{2-} and the central Ti(IV) atoms, while octahedral Ti (Oh) is observed at *ca.* 260-330 nm [27, 29]. Figure 3 shows that, for TS-1 sample, only single high intense band at around 208 nm is observed. This band is attributable for titanium in the tetrahedral structure. This finding further support that TS-1 contains Ti in the tetrahedral structure. As for SO_4^{2-}/TS-1 and SO_4^{2-}-Ti/TS-1 samples, a medium intense band at *ca.* 215 - 228 nm and a shoulder band at *ca.* 270 - 312 nm are observed, which are characteristic for titanium with tetrahedral and octahedral structures, respectively. The intensity of tetrahedral titanium for both samples has decreased as compared

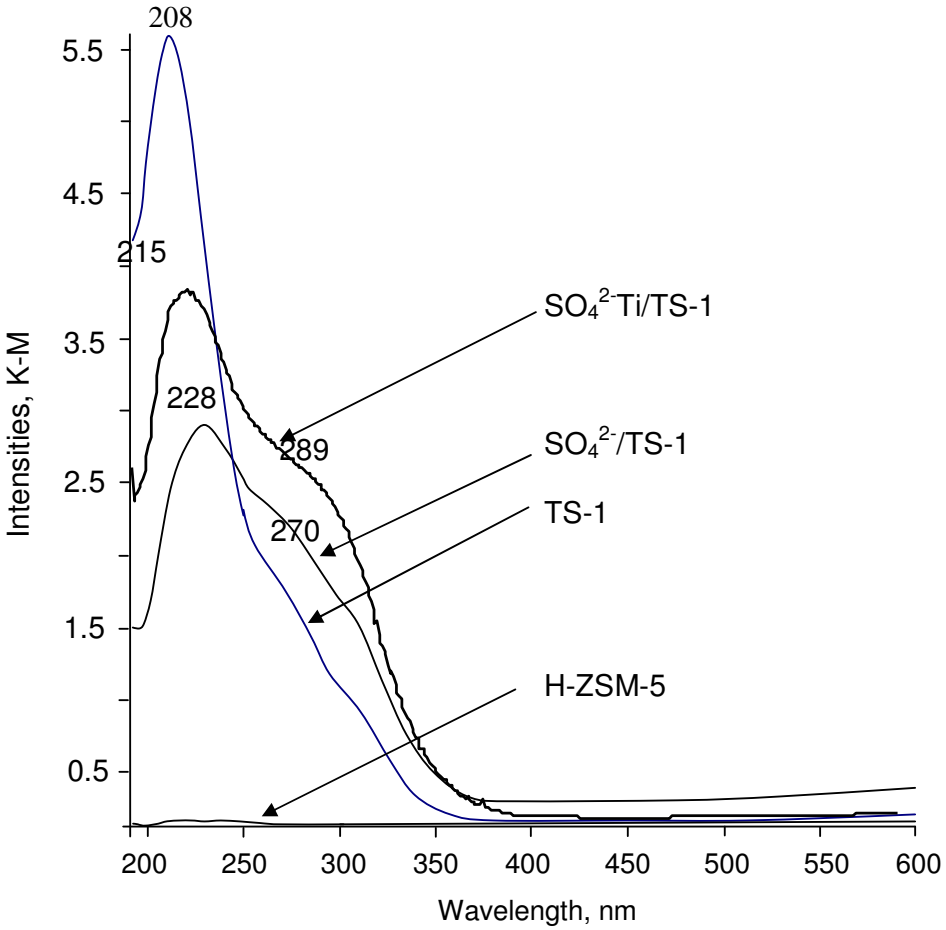

Figure 3 : UV-Vis DR spectra of the samples

to parent sample TS-1, in which the tetrahedral titanium intensity for SO_4^{2-}-Ti/TS-1 sample is significantly higher than SO_4^{2-}/TS-1 sample. The decrease in the intensity of the tetrahedral titanium band followed by the formation of the octahedral titanium band clearly indicates that some of the tetrahedral titanium framework has been expelled from the framework, and becomes extraframework titanium, with octahedral structure.

The oxidation activity depends on the amount of titanium in the tetrahedral structure [27]. The purpose of deposition of the titanium in the TS-1 is to add the extraframework titanium on the TS-1 surface such that the SO_4^{2-} anion only react with the titanium extraframework on the surface of TS-1 instead of tetrahedral titanium of TS-1. Thus, we would expect the spectrum of UV-Vis DR for this sample would give a band for tetrahedral titanium with similar intensity as for the TS-1. Table 1 shows the percentage of tetrahedral titanium in the samples (calculated based on the intensity of tetrahedral titanium in TS-1, in which TS-1 is taken as 100%) and also the position of the band. The results from the UV-Vis DR spectrum show that the intensity of the band for tetrahedral titanium species of SO_4^{2-}-Ti/TS-1 sample is lower than that of TS-1 sample, and shift to the higher wavelength to about 215 nm. Meanwhile, for the SO_4^{2-}/TS-1 sample, its intensity is much lower than that of TS-1 sample, and also shifts to the higher wavelength to about 228 nm. The shifting of the band to higher wavelength suggests that the SO_4^{2-} anions has reacted with the tetrahedral titanium in both samples. However, the amount of tetrahedral titanium which has been reacted with $SO4^{2-}$ anion is lower for SO_4^{2-}-Ti/TS-1 sample as compared to the SO_4^{2-}/TS-1 sample. It indicates that for sample SO_4^{2-}-Ti/TS-1, the SO_4^{2-} anion has reacted not only with the tetrahedral titanium but also with the titanium extraframework (which is in the octahedral structure) on the surface of TS-1.

The band shifting in the range of tetrahedral titanium of the SO_4^{2-}/TS-1 and SO_4^{2-}-Ti/TS-1 samples to higher wavelength at ca. 228 and 215 nm shows that the charge transfer of the tetrahedral titanium sites between O^{2-} and the Ti(IV) atoms for both samples is lower than that of the TS-1. This finding indicates that the oxygen atom in the tetrahedral titanium which has charge transfer of O(2p) $\rightarrow$ Ti(3d) is bonded with the sulfur atom in the form of SO_4^{2-}. The electronegativity of the sulfur atom (2.58, Pauling unit) is higher than that of silicon atom (1.90, Pauling unit). Therefore, for SO_4^{2-}/TS-1 and SO_4^{2-}-Ti/TS-1 samples, electron

density in the oxygen atom decreases, consequently, the charge transfer energy of O(2p) → Ti(3d) decreases, compare to TS-1 sample. As a result, the tetrahedral titanium band shifted to the higher wavelength (lower energy) in the UV-Vis DR spectroscopy.

Acidity studies

The acid strength of the sample was measured by observing the changing of the color of Hammet indicators [5], when the dried solid sample was poured into the solution of the indicator in benzene. Table 2 shows the acidic strength of the samples measured by Hammet indicators. H-ZSM-5 sample is found to have an H_0 value around –11.35 (measured in 1-nitrotoluene), in which the strength is similar with 98% of sulfuric acid. The TS-1 sample does not show any color changing of all Hammet indicators up to the pKa = -5.6 (measured in benzalacetophenone), indicating that the samples have low acid strength. Meanwhile, the SO_4^{2-}/TS-1 and SO_4^{2-}-Ti/TS-1 samples show color changing for all Hammet indicators, including measured in 2,4-dinitrobenzene (pKa = -14.52). This result suggests that both samples contain superacidity.

The type of acid sites of the samples were monitored by pyridine adsorption after evacuation of the samples at 400°C under vacuum, followed by adsorption of pyridine at room temperature, and evacuation at 150°C for an hour under vacuum. Samples were recorded by FTIR spectroscopy at room temperature in the range wavenumber of 2000 – 1400 cm^{-1}. The main peaks at *ca.* 1450 cm^{-1} and 1545 cm^{-1} are characteristic for Lewis and Brønsted acid sites, respectively. While the peak at *ca.* 1880 cm^{-1} is characteristic for vibration of the titanium silicalite framework. Figure 4 shows the spectra of the samples after evacuation at 150°C. All samples only show the peak at *ca.* 1445 cm^{-1} which corresponds to Lewis acid sites, while the peak for Brønsted acid sites at *ca.* 1545 cm^{-1} was not observed. This finding indicates that all samples only contain Lewis acid sites. The amount of the acid sites increase in sample SO_4^{2-}-Ti/TS-1 after the Ti loaded on the surface of TS-1 was treated by sulfuric acid.

It has been reported that the introduction of sulfate anions on the surface of zirconia has been found to increase the number and strength of the Lewis acid sites. It has been proposed that superacid sites of the sulfated oxides material such as zirconia is formed via oxidation of zirconia hydroxide in the presence of sulfate ion at high temperature, regardless of the types of starting materials used for sulfation [14]. It has further been suggested that such a structure may develop at the edge or corner of the metal oxide surfaces. In this study, for the samples SO_4^{2-}/TS-1 and SO_4^{2-}-Ti/TS-1, based on the characterization results especially the UV-Vis DR spectroscopy technique, the proposed structure of sulfated titanium on TS-1 is shown in Figure 5. The SO_4^{2-} ion is bonded with the titanium framework and titanium extraframework.

Table 2 : Acid strength by Hammet indicator

Hammet Indicator (*)	pKa of indicator	Sample				
		H_2SO_4	H-ZSM-5	TS-1	SO_4^{2-}/TS-1	SO_4^{2-}-Ti/TS-1
1	-5.60	+	+	-	+	+
2	-8.20	+	+	-	+	+
3	-11.35	+	+	-	+	+
4	-12.70	-	-	-	+	+
5	-13.75	-	-	-	+	+
6	-14.52	-	-	-	+	+

(*) 1=Benzalacetophenone; 2=Anthraquinone; 3=1-nitrotoluene; 4=1-chloro 4-nitrobenzene; 5=2,4-dinitrotoluene; 6=2,4-dinitrofluorobenzene

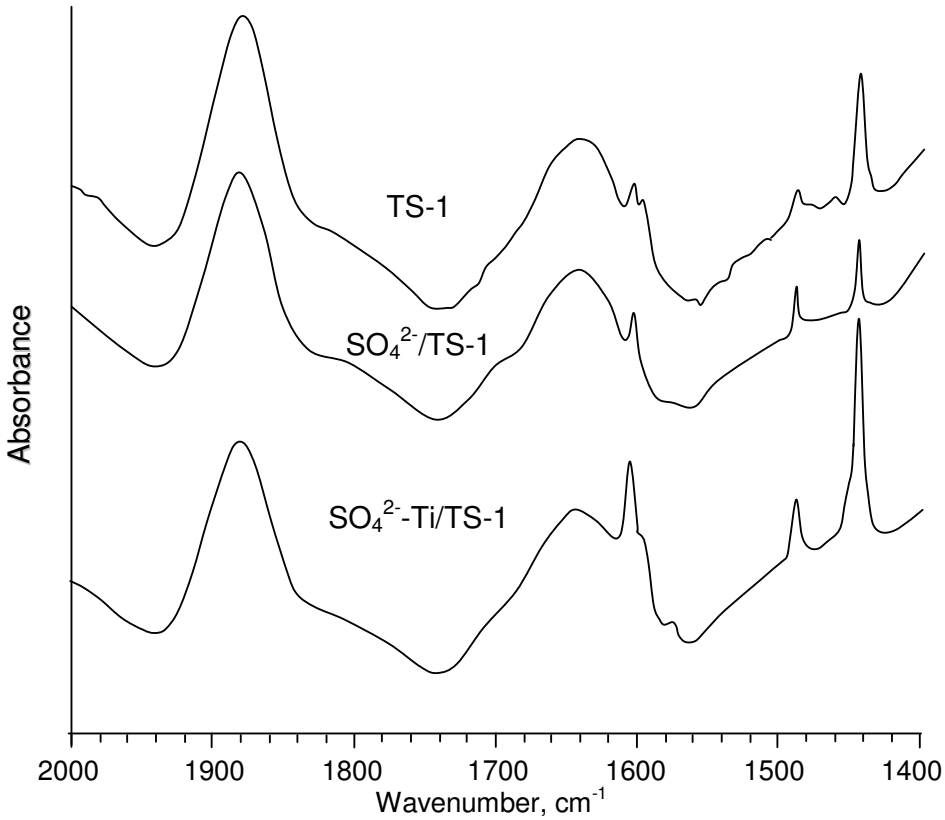

Figure 4 : FTIR spectra of the samples after following treatments: heated at 400°C for 4 hrs in vacuum, adsorbed pyridine at room temperature, and desorbed pyridine at 150°C for an hour.

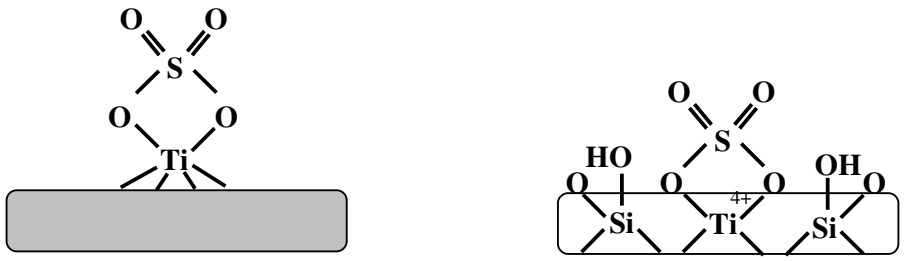

Ti extraframework (SO_4^{2-}-Ti/TS-1)

Ti framework (SO_4^{2-}/TS-1)

Figure 5 : Proposed structure of the sulfated titanium on TS-1

Conclusions

Bifunctional oxidative and superacid catalysts have been prepared. The SO_4^{2-}/TS-1 and SO_4^{2-}-Ti/TS-1 samples showed both oxidative and acidic sites. The amount of oxidative site is higher for SO_4^{2-}-Ti/TS-1 sample than of SO_4^{2-}/TS-1 sample, while the superacid strength is similar in both samples. However, creation of superacid sites caused the decrease in the oxidative sites.

Acknowledgements

We gratefully acknowledge funding from The Ministry of Science Technology and Environment Malaysia, under IRPA grant no: 09-02-06-0057 SR0005/09-03.

References

1. Trong On., D., Nguyen, S.V., Hulea, V., Dumitriu, E. and Kaliaguine, S. (2003) *Microporous and Mesoporous Mater,* **57**, 169–180.

2. van der Waal, J.C., Rigutto, M.S. and van Bekkum, H. (1998) *Appl. Catal. A: General,* **167**, 331-342.
3. Taramasso, M., Perego, G. and Notari, B. (1983) *US Patents No*., **4**,410,501.
4. Dias, S.C.L. (1997) Characterization of zeolites and zeotypes. PhD Thesis, University of Florida.
5. Yang, H., Lu, R., Zhao, J., Yang, X., Shen, L. and Wang, Z. (2003) *Mater. Chemistry and Physics,* **80**, 68–72.
6. Jung, S. M., Dupont, O. and Grange, P. (2001) *Appl. Catal. A: General*, **208**, 393-401.
7. Huang, Y., Zhao, B. and Xie, Y. (1998) *Appl. Catal. A: General*, **171**, 75-83.
8. Miao, C.X. and Gao, Z. (1997) *Mater. Chemistry and Physics*, **50**, 15–19.
9. Matsuhashi, H., Miyazaki, H., Kawamura, Y., Nakamura, H. and Arata, K. (2001) *Chem. Mater*, **13**, 3038-3042.
10. Arata, K. (1996) *Appl. Catal. A: General*,**146**, 3-32 .
11. Das, D., Mishra, H.K., Dalai, A.K. and Parida, K.M. (2003) *Appl. Catal. A: General*, **243**, 271–284.
12. Moreno, J.A. and Poncelet, G. (2001) *Appl. Catal. A: General*, **210**, 151-164
13. Grau, J.M., Vera, C.R. and Parera, J.M. (1998) *Appl. Catal. A: General*, **172**, 311-326.
14. Yadav, G.D. and Nair, J.J. (1999) *Microporous and Mesoporous Mater*, **33**, 1-48.
15. Huang, Y., Zhao, B. and Xie, Y. (1998) *Appl. Catal. A: General*, **173**, 27-35.
16. Huang, Y., Zhao, B. and Xie, Y. (1998) *Appl. Catal. A: General*, **171**, 65-73.
17. Huang, Y., Zhao, B. and Xie, Y. (1998) *Appl. Catal. A: General*, **172**, 327-331.
18. Damyanova, S., Grange, P. and Delmon, B. (1997) *J. Catal*., **168**, 421-430.
19. Lei, T., Xu, J.S., Tang, Y., Hua, W.M. and Gao, Z. (2000) *Appl. Catal. A: General*, **192**, 181–188.
20. Sohn, J.R. and Seo, D.H. (2003) *Catal. Today*, **87**, 219–226.
21. Arata, K. and Hino, M. (1990) *Appl. Catal*., **59**, 197-204.
22. Clearfield, A., Serrette, G.P.D. and Khazi-Syed, A.H. (1994) *Catal. Today*, **20**, 295-312
23. Hua, W., Goeppert, A. and Sommer, J. (2001) *J. Catal*., **197**, 406-413.
24. Xia, Q.-H., Hidajat, K. and Kawi, S. (2000) *Chem. Commun*., **2229**–2230.
25. van der Pol, A.J.H.P., Verduyn, A.J. and van Hooff, J.H.C. (1992) *Appl. Catal. A: General*, **92**, 113-130.
26. Flanigen, E. M. (1976) in Rabo, J.A. "Zeolite chemistry and catalysis". *ACS Monograph*, **171**, 80-117.
27. Zecchina, A., Bordiga, S., Lamberti, C., Ricchiardi, G., Lamberti, C., Ricchiardi, G., Scarano, D., Petrini, G., Leofanti, G. and Mantegazza, M. (1996) *Catal. Today*, **32**, 97-106.
28. Smirnov, K.S. and van de Graaf, B. (1996) *Microporous Mater*, **7**, 133-138.
29. Astorino, E., Peri, J.B., Willey, R.J. and Busca, G. (1995) *J. Catal*., **157**, 482-500.

Available online at www.sciencedirect.com
SCIENCE DIRECT®
Catalysis Communications 5 (2004) 725–728
CATALYSIS COMMUNICATIONS
www.elsevier.com/locate/catcom

Sulfation: a simple method to enhance the catalytic activity of TS-1 in epoxidation of 1-octene with aqueous hydrogen peroxide

Hadi Nur [a,*], Didik Prasetyoko [b], Zainab Ramli [b], Salasiah Endud [b]

[a] *Ibnu Sina Institute for Fundamental Science Studies, Universiti Teknologi Malaysia, 81310 UTM Skudai, Johor, Malaysia*
[b] *Department of Chemistry, Faculty of Science, Universiti Teknologi Malaysia, 81310 UTM Skudai, Johor, Malaysia*

Received 17 March 2004; revised 9 September 2004; accepted 10 September 2004

Abstract

Titanosilicalite (TS-1) has been successfully modified by sulfation to exhibit enhanced catalytic activity in the oxidation of 1-octene with aqueous H_2O_2. A high activity of the sulfated TS-1 was related to modifications of the local environment of Ti active site upon interaction with the SO_4^{2-}.

Keywords: TS-1; Epoxidation; Sulfation; Enhancement of catalytic activity

1. Introduction

The discovery of the framework substituted microporous materials titanium silicalite-1 (TS-1) was one of the most important developments in heterogeneous catalysis with in the last decade [1]. These materials exhibit extremely high selectivity in oxidation reactions using hydrogen peroxide, with water as the major byproduct. Since there is a low concentration of Ti present in TS-1 the catalytically active Ti centers are believed to be site isolated from each other. This site isolation is thought to give rise to its unique catalytic activity and selectivity. It has been reported that the catalytic activity of TS-1 for olefin epoxidation with aqueous H_2O_2 could be enhanced by trimethylsilylation in order to produce hydrophobic TS-1 [2]. However, trimethylsilyl group can block the pore of the TS-1 since its size is considerably big. Here, we demonstrated a simple method to enhance the catalytic activity of TS-1 in epoxidation of 1-octene with aqueous H_2O_2 by sulfation. This simple method can eliminate the possibility of pore blockage.

2. Experimental

2.1. Synthesis

TS-1 (2% of Titanium, mol%) was prepared according to a procedure described earlier [1,3], using reagents, i.e., tetraethyl orthosilicates (Merck, 98%), tetraethyl orthotitanate (Merck, 95%) in isopropyl alcohol, tetrapropylammonium hydroxide (Merck, 20% TPAOH in water) and distilled water. The hydrothermal crystallization was carried out at 175 °C under static condition in the stainless steel autoclave for 4 days.

Sulfated TS-1 was prepared by impregnation method as follows: About 1 g of TS-1 was added into 25 ml of H_2SO_4 0.5 M under vigorous stirring at 80 °C for 3 h. After evaporation of water, the solid was dried at 100 °C for 24 h. The solid sample was then calcined at 550 °C for 3 h. The sample was denoted as SO_4/TS-1.

* Corresponding author.
E-mail address: hadi@kimia.fs.utm.my (H. Nur).

1566-7367/$ - see front matter © 2004 Elsevier B.V. All rights reserved.
doi:10.1016/j.catcom.2004.09.007

2.2. Characterizations

The solid structure was determined by using X-ray diffraction (XRD), infrared (IR) and UV–Vis Diffuse Reflectance (UV–Vis DR) spectroscopy techniques. All samples were characterized by powder XRD for the crystallinity and phase content of the solid materials using a Bruker Advance D8 Diffractometer with the Cu Kα (λ = 1.5405 Å) radiation as the diffracted monochromatic beam at 40 kV and 40 mA. The sample was scanned in the 2θ range between 5° and 50°. IR spectra of the samples were collected on a Perkin–Elmer Fourier Transform Infrared, with a spectral resolution of 2 cm^{-1}, scans 10 s, at room temperature by KBr pellet method. The framework spectra were recorded in the region of 1400–400 cm^{-1}. UV–Vis DR spectra were recorded under ambient conditions on a Perkin–Elmer Lambda 900 UV/Vis/NIR spectrometer. The acidity of the solids characterized by absorbed base probe molecule. The wafer of the sample (10–12 mg) was locked in the cell equipped with CaF_2 windows, and evacuated at 400 °C under vacuum condition for 4 h. Pyridine as probe molecule was introduced into the evacuated sample at room temperature. IR spectra of the sample was monitored at room temperature after desorption of pyridine at 150 °C for 1 h.

2.3. Epoxidation of 1-octene

All reactions were carried out at room temperature with 1-octene (1.0 ml), 30% H_2O_2 (0.5 ml), a mixture of methanol (5 ml) and acetone (5 ml) as solvent, and catalyst (50 mg) with stirring. The products of reaction were analyzed by GC and GC–MS.

3. Results and discussion

XRD was used to characterize the structure and the crystallinity of the TS-1 and SO_4/TS-1. All samples show similar XRD patterns characteristic of MFI structure type of zeolite. Introduction of SO_4^{2-} anions into the TS-1 has no effect on the sample crystallinity, with less than 1% changes. This suggests that the MFI structure of TS-1 is still maintained after the introduction of SO_4^{2-}. IR spectra of TS-1 and SO_4/TS-1 samples show a peak at around 970 cm^{-1} which is a characteristic for titanium with tetrahedral structure (Fig. 1). This band appears to be diminished in the sulfated material, suggesting the decrease in the amount of tetrahedral titanium in SO_4/TS-1. IR spectrum of SO_4/TS-1 shows a new peak at around 1384 cm^{-1} which is corresponded to the asymmetric stretching vibration of the covalent S═O for SO_4^{2-} ion.

Fig. 2 shows UV–Vis DR spectra of TS-1 and SO_4/TS-1. The band in the range of 190–220 nm is attributed

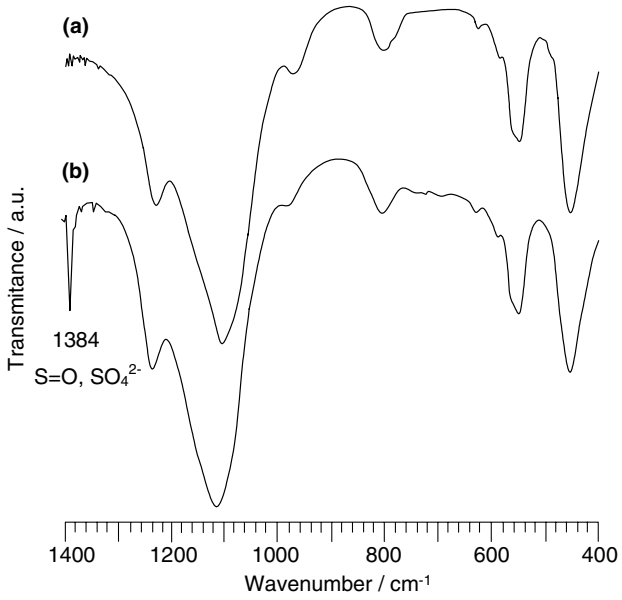

Fig. 1. FTIR spectra of: (a) TS-1; (b) SO_4/TS-1.

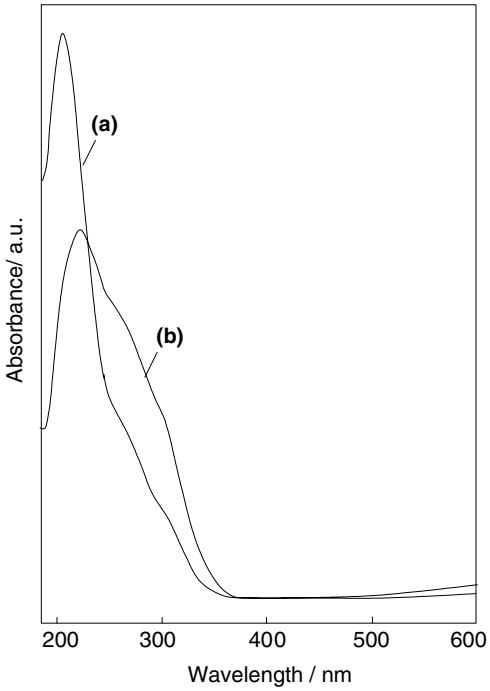

Fig. 2. Absorption spectrum of: (a) TS-1; (b) SO_4/TS-1.

to a charge-transfer of the tetrahedral titanium sites between O^{2-} and the central Ti(IV) atoms, while octahedral Ti is observed at around 310–330 nm [4,5]. It shows that, for TS-1, only single high intense band at around 208 nm can be observed. This band is attributable to titanium in the tetrahedral structure. Impregnation of SO_4^{2-} into the TS-1 shows a medium intense band at around 215–228 nm and a shoulder band at around 270–312 nm, characteristic for titanium with tet-

rahedral and octahedral structure, respectively. The peak intensity of tetrahedral titanium for SO_4/TS-1 is lower than that of the parent sample (TS-1). The decrease in intensity of the tetrahedral titanium and the formation of the octahedral titanium indicate the occurrence of the transformation of some of the tetrahedral titanium framework to the octahedral structure or the extraframework during the sulfation. It has been calculated that 49% of tetrahedral titanium in the parent sample have been modified by sulfation.

As shown in Fig. 2, the wavelength of absorption band of the tetrahedral titanium sites (i.e., 288 nm) of SO_4/TS-1 is higher than that of TS-1 (i.e., 208 nm). It could be that the Ti–O–S bonding in SO_4/TS-1 lowered the charge-transfer excited state involving an electron transfer from O^{2-} to Ti^{n+} [6]:

$$[Ti^{n+}–O^{2-}] \xrightarrow{h\nu} [Ti^{(n-1)+}–O^{-}]^*$$

This phenomenon is supported by the fact that the band at 970 cm^{-1} of TS-1, which is corresponded to tetrahedral titanium, is shifted to higher wavenumber in SO_4/TS-1 (see Fig. 1). The shift to higher wavenumber is expected since the presence of SO_4^{-2} species in SO_4/TS-1 weakened the Ti–O–Si bonding, resulting in a longer bond length and hence decreasing the force constant of Ti–O–Si.

The acidity of the samples was characterized by pyridine adsorption. TS-1 and SO_4/TS-1 only show the peak at around 1450 cm^{-1} (which is corresponded to Lewis acid site), while the peak at around 1545 cm^{-1} (which is corresponded to Brönsted acid site) was not observed (Fig. 3). This indicates that all samples only contain Lewis acid sites. It has been calculated that the amount of the Lewis acid sites in TS-1 and SO_4/TS-1 were 12 and 8 μmol g^{-1}, respectively, indicating a decrease of 33% in the Lewis acid concentration of SO_4/TS-1 from the TS-1. This result suggests that the removal of tetrahedral titanium from the lattice to form octahedral species is the reason for the decrease in the acidity, since the amount of the Lewis acid sites correlate to the amount of tetrahedral titanium. No diol is observed in the reaction product of the epoxidation of 1-octene with aqueous H_2O_2 confirming that no Brönsted acid sites are present in the samples.

The infrared spectra of the TS-1 and SO_4/TS-1 in the range of hydroxyl stretching regions at 4000–3000 cm^{-1} were recorded after evacuation in vacuum at 400 °C for 4 h (Fig. 4). TS-1 shows an intense band at 3736 cm^{-1} and a broad band at 3526 cm^{-1}, characteristics for terminal silanol hydroxyl groups and hydroxyl groups with hydrogen bonding of water molecule with silanol groups, respectively [5]. The sulfation of TS-1 caused the sharp band of silanol groups to decrease significantly and becomes broader in the ranges of 3740–3726 cm^{-1}, suggesting the formation of defect sites in the surface of TS-1. Meanwhile, the broad band for hydroxyl groups around 3500 cm^{-1} increases due to the hydroxyl groups are bounded on the sulfur centers.

As shown in Fig. 5, sulfation onto the surface of TS-1 increases its epoxidation activity. This phenomenon may be explained in terms of the local environment of Ti active site. It is generally accepted that isolated Ti(IV) are considered the most active species in epoxidation reaction. It has been found that tripodal open lattice site

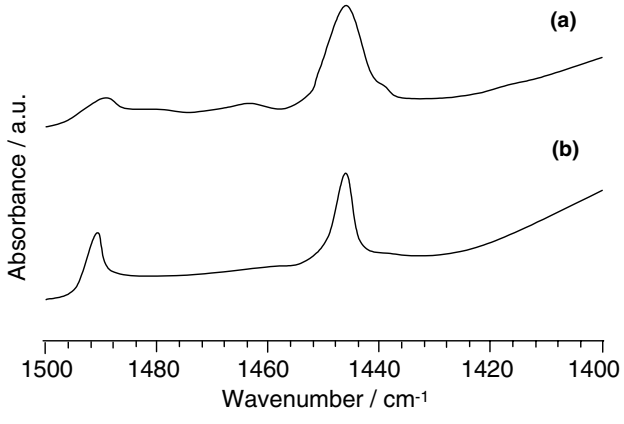

Fig. 3. FTIR spectra of: (a) TS-1; (b) SO_4/TS-1 after following treatments: heated at 400 °C for 4 h in vacuum, adsorbed pyridine at room temperature, and desorbed pyridine at 150 °C for 1 h.

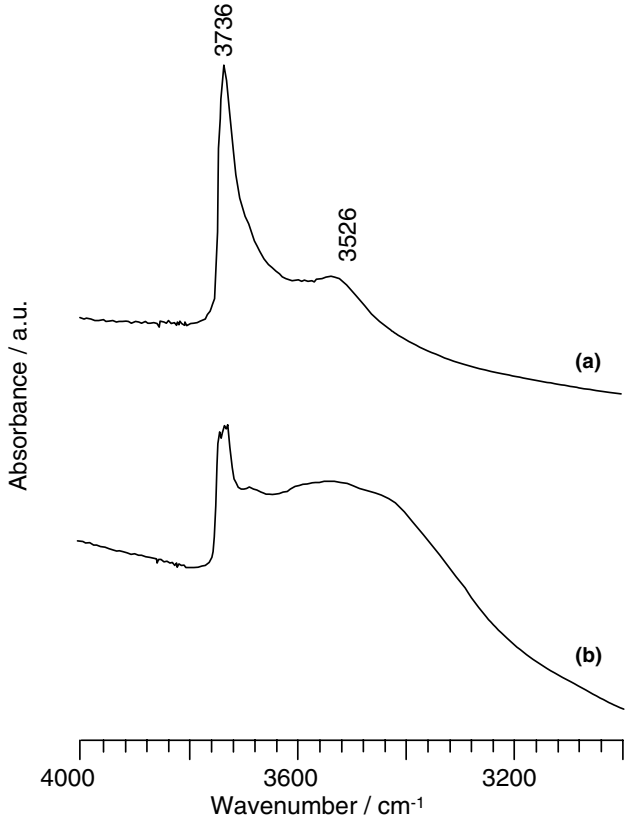

Fig. 4. FTIR spectra of: (a) TS-1; (b) SO_4/TS-1 after heated at 400 °C for 4 h in vacuum.

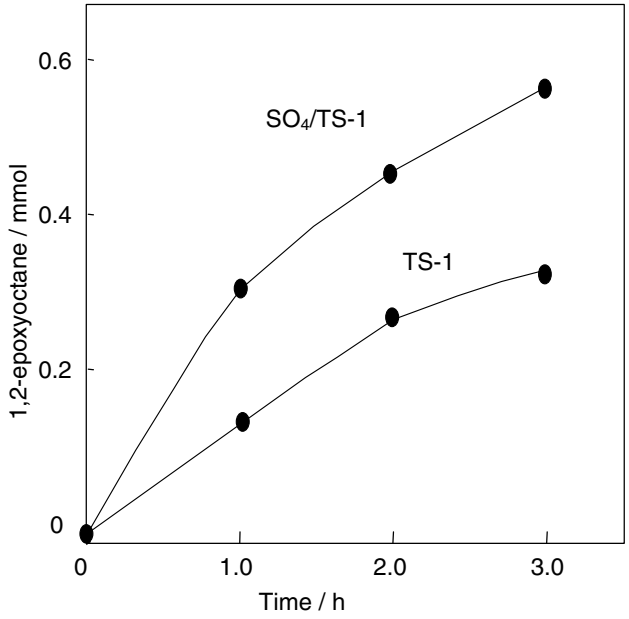

Fig. 5. The yield of 1,2-epoxyoctane on the epoxidation of 1-octene using TS-1 and SO_4/TS-1. The reactions were carried out at room temperature with 1-octene (1.0 ml), 30% H_2O_2 (0.5 ml) and catalyst (50 mg).

[i.e., $Ti(OSi)_3OH$] of Ti on the TS-1 surface was more active compared to the bipodal [i.e., $Ti(OSi)_2(OH)_2$] and the tetrapodal closed lattice sites [i.e., $Ti(OSi)_4$] [7,8]. Based on these findings, the effect of sulfation on increasing the epoxidation activity of SO_4/TS-1 can be explained by the presence of tripodal Ti active site. As shown in Fig. 6, it proposes that the bipodal Ti reacted with SO_4^{2-} giving $Ti(SiO)_2SO_4$ and followed by the hydration of $Ti(SiO)_2SO_4$ resulting in the tripodal Ti site [i.e., $Ti(OSi)_2(SO_3)OH$].

The alternative explanation for the higher activity of SO_4/TS-1 is that the possibility of the formation of new sites generated by sulfation on the surface TS-1. The UV–Vis DR spectra shown in Fig. 2 clearly show that Ti has been removed from the lattice to form octahedral species. It is possible that it can migrate to the external surface. Since 1-octene is a relatively large molecule, one considers that an increase the number of external active sites and access on them could be a cause for the higher activity.

Based on the above considerations, the high activity of SO_4/TS-1 for epoxidation of 1-octene by aqueous hydrogen peroxide can be considered as the influence of the attachment of SO_4^{2-} to the Ti active sites or alternatively, the formation of new sites generated by sulfation in the surface TS-1.

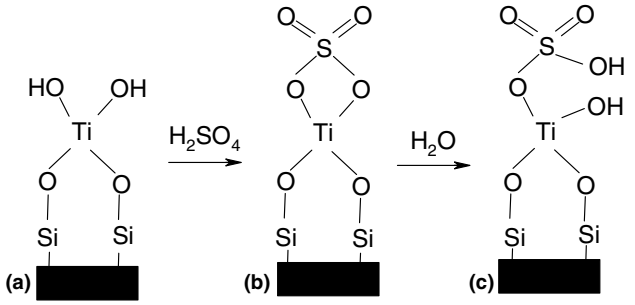

Fig. 6. Proposed model of the local environment structure of Ti: (a) bipodal; (b) tetrapodal; (c) tripodal.

Acknowledgements

The authors thank the anonymous international referees for helpful suggestion and comments on an earlier draft. A research grant from the Ministry of Science Technology and Environment Malaysia (Grant No. 09-02-06-0057 SR0005/09-03) is gratefully acknowledged.

References

[1] M. Taramasso, G. Perego, B. Notari, US Patents, No. 4,410,501, 1983.
[2] M.B. D'Amore, S. Schwarz, Chem. Commun. 121 (1999).
[3] A.J.H.P van der Pol, A.J. Verduyn, J.H.C. van Hooff, Appl. Catal. A: Gen. 92 (1992) 113.
[4] A. Zecchina, S. Bordiga, C. Lamberti, G. Ricchiardi, C. Lamberti, G. Ricchiardi, D. Scarano, G. Petrini, G. Leofanti, M. Mantegazza, Catal. Today 32 (1996) 97.
[5] E. Astorino, J.B. Peri, R.J. Willey, G. Busca, J. Catal. 157 (1996) 482.
[6] M. Matsuoka, M. Anpo, J Photochem. Photobiol. C: Photochem. Rev 31 (2003) 225.
[7] M. Crocker, R.H.M. Herold, B.G. Roosenbrand, K.A. Emeis, A.E. Wilson, Coll. Surf. A 139 (1996) 351.
[8] D. Gleeson, G. Sankar, C.R.A. Catlow, J.M. Thomas, G. Spano, S. Bordiga, A. Zecchina, C. Lamberti, Phys. Chem. Chem. Phys. 2 (2000) 4812.

Title of thesis : Bifunctional Oxidative and Acidic Catalysts for One Pot Synthesis of 1,2-Octanediol from 1-Octene

Name : Didik Prasetyoko

ABSTRACT

New bifunctional catalysts containing both oxidative and Brønsted acidic sites have been prepared and used for the consecutive transformation of alkenes to the corresponding diols via the formation of epoxides with aqueous hydrogen peroxide as oxidant. The catalytic system was designed in order that the two kinds of active sites allow the epoxidation of alkenes to take place within the pore channels of titanium-containing molecular sieve while acid catalysis of the epoxides to diols occurs on the catalyst external surface. Based on this design, titanium silicalite (TS-1), a known excellent and commercial oxidation catalyst so far, has been chosen as oxidative sites of the bifunctional catalyst. The TS-1 was then modified with different acidic oxide precursors. Synthesis of the series of bifunctional catalysts was achieved by deposition of various loadings of acidic oxide precursors up to 25 wt% onto TS-1 powder. The Ti^{4+} and acidic oxides in the TS-1 molecular sieve served as oxidative and acidic sites, respectively. The thus obtained bifunctional catalysts were sulfated TS-1 (SO_4^{2-}/TS-1), sulfated titanium oxide supported on TS-1 (SO_4^{2}-Ti/TS-1), tungsten oxide supported on TS-1 (WO_3/TS-1), sulfated zirconia supported on TS-1 (SZ/TS-1), and niobium oxide supported on TS-1 (Nb/TS-1). The X-ray diffraction analysis revealed that TS-1 still retained the MFI structure after incorporation of the acidic oxides even if the crystallinity is lower. The infrared (IR) and ultra-violet diffuse reflectance (UV-Vis DR) spectra showed that the titanium in TS-1 was mainly in tetrahedral coordination after incorporation of acidic oxides. Results of pyridine adsorption followed by IR spectroscopy showed the presence of Brønsted acid sites in WO_3/TS-1, Nb/TS-1 and highly loaded SZ/TS-1 but not sulfated samples of TS-1 (SO_4^{2-}/TS-1 and SO_4^{2}-Ti/TS-1). In the consecutive transformation of 1-octene to 1,2-octanediol through the formation of 1,2-epoxyoctane, all the catalysts showed a significant increase in the rate of formation of 1,2-epoxyoctane with respect to TS-1. The presence of acidic oxides in TS-1 was proposed to explain the increased hydrophilic character of the catalysts, which is responsible for the higher rate of formation of reactive oxo-titanium species. Moreover, the acid sites have been shown to effectively catalyze the formation of 1,2-octanediol with the 10 wt% niobium oxide supported

on TS-1 giving the highest yield. Comparison of the catalytic performance of the prepared bifunctional catalysts with that of the mechanical mixture comprising TS-1 and H-ZSM-5 (Brønsted acid), has shown that the bifunctional catalysts were more active suggesting that specific location of the two active sites plays an important role in the consecutive transformation of alkenes to epoxides and then diols. The higher activity of the bifunctional catalysts was proposed due to the location of the acidic sites in the immediate vicinity of the oxidative sites which enables the epoxidation products to undergo hydrolysis rapidly at the Brønsted acid sites located on the external surface of TS-1.

Title of thesis : **Bifunctional Nb/Ti-MCM-41 Catalyst in Oxidative Acidic Reaction of Cyclohexane to Diols**

Name : Mazidah Abd Shukor

ABSTRACT

Bifunctional oxidative and acidic catalyst was prepared by incorporating titanium ion (Ti^{4+}) and niobic acid in mesoporous molecular sieves MCM-41 structure. The catalyst being active both in oxidation reaction due to the presence of tetrahedral Ti^{4+}, and acid-catalyzed reaction due to the presence of niobic acid. Nb/Ti-MCM-41 was prepared by first synthesizing Ti-MCM-41 by direct hydrothermal method, followed by calcinations in air and subsequent impregnation of niobium into Ti-MCM-41 at various %wt niobium loading. The sample was characterized by XRD, FTIR and UV-Vis DR spectroscopy techniques. The types and the amount of acid sites were studied by FTIR spectroscopy using pyridine as probe base molecule. The catalyst performances were tested in the oxidation reaction of cyclohexene with aqueous H_2O_2 as oxidant. The XRD analysis of Nb/Ti-MCM-41 showed that the framework structure of MCM-41 has collapsed. UV-Vis DR showed that the Ti^{4+} in Ti-MCM-41 sample is in tetrahedral form while in sample Nb/Ti-MCM-41 both the tetrahedral Ti^{4+} and the peak characteristic for niobic acid in octahedral form are observed. Pyridine adsorption study showed that both Brønsted and Lewis acid sites are present in all Nb/Ti-MCM-41 samples. The Brønsted acid sites increased with increasing amount of niobium. The catalytic testing of the catalysts using cyclohexene as reactant gave cyclohexenediol as the main product through the formation of cyclohexene oxide. No trend was observed for conversion of cyclohexene to cyclohexanediol but the selectivity and yield were found to increase with the increase amount of niobium. In this case the amount of Brønsted acid sites provided by Nb species is responsible for the increased yield of cyclohexanediol.

Title of thesis : Dihydroxylation of Butenol Over Bifunctional Catalyst

Name : Yeow Kian Wee

ABSTRACT

Zeolites are important solid acid catalysts and have wide applications in chemical industries. In this study, TS-1 was synthesized through modification of the conventional method and followed by the impregnation of 1%, 3% and 6% w/w of niobic acid on TS-1 to form bifunctional oxidative and acidic catalyst XNb/TS-1 (X=%w/w Nb). The catalyst is active in oxidation reaction due to the presence of tetrahedral Ti^{4+}, and acid-catalyzed due to the presence of niobic acid. The structure and the properties of the sample were characterized by XRD, FTIR, UV-vis DR and pyridine adsorption techniques. XRD and FTIR showed that the impregnation of niobic acid did not affect the MFI framework structure of TS-1. UV-vis DR showed the presence of niobium species in octahedral form. Acidic study by pyridine adsorption technique showed the Nb/TS-1 has Brønsted and Lewis acid sites but TS-1 only has the Lewis acid site. The catalytic properties of Nb/TS-1 were investigated in the dihydroxylation of 3-methyl-2-buten-1-ol with dilute H_2O_2 as oxidizing agent. The products of the reaction were analyzed by GC and identification of the product were done by GC-MS. 1,2,3-pentanetriol is obtained as the major product showing that the sample Nb/TS-1 is a bifunctional oxidative and acidic catalyst. Sample Nb/TS-1 with 6% w/w niobic acid exhibits the highest performance in the cis-2-pentene-1-ol dihydroxylation with 50.52% conversion, 73.32% selectivity and 37.04% yield, whereas the TS-1 gave 30.35% conversion, 32% selectivity and 9.71% yield. The catalytic activity of Nb/TS-1 in the dihydroxylation of unsaturated alcohols is a significant improvement as compare to the support TS-1. In this study Nb is responsible for the increase performance of the bifunctional TS-1 catalyst.

A New Approach To Probe The Dispersion Capacity Of Tungsten Oxide On The Surface Of Titanium Silicalite By Infrared Spectroscopy

Didik Prasetyoko, Zainab Ramli, Hadi Nur, and Salasiah Endud

Department of Chemistry, Faculty of Sciences, Universiti Teknologi Malaysia, 81310 UTM Skudai-Johor, Malaysia.

Abstract

The dispersion capacity of WO_3 on the surface of titanium silicalite (TS-1) was evaluated by XRD and FTIR spectroscopy techniques. The dispersion capacity of WO_3 on TS-1 in the region of the hydroxyl groups using 3726 and 3505 cm^{-1} wavenumber are 0.40 and 0.38 W^{6+}/nm^2 TS-1, respectively, while the dispersion capacity using bands in the framework region between 900-700 cm^{-1} wavenumber gave 0.40 W^{6+}/nm^2 TS-1. These values are in a good agreement with the result from XRD analysis, i.e. 0.35 W^{6+}/nm^2 TS-1.

Keywords: Oxides,. Structural materials, Infrared spectroscopy, Surface properties.

Introduction

The structures and properties of supported metal oxide materials are strongly influenced by the metal oxide precursor, the loading amount of the metal oxide, the nature of support, and the experimental conditions. The generation of monolayer metal oxides dispersed on the solid supports is important in the performance of monolayer-type catalyst [1-4]. The optimum catalytic activity of the catalysts is often near its monolayer dispersion capacity. For example, Wang et al. [5] investigated the effect of the amount of tungsten oxide loaded on the different silica supports, WO_3/SiO_2 in the 1-butene metathesis. The yields of butene metathesis products increased with the increase of tungsten oxide loadings and reached maximum values over the sample with 6 wt.% WO_3 loadings. This loading value is close to monolayer loading of WO_3 on silica. Jiang et al. [6] found that for the solid base, the basic sites on the surface of $MgO/\gamma\text{-}Al_2O_3$ should mainly originate from monolayer-dispersed MgO. The MoO_3/SnO_2 catalyst with 8 wt.% MoO_3 loading showed high catalytic activity in oxidation of methanol [1].

The examples of catalytic applications suggest that the monolayer capacity can be related to the catalytic activity [1-10]. Therefore, determination of the dispersion capacity of supported catalysts is significant in the area of catalysis by supported metal oxides. Several methods have been reported to determine the dispersion capacity of metal oxide supported on the solid support. The XRD quantitative phase analysis and XPS characterization techniques are the common method that has been used to determine the monolayer capacities of metal oxides supported on various supports [5, 11-14]. However, the use of infrared spectroscopy to measure the dispersion capacity of the metal oxides on the supports has not been reported. The infrared technique has been used to characterize the structure and properties of the supported metal oxides [15-20]. Therefore, this present work concentrates on the evaluation of the monolayer capacity of supported metal oxide, tungsten oxide supported on the titanium silicalite (WO_3/TS-1) by using infrared technique in the hydroxyl and framework regions. As a comparison, the XRD technique was also used to determine of monolayer capacity of the WO_3/TS-1.

Experiment

Preparation of sample

The support, titanium silicalite (TS-1, 3% of titanium, %mol) was prepared according to a procedure described earlier [21]. The WO_x/TS-1 catalysts were prepared by incipient wetness impregnation of TS-1 with an aqueous solution containing sufficient amount of ammonium metatungstate hydrate $(NH_4)_6\ H_2W_{12}O_{41}.\ 18H_2O$, to yield materials with loading in the ranges of 2 – 25 wt% of WO_3 in the calcined state. The suspension was heated at 110^{o}C for 3 hours under stirring condition, followed by evaporation of water, drying at 110^{o}C for 24 hours, and calcination at 550^{o}C for 6 hours. The samples denoted by their weight percentage of WO_3 on TS-1 are .

Table 1. Preparation conditions of the samples

Sample	Support	WO_3, wt%	Conditions
TS-1	TS-1	0	-
2WO_3/TS-1	TS-1	2.4	Neutral
5WO_3/TS-1	TS-1	4.9	Neutral
7WO_3/TS-1	TS-1	7.2	Neutral
10WO_3/TS-1	TS-1	9.7	Neutral
15WO_3/TS-1	TS-1	14.6	Neutral
25WO_3/TS-1	TS-1	24.9	Neutral

Characterization

The solid structure was determined by using XRD and infrared spectroscopy techniques. The samples were characterized by powder X-ray diffraction (XRD) for the crystallinity and phase content of the solid materials using a Bruker Advance D8 Difractometer with the Cu Kα (λ=1.5405 Å) radiation as the diffracted monochromatic beam at 40 kV and 40 mA. The pattern was scanned in the 2θ ranges from 5^o to 50^o at a step size 0.010^o and step time 1s. Infrared (IR) spectra of the samples were collected on a Shimadzu Fourier Transform Infrared (FTIR), with a spectral resolution of 2 cm^{-1}, scans 10 s, at temperature 20^{o}C by KBr pellet method. The framework spectra were recorded in the region of 1400 – 400 cm^{-1}. The hydroxyl groups of the samples were monitored by FTIR spectroscopy technique. The wafer of the sample (10-12 mg) was locked in the cell equipped with CaF_2 windows, and evacuated at 400^{o}C under vacuum condition for 4 hrs. Infrared spectra of the sample were recorded at room temperature in the region of 4000 – 3000 cm^{-1}.

Results and discussions

X-ray diffraction

The XRD patterns of the TS-1 and WO_3/TS-1 samples with various tungsten loading and condition are shown in Fig. 1. The peaks corresponding to the crystalline phase of WO_3 at 2θ = 23.1, 23.7, 24.4, 33.2-34.6, and 41.5^o (marks by arrow, in which the peaks at 2θ = 23-25^o overlapping with the peaks of TS-1) is only observed for the WO_3/TS-1 samples with high amount of tungsten loading, ca. 10, 15 and 25%. The crystalline phase of WO_3 were not observed for the WO_3/TS-1 samples with low loading amount of WO_3, ca. 2, 5 and 7%. The result demonstrates that crystalline WO_3 appears only in samples with high loading while the WO_3 exists as highly dispersed species in the low loading samples. This finding is in a good agreement with Wang, et al. [5] in which the characteristic peaks of crystalline WO_3 were clearly seen for the samples with high loading amount of WO_3, ca. >6% and 10%, depending on the nature of support.

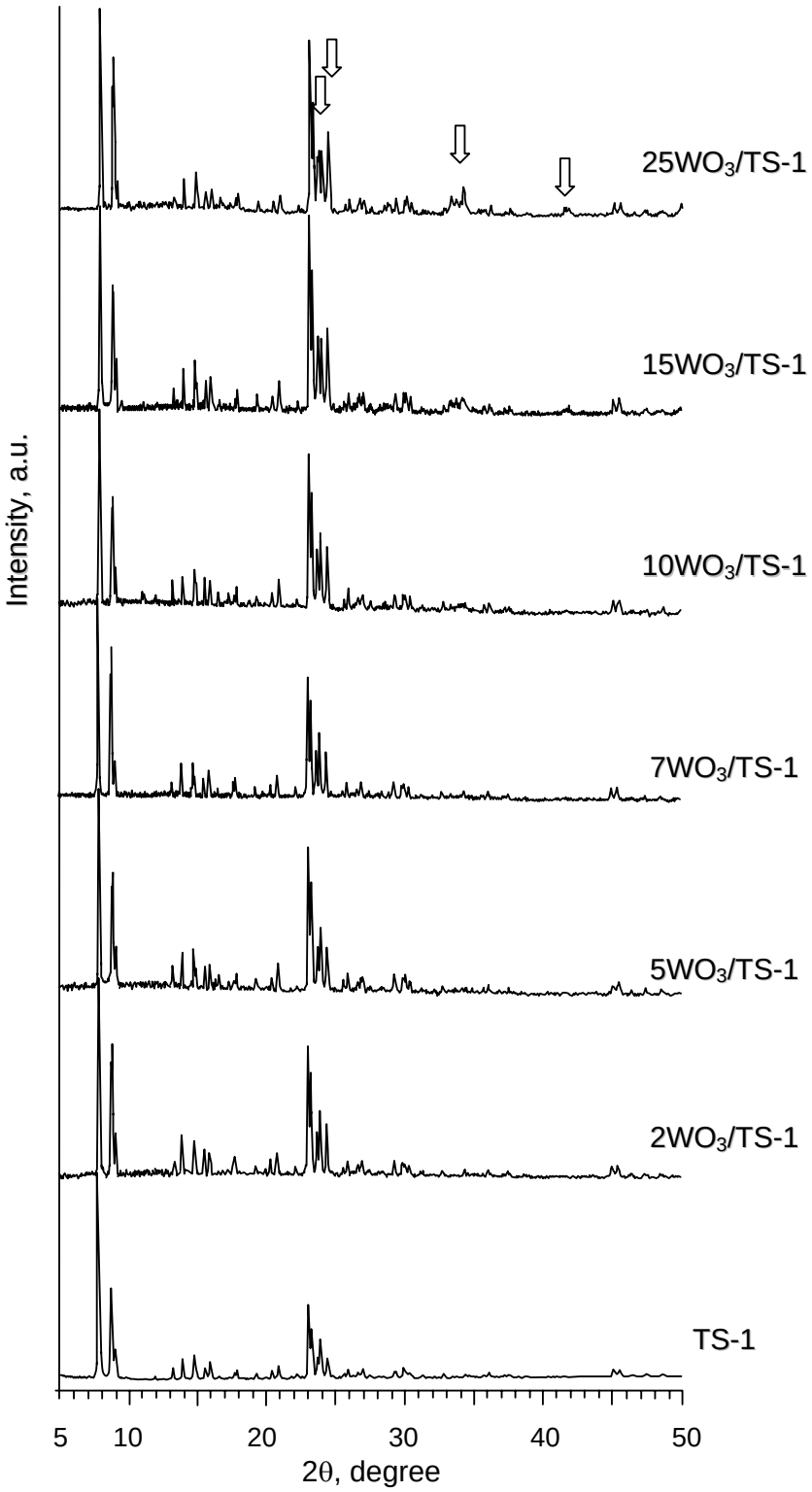

Fig. 1. XRD patterns of the TS-1 and tungsten-coated TS-1 samples

The peak intensities of the crystalline WO_3 in the WO_3/TS-1 samples increase with the increase of WO_3 loading, due to the increase concentration of the WO_3 on the surface of the TS-1 support. The surface concentration of metal dispersed in the support can be calculated quantitatively based on the amount of metal oxide loading, by the equation as following [5].

$$C_W = \left(\frac{L_{WO3}/100}{238.1}\right)\left(\frac{N_0}{S_{BET} \times 10^{18}}\right)$$

with, C_W denotes as the surface concentration of tungsten (W^{6+} cations nm^{-2}); L_{WO3}, the loading amount of tungsten oxide (wt.%); 238.1 is the formula weight of WO_3; N_0, the Avogadro constant (6.023×10^{23}), and S, the specific surface area ($m^2\ g^{-1}$).

Fig. 2 shows the correlation of the surface concentration of the tungsten vs the ratio of the diffraction peak intensity of WO_3 to that of TS-1 (I_{WO3}/I_{TS-1}; 2θ: $34.17^o/23.04^o$) in various WO_3 loading. Based on this graph, the dispersion capacity of tungsten on the titanium silicalite support was evaluated to be 0.35 W^{6+} cations/nm^2, by extrapolating the straight line to get the intercept on the abscissa. Obviously, the dispersion capacity of a metal oxide, which relates to monolayer coverage of oxide at maximum value is refer to a critical value. Any value lower than this value, the oxide might become highly dispersed on the support, while at higher value results in the formation of its crystalline phase. For comparison, the dispersion capacity of the WO_3 on anatase by using the similar characterization and technique was reported to be 4.85 W^{6+}/nm^2 of TiO_2 [12], which comparable with dispersion capacity of the WO_3 on ceria, ca. 4.8 W^{6+}/nm^2 [13]. While on silica support, with the dispersion capacity of WO_3 was 0.5 W^{6+}/nm^2 [5]. On TS-1 support, the dispersion capacity of WO_3 is much lower than that of anatase and ceria supports, and near with the silica support, in which these supports have lower surface area (below 300 m^2/g). It seems to deduce that surface interaction between WO_3 with TS-1 is evidently different from that of WO_3 with anatase and ceria, but almost the same with WO_3 and silica. This might be due to the TS-1 has highly crystalline phase of TS-1, cause weak interaction with the metal oxide, taking into account to reduce the dispersion capacity of the supported metal oxides.

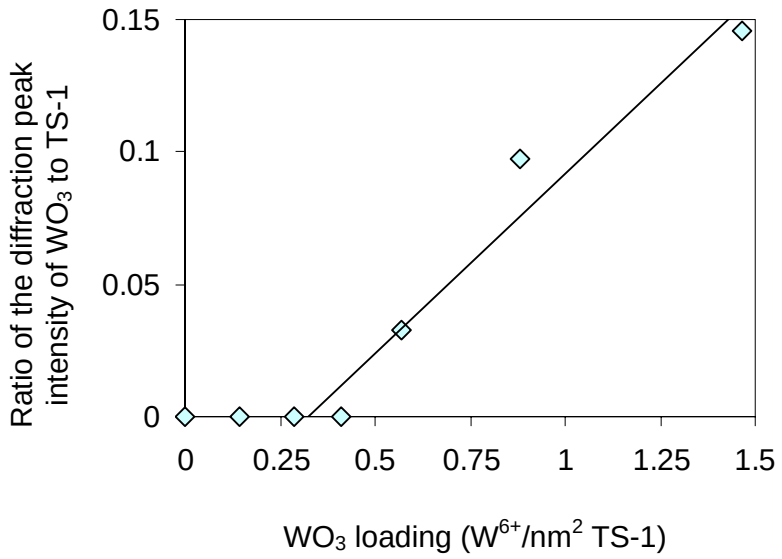

Fig. 2. The WO_3 content vs XRD peak intesity ratio of WO_3 to TS-1 in the samples

FTIR spectroscopy

Hydroxyl stretching region

The infrared spectra of the TS-1 and WO_3/TS-1 samples were recorded in the range of hydroxyl stretching region at 4000 –3000 cm^{-1}. The infrared spectra of all samples are shown in Fig. 3. The noise of the spectra is very high for sample with high tungsten loading, ca. >10wt% renders any other hydroxyls vibration detected in this region. After evacuation in vacuum at 400^oC for 4 hrs, the parent support, TS-1 sample shows an intense band at 3726 cm^{-1} and a broad band centered at 3505 cm^{-1}. A shoulder band also can be detected between those bands, centered at 3680 cm^{-1}. The higher frequency intense band at 3726 cm^{-1} is characteristics for silanol hydroxyl groups. However, the frequency of this band is slightly lowers with respect to the typical of amorphous silica (3741 cm^{-1}) [22]. The broad band at 3505 cm^{-1} associated to hydroxyl groups with hydrogen bonding of water molecule with silanol groups [22]. The last band (3680 cm^{-1}) has been assigned by Zecchina, et al. [23] to different structure of terminal hydroxyl groups in the zeolitic pores. After deposition of tungsten in the TS-1 sample, the hydroxyl region of the spectrum changed as can be seen in Fig. 3. The band position of TS-1 sample at 3726 cm^{-1} does not shifted to lower/higher frequency. However, this band become slightly broader with lower intensity compare to the TS-1 sample, were observed for the lower WO_3 loading, 2WO_3/TS-1, 5WO_3/TS-1 and 7WO_3/TS-1 samples. Similar phenomenon also appeared for a broad band at around 3505 cm^{-1}, although only observed for 2WO_3/TS-1 and 5WO_3/TS-1samples. For samples with high WO_3 loading, 10WO_3/TS-1, 15WO_3/TS-1 and 25WO_3/TS-1 samples, the isolated silanol peak is not displayed. While the peak for hydroxyl groups with hydrogen bonding started to disappear for 7WO_3/TS-1sample. These fact shows that both of the hydroxyl groups of TS-1 (silanol and hydrogen bonding) are involved in the reaction with tungsten, in which reactivity of the hydroxyl groups with hydrogen bonding is higher than that of silanol groups. In the previous study, Wang, et al. [5] found that only silanol groups involved in the reaction with tungsten. However, determination of the dispersion capacity by using hydroxyl groups has not been reported.

In the XRD technique, the dispersion capacity of the WO_3 on titanium silicalite support was evaluated using the crystalline WO_3 existed in the WO_3/TS-1 samples with high WO_3 loading, in which the peak intensities increases with the increasing of WO_3 loading was observed. On the other hand, using FTIR technique, the hydroxyl groups provided by WO_3/TS-1 samples with low amount of WO_3 loading is considered the important data to determine the dispersion capacity of WO_3 on the TS-1 support. It is found that the intensity of the hydroxyl groups decreases as the WO_3 loading increased, and disappear for WO_3/TS-1 samples at high WO_3 loading. Therefore, the dispersion capacity of the WO_3 on TS-1 is evaluated based on the decreasing in intensities of the hydroxyl groups in the samples of WO_3/TS-1. Fig. 4 shows the correlation of the tungsten surface concentration vs the peak area ratio of the silanol hydroxyl groups (3726 cm^{-1}) and the hydroxyl groups with hydrogen bonding (3505 cm^{-1}) to that of the framework TS-1 (1880 cm^{-1}) in the TS-1 and WO_3/TS-1 samples. The dispersion capacity of WO_3 on TS-1 support is determined by extrapolating the straight lines of the graph to get the intercept on the abscissa. The dispersion capacity of WO_3 on TS-1 based on the silanol hydroxyl groups evaluation is found to be 0.40 W^{6+}/nm^2 TS-1. This value is close with the dispersion capacity of WO_3 on TS-1 that is calculated by hydroxyl groups with hydrogen bonding, i.e. 0.38 W^{6+}/nm^2 TS-1. The dispersion capacity results by FTIR technique in the hydroxyl region are basically in agreement with that from XRD quantitative analysis.

Framework vibration region

FTIR spectra of the TS-1 and WO_3 containing TS-1 samples in the framework region at 1400-400 cm^{-1} are shown in Fig. 5. From the literature, the formation of WO_4^{2-} monomer gives a peak at 830 cm^{-1}, while for WO_3 dimer at 830 and 900 cm^{-1} [15]. Scheithauer, et al. [17], observed a broad W=O absorption band at 995 cm^{-1} in the spectrum of tungsten loaded zirconia sample with low tungsten loading and at around 1021 and 1014 cm^{-1} for high tungsten loading, in which these W=O stretching modes is not evident in our samples. According to Tsipis, et al. [18], the WO_3 species show peaks in the high-frequency normal modes in the region of 925-992 cm^{-1}

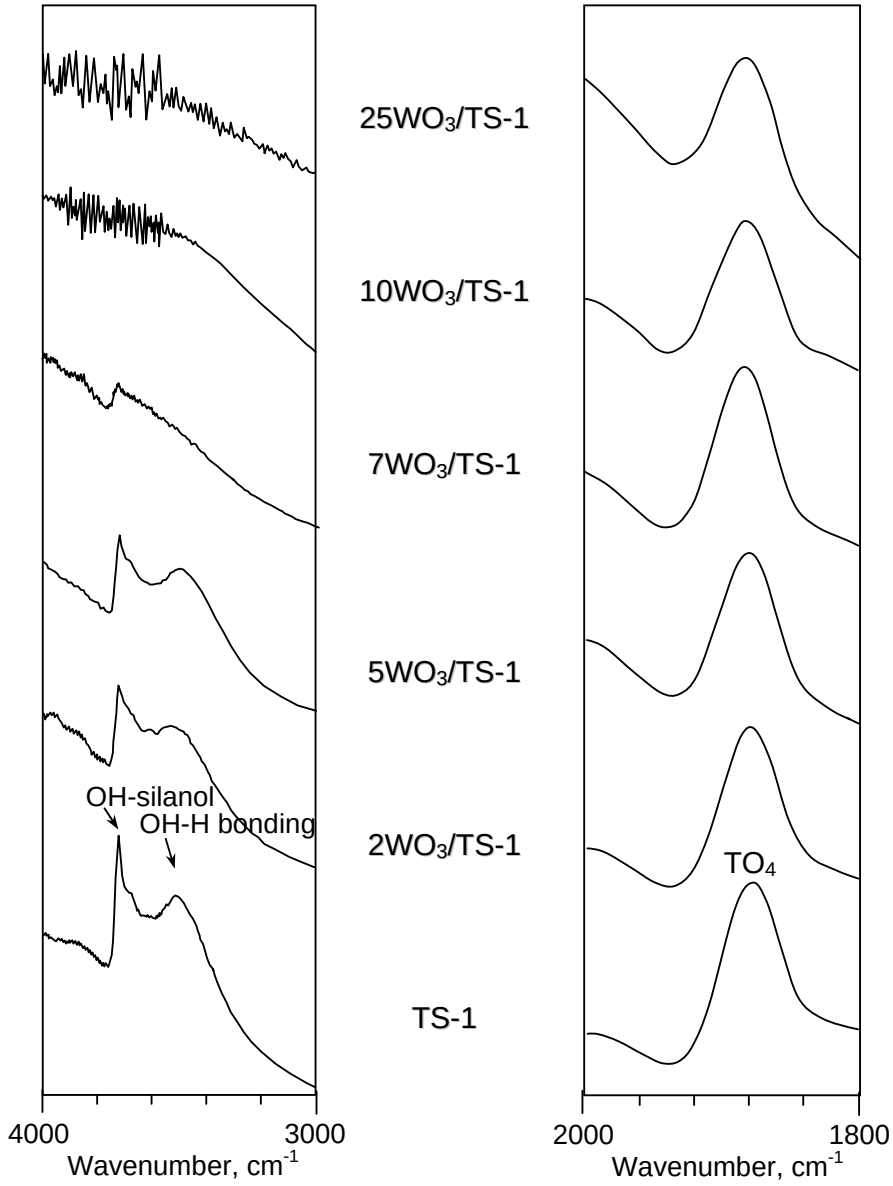

Fig. 3. Infrared spectra in the range of hydroxyl groups observation for titanium silicalite samples with different WO_3 content.

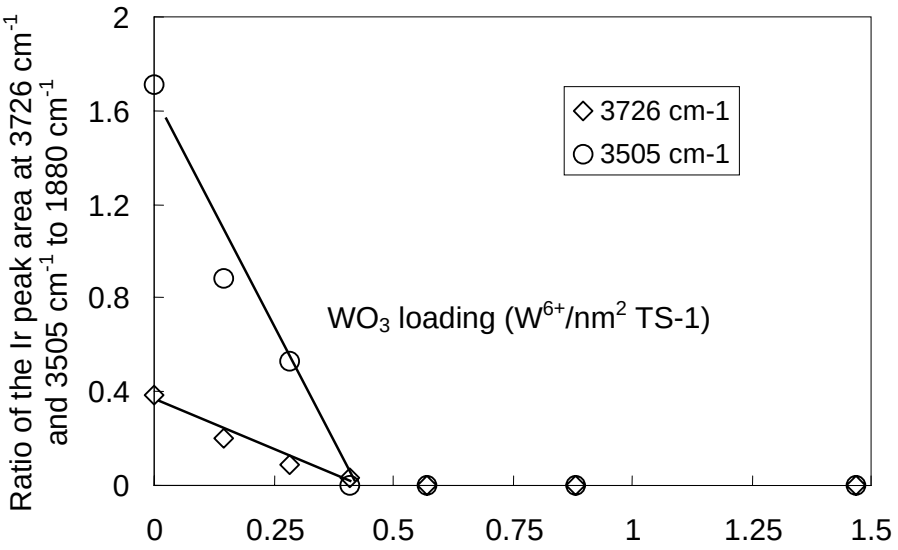

Fig. 4. The WO_3 content vs ratio of the IR peak area at 3726 cm^{-1} to 1880 cm^{-1} and 3505 cm^{-1} to 1880 cm^{-1} in the samples

assigned to *v*(W-O) stretching vibrations, while for the WO_4^{2-} (T_d) dianion show W-O-Na bending deformations at 862 and 835 cm^{-1}, *v*(W-O) stretching vibrations at 814 cm^{-1} and W-O stretching mode involving the triply bridged oxygen atom at 749 cm^{-1}. In this study, samples WO_3/TS-1 with WO_3 loading up to 7%wt gave similar spectra with that of the support TS-1. Such that no conclusive evidence for the presence of WO_3 with low WO_3 loading (2-7%wt) can be deduced. However, for higher WO_3 loading ca. 10-25%wt, a very small new peak at 873 cm^{-1} appeared and a peak at around 800 cm^{-1} shifted to the higher frequency at about 812 cm^{-1} for 25WO_3/TS-1 sample. The band at 873 cm^{-1} is interpreted as asymmetric stretching mode (triply degenerate) of tetrahedral WO_4^{2-} dianion [19]. This finding suggests that the WO_4^{2-} (T_d) dianion can only be monitored at high WO_3 loading. In addition, it is observed that the band in the region of 900-700 cm^{-1} becomes broader, which attributed to the presence of bulk WO_3. For the last three samples, 10-25WO_3/TS-1 exist both the surface tungsten oxide species and bulk WO_3 on the TS-1.

From the XRD data, it was found that the dispersion capacity of WO_3 on the TS-1 is 0.35 W^{6+}/nm^2, close to the 7%wt of WO_3. Similar to the XRD finding, the FTIR data provide important information regarding the formation of WO_4^{2-} dianion, i.e. the peak at 873 and 812 cm^{-1} and also the broad band in the region 900-700 cm^{-1}. Therefore, the dispersion capacity of WO_3 on the TS-1 can be determined using the framework vibration of these peaks. Because of the peak at 873 cm^{-1} is very small, while the peak at 812 cm^{-1} is exposed as shoulder band, it is difficult to measure the area under this peak. Accordingly, we utilize the area in the region 900-700 cm^{-1}, using the peak of T-O-T (T = Si or Ti) bending at around 548 cm^{-1} as a standard. The ratio of the infrared area of the peak in the region of 900-700 cm^{-1} to that of the peak at 548 cm^{-1} in the samples with various WO_3 loading as function of the loading amounts of tungsten is shown in Fig. 6. A linear relationship is found for the highly dispersed samples, as shown in line A. When the loading amounts of WO_3 is higher than its dispersion capacity, another straight line can be drawn, line B. The interception point of the two lines (A and B) occurs at 0.4 W^{6+} cations/nm^2, which corresponds to the dispersion capacity of WO_3 on the TS-1. This value is consistent with the result obtained from the hydroxyl stretching region, and not much different with respect to the XRD result. The evident of different slopes of line A and B (line A is lower than line B) could be understood by taking into consideration the differences on the dispersed states of the supported oxides. It is also found that the slightly increase of area ratio with the increase of

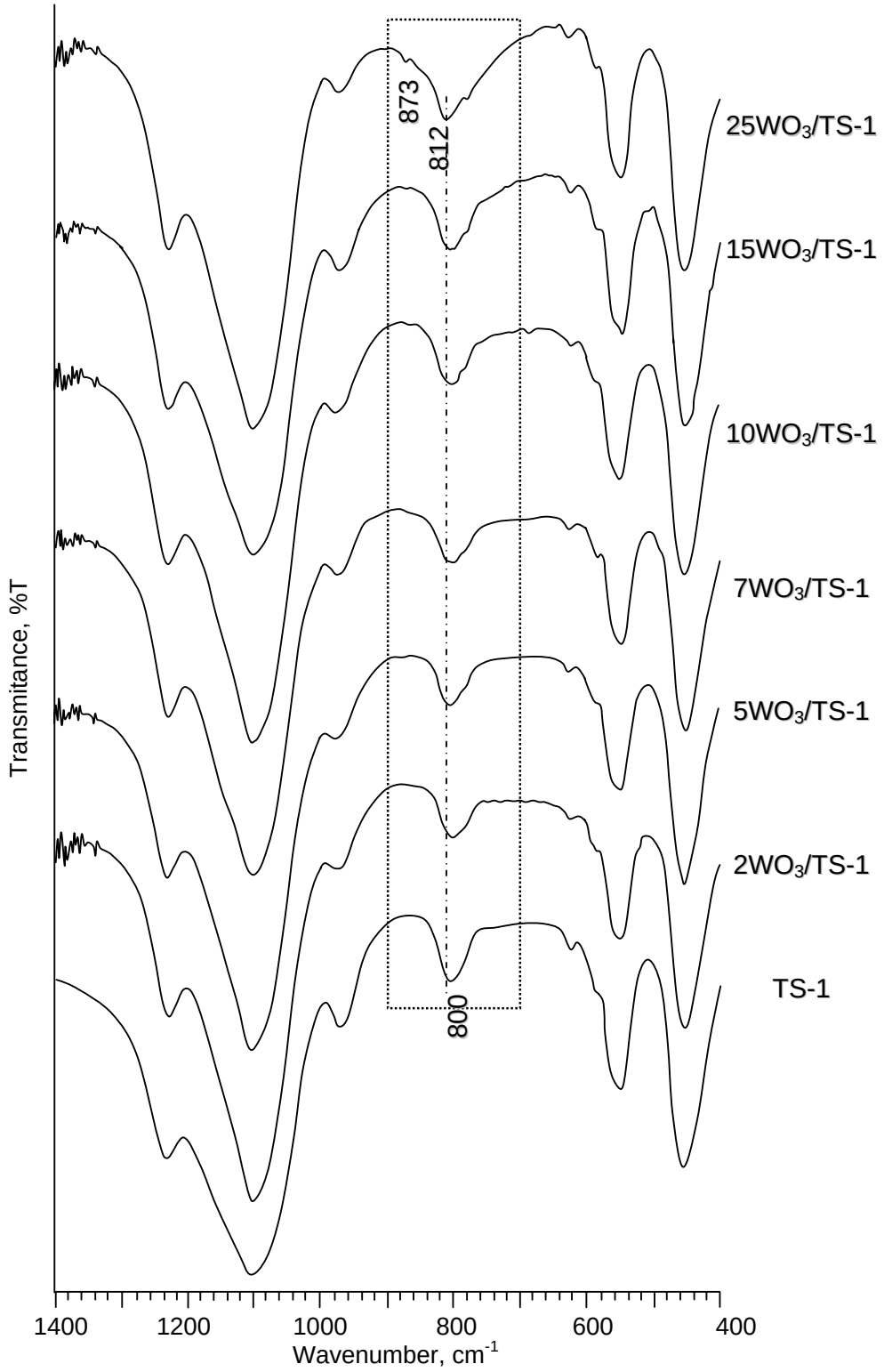

Fig. 5. The framework vibration of the TS-1 and tungsten-coated TS-1 samples

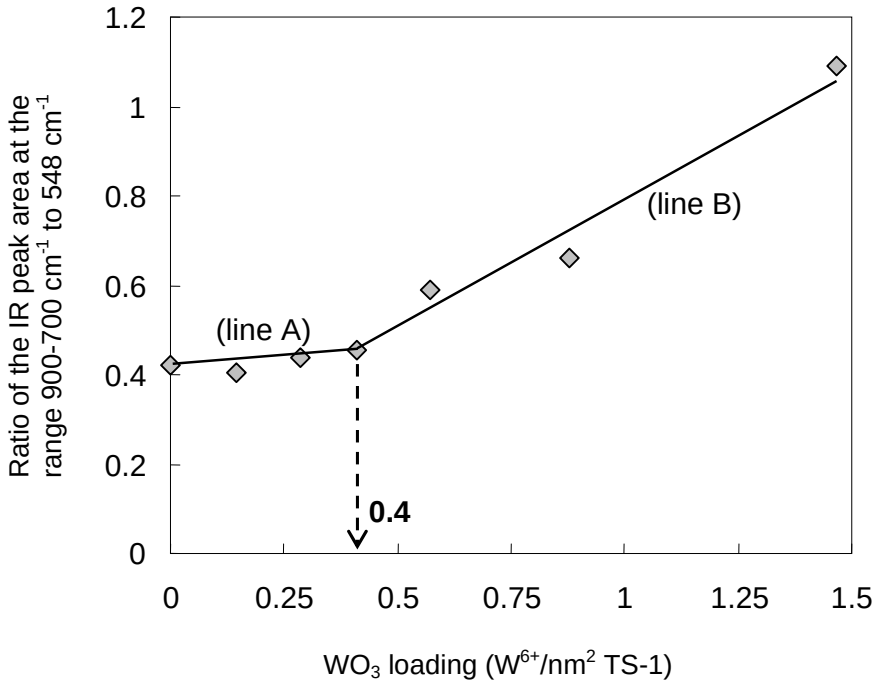

Fig. 6. The WO_3 content vs ratio of the IR peak area at the range 900-700 cm^{-1} to 548 cm^{-1} in the samples

tungsten loading for monolayer dispersion of the dispersed W^{6+} species, suggests that the formation of double layer is slow. The positive slope of the line A suggests that the WO_4^{2-} already formed in the samples with low WO_3 loading, although no peak can be detected in the FTIR spectra of the low WO_3/TS-1 samples.

4. Conclusions

The FTIR technique (hydroxyl and framework region) has proved to be an accurate method to determine quantitatively the monolayer dispersion of supported metal oxide. In this study, the dispersion capacity of WO_3 on the TS-1 by using two hydroxyls groups and framework region of FTIR method was found to be 0.40, 0.38, and 0.40 W^{6+}/nm^2 TS-1, respectively, which comparable to the XRD technique.

Acknowledgements
We gratefully acknowledge funding from The Ministry of Science Technology and Environment Malaysia, under IRPA grant no: 09-02-06-0057 SR0005/09-03.

References

[1] M. Niwa, J. Igarashi, Catal. Today 52 (1999) 71.
[2] N. Katada, J. Endo, K. Notsu, N. Yasunobu, N. Naito, M. Niwa, J. Phys. Chem. B. 104 (2000) 10321.
[3] M. Niwa, Y. Habuta, K. Okumura, N. Katada, Catal. Today 87 (2003) 213.
[4] Y. Habuta, N. Narishige, K. Okumura, N. Katada, M. Niwa, Catal. Today 78 (2003) 131.
[5] Y. Wang, Q. Chen, W. Yang, Z. Xie, W. Xu, D. Huang, Appl. Catal. A: General 250 (2003) 25.
[6] D. Jiang, B. Zhao, Y. Xie, G. Pan, G. Ran, E. Min, Appl. Catal. A: General 219 (2001) 69.
[7] J. Kijenski, P. Winiarek, T. Paryjczak, A. Lewicki, A. Mikolajska, Appl. Catal. A: General 233 (2002) 171.

[8] M. Scheithauer, R. K. Grasselli, H. Knozinger, Langmuir 14 (1998) 3019.
[9] D. G. Barton, S. L. Soled, G. D. Meitzner, G. A. Fuentes, E. Iglesia, J. Catal. 181 (1999) 57.
[10] J. Ramýrez, A. G. Alejandre, J. Catal. 170 (1997) 108.
[11] X. Wang, B. Zhao, D. Jiang, Y. Xie, Appl. Catal. A: General 188 (1999) 201.
[12] B. Xu, L. Dong, Y. Fan, Y. Chen, J. Catal. 193 (2000) 88.
[13] L. Dong, Y.Hu, F. Xu, D. Lu, B. Xu, Z. Hu, Y. Chen, J. Phys. Chem. B 104 (2000) 78.
[14] M. Shen, Y. Hu, H. Zhu, T. Liu, S. Wei, L. Dong, Y. Chen, J. Colloid and Interface Science 257 (2003) 408.
[15] G. Ozin, S. Oskar, J. Phys. Chem. 94 (1990) 7556.
[16] S. Damyanova, P. Grange, B. Delmony, J. Catal. 168 (1997) 421.
[17] M. Scheithauer, T. K. Cheung, R. E. Jentoft, R. K. Grasselli, B. C. Gates, H. Knozinger, J. Catal. 180 (1998) 1.
[18] A. C. Tsipis, C. A. Tsipis, J. Phys. Chem. A 104 (2000) 859.
[19] C. Lau, S. Brück, H. -J. Mai, U. Kynast, Microporous Mesoporous Mater. 47 (2001) 339.
[20] S. Eibl, B. C. Gates, H. Knozinger, Langmuir 17 (2001) 107.
[21] M. Taramasso, G. Perego, B. Notari, US Patents (1983) No. 4,410,501.
[22] E. Astorino, J. B. Peri, R. J. Willey, G. Busca, J. Catal. 157 (1995) 482.
[23] A. Zecchina, S. Bordiga, G. Spoto, L. Marchese, G. Petrini, G. Leofanti, M. Padovan, J. Phys. Chem. 96 (1992) 4991.

Proceeding of the Annual Fundamental Science Seminar 2004 (AFSS2004), pg. 207-216

Proceeding of the Annual Fundamental Science Seminar 2004 (AFSS2004), pg. 207-216

Wong Kah Man (2004). M.Sc (Chemistry). UTM

Title of thesis : Modification of Zeolite Beta as Base Catalyst: Characterization and catalytic study

Name : Wong Kah Man

ABSTRACT

Zeolites are well known as acid catalysts. However, zeolites do have base sites and capable of catalyzing reactions, in which its base properties is not widely explored. Studies on base zeolites were focused mainly on faujasites types zeolite (Si/Al = ~2.5) due to its high aluminum content. In this study, zeolite Beta (Si/Al = ~13) was chosen due to its high thermal stability and large pore property as faujasite that desirable for catalyst modification and catalytic activity. Zeolite Beta was modified by 3 method; alkali metal cations (Na^+, K^+, Cs^+) exchange, incorporation of alkali metal through wet impregnation, and alumination methods, in order to create and enhance the basicity in zeolite Beta. XRD, IR and nitrogen adsorption were carried out to study the structural properties of zeolite Beta after the modifications. Whereas, the acid-base properties were investigated by TPD, where NH_3 and CO_2 were use as probes for acidity and basicity studies, respectively. Results showed the decrease in relative crystallinity in zeolite Beta after modifications. Alkali metal impregnated samples turned into amorphous at Na^+ and K^+ loading of > 6%w/w, whereas cesium impregnated sample retained its crystallinity. In basicity study, insignificant increment in basicity was obtained by ion exchange method. However the acidity of the sample were suppressed significantly after this modification. On the other hand, a higher basicity was obtained through impregnation and alumination methods. The acid-base properties and catalytic performance of these base zeolites were tested on aldol condensation of propanal and dehydration-dehydrogenation of cyclohexanol. The exchanged samples yielded lower selectivity of 2-methyl-2-pentenal in aldol reaction. Rather than basicity, acidity was found to be the main factor in catalyzing this reaction. However, for dehydration-dehydrogenation of cyclohexanol, the selectivity of cyclohexanone that produced through base sites was increased with the increase in basicity. Nevertheless, cyclohexene was still the domain product that obtained through acid catalyzed reaction. This indicates the favorable of the catalysts at acid sites in this reaction. Thus, the obtained modified zeolite Beta showed the present of conjugated acid-base pairs, in which acting as bifunctional catalysts in catalyzing dehydration-dehydrogenation of cyclohexanol at both sites.

Chew Ann Nee (2005). Thesis Projek Sarjana Muda. UTM

Title of thesis : Modification of Zeolite Beta as Base Catalyst: Characterization and catalytic study

Name : Chew Ann Nee

ABSTRACT

Zeolites are important solid acid catalysts and have wide applications in chemical industries. However, few works had been done to study the basicity of zeolites. In this study, the base property of zeolite Beta was explored due to its large pore size and high thermal stability. Zeolite Beta (SiO_2/Al_2O_3 = 20 and 50) was synthesized from rice husk ash by using hydrothermal method. Characterization by XRD and IR confirmed the formation of zeolite Beta. The as-synthesized zeolite, NaBEA-20 and commercial zeolite Beta in NH_4^+ form were modified to their base properties by using ion- exchange method. They were modified to potassium, KBEA-20 and sodium form, com-NaBEA, respectively. Elemental analysis of the modified samples showed 40.23% of Na^+ ions had been successfully exchanged to K^+ ions in KBEA-20. XRD results revealed the retaining of the framework structure after the ion exchange process. The reactivity of zeolite Beta samples as base catalyst was tested in the nitroaldol condensation of nitroethane by 4-chlorobenzaldehyde. The products formed after 24 hours of reaction were analyzed by GC and identification of the product was done by GC-MS. Analysis of GC showed that 1-(4-chlorophenyl)-2- nitropropene was the main product. The as-synthesized zeolite Beta, NaBEA-20 showed the highest conversion (46.62%) whereas the reaction catalyzed by KBEA-20 was more selective towards the product (62.16%). In comparison with NaBEA-20, the reaction catalyzed by com-NaBEA showed the highest selectivity (98.75%). This is due to the large amount of Na^+ ions present in the commercial NaBEA sample.

Proceeding of the Annual Fundamental Science Seminar 2003, pg. 96-102

ZEOLITE AS BASE CATALYST: PREPARATION AND CHARACTERIZATION OF ZEOLITE BETA ION-EXCHANGED WITH ALKALINE METAL CATIONS.

Zainab Ramli, Abdul Rahim Yacob and Wong Kah Man

Department of Chemistry, Faculty of Science, Universiti Teknologi Malaysia, 81310 UTM Skudai, Johor, Malaysia.
Tel.: 07-5534491 Fax: 07-5566162
Email: zainab@kimia.fs.utm.my

ABSTRACT

The preparation of basic zeolite beta was carried out by ion-exchanged of the zeolite beta in hydrogen form, H-BEA (SiO_2/Al_2O_3=25) with alkaline metal cations of Na^+, K^+ and Cs^+. The crystallinities of the samples were monitored by XRD and FTIR, while the basicity was tested on a model base-catalyzed reaction, i.e. aldol condensation of propanal. Results showed that crystallinity decreased slightly in the order of $Na^+ > K^+ > Cs^+$. Structural IR spectra of the samples detected a band at 950 cm^{-1} in all the samples, indicating the presence of occluded alkaline metal oxides at the defect sites. This was confirmed by the decreased in the intensities of the silanol terminal/defect sites of the framework. The prepared K-Beta was tested on the aldol condensation reaction and it proved to be an effective base catalyst in this reaction where it shows a high conversion of propanal (60%) with 70% product selectivity of 2-methyl-2-pentenal.

1.0 INTRODUCTION

Very intensive studies on the acidic nature of zeolites have been done and an enormous number of data has been accumulated. On the other hand, a growing interest for the basic sites in zeolites is being observed due to their applications in catalysis and adsorption.

The origin of the basicity in zeolite framework [1-4] is due to the oxygen atoms of zeolite framework that derived from alumina tetrahedra. The average oxygen charge, which is known as intrinsic basicity increased with the increasing in Al content and the ionic radius of the alkali cation balancing. This can be achieved, respectively, by preparing a lower Si/Al ratio zeolite and by ion-exchanging the cation balancing in the zeolite framework, with a larger radius of alkali cation [3,5-7].

The existence of basic sites in alkali exchanged zeolites has been postulated where the framework oxygen atoms of zeolites behaving as Lewis basis sites. These zeolites do not show any Brönsted basicity. The average charge on the oxygen atoms, which determines the site strength, can be calculated based on the Sanderson electronegativity equalization principle [3,8].

Recent studies have reported that the basicity in zeolite can be increased by having an excess alkali in the framework. This can be achieved by introducing a basic guest into the zeolite framework, either by impregnation method or through metal vapors decomposition method [3]. Not much work has been done in preparing a basic zeolite. Several works have been carried out to prepare a basic site in zeolite X and Y and have shown encouraging results as base catalyst. The greatest challenge in preparing a basic zeolite is the low resistant of the framework structure towards the basicity. The destruction of zeolite framework that easily occurs during calcination is due to the hydrolysis of the Si-O-Al bonds.

Zeolite beta, which has potential as catalyst in the petrochemical industry, has been reported to possess a basicity which is stronger than that expected from its chemical composition and to exhibit base-catalyzed activity [3,9]. In this work, an attempt to prepare a basic zeolite beta has been carried out by ion-exchanged of the zeolite beta in hydrogen form, H-BEA with various alkaline metal cations (Na^+, K^+ and Cs^+). XRD and FTIR have been used for structural studies, while the effectiveness as basic catalyst has been tested on the aldol condensation of propanal with the exchange K-Beta.

2.0 EXPERIMENTAL

2.1 Catalysts Preparation

The zeolite Beta with SiO_2/Al_2O_3=25 in ammonium form (Zeolyst) was used as a starting material. The NH_4-Beta was calcined to decompose the ammonium and changed it the hydrogen form at 450°C for 7 h. After calcination, the hydrogen form, H-Beta, was used as the parent material for ion-exchanged with various alkali metal cations.

Na-Beta, K-Beta and Cs-Beta were prepared by ion-exchanging the H-Beta in 1.0 M solution of sodium acetate, potassium nitrate and cesium acetate, respectively, at 80°C overnight, using a liquid to solid ratio of 10. The ion-exchange procedures were repeated 6 times in order to have the maximum exchanged. The exchanged samples were filtered, washed and dried overnight at 100°C.

2.2 Characterizations

Structural characterization was performed by XRD and FTIR. Diffractograms of the samples were recorded using D500 Siemens Kristalloflex X-ray diffractometer with $CuK\alpha_1$ as the radiation source with λ = 1.5418 Å at 40 kV and 30 m, in the range of 2θ of 2° to 60° at room temperature with step time of 0.02°. The FTIR spectra were recorded at room temperature with 4 cm^{-1} resolutions between 1400-400 cm^{-1} by using FTIR Perkin Elmer 1600 series.

The IR spectra of hydroxyl groups for the exchanged zeolite beta were recorded on the FTIR Shimadzu 8000 series. Self-supported wafers (~10 mg) were heated at 400°C under vacuum for 2 h. The spectra were then recorded at room temperature in absorbance mode with 2 cm^{-1} resolutions.

2.3 Catalytic Reaction

Aldol condensation of propanal was chosen as a model base-catalyzed reaction by using K-Beta as catalyst. The catalyst was first activated at 500°C in the flow of N_2 The reaction was carried out in a stainless steel autoclave, where the activated K-Beta (0.35 g) was added into the freshly distilled propionaldehyde (5mL) and heated in an oven at 140°C for 2h. A blank study has also been done, where the reaction was performed without the presence of zeolite at the same condition as stated above. The product obtained was analyzed by a Gas Chromatography-FID Hewlet-Packard 6890 Series using Ultra-1 column and Hewlet-Packard GC-MSD using HP5 column for product identification.

3.0 RESULTS AND DISCUSSION

3.1 Structural caharacterization

The X-ray diffraction patterns of the exchanged zeolite beta samples are presented in Fig. 1. All samples exhibit similar diffraction pattern to that of the parent zeolite beta (Fig. 1(a)), where is the typical phases for zeolite beta, as reported by Pariente et.al. [10]. Both intense peaks at 2θ 7.8° and 22.5° are assigned to the d_{001} and d_{302}, respectively, where the broad peaks at 2θ 7.8° is the characteristic peak for the faulted structure, while the sharp peak at 2θ 22.5° is due to the tetragonal and monoclinic symmetry structure of zeolite beta [11-12]. The presence of all diffractions peaks for each sample indicates that the framework structure of zeolite beta is retained after ion exchanging with alkaline metal cations of Na^+, K^+ and Cs^+. However it is observed that the intensity of the diffraction peaks of the exchanged samples decreased successively from parent sample H-Beta to Na-Beta, K-beta and Cs-Beta. This indicates that the deterioration of the crystal structure of zeolite beta has occurred when the exchanged involves cations of larger size.

Fig. 2 shows the crystallinity curves for the exchanged samples. The relative crystallinity was evaluated from the intensity of the most intense reflection XRD peak (302) appeared at 2θ = 22.4° of each sample relative to the similar peak in the parent H-beta sample. The crystallinity of zeolite beta decreased with the increase of size and the electropositive chararacter of alkali metal cations, in the order of Na^+<

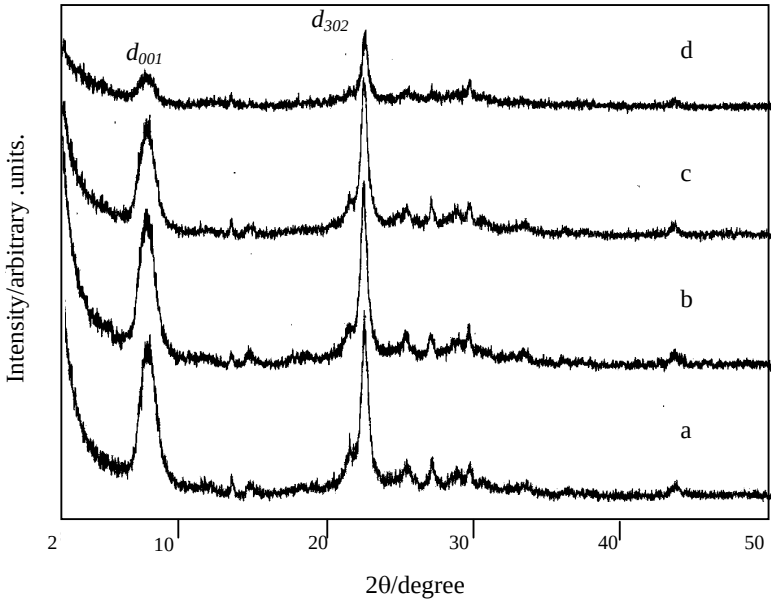

Fig. 1: X-ray diffraction patterns of the exchanged zeolite beta: (a) H-Beta, (b) Na-Beta, (c) K-Beta (d) Cs-Beta.

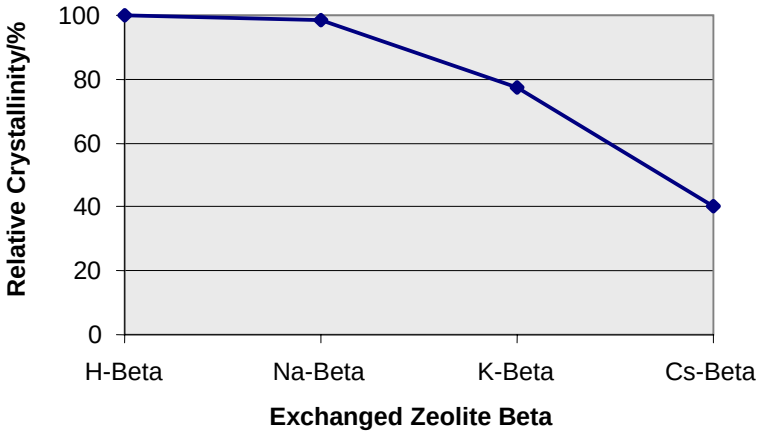

Fig. 2: Relative cystallinity of the exchanged zeolite beta.

$K^+ < Cs^+$. It was suggested that the decreased in the crystallinity is due to the strong interaction of the cation with the oxygen atom of the alumina tetrahedral in the zeolite framework. As the electropositive characteristic of the cations increased from Na^+ to Cs^+, stronger interaction of the cations with the oxygen atoms of the alumina tetrahedra is expected, thus weaken the bond of the oxygen with the rest of zeolite framework. It then explained the decrease of about 60% of the crystallinity of Cs-Beta compared to the parent H-Beta.

The IR spectrums of the exchanged zeolite beta samples are shown in Fig. 3. There are several typical bands that can be observed in the spectrums for all the samples. The bands in the region of 1250 – 1200 cm^{-1}, 1100 – 1050 cm^{-1} and 800 – 750 cm^{-1} are assigned to the external asymmetric stretching, internal asymmetric stretching and symmetric stretching of TO_4 (T=Si, Al) respectively. The double 6-membered ring and double 4-membered ring vibrations that can be observed respectively at 570 – 560 cm^{-1} and 520 – 510 cm^{-1} indicate the framework structure of zeolite. Meanwhile, band at around 462 cm^{-1} is assigned to the T-O bending. All the peaks that corresponds to the IR spectra of zeolite beta as reported by Perez-Pariente et al. [10] can be observed in all the exchanged samples.

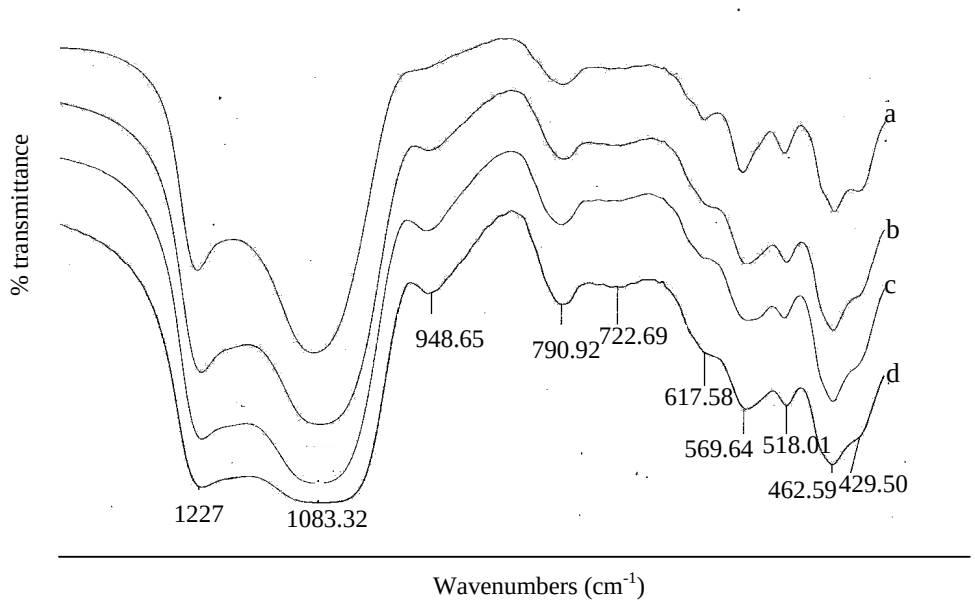

Fig. 3: IR spectra of the exchanged zeolite beta: (a) H-Beta, (b) Na-Beta, (c) K-Beta, (d) Cs-Beta.

However, a band at ~950 cm^{-1} was detected in all the exchanged samples. This band is suggested to attribute to the vibration of Si-O-M (M=other elements). In siliceous zeolite, this band is assigned to the vibration Si-O- of silanol at the defect sites. The band is not significantly observed in the parent H-Beta zeolite, indicating that the sample contains only a small amount of the defect sites. However this band is significantly observed in all samples of the exchanged zeolite beta. There are two possibilities of the presence of this band in the samples. First, it might constitute of silanol at the defect sites, which indicate of the deterioration of the framework structure. This is in agreement with the results obtained from the XRD i.e. the crystallinity decreased in the exchanged zeolite beta samples. However, peaks assigned to the double ring vibration at ~ 569 cm^{-1} and ~ 518 cm^{-1}, which are sensitive to the framework changes remain the same in term of intensity, showing that the framework are still intact. The second possibility is, the band could be due to the occluded alkaline metal oxides at the defect sites. This suggestion is based

on the results obtained for TS-1 (Ti-silicalite) in which the band is attributed to the vibration of SiOH-(OH)Ti defective sites [16].

In order to confirm this, the spectrums of the IR of the dehydration samples after heated at 400^{o}C in vacuum to remove the zeolitic water, were taken. Figure 4 shows the IR spectrums of the dehydrated exchanged zeolite samples in the OH stretching region. The vibration band at 3743 cm^{-1}, which is assigned to the O-H of silanol group, is clearly observed in H-Beta. However, the intensity of this band decreased with the increase of the size of the cations in the exchanged zeolite beta samples. This suggests that besides the ion-exchange process which occurred at the oxygen vicinity of the alumina tetrahedral framework, some of the alkaline metals might have exchanged with the silanol at the defect sites and occluded at this sites, causing the decrease in the intensity of the silanol group. This observation then supports the results from the structural IR sprectrums of the exchanged samples in which the band at ~ 960 cm^{-1} is most probably due to vibration of the occluded alkaline metal oxides. Since Cs^{+} has the largest size than Na^{+} and K^{+} most of the cations prefers to occupy the defect sites rather than the normal ion-exchanged process in the narrow channels of the zeolite framework. This explained the missing band of the OH silanol group in Cs-Beta sample. Other bands appeared in the samples are assigned to Si–(OH)–Al groups in the framework (3606.6 cm^{-1}), and the hydroxyl group that bonded with the extraframework aluminium (3668.4 cm^{-1}). A small band near ~3780 cm^{-1} is only observed in parent H-Beta. This band is assigned to the isolated extra-framework $AlOOH^{+}$ species [13-15].

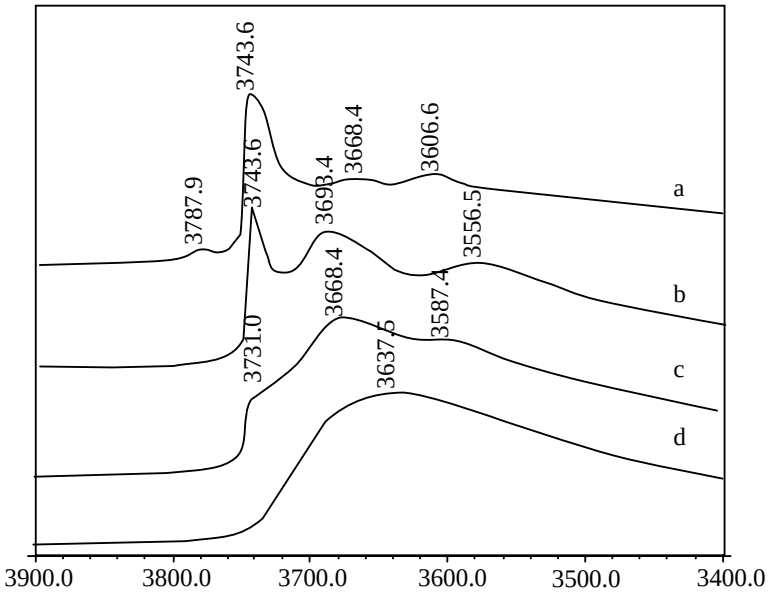

Fig. 4: IR spectra of the exchanged samples after heated at 400°C for 2 h under vacuum: (a) H-Beta, (b) Na-Beta, (c) K-Beta, (d) Cs-Beta.

3.2 The aldol condensation of propanal.

The aldol condensation of propanal proceeds in the presence of base catalyst. The reaction is shown in the following reaction.

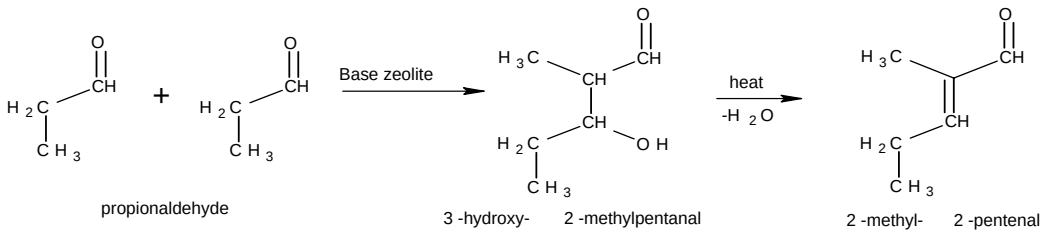

The product obtained from the catalytic experiment has been identified as 2-methyl-2-pentenal by using GC-MS. Figure 5 shows the result of the aldol condensation reaction that obtained from GC-FID. By using K-Beta as basic catalyst, the conversion of propionaldehyde has increased to about 10-fold (i.e. 60.26%) with a high product selectivity (~70%). This selectivity is comparable to the reaction that undergo without the presence of K-Beta

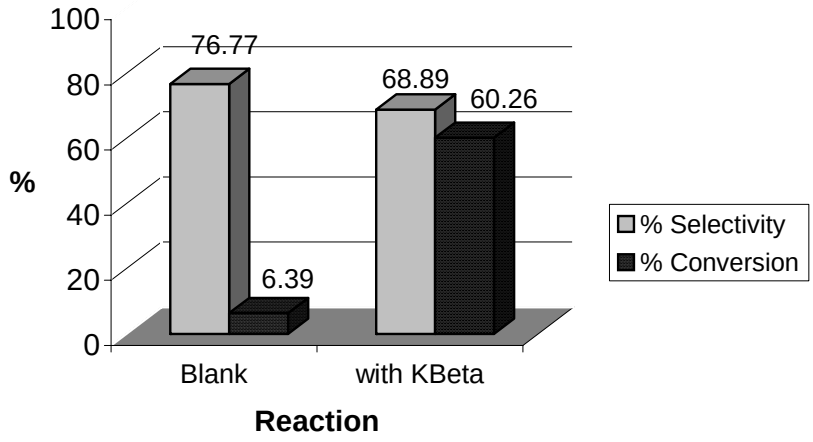

Fig. 5: Selectivity and conversion in aldol condensation of propanal.

4.0 CONCLUSION

Zeolite beta prepared by ion exchange with alkaline metal cations has shown basic character. The exchanged K-Beta has proven to be a basic catalyst in which it catalysed aldol condensation of propanal, giving a significant increased in the conversion and product selectivity. Characterization on Na-Beta, K-Beta and Cs-Beta has shown that the crystallinity of the zeolite beta decreased with the increase in the size of the exchange alkaline metal cations. Besides ion exchange process, some of the metal cations were occluded in the defect sites of zeolite beta framework.

ACKNOWLEDGEMENT

The authors would like to thank Ministry of Science, Technology and Environment, Malaysia for financial support under IRPA vot. 74507.

REFERENCES

1. K. Tanabe, Academic Press Inc: UK, (1970) 78.
2. Y. Ono, *Stud. Surf. Sci. Catal.*, **5** (1980)19.
3. D. Barthomeuf, *Catal. Rev. Sci. Eng*., **38** (1996) 521.
4. J. Zhu, Y. Chun, Y. Wang and Q. Xu, *Catal. Today*, **51** (1999) 103.
5. J. Weitkamp, M. Hunger and U. Rymsa, *Microporous and Mesoporous Material*s, **48** (2001) 255.
6. G. Martra, R. Ocule, L. Marchese, G. Centi and S. Coluccia, *Catal. Today*, **73** (2002) 83.
7. U.D. Joshi, P.N. Joshi, S.S. Tamhankar, V.V. Joshi, C.V. Rode, and V.P. Shiralkar, *Applied Catalysis A: General*, **6215** (2002) 1.
8. C.O. Veloso, J.L.F. Monteiro and E.F. Sousa-Aguiar, *Stud. Surf. Sci. Catal*., **84** (1994) 1913.
9. C. Yang, J. Wang and Q. Xu, *Microporous Materials*. **11** (1997) 261.
10. J.P. Pariente, J.A. Martens and P.A. Jacobs, *Applied Catalysis*. **31** (1987). 35.
11. J.B. Higgins, R.B. LaPierre, J.L. Schlenker, A.C. Rohrman, J.D. Wood, G.T. Kerr and W.J. Rohrbaugh, *Zeolites*. **8** (1988) 446.
12. X. Zaiku, Q.L. Chen, B. Chen and C.F. Zhang, *Crystal Engineering*. **4** (2001) 359.
13. M.A. Camblor, A. Corma, and S. Valencia, *Microporous and Mesoporous Materials*. **25** (1998) 59.
14. P.J. Kunkeler, B.J. Zuurdeeg, J.C.V.D. Waal, J.A.V. Bokhoven, D.C. Koningsberger and H.V. Bekkum, *J. Catal*., **180** (1998) 234.
15. D. Prasetyoko, Thesis of master. UTM: Malaysia. (2001).
16. D. Scarano, A Zecchina, S. Bordiga, F. Geobaldo, G. Spoto, G. Petrini, G. Leofanti, M. Padovan and G. Tozzola, *J. Chem. Soc. Faraday Trans*. **89** (1993) 4123

LIST OF PUBLICATION AND THESES

PUBLICATIONS

1. Zainab Ramli, Mazidah Abdul Shukor and Didik Prasetyoko (2006) "Bifunctional Nb/Ti-Mcm-41 Catalyst in Oxidative Acidic Reaction of Cyclohexene To Diols" – *Malay. J. Anal. Sci*., in press.

2. Zainab Ramli, Noor Aishikin Mohd Yusoff and Halimaton Hamdan (2006) "Delaminated Zeolite, ITQ-6 as Heterogeneous Catalyst For Friedel Crafts Alkylation" – *Malay. J. Anal. Sci*., in press

3. Didik Prasetyoko, Zainab Ramli, Salasiah Endud, Halimaton Hamdan, Bogdan Sulikowski, (2006) Conversion of rice husk ash to zeolite beta", *Waste Management* , 26 , 1173-1179

4. Didik Prasetyoko, Zainab Ramli, Salasiah Endud, Halimaton Hamdan, Bogdan Sulikowski (2006) Synthesis of Zeolite Beta Directly from Rice Husk Ash: Effect of Reaction Composition on Crystallinity of Zeolite Beta, *Indo. J. Chem*., 6(1),11-15

5. Didik Prasetyoko, Zainab Ramli, Salasiah Endud and Hadi Nur (2005) Niobic Acid Dispersed on the Surface of TS-1: Acidity Atudy, Acta Kimia Indonesia., 1(1)11-16.

6. Aiman Najati Akmar Rahman, Zainab Ramli and Farediah Ahmad (2005) "Isomorphous substitution of Gallium into Zeolite Beta of Rice Husk Ash" *Buletin Kimia* . 21 (1&2) 39 40

7. Didik Prasetyoko, Zainab Ramli, Salasiah Endud and Hadi Nur, (2005) Enhancement of Catalytic Activity of Titanosilicalite-1 – Sulfated Zircona

Combination Towards Epoxdation of 1-Octene With Aqueous Hydrogen Peroxide , React. *Minect. Catal. Lett*., 86(1), 83-89

8. Didik Prasetyoko, Zainab Ramli, Salasiah Endud and Hadi Nur (2005) "TS-1 Loaded with Sulfated Zirconia as Bifunctional Oxidative and Acidic Catalyst for the Transformation of 1-Octene to 1,2-Octanediol, *J. Mol Catal.* 241, 118-125

9. Wong Kah Man, Zainab Ramli and Hadi Nur (2005) "Effect of Loaded Alkali Metals on the Structural, Basicity and Catalytic Activity of Zeolite Beta", *Jurnul Teknologi C:* Sains and Matematik, No. 42, 43-55.

10. Didik Prasetyoko, Zainab Ramli, Salasiah Endud and Hadi Nur (2005). "Preparation and characterization of bifunctional oxidative and acidic catalysts Nb_2O_5/TS-1 for synthesis of diols". *Material Chemistry and Physics.* 93, 443-449

11. Didik Prasetyoko, Zainab Ramli, Salasiah Endud and Hadi Nur (2005) "Structural and Superacidity Study of Bifunctional Catalyst, Sulfated-Titanium/TS-1" *Malay. J. Chem.*, 7(1) 11- 18

12. Hadi Nur, Didik Prasetyoko, Zainab Ramli and Salasiah Endud "Sulfation: A simple method to enhance the catalytic activity of TS-1 in epoxidation of 1-octene with aqueous hydrogen peroxide" "*Catalysis Communication*" 5 (2004), 725-728 .

13. Didik Prasetyoko, Zainab Ramli, Hadi Nur and Salasiah Endud (2004) " A new Approach to Probe the Dispersion Capacity of Tungsten Oxide on the Surface of Titanium Silicalite by Infra Red" Proceeding of the 2nd Annual Fundamental Science Seminar 2004 AFSS 2004, pg 207-216

14. Wong Kah Man, Hadi Nur, Abdul Rahim Yacob, and Zainab Ramli (2004) " The Basicity and Acidity of Beta Zeolites after Ion exchanged with Alkali Metal

Cations: A Physicochemical Characterization" '*Physic J. of Indonesian Physical Society'* Vol A7, 0211 to 211-6

15. Hadi Nur, Didik Prasetyoko, Zainab Ramli and Salasiah Endud. 2004 "Enhancement Of Catalytic Activity Of TS-1 Catalyst In Epoxidation Of 1-Octene With Aqueous Hydrogen Peroxide By Sulfation. The proceedings of the 3rd Hokaido Indonesian student association scientific meeting, Sapporo. Japan, , 130-133.

16. Zainab Ramli and Hasliza Bahruji (2003), "Synthesis of ZSM-5 Type Zeolite using Crystalline Silica of Rice Husk Ash", *Malay. J. Chem*. 5(1) 48-55.

17. Zainab Ramli, Abdul Rahim Yacob and Wong Kah Man. (2003) "Structural and Basicity Studies of Potassium Impregnated- Zeolite Beta" Proceeding of the Inetrnational Conference on the Advancement in Science and Technology, *i*CAST, pg. 111-113

18. Marzita Abd Mazak, Farediah Ahmad and Zainab Ramli "Effect Of SiO_2/Al_2O_3 Ratios Towards The Acidity and Activity of Zeolite Beta in Friedel-Crafts Reaction." – Proceeding of the AFSS 2003, 20-21 May 2003, JB. pg. 184-190

19. Zainab Ramli, Abdul Rahim Yacob and Wong Kah Man "Zeolite as Base Catalyst: Preparation and Characterization of Zeolite Beta Modified by Ion-exchanged of Alkaline Metal Cations" Proceeding of the AFSS 2003, 20-21 May 2003, JB pg. 96-102

20. Zainab Ramli, Halimaton Hamdan, Bogdan Sulikowski, Hasliza Bahruji "Effect of Molar Oxides Composition in the Synthesis of Ferrierite from Rice Husk Ash"- Proceeding of the AFSS 2003, 20-21 May 2003, JB pg. 147-152

21. Didik Prasetyoko dan Zainab Ramli (2003) “Analisis kumpulan hidroksil permukaan dan tapak asid zeolite beta daripada abu sekam padi dengan kaedah Spektroskopi FTIR: *Jurnul Teknologi C, No. 38*., 1-14.

22. Didik Prasetyoko, Salasiah Endud dan Zainab Ramli, (2002) “Analisis Struktur Zeolit Beta daripada Abu Sekam Padi: Kesan Suhu Pengkalsinan, *Buletin Kimia*, I8(2)

23. Didik Prsetyoko dan Zainab Ramli ‘Transformasi Abu Sekam Padi Kepada Zeolit Beta: Kaedah Alternatif Penentuan Kehabluran Menggunakan Analisis Terma (TGA-DTG), Paper accepted for publication in *Jurnul Teknologi C: Sains dan Matematik* (2000)

24. Zainab Ramli, Didik Prasetyoko, Salasiah Endud,(2002) Friedel-Crafts Acylation of Anisole Catalysed by H-Zeolite Beta of Crystalline Rice Husk Ash. *Jurnul Teknologi C*: 36, 41-54

THESES

1. Didik Prasetyoko (2006) Bifunctional oxidative and Acidic Titanium Silicalite (TS-1) Catalysts for One Pot Synthesis of 1,2-octenediol from 1-octene. Ph. D Tesis, UTM

2. Aiman Najati Akmar binti Rahman (2006) Gallium Modified Zeolite Beta for Friedel Crafts Alkylation of Resorcinol. M.Sc Thesis , UTM

3. Marzita Abd. Mazak (2006) “Modified Zeolite Beta as Catalysts in Friedel Crafts alkylation of Resorcino*l*. M.Sc Tesis, UTM

4. Hasliza binti Bahruji (2005) Synthesis of zeolite Ferrierite from Rice Husk Ash, Characterization and Activity Towards Friedel Crafts Acylation of Anisole with propyl anhydride M.Sc Thesis, UTM

5. Wong Kah Man (2004) Acid-base Properties of Modified Zeolite Beta: Modification, Characterization and Catalytic Testing. M.Sc Thesis, UTM

6. Nur Ain Binti Ibrahim (2007) Bifunctional Nb/Ti-ITQ6 Catalyst in Oxidative Acidic Reaction of Cyclehexane to Diol (Thesis PSM, UTM Skudai)

7. Azilia Hani Binti Abd Aziz (2007) Sintesis Prefer Untuk Zeolite ITQ-6 Daripada Abu Sekam Padi (Thesis PSM, UTM Skudai)

8. Siti Syazlina Alyssa Alias (2007) Synthesis of Zeolite P from Rice Husk Ash Using Different Mineralizing Agents as Anion Exchanger (Thesis PSM, UTM Skudai)

9. Mazidah Abdul Shukor (2006) Bifunctinal Nb/Ti-MCM-41 Catalyst of Oxidative Acidic Reaction of Cyclohexene to Diols. Thesis PSM, UTM.

10. Nur Hidayah Deris (2006) Sintesis Zeolit Beta daripada Abu Sekam Padi Sebagai Mangkin Asid Dalam Tindak Balas Pengalkilan Friedel-Crafts. Thesis PSM, UTM

11. Yeow Kian Wee (2006) Dihydroxylation of Butenol over Bifunctional Catalyst. Thesis PSM, UTM

12. Jasmie bin Marutai (2005) Sintesis zeolite Ferrierit daripada abu sekam padi sebagai mangkin asid dalam tindak balas pengalkilan Friedel Crafts. Thesis PSM, UTM

13. Aiman Najati Akmar Rahman (2004) Pengalkilan Dan Pengasilan Friedel-Crafts P-Kresol Bermangkinkan Zeolit Beta Bagi Menghasilkan Antioksida. Thesis PSM, UTM

14. Chong Kwok Feng (2004) Rietveld Refinement For Zeolite A And Ferrierite. (Thesis PSM, UTM Skudai)

15. Kwek Siang Sing (2004) Siliceuos Zeolite Beta: Synthesis, Characterization And Its Activities In Friedel-Crafts Acylation Of Anisole. Thesis PSM, UTM

16. Abdul Rahman bin Ali (2004) Sintesis Zeolit X Daripada Abu Sekam Padi dan Penggunaannya sebagai Penukar Ion. Thesis PSM, UTM

17. Tan Teck Yee (2003) Zeolit Beta Abu Sekam Padi: Sintesis, Pencirian dan Keaktifan Dalam Pengalkilan Anisol. Thesis PSM, UTM

18. Ng Yun Hau (2003) Simulasi Difraktrogram XRD Melalui Pendekatan Rietveld bagi Penentuan Struktur Hablur Zeolit P yang disintesis Daripada Abu Sekam Padi dengan Pelbagai Kation Pengimbang. (Thesis PSM, UTM Skudai)

29. Nurjannah Binti Jan (2003) Sintesis Zeolit X Secara terus daripada Abu Sekam Padi dan Penggunaan Sebagai Penukar Ion. Thesis PSM, UTM

20. Mohammad Fauzan Bin Esa (2003) Pengasilan Friedel Crafts Fenol Bermangkinkan Zeolit Beta daripada Abu Sekam Padi. Thesis PSM, UTM
- won 2nd place for best Thesis for Final Year Project Undergraduate awarded by ANALIS

21. Hasliza Binti Bahruji (2002) Synthesis of Zeolite ZSM-5 Using Crystalline Rice Husk Ash As Silica Source. Thesis PSM, UTM

CONCLUSIONS

This project has proved the reactivity of rice husk ash (RHA) as silica source for producing zeolites. Almost all kind of zeolites have successfully formed when using RHA as silica source. In this project zeolite P (small pore) zeolite ferrierite (FER), precursor of ferrierite (PREFER) (medium pore zeolite), zeolite Beta and zeolite X has have been synthesized in pure and highly crystalline form. The pure FER phase was obtained from gel compositions in the range of 1.31 – 1.5 Na_2O : Al_2O_3 : 10 – 30 SiO_2 : 4.0 – 10.0 Pyrrolidine : 410 H_2O with narrow range of SiO_2/Al_2O_3 ratios from 10 to 30. The stable FER was obtain in 4 days crystallization time at 200^oC, shorter than when using commercial silica source like fume silica, which usually take 8-12 days. Pure zeolite Beta phase is obtained from the oxide gel ratios of 1.9-8 Na_2O: Al_2O_3: 27-90 SiO_2: 5-20 TEA_2O: 240-800 H_2O at 150^oC for 7 days crystallization. Silicieous zeolite Beta (aluminium free) failed to obtain due to the presence of aluminium containment which facilitate the formation of Al-Beta. However gallosilicate zeolite Beta (aluminium free zeolite Beta containing gallium in the framework) has been successfully synthesized from hydrothermal synthesis at 135^oC with molar oxide composition of 6.0 Na_2O : 67 SiO_2 : Ga_2O_3 : 13.3 TEA_2O : 1000 H_2O. Another successful formation of zeolite PREFER was obtained from gel composition in the range of 10-60 SiO_2 : 0.5-1Al_2O_3 : 7.5-15NH_4F : 2.5-5HF : 10 (4-amino-2,2,6,6- tetramethylpiperidinr) : 50-100H_2O at 175^oC for 5 days crystallization time. For a small pore zeolite P can be formed in 1 days time at 100^oC using 6.0-6.2 Na_2O : Al_2O_3 : 8 SiO_2 : 112 H_2O gel composition. For half day crystallization time at the same temperature and composition will produced zeolite X or Y showing that zeolite X and Y are metastable zeolites which will transform to other phases. Another successfull attemp in producing zeolitic mesoporous zeolite Ti-PREFER and Ti-ITQ-6 amphasized the reactivity of rice RHA as silica source. In all cases the RHA must be in amorphous form.

In the reactivity of the prepared zeolites for the Friedel Crafts alkylation/acylation, the study was carried out using mainly zeolite Beta, gallosilicate Beta, FER and ITQ-6. The prepared zeolites were modified into its H-form by ion-exchanged, incorporation of metal oxides namely niobium oxide (Nb), and gallium oxide at different %wt loading by impregnation methods. The reactivity of the catalysts was tested in the alkylation of resorcinol with tert-butyl agents producing antioxidant 4-tert-butylresorcinol (mono substituted) and 4,6-diterbutylresorcinol(disubstituted) as the main products. The reactivity of the catalyst varies with the types of zeolites and depends on the crystallinity which related closely to the amount and strength of acidic sites. The higher the crystallinity, the higher the amount and strength of acidic sites, the higher the reactivity of the catalyst.

In general, the activity of zeolite Beta catalyst increased with the decreased in Si/Al ratios in zeolite Beta samples. Zeolite Beta with Si/Al =11 ratio gave the highest conversion (95 %) followed by zeolite Beta with Si/Al =19 ratio with 70 % and lastly zeolite Beta with Si/Al = 21 ratio which only gave 64 %. Similarly, zeolite Beta with Si/Al =11 ratio gave the highest selectivity of 4,6-di-*tert*-butylresorcinol (81 %) followed by Zeolite Beta with Si/Al =19 ratio (78 %) and Zeolite Beta with Si/Al = 21 ratio (56 %). The conversion of resorcinol and the selectivity of 4,6-di-*tert*-butylresorcinol increased with the increase of Brönsted acid sites while there has no correlation between the conversions of resorcinol and the selectivity of 4,6-di-*tert*-butylresorcinol with the amount of Lewis acid sites. This finding indicated that the activity of the zeolite Beta catalysts is largely relates to the Brönsted acid sites. The catalytic performance increased with the increased of the crystallinity and the surface area of the zeolite Beta at different Si/Al ratios. The conversion of resorcinol in zeolite Beta sample with 2 % niobium loading is more active and reached equilibrium faster than the parent zeolite Beta. In addition, the selectivity of 4,6-di-*tert*-butylresorcinol has increased to 100 % in zeolite Beta samples with 2 % w/w niobium loading from 78 % in the parent zeolite Beta. In this study, zeolite Beta with 2 % w/w niobium loading was identified as the most active catalyst and has a potential to be selective catalysts in the Friedel-Crafts alkylation of resorcinol.

Catalytic activity of aluminosilicate and gallosilicate zeolite Beta in Friedel-Crafts alkylation of resorcinol shows that aluminosilicate analogue is a better catalyst compared to gallosilicate zeolite Beta as it gives higher reactant conversion and amount of products yield. The low amount of Brønsted acid sites due to the low crystallinity of sample after continuous modification treatment and the decrease in the strength of this acid sites due to replacement of Al with Ga is responsible for the low catalytic performance of [Ga]-Beta in this reaction. Catalytic activity of samples of gallium impregnated zeolite Beta as the optimum yield of 4-*tert*-butylresorcinol (60.3%) as the major product with highest conversion of resorcinol (63.0%) was obtained at 8 wt% of Ga loading. The 100% selectivity of major product was achieved for 10 – 15 wt% of Ga loading zeolite Beta which contain higher amount of Lewis acid sites. TOF increased gradually with the increase amount of Ga in the samples, and at 7.3 wt% of Ga loading, both Brønsted and Lewis acid sites contributed evenly in producing the major product which lead to optimum yield of product and reactant conversion. This finding suggests that the presence of gallium on zeolite Beta influenced the catalytic activity based on the amount of Ga loading into the sample.

Catalytic activity of FER on the acylation of anisole with acetic anhydride and propionic anhydride depend largely on the size of the substrates. All H-ferrierite catalysts used, produced only *p*-methoxypropiophenone as a main product with propionic acid as the side product reaction when using propionic anhydride as acyl agent. The conversion increased relatively with the decreasing SiO_2/Al_2O_3 ratios due to the increase in Brønsted acid sites in the ferrierite framework. The effect of different size of acylating agent (acetic anhydride as compared with propionic anhydride) in acylation of anisole shows that the product obtained is also in *para* orientation. However, the product selectivity and the anisole conversion were 98 % and 55 %, were higher as compared to propionic anhydride. From the product obtained, we proposed that the mechanism of this reaction involved electrophile aromatic substitution which included the formation of acylium ions from the Brønsted acid sites in the catalysts

Catalytic activity of bifunctional oxidative acidic TS-1 based catalyst on the transformation of 1-octene to 1,2-octanediol showed that the production of diol via 1,2 epoxyoctane depend largely of the presence of Bronsted acid rather than Lewis acid.

SO_4^{2-}/TS-1 and SO_4^{2-}-Ti/TS-1 catalyst were shown to display only Lewis acidity. The catalysts greatly enhanced the yields of 1,2-epoxyoctane, but decreased in activity towards the formation of 1,2-octanediol when compared to the parent TS-1. WO_3/TS-1 catalysts with different amounts of tungsten loading contain similar amount of Brønsted acid sites. Consequently, the activities of the WO_3/TS-1 catalysts for the formation of 1,2-octanediol from 1-octene were found to be similar suggesting that the Brønsted acid sites were formed due to formation of Si-O-W bond in the WO_3/TS-1 catalysts. The Nb/TS-1 catalysts were active towards the consecutive transformation of 1-octene to 1,2-octanediol through the formation of 1,2-epoxyoctane. Both the amount of Brønsted and Lewis acid sites increased as the niobium loading increased. It was demonstrated that the tetrahedral titanium species and niobic acid act as oxidative and acidic active sites, respectively.

On the basis of the catalytic activity results, two new properties of the bifunctional catalysts can be highlighted. The first property is based on the higher rate of epoxidation of 1-octene. Generally, it has been found that introduction of acidic sites onto the TS-1 results in a significant increase of the rate of the formation of 1,2-epoxyoctane at the initial time of reaction, due to increased rate of formation of reactive oxo-titanium species. The acidic sites present on the surface of TS-1 leads to the increased hydrophilic character of the catalysts, because they facilitate the adsorption of aqueous H_2O_2 onto the TS-1. Consequently, the rate of the formation of oxo-titanium species increases and the production of epoxides is also increased. Secondly, in the formation of diol, the activity of the bifunctional catalyst was observed to be higher than that of the mechanical mixture of oxidative and acidic active sites. It is concluded that the specific location of the acidic sites on the external surface of TS-1 which is in vicinity of the Ti oxidative active sites is responsible for the increased catalytic activity. In consequence, after leaving the pores of TS-1, the epoxidation products could immediately undergo hydrolysis at the Brønsted acid sites that are distributed homogeneously on the external surface of TS-1.